

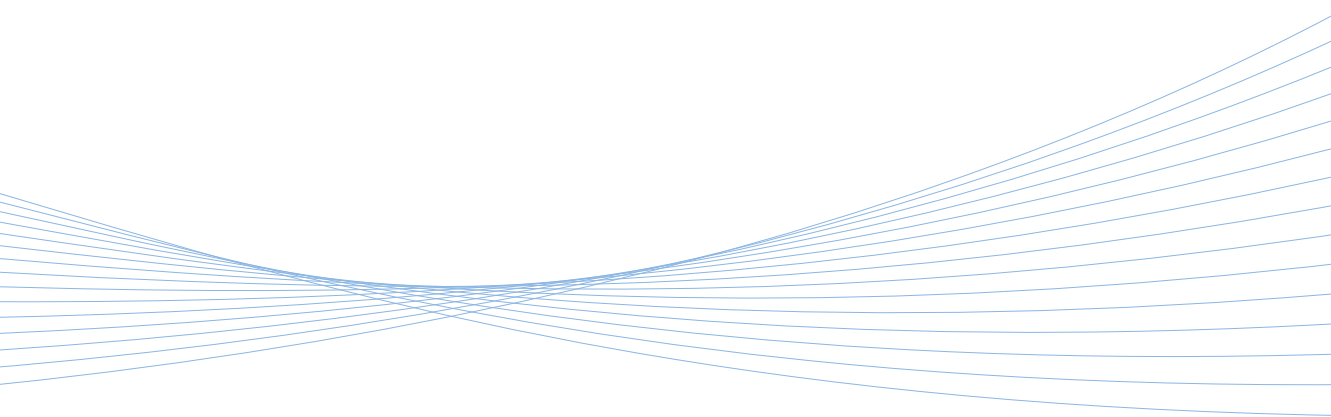


ILMATIETEEN LAITOS
METEOROLOGISKA INSTITUTET
FINNISH METEOROLOGICAL INSTITUTE

131
CONTRIBUTIONS

ADVANCED SEPARATION TECHNIQUES
COMBINED WITH MASS SPECTROMETRY
FOR DIFFICULT ANALYTICAL TASKS
- ISOMER SEPARATION AND OIL ANALYSIS

JAAKKO LAAKIA



Department of Chemistry
University of Helsinki
Finland

**Advanced separation techniques combined with mass spectrometry
for difficult analytical tasks – isomer separation and oil analysis**

Jaakko Laakia

Academic Dissertation

To be presented, with the permission of
the Faculty of Science of the University of Helsinki,
for public criticism in Auditorium A129 of the Department of Chemistry
(A.I. Virtasen aukio 1, Helsinki)
on May 12th, 2017, at 12 o'clock noon.

Helsinki 2017

Supervisors	<p>Professor Tapio Kotiaho Department of Chemistry Faculty of Science</p> <p>and</p> <p>Division of Pharmaceutical Chemistry and Technology Faculty of Pharmacy University of Helsinki</p> <p>Docent Tiina Kauppila Division of Pharmaceutical Chemistry and Technology Faculty of Pharmacy University of Helsinki</p>
Reviewers	<p>Professor Janne Jänis Department of Chemistry Faculty Science and Forestry University of Eastern Finland</p> <p>Docent Velimatti Ollilainen Department of Food and Environmental Sciences Faculty of Agriculture and Forestry University of Helsinki</p>
Opponent	<p>Professor Wolfgang Schrader Max-Planck-Institut für Kohlenforschung Mülheim an der Ruhr, Germany</p>
Custos	<p>Professor Marja-Liisa Riekkola Department of Chemistry University of Helsinki</p>

ISBN 978-952-336-016-7 (Paperback)
ISSN 0782-6117
Erweko Oy
Helsinki 2017

ISBN 978-952-336-017-4 (PDF)
<http://ethesis.helsinki.fi>
Helsingin yliopiston verkkojulkaisut

TABLE OF CONTENTS

ABSTRACT	4
TIIVISTELMÄ	5
LIST OF ORIGINAL PAPERS	6
ACKNOWLEDGEMENTS	7
ABBREVIATIONS	8
1. INTRODUCTION	10
1.1.1 Basic operation principles of ion mobility 12 spectrometry	11
1.1.2 Applications of ion mobility spectrometry	16
1.2 Basic operation principles and applications of two-dimensional gas chromatography – time-of-flight mass spectrometry	19
1.3 Aims of study	23
2. EXPERIMENTAL	24
2.1 Chemicals	24
2.2 Oil fractioning (Paper IV-V)	27
2.3 Separation of <i>n</i> -alkanes from branched and cyclic saturated hydrocarbons by urea adduct formation (Papers IV-V)	27
2.4 Ion mobility spectrometry instrumentation (Papers I-III)	29
2.5 Temperature of ion mobility drift tube (Paper I)	31
2.6 Two-dimensional gas chromatography – time-of-flight mass spectrometry instrumentation (Papers IV-V)	32
2.7 Principle component analysis (Papers IV-V)	33
3. RESULTS AND DISCUSSIONS	34
3.1 Sterically hindered phenols (Paper I)	34
3.2 Separation of different ion structures (Paper II)	38
3.3 Separation of isomers	41
3.4 Geochemistry of Recôncavo Basin, Brazil, oils (Paper IV)	46
3.5 Geochemistry and identification of compounds in Brazilian crude oils (Paper V)	53
4. CONCLUSIONS	63
REFERENCES	66
PUBLICATIONS I, II, III, IV and V	77



publication		Series title, number and report code of
Published by	Finnish Meteorological Institute (Erik Palménin aukio 1), P.O. Box 503 FIN-00101 Helsinki, Finland	Finnish Meteorological Institute Contribution 131, FMI-CONT-131
		Date May 2017

Author:
Jaakko Laakia

Title:
Advanced separation techniques combined with mass spectrometry for difficult analytical tasks – isomer separation and oil analysis

Abstract

This thesis covers two aspects of utilisation of advanced separation technology together with mass spectrometry: 1. Drift tube ion mobility spectrometry – mass spectrometry (IMS-MS) studies of the behaviour of ions in the gas phase and 2. Comprehensive two dimensional gas chromatography – time-of-flight mass spectrometry (GC×GC-TOF-MS) studies for characterization of crude oil samples.

In IMS studies, the focus was on the separation of isomeric compounds. For example, [M-H]⁻ ions of 2,4-di-tert-butylphenol (2,4-DtBPh) and 2,6-di-tert-butylphenol (2,6-DtBPh) were separated. It was also observed that shielding of the charge site by the functional groups of a molecule has a large effect on the separation of the isomeric compounds. For example, amines with a shielded charge site were separated from those with a more open charge site, while some of the isomeric amines studied were not separated. Different kinds of adduct ions were observed for some of the analytes. Dioxygen adducts were seen for 2,4-DtBPh [M+O₂]⁻, 2,6-di-tert-butylpyridine (2,6-DtBPyr) [M+O₂]^{+·} and 2,6-di-tert-butyl-4-methylpyridine (2,6-DtB-4MPyr) [M+O₂]^{+·}. The adduct formation increases the total mass of the analyte ion, and therefore, for example the 2,4-DtBPh [M+O₂]⁻ ion could be separated from its isomeric compound 2,6-DtBPh [M-H]⁻, which did not form the dioxygen adduct ion. In the case of 2,6-DtBPyr and 2,6-DtB-4MPyr, the [M]⁺ ions formed dioxygen adduct [M+O₂]^{+·} ions. The both ions, [M]⁺ and [M+O₂]^{+·}, shared the same drift time which was longer than their [M+H]⁺ ion species. This work demonstrates that measuring with IMS the mobility of different ion structures of the same molecule, especially dioxygen adducts, results in a better understanding of the role of adduct ions in the IMS-separation process.

In GC×GC-TOF-MS studies, the focus was on detailed characterization of crude oil samples. For instance, oils from the Recôncavo Basin were classified to two different groups by using minor oil components. The GC×GC-TOF-MS data showed the correlation between 2D retention time and the number of carbons in a ring for several hydrocarbons as known from the literature. This information was used to achieve more structural information about eight new tetracyclic compounds, some of them similar to nor-steranes, detected during analysis. Some of these new compounds could be used as maturity indicators. This study demonstrated how GC×GC-TOF-MS can be used to separate geochemically interested isomers, identify minor geochemical differences between oils and achieve structural information about unknown biomarkers.

Publishing units

Atmospheric Composition Research and Expert Services

Classification (UDC)

543.544.3 543.51 539.144.7

Keywords

Ion mobility spectrometry, Two-dimensional gas chromatography, mass spectrometry, oil analysis, isomer separation

ISSN and series title

0782-6117 Finnish Meteorological Institute Contributions

ISBN

978-952-336-016-7 (Paperback)
978-952-336-017-4 (PDF)

Language

English

Pages

132



Tekijä:

Jaakko Laakia

Nimeke

Massaspektrometriin kytkeytyneet esierotustekniikat vaikeissa analyttisissä tehtävissä – isomeerien erotuksessa ja öljyanalytiikassa

Tiivistelmä

Väitöskirja koostuu kahdesta osiosta. Ensimmäisessä osiossa perehdytään ioniliikkuvuuspektrometria-massaspektrometriaan (IMS-MS), jolla tutkittiin ionien liikkuvuutta kaasufaasissa, ja toisessa kaksiosuotteiseen kaasukromatografia-massaspektrometriaan (GC×GC-TOF-MS), jolla karakterisoiitiin raakaöljynäytteitä.

Yksi IMS tutkimuksen tavoitteista oli erotella isomeerejä. Osa tutkituista isomeereistä erottui hyvin ja osa ei. Tarkemmassa tarkastelussa huomattiin, että yhdisteiden tietyt funktionaaliset ryhmät pystyvät ”suojamaan” molekyylin varautunutta funktionaalista ryhmää. Tällä efektillä oli suuri merkitys isomeerien erottumisessa, sillä esimerkiksi amiinit, joiden varauskohta oli ”suojattu” erottuivat IMS:llä ioneista, joiden varauskohta oli ”avoimpi”. Erilaisia addukti-ioneja (analyysin ja pienmolekyylin yhteenliittymä) havaittiin joillekin mitatuille yhdisteille. Mikäli adduktin muodostus tapahtuu vain toiselle isomeerille niin isomeerit erottuvat IMS:lla esim. 2,4-di-tert-butylphenolin (2,4-DtBPh) muodosti [M+O₂]⁻ addukti-ionin ja erottui 2,6-DtBPh-isomeeristä mikä ei muodostanut vastaavaa addukti-onia. di-tert-butylipyridiini taas muodosti [M]⁺ ja [M+O₂]⁺ ionin. Näille molemmille ioneille mitattiin sama liikkuvuus, mutta se pystyttiin erottamaan saman yhdisteen eri ioni muodosta, [M+H]⁺, IMS:llä. Tutkimuksessa osoitettiin, että on tärkeää mitata liikkuvuus saman yhdisteen eri ionimuodoille, erityisesti dihappiaddukteille, jotta ymmärrettäisiin paremmin ionien muodostusmekanismeja sekä adduktien vaikutusta eri ionimuotojen ja isomeerien erottumiselle IMS:ssä.

Väitöskirjan GC×GC-TOF-MS osiossa karakterisoiitiin raakaöljynäytteitä. Esimerkiksi Brasilian Recôncavo Basin öljykentältä kerätyt näytteet voitiin jakaa kahteen ryhmään käyttämällä näytteiden luokitukseen alhaisen pitoisuuden näytekomponentteja. GC×GC-TOF-MS mittaukset osoittivat korrelaation toisen dimensio GC-erotuksen retentioajan ja tunnettujen saturoituneiden hiilivetyjen renkaiden määrän ja niissä olevien hiiliatomien lukumäärän välillä. Tätä tietoa käytettiin hyödyksi tutkittaessa kahdeksan tuntemattoman yhdisteen rakennetta, joista osalla oli samankaltainen rakenne kuin nor-steraneilla. Kahta näistä yhdisteistä voitiin hyödyntää öljyjen maturaatio-asteiden määrittämisessä. Tutkimuksessa näytettiin että GC×GC-TOF-MS:llä voidaan erotella toisistaan geokemiallisesti kiinnostavia isomeerejä, tunnistaa pieniä geokemiallisia eroja öljyjen välillä ja saada rakenteellista tietoa ennestään tuntemattomista biomarkkereista.

Julkaisijayksikkö

Ilmakehän koostumuksen tutkimus ja asiantuntijapalvelut

Luokitus (UDK)

543.544.3 543.51 539.144.7

Asiasanat

Ioniliikkuvuuspektrometria, kaksiosuotteinen kaasukromatografia, massaspektrometria, isomeerien erottelu, öljytutkimus

ISSN ja avainnimeke

0782-6117 Finnish Meteorological Institute Contributions

ISBN

978-952-336-016-7 (Nidottu)

978-952-336-017-4 (PDF)

Kieli

Englanti

Sivumäärä

132

LIST OF ORIGINAL PAPERS

This thesis is based on the following papers, hereafter referred to by their Roman numerals [I-V]:

- I** J. Laakia, C. S. Pedersen, A. Adamov, J. Viidanoja, A. Sysoev, T. Kotiaho, Sterically Hindered Phenols in Negative Ion Mobility Spectrometry-Mass Spectrometry. *Rapid Comm. Mass Spectrom.* 2009, 23, 3069-3076
- II** J. Laakia, A. Adamov, M. Jussila, C. S. Pedersen, A. Sysoev, T. Kotiaho, Separation of Different Ion Structures in Atmospheric Pressure Photoionization - Ion Mobility Spectrometry - Mass Spectrometry (APPI-IMS-MS). *J. Am. Soc. Mass Spectrom.* 2010, 21, 1565-1572
- III** J. Laakia, T. J. Kauppila, A. Adamov, A. A. Sysoev, T. Kotiaho, Separation of isomeric amines with ion mobility spectrometry (IMS), Short communication, *Talanta.* 2015, 135, 889-893
- IV** A. Casilli, R. C. Silva, J. Laakia, C. J. F. Oliveira, A. A. Ferreira, M. R. Loureiro, D. A. Azevedo, F. R. Aquino Neto, High resolution molecular organic geochemistry assessment of Brazilian lacustrine crude oils, *Org. GeoChem.* 2014, 68, 61-70
- V** J. Laakia, A. Casilli, Bruno Q. Araújo, F. T. T. Gonçalves, E. Marotta, C. J. F. Oliveira, C. A. Carbonezi, M. R. B. Loureiro, D. A. Azevedo, F. R. Aquino Neto, Characterization of unusual tetracyclic compounds and possible novel maturity parameters for Brazilian crude oils using Comprehensive Two-Dimensional Gas Chromatography - Time of Flight Mass Spectrometry, *Org. GeoChem.* 2017, 106, 93-104

Author's contribution to the publications included in the doctoral thesis:

Papers I-III. Main responsibility in planning and carrying out measurements, data processing and writing the article. Associate professor Alexey Sysoev has used his contribution (consulting in physics of IMS and IMS/MS) in Papers I and II in his Doctor of Science degree at the National Research Nuclear University MEPhI, Moscow, Russia.

Paper IV Main responsibility in data processing and shared responsibility in geochemical analysis and in writing of the article, excluding the maturation (diamondoids) results, which were carried out by Renzo C. Silva and used as part of his PhD thesis "Applications of modern analytical techniques in petroleum organic geochemistry studies" at Federal University of Rio de Janeiro, Rio de Janeiro, Brazil.

Paper V Main responsibility in data processing and in geochemical analysis and in writing of the article.

ACKNOWLEDGEMENTS

This thesis is based on research conducted by the Ion Mobility Group of the Laboratory of the Analytical Chemistry at the University of Helsinki and the Laboratory of the Molecular Organic Geochemistry and Environmental at the Federal University of Rio de Janeiro, Brazil. The Academy of Finland (project numbers: 114132 and 122018), is acknowledged for financial support for the ion mobility research during the years 2007-2010 and PETROBRAS (Contract 00500072201.11.9) for funding the geochemistry research during the years 2012-2014. The Brazilian organizations CNPq, FAPERJ and FUJB are thanked for their financial support. Water och Lisi Wahls stiftelse för naturevetenskaplig forskning is thanked for funding a new nitrogen generator.

All of the staff (especially Pena) of the Laboratory of Analytical Chemistry and of the Laboratory of the Molecular Organic Geochemistry and Environmental (especially Vinicius) are acknowledged for providing assistance and the facilities.

I would like to thank all of the ion mobility team members: Ph.D. Alexey Adamov and Prof. Alexey Sysoev for their technical assistance, Ph.D. Christian Pedersen for supportive and innovative comments and Dos. Tiina Kauppila and Prof. Tapio Kotiaho for supervising my work and the geochemistry team: Prof. Débora Azevedo, Ph.D. Alessandro Casilli and Prof. Francisco R. Aquino Neto for constructive comments, Prof. Maria Regina Loureiro is especially thanked for her great help in Geochemistry, Portuguese and English.

Acknowledgements are also directed to helpful colleagues: Ph.D. Jaroslaw Puton, Ph.D. Anna-Kaisa Viitanen, Ph.D. Elina Kalenius, Ph.Lic. Matti Jussila, Ph.D. Timo Mauriala, Ph.D. Markus Haapala, Ph.Lic. Jyrki Viidanoja, Ph.D. Renzo C. Silva, M.Sc. Cleverson J.F. Oliveira and Ph.D. Alexandre A. Ferreira.

ABBREVIATIONS

¹ D	First chromatographic dimension
² D	Second chromatographic dimension
ACN	Acetonitrile
APCI	Atmospheric pressure chemical ionization
APPI	Atmospheric pressure photoionization
B/C	Branched and cyclic hydrocarbon fraction
B-N	Bradbury-Nielsen gate
2- <i>t</i> BPh	2- <i>tert</i> -Butylphenol
2- <i>t</i> BPyr	2- <i>tert</i> -Butylpyridine
β-car	β-Carotane
DBE	Double bond equivalence
CENPES	The Research Center of Petrobras (Centro de Pesquisas Leopoldo Américo Miguez de Mello, Rio de Janeiro, RJ, Brazil)
2,4,6-Col	2,4,6-Collidine
CV	Compensation voltage
2,6-D <i>t</i> B-4-MPh	2,6-Di- <i>tert</i> -butyl-4-methylphenol
2,4-D <i>t</i> BPh	2,4-Di- <i>tert</i> -butylphenol
2,6-D <i>t</i> BPh	2,6-Di- <i>tert</i> -butylphenol
2,6-D <i>t</i> B-4-MPyr	2,6-Di- <i>tert</i> -butyl-4-methylpyridine
2,6-D <i>t</i> BPyr	2,6-Di- <i>tert</i> -butylpyridine
DH ₃₀ (or DiaH ₃₀)	C ₃₀ 17α-Diahopane
<i>N,N</i> -DMA	<i>N,N</i> -Dimethylaniline
DMS	Differential mobility spectrometry (= also FAIMS)
EI	Electron ionization
ESI	Electrospray ionization
4-EA	4-Ethylaniline
FAIMS	Field asymmetric waveform ion mobility spectrometry (= also DMS)
FID	Flame ionization detector
Gam	Gammacerane
GC	Gas chromatography
GC×GC	Two-dimensional gas chromatography
GC×GC-TOF-MS	Two-dimensional gas chromatography – time-of-flight mass spectrometry
H ₃₀	17α(H),21β(H)-Hopane
H ₃₁ R	C ₃₁ 17α(H),21β(H)-homohopane
IMS	Ion mobility spectrometry
IMS-FP	Ion mobility spectrometer – faraday plate detector
IMS-MS	Ion mobility spectrometer – mass spectrometer
LC	Liquid chromatography
<i>m/z</i>	Mass to charge ratio
M ₃₀	Moretane, 17β(H),21β(H)-hopane
3βMH ₃₁	C ₃₁ 3β-Methylhopane
MeOH	Methanol
<i>n</i> -M- <i>o</i> -T	<i>N</i> -Methyl- <i>o</i> -toluidine

x-MBA	x-Methylbenzylamine (x = 2, 3, or 4)
ONII	8 α (H), 14 α (H)-Onocerane
ONIII	8 α (H), 14 β (H)-Onocerane
PEA	2-Phenethylamine
R _o (%)	Vitrinite reflectance
RF	Radio-frequency
RIP	Reaction ion peak
SIM	Selected ion monitoring
St	20S + 20R C ₂₇ 5 α ,14 α ,17 α -Cholestanes
TeT ₂₄	C ₂₄ Tetracyclic terpane
Tm	C ₂₇ 17 α -22,29,30-Trisnorhopane
t _R	Retention time
TIMS	Trapped ion mobility Spectrometer
Tr _x	C _x tricyclic terpane
Ts	C ₂₇ 18 α -22,29,30-Trisnorneohopano
TOF-MS	Time-of-flight mass spectrometry
TWIMS	Traveling wave ion mobility spectrometry
2,4,6-T <i>t</i> BPh	2,4,6-Tri- <i>tert</i> -butylphenol
2,4,6-TNT	2,4,6-Trinitrotoluene

1. INTRODUCTION

Mass spectrometry (MS) is a powerful analytical technique, which is used for the identification of unknown compounds and for the quantitation of known compounds in various types of samples [1]. It is used in many fields of science for these purposes, for example in pharmaceutical chemistry, environmental and food analysis, forensic science and industrial process analysis. The working principle of MS involves first the ionization of the compounds to be measured and the subsequent separation of the ions based on their differing mass-to-charge (m/z) ratios. Ionization can be carried out in atmospheric pressure or in a vacuum, but ion separation is always done in a vacuum. Production of m/z data is the key feature of MS, since it allows the determination of the molecular weight of a compound. The current mass spectrometers can measure very precisely the m/z ratios, which allows the determination of elemental composition of the analytes. However, the elemental composition of a compound does not necessarily give information about the chemical structure, since compounds can have the same elemental compositions, but different structures (isomeric compounds). One solution for this is the separation of isomeric compounds before the mass spectrometric analysis. In addition, mass spectrometric analysis of very complex samples, such as biological or crude oil samples, often requires additional pre-separation of the sample components for reliable analysis.

The two most common pre-separation techniques used with MS are liquid chromatography (LC) [2] and gas chromatography (GC) [3]. However, they are not always sufficient for reliable compound identification, for example in complex samples containing isomeric compounds, which are not separated (co-elutes) in LC or GC. Therefore, alternative and advanced pre-separation techniques, such as ion mobility spectrometry (IMS) [4] and two dimensional gas chromatography (GC×GC) [5], that can be combined with MS, have been developed. Their analytical characteristics are studied in this thesis.

Similar to MS, in IMS the compounds are first ionized and subsequently separated. However, in IMS the ion separation typically occurs in the gas phase under atmospheric pressure or in a reduced pressure, which is higher than in MS. The other main difference is that in IMS the ions are separated based on their shape (i.e. collision cross-section)

[4] instead of m/z ratios as in MS. In many cases IMS is more capable to separate isomers than MS.

In GC×GC the main idea is to use two different column phases in line, for example, a non-polar column in the first dimension (¹D) and a semi-polar column in the second dimension (²D). This results in GC×GC providing clearly higher peak capacity than one dimensional GC, and very complex samples, such as crude oil samples containing thousands of compounds, can be more efficiently separated into individual compounds [5-9]. This makes GC×GC-MS analysis more reliable than GC-MS analysis.

1.1.1 Basic operation principles of ion mobility spectrometry

The operation principle and main parts of the most common IMS, the drift tube, is presented in Figure 1. A drift tube IMS consists of an ion source, a desolvation region, a drift region, a detector, control electronics and software to run the instrument.

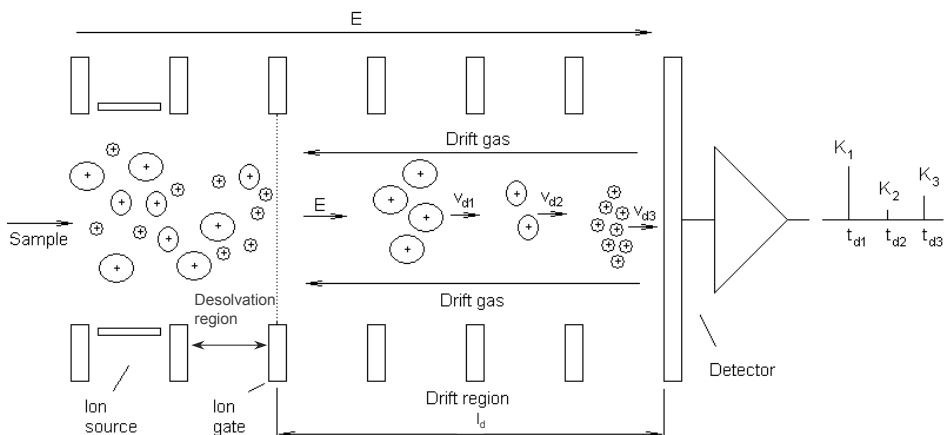


Figure 1. Schematic diagram of a drift tube IMS (permission and courtesy of Alexey Sysoev, unpublished material). l_d = length of the drift region, E = electric field, v_{dx} = drift velocity of an ion, K_x = mobility coefficient of an ion and t_{dx} = drift time of an ion.

A typical measurement sequence has the following steps: After sample introduction the analyte molecules are ionized in an atmospheric pressure ion source and the ions are transferred to the desolvation area, where the ions are stored before they are pulsed with a Bradbury-Nielsen (B-N) gate [11] into the drift region. Next, the ions move by an electric field (typically 100-300 V/cm) across the drift region, in which a neutral gas

(e.g. nitrogen or air) is flowing in the opposite direction. After the IMS separation, the separated ions are usually detected with a faraday plate detector or with MS.

The separation of ions is based on their collisions with neutral gas molecules, which produce different drift times for ions with differing shapes, i.e. differing collision cross-sections (cm² or Å). For example, an ion with a small collision cross-section moves faster through the drift region than an ion with a larger collision cross-section. The drift velocity (v_d , [cm/s]) of an ion through the drift region can be presented by Equations 1 and 2 [4, 10].

$$v_d = KE \quad (1)$$

$$v_d = \left(\frac{l_d}{t_d} \right) \Rightarrow K = \left(\frac{l_d^2}{t_d V} \right) \quad (2)$$

where K = mobility coefficient (cm²V⁻¹s⁻¹), E = electric field in the drift region (V/cm), l_d = length of the drift region (cm), t_d = drift time of the ion through the drift region (ms) and V = voltage drop over the drift region (V).

The mobility coefficient (K) (Equation 2) is inversely proportional to collision cross-section (Ω) [10] (Equation 3).

$$K = \frac{3ez\sqrt{2\pi}(1 + \alpha_c)}{16N\sqrt{\mu kT_{eff}}\Omega} \quad (3)$$

Where e = charge of electron (C), z = charge number, α_c = correction factor for large molecules <0.02 , N = drift gas density (molecules m⁻³), μ = reduced mass ion-neutral pair (g), k = Boltzmann's constant (J/K), T_{eff} = effective temperature of ion (K).

K is often presented as reduced mobility coefficient K_0 according to Equation 4 [4]:

$$K_0 = \left(\frac{l_d^2}{t_d V} \right) \left(\frac{273}{T} \right) \left(\frac{P}{760} \right) \quad (4)$$

where, T = temperature (K) and P = pressure (Torr).

Even though mobilities in IMS are typically reported as reduced mobility (K_0) values (Equation 4), which are normalized with standard pressure and temperature, variations in reduced mobility values are observed. This can be due to moisture or other impurities in the drift gas, or instrumental factors, such as an imperfect electric field or variation of the drift length. Due to these facts different compounds have been tested as reference compounds, which would allow standardization of mobilities. It has been observed that mobilities of compounds such as tetraalkylammonium halides [11] and 2,6-di-*tert*-butylpyridine [12-14], are not much affected by moisture or other drift gas impurities. Therefore, these compounds can be used for comparison of different instruments as instrumental standards [15]. On the other hand, model compounds such as lutidine [16] and dimethyl methylphosphonate [12], which also respond to the quality (e.g. impurities) changes of the drift gas, can be used as mobility standards. All the above-mentioned compounds are used as standards in positive ion mode measurements. Standard compounds, such as methyl salicylate [17] and 2,4,6-trinitrotoluene [18], to be used as mobility standards in negative ion mode, have also been presented.

Ionization is the heart of an ion mobility spectrometer. Ions are generated in drift tube IMS commonly with a radioactive source (e.g. ^{63}Ni) [19], electrospray ionization (ESI) [4, 11, 20-23], atmospheric pressure chemical ionization (APCI) [24, 25] or atmospheric pressure photoionization (APPI) [26-28]. All these techniques work under atmospheric pressure conditions, and can be considered as soft ionization techniques, which produce mostly protonated and deprotonated molecules with little fragmentation. Since APCI and APPI were used in this study, they are presented in more detail.

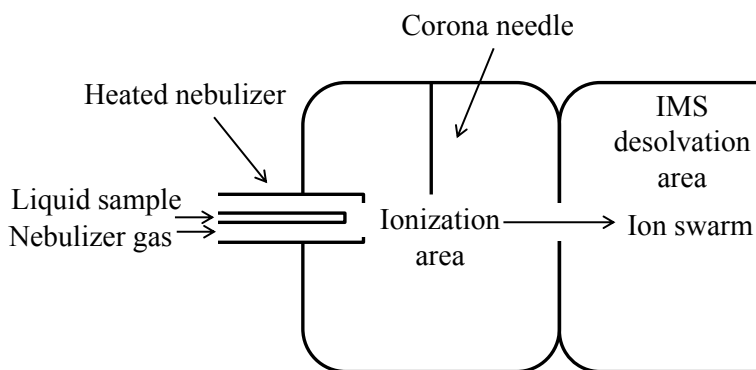


Figure 2. A schematic drawing of a typical atmospheric pressure chemical ionization source for IMS.

As shown in Figure 2, in a typical APCI ion source a liquid sample is pumped through a heated nebulizer, in which a vaporized sample stream is produced with the aid of heat and nebulizer gas [29]. Ionization reactions in APCI are initiated by corona discharge, which is obtained by conducting high voltage to a corona needle. The reactant ions in APCI depend on the solvent composition and reaction ions available in the ionization chamber, and components such as $[\text{H}_3\text{O}]^+$ and $[\text{NH}_4]^+$ ions are formed in positive ion mode, and $[\text{HO}]^-$, $[\text{O}_3]^-$ and $[\text{NO}_x]^-$ ions in negative ion mode [30-34]. In IMS, the reactant ions settle to equilibrium in the desolvation area and typically, a cluster of ions, also called a reactant ion peak (RIP), is observed [4]. The most common analyte ions formed in the ionization reactions with the reactant ions and neutral analyte molecules in APCI are protonated molecules $[\text{M}+\text{H}]^+$ in positive ion mode and deprotonated molecules $[\text{M}-\text{H}]^-$ in negative ion mode [4].

APPI ion source resembles the APCI ion source, except that in APPI an ultraviolet (UV) lamp is used to initiate the ionization instead of a corona needle. Often, APPI uses a dopant, an additional solvent, which is introduced to the ion source, in order to enhance the ionization of analytes. In APPI, the ionization sequence typically starts with the ionization of the vaporized solvent or dopant due to radiation emitted by the UV lamp. Various types of reactant ions can be formed in positive APPI, e.g., protonated molecules $[\text{S}+\text{H}]^+$ or radical cations $[\text{S}]^+$ of solvent and / or dopant [35]. In negative APPI, deprotonated molecules $[\text{S}-\text{H}]^-$ or negative molecular ions $[\text{S}]^-$ of solvent and/or atmospheric gases are typically formed [36, 37]. Subsequent reactions of analytes with the reactant ions produce analyte ions; in positive APPI mainly radical cations M^+ and/or protonated molecules $[\text{M}+\text{H}]^+$, and in negative APPI negative molecular ions M^- and/or deprotonated molecules $[\text{M}-\text{H}]^-$.

The drift tube ion mobility instrument presented above is the main type of IMS instrument used nowadays, but many other types of instruments have been developed and are also commercially available. One of them is field asymmetric waveform ion mobility spectrometry (FAIMS) or differential mobility spectrometry (DMS). The ion separation principle for FAIMS and DMS is the same [38], but the electrode in FAIMS has cylindrical geometry and in DMS planar geometry. The electric field can be varied quickly between high (~ 20 kV/cm) and low field (~ 1 kV/cm) using high radio-frequency (RF) voltage also called dispersion or direct voltage (DV) (Figure 3) [39]. An additional superimposed direct current (DC) voltage, a so-called compensation voltage

(CV) is used to allow the passage of the desired ions through the electrode pair to the detector. Scanning the CV creates an analyte spectrum [40].

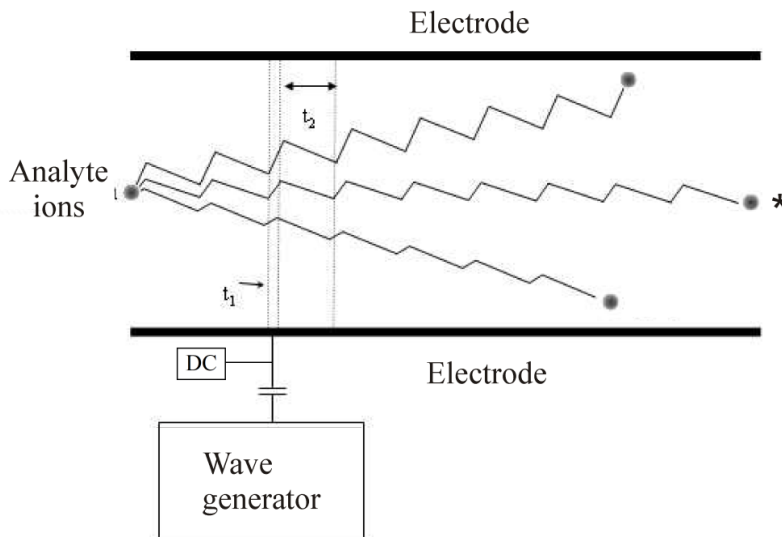


Figure 3. The schematic picture of a field asymmetric waveform ion mobility spectrometry (FAIMS) or differential mobility spectrometry (DMS) represents the situation where the ion (marked with an asterisk) is collected onto the detector. Commonly, the drift gas flow is parallel to the analyte movement (from left to right). t_1 = dispersion voltage (DV) at high field, t_2 = DV at low field and DC = direct current (Reused with permission from ref. [4])

Another IMS approach, which has been combined with mass spectrometry is travelling wave ion mobility spectrometry (TWIMS, Waters Corp., Milford, MA, USA) [41, 42]. In TWIMS a low electric field is used to produce voltage waves (~ 20 V), which travel through a set of electrodes forming the drift region. Analyte ions are separated as the wave travels through the drift region under reduced pressure (~ 1 mbar), which is higher than the typical pressure inside a mass analyzer ($< 10^{-5}$ mbar).

Recently a trapped ion mobility spectrometer (TIMS)-q-TOF instrument has been developed. In TIMS analyte ions are held stationary in the gas flow [43].

All the presented IMS instrument types have been combined with MS, (IMS-MS [4, 20, 44]) or LC and MS (e.g. LC-FAIMS-MS [45] and LC-IMS-MS [46]). For instance, in biomolecule analysis, where samples are very complex, the IMS-MS combination has increased the component separation [47, 48] and a further increase is obtained with LC-IMS-MS, as thousands of peaks have been separated with different retention times, drift times and m/z ratios from plasma proteome [49].

1.1.2 Applications of ion mobility spectrometry

The most important applications of traditional stand-alone IMS instruments are detection of explosives and chemical weapons [50-52]. Besides these, IMS is nowadays used in many fields of science [53, 54]. Ion mobility instruments are typically operated at atmospheric pressure, and therefore do not require heavy vacuum pumps as MS. Due to this, stand-alone ion mobility spectrometers are light enough for field applications, such as detection of chemical warfare agents [4], explosives [50], herbicides [55], pesticides [56] and organic volatile compounds [18]. IMS can also be used to detect specific compounds, such as ethanol in a fermentation process [57] or volatile compounds in food [58, 59], or identifying chemical classes of biologically relevant compounds, such as lipids, peptides and carbohydrates [60]. IMS instruments can also be used as detectors for GC [61]. The main applications of IMS-MS instruments are in metabolomics [62, 63], glycomics [63, 64] and proteomics [20, 49, 66]. Recently, TWIMS and IMS-MS instruments have been used to identify contaminants and additives in crude oil and gasoline samples, respectively [67, 68]. IMS-MS has been used to study the shape of model aromatic compounds that can be present in crude oils [69] and TWIMS has been used to produce information about sizes and shapes of compounds in the asphaltene fraction of crude oil [70].

In Table 1 are examples of situations where IMS is capable of separating isomers, e.g. hydrocarbons [71, 72], dihalogenated benzenes [73], terpenes [74] and anilines [75]. Isomers can be separated in IMS because they usually have different shapes and therefore different collision cross-sections. IMS separation before MS detection has been used to distinguish isomeric hydrocarbons [76] and polycyclic aromatic hydrocarbons [43], and to separate stereoisomers, such as *cis*- and *trans*-conformations of singly and doubly charged tryptic peptides [77]. However, it has been reported that singly protonated $[M+H]^+$ ions of two peptide isomers do not necessarily have large enough differences in their shapes, and therefore they cannot be separated by IMS, but the doubly charged $[M+2H]^{2+}$ ions of the same peptides can be [78]. Ionization of isomeric analytes can sometimes be enhanced by forming adducts (e.g. sodium, potassium or metal ions), which can be separated by IMS. For example, this has been done with sodium adducts of disaccharide-aldodols and trisaccharides [79], with

sodium, potassium and silver adducts of flavonoid diglycosides [80] and with sodium, silver, cobalt, copper, mercury and lead metal cation adducts of stereoisomers of methyl galactoside [76]. Separation of enantiomeric model compounds can be done by adding chiral modifiers (e.g. (S)-(+)-2-butanol) in the drift gas stream [81, 82]. The modifier reduces the drift time of both enantiomers, but for one enantiomer it is reduced more than for the other, which is assumed to be due to stronger interaction between the chiral centre of the enantiomer and the modifier. The TWIMS instrument has been used, e.g., to separate $[M+H]^+$ ions of the isomeric 4-butylaniline and *N*-butylaniline [83], and in protein analysis [84]. In another study, it was observed that model isomeric steroid pairs of estradiols, androsterones and testosterone showed hardly any separation with TWIMS, but their *p*-toluenesulfonyl isocyanate derivatives resulted in better separation of α - and β -estradiols, 3 α - and β -androsterones and 17 β - and 17 α -testosterone [85].

Table 1. Examples of isomeric compounds separated with IMS, FAIMS and TWIMS.

Compound	Drift gas and separation conditions	Ionization	IMS instrumentation	Ref
Hydrocarbons	air	Radioactive, APCI and APPI	IMS-FP ^a	[71,72]
Dihalogenated benzenes	air	Radioactive, APCI and APPI	IMS-FP ^a	[73]
Terpenes	air	Radioactive, APCI and APPI	IMS-FP ^a	[74]
Anilines	air	Radioactive, APCI and APPI	IMS-FP ^a	[75]
Hydrocarbons	^b	ESI	IMS-MS	[76]
PAH	N ₂	APPI	Trapped IMS-MS	[43]
Tryptic peptides	He	ESI	IMS-MS	[77]
Peptides	N ₂ ^c	ESI	IMS-MS	[78]
Saccharides	N ₂ ; Sodium adducts	ESI	IMS-MS	[79]
Flavonoid diglycosides	N ₂ ; Cation adducts	ESI	IMS-MS	[80]
Model compounds	N ₂ ; Chiral modifier	ESI	IMS-MS	[81, 82]
Hydrocarbons	N ₂	APPI	DMS-MS	[86]
Disaccharide	N ₂ ; Cation adducts ^d	ESI	FAIMS-MS	[87]
Phthalic acids	N ₂ or CO ₂	ESI	FAIMS-MS	[88]
Model aniline compounds	Ar or CO ₂	ESI	TWIMS	[83, 89]
Protein	N ₂	nano-ESI	TWIMS	[84]
Steroids	N ₂ or CO ₂ ^e	ESI	TWIMS	[85]

APCI, Atmospheric pressure chemical ionization; APPI, Atmospheric pressure photoionization; ESI, Electrospray ionization; IMS-MS, Ion mobility spectrometer – mass spectrometer; DMS-MS, Differential mobility spectrometry (= also FAIMS); TWIMS, Traveling wave ion mobility spectrometry; PAH, Polycyclic aromatic hydrocarbons; N₂, nitrogen; He, Helium; CO₂, carbon dioxide; Ar, Argon; ^a IMS-MS is used to confirm ion structures; ^b Metal cations Na⁺, Ag⁺, Co⁺², Cu⁺², Ca⁺², Hg⁺² and Pb⁺²; drift gases He, N₂, Ar and CO₂; ^c Doubly charged ions are separated; ^d Cations studied were H⁺, NH₄⁺, Li⁺, Na⁺, K⁺, Rb⁺, and Cs⁺; ^e *p*-toluenesulfonyl isocyanate derivatives of steroids

1.2 Basic operation principles and applications of two-dimensional gas chromatography – time-of-flight mass spectrometry

Two-dimensional gas chromatography (GC×GC) is similar to the conventional one-dimensional gas chromatography (GC) in the sense that the analyte compounds are separated in the gas phase by their interactions with a stationary phase on the column surface. The GC and GC×GC have three main components: (i) injector, (ii) column (inside the oven) and (iii) detector. The main additional parts in GC×GC are a modulator and a second column, which are located between the first column and the detector (Figure 4).

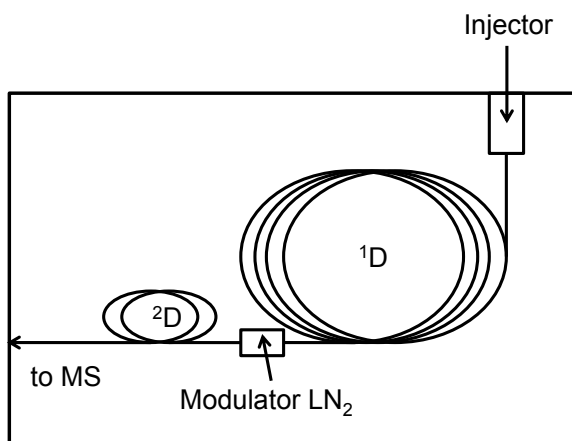


Figure 4. Schematic diagram of a two-dimensional GC×GC instrument. Modulator LN₂ = cryogenic modulator which uses liquid nitrogen as a cold jet.

There are various GC injectors for different kinds of samples. The split-splitless injector type is the most common due to the possibility to switch between two modes allowing for a wide concentration working range: split mode for highly concentrated or dirty samples and splitless mode for trace level analysis.

GC columns for GC×GC have many options with different length, diameter and film material (stationary phase). A large amount of different materials and their combinations are available for stationary phases, but generally non-polar columns are suitable for separation of non-polar compounds and polar columns for separation of polar compounds. The separation in non-polar ¹D column may be explained by the boiling point of the analyte. For example, 2,2-dimethylpropane with a more spherical shape has a lower boiling point (282.6±0.5 K) than pentane with a linear shape

(309.2±0.2 K), and therefore they are separated in ¹D. In a semi-polar ²D column the separation is driven by interactions between analytes and the stationary phase of the column, where the polarity of the molecule has commonly a key role. A common combination of columns is a non-polar in the first dimension (¹D) column and a semi-polar in the second dimension (²D) column [90]. After the separation in the ¹D column the sample compounds are continuously introduced by the modulator during the chromatographic run into the ²D column for further separation. Different kinds of modulators are available, and they are described elsewhere [90]. In a cryogenic modulator the sample compounds are held and then released, with a cold and a hot jet, resulting in a two-dimensional separation field (Figure 4) [91].

Typical carrier gases are nitrogen, argon, helium, hydrogen and air. Linear velocity of the carrier gas has an important role in the efficiency of the chromatographic separation. Golay plots and van Deemter curves for each carrier gas are used to demonstrate the optimal linear velocities against the number of theoretical plates (resolution). For instance, hydrogen has the longest linear velocity range, but it is an expensive and flammable gas. Helium has the second longest linear velocity range after hydrogen, and therefore it is selected for applications, where a wide variety of compounds are to be analyzed with the same GC setup.

For GC×GC, MS is a common detector, especially time-of-flight mass spectrometry (TOF-MS), which has the advantage of producing full mass spectral data with high frequency to ensure a sufficient number of data points for a good peak shape.

Different detectors can be attached to GC×GC, for example a flame ionization detector (FID). It is cheap, easy to maintain, and good for quantitative analysis with a large linear response range for organic compounds.

In most GC×GC-MS instruments the analytes are ionized after the ²D separation by electron ionization (EI, 70 eV). The electrons collide with analyte molecules by knocking out an electron, and typically molecular ions M⁺ and their fragments are observed. EI is a stable and repeatable ionization technique with already existing large mass spectral libraries; the most important is the one by the National Institute of Standards and Technology (NIST) [92].

GC×GC instruments have a high peak capacity [8], and therefore they are good for many kinds of applications in different fields of chemistry, such as environmental [93], food [94], metabolomics [95, 96], biological [97] and geological [98]. GC×GC is an

attractive tool for difficult analytical applications, and it is a good tool for screening complex samples in order to find compounds such as illegal drugs [99] and anabolic agents in doping control [100] and crude oil samples [101].

GC×GC-TOF-MS has been used in petroleum research to analyze different kinds of samples, the examples of which are presented in Table 2.

Table 2. Examples of petroleum studies with GC×GC-TOF-MS.

Research topic	Reference
Fischer-Tropsch reaction	[102]
Extra heavy gas oil	[103, 104]
Heavy petroleum fraction	[105, 106]
Crude oils from Cear Basin	[107]
Biodegradation of oils	[108-110]
Depositional paleoenvironmental conditions	[111-113]
Maturation of oils	[114]
Trace analysis	[115]
Modified white gasoline	[116]
Higher plant biomarkers in oils and rock extracts	[101]
Marine diesel fuel	[117]
Petroleum contaminated sediment	[98]
Sulfur compounds in diesel oils	[118]

In oil research, Fourier transform ion cyclotron resonance mass spectrometry (FT-ICR-MS) is also an important instrument, which has been commonly used to analyze polar crude oil fraction or whole oil [119, 120]. In FT-ICR, without chromatographic separation, the geochemical evaluation is conducted based on accurate mass data, which can be used to determine the chemical compositions of each mass peak observed [121, 122]. However, the isomers with the same chemical composition are not distinguished.

An interesting compound group present in all crude oils are biomarkers that originate from living organisms which populated the earth a long time ago. They reflect different kinds of initial organic input material, environmental and diagenesis conditions, maturation and biodegradation during the crude oil formation process [123, 124].

Crude oil contains many isomeric hydrocarbons and the examples of important studies where isomers have been separated by GC×GC are illustrated in Table 3. Many of these isomers share the same retention time in ¹D, and also share the same exact mass. These co-eluting isomers can be separated sometimes in ²D, for example C₂₄ tricyclic terpane and C₂₄ demethylated tricyclic terpane, and C₃₀R 25-norhomohopane

and C₃₀ hopane are separated [108]. In some cases isomeric compounds have an increase in retention time in both ¹D and ²D, for example the isomers of alkyl tetramantane [114]. The most important factors for isomer separation in GC×GC are the different properties of the stationary phase of the columns used.

Table 3 Examples of studies where isomers have been separated in petrochemical samples with GC×GC.

Isomers	GC×GC column	Ref
C ₁₉ –C ₂₄ tricyclic terpanes	*HP-5 and BPX-50	[112]
C ₂₇ –C ₂₉ steranes	*HP-5 and BPX-50	[112]
C ₃₁ –C ₃₅ hopane	*HP-5 and *BPX-50	[108, 112]
Oleanane	*HP-5 and *BPX-50	[124]
Alkyl tetramantanes	*HP-5 and *BPX-50	[114]
Branched alkanes	*HP-1 and BPX-1701	[98, 117]
Alkylcycloalkanes	*HP-5 and BPX-50	[125]
Dibenzothiophenes	*HP-5 and BPX-50	[113]
Triaromatic stereroids	*HP-5 and BPX-50	[113]
Alkylpyrenes	*HP-5 and BPX-50	[104]

* The column where separation of isomers occurred.

1.2 Aims of the study

The first part of the thesis discusses a negative mobility standard for IMS (Paper I), the separation of different ion structures with IMS (Paper II) and the factors affecting the separation of isomers in linear drift tube IMS (Papers I-III). The second part of the thesis discusses the geochemical assessment of Recôncavo Basin, Brazil (Paper IV) and new biomarkers detected with GC×GC-TOF-MS in Brazilian crude oils (Paper V).

The specific aims of the thesis were the following:

- Search for new negative IMS mobility standard by analysing sterically hindered phenols with negative APCI-IMS (Paper I)
- Separate different ion structures of pyridine and naphthol compounds with positive APPI-IMS (Paper II)
- The capability of IMS to separate isomers was studied with two phenolic (Paper I), two naphthol (Paper II) and eight amine (Paper III) isomers.
- During the analysis, new peaks were observed in the IMS spectra. MS was applied to the study of the identity of these peaks (Papers I-III)
- Distinguishing minor geological differences in the Recôncavo Basin (oil field), Brazil, with GC×GC-TOF-MS using β -carotane and other biomarkers (Paper IV)
- Geochemical evaluation of selected Brazilian crude oils with GC×GC-TOF-MS. Novel biomarkers were detected during the analysis and their tentative identification and geochemical significance were studied (Paper V).

2. EXPERIMENTAL

2.1 Chemicals

The solvents and gases used in the thesis are presented in Table 4, the analytes in Table 5 and analyte structures in Figures 5 and 6. All the analytes in the IMS experiments (Papers I-III) were first dissolved in solvents, according to Table 4, to achieve 5 mM stock solutions, which were further diluted to give 50 μ M, 100 μ M and 500 μ M working concentrations. The isomeric amines studied in Paper III (Figure 6) were diluted further with methanol:toluene (95:5%) to give 50 and 100 μ M solutions and following mixtures were prepared: Mix A (2,4,6-Col, *N,N*-DMA, *n*-M-*o*-T and 2-MBA), Mix B (PEA, 4-EA and 2,6-DtBPyr) and Mix C (2-, 3-, 4-MBA, and 2,6-DtBPyr).

Table 4. The solvents and gases used in this thesis.

Solvent / gas	Purity	Manufacturer	Paper
Acetonitrile		Lab-Scan, Dublin, Ireland	I
<i>n</i> -Hexane	>95%	Poch SA, Gliwice, Poland	I & II
<i>n</i> -Pentane	>99%	Fluka, Steinheim, Germany	II
Methanol	HPLC grade	Baker, Deventer, Holland	II
Toluene	HPLC grade	Lab-Scan, Dublin, Ireland	II
Toluene	HPLC grade	Baker, Deventer, Holland	III
Methanol	HPLC grade	Lab-scan, Dublin, Ireland	III
Dichloromethane, <i>n</i> -hexane and methanol	Chromatographic grade	Tedia, Rio de Janeiro, Brazil	IV & V
Nitrogen	NGLCMS20 nitrogen generator 99.5%	Labgas Instrument Co., Espoo, Finland	I-III
Bottled air (80% N ₂ , 20% O ₂)	4.0	AGA Ltd., Espoo, Finland	I

Table 5. The standards used in this thesis. All the standards were purchased from Sigma-Aldrich (Steinheim, Germany) unless otherwise stated.

Paper I	Abbreviation	Solvent / dopant	Purity (%)
2- <i>tert</i> -Butylphenol	2- <i>t</i> BPh	Hexane	>99
2,4-Di- <i>tert</i> -butylphenol	2,4-D <i>t</i> BPh	Hexane	>99
2,6-Di- <i>tert</i> -butyl-4-methylphenol	2,6-D <i>t</i> B-4-MPh	Hexane	>99
2,4,6-Tri- <i>tert</i> -butylphenol	2,4,6-T <i>t</i> BPh	Hexane	>98
2,4,6-Trinitrotoluene ^a	2,4,6-TNT	Acetonitrile	99
2,6-Di- <i>tert</i> -butylpyridine	2,6-D <i>t</i> BPyr	Hexane	>97
Paper II			
Pyridine ^b		Hexane and hexane:toluene (90:10%)	>99.5
1-Naphthol		Hexane and hexane:toluene (90:10%)	>97
2-Naphthol		Hexane and hexane:toluene (90:10%)	>97
2- <i>tert</i> -Butylpyridine	2- <i>t</i> BPyr	Hexane and hexane:toluene (90:10%)	>97
2,6-Di- <i>tert</i> -butylpyridine	2,6-D <i>t</i> BPyr	Hexane and hexane:toluene (90:10%)	>97
2,6-Di- <i>tert</i> -butyl-4-methylpyridine	2,6-D <i>t</i> B-4-MPyr	Hexane and hexane:toluene (90:10%)	>98
Paper III			
2,4,6-Collidine ^b	2,4,6-Col	Methanol:toluene (95:5%)	>99
<i>N,N</i> -Dimethylaniline	<i>N,N</i> -DMA	Methanol:toluene (95:5%)	>99.5
<i>N</i> -methyl- <i>o</i> -Toluidine	<i>n</i> -M- <i>o</i> -T	Methanol:toluene (95:5%)	>95
2-Phenethylamine	PEA	Methanol:toluene (95:5%)	>99
4-Ethylaniline	4-EA	Methanol:toluene (95:5%)	>98
2-Methylbenzylamine	2-MBA	Methanol:toluene (95:5%)	>96
4-Methylbenzylamine	4-MBA	Methanol:toluene (95:5%)	>97
3-Methylbenzylamine	3-MBA	Methanol:toluene (95:5%)	>98
2,6-Di- <i>tert</i> -butylpyridine	2,6-D <i>t</i> BPyr	Methanol:toluene (95:5%)	>97
Papers IV-V			
<i>n</i> -tetracosane-D ₅₀ ^c		Dichloromethane	>98%
pyrene-D ₁₀ ^c		Dichloromethane	

^a *Supelco* (Bellefonte, PA, USA), ^b *Merck* (Darmstadt, Germany) and ^c *Cambridge Isotope Laboratories*, Andover, MA, USA.

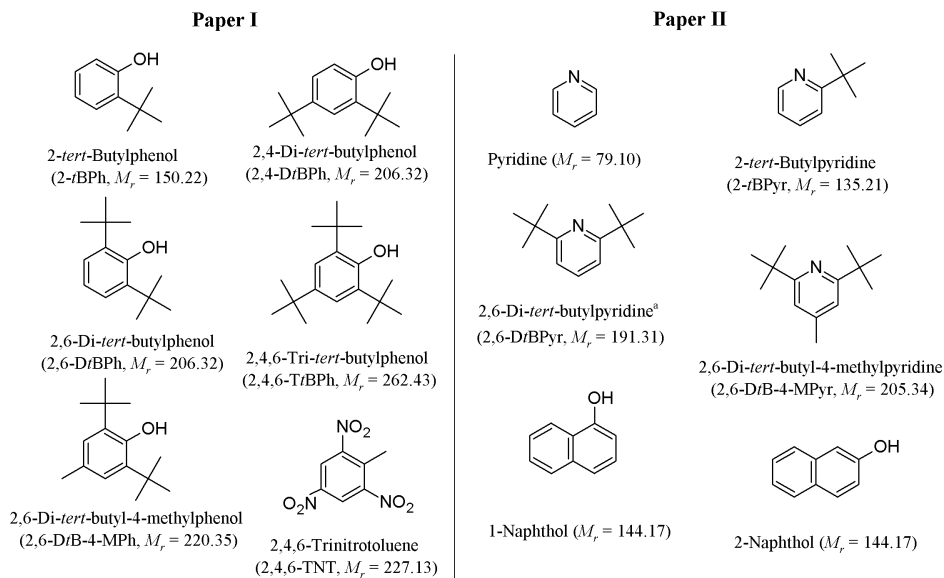


Figure 5. Compounds studied with IMS in Papers I and II. ^a = also studied in Papers I and III (modified from ref. [127]).

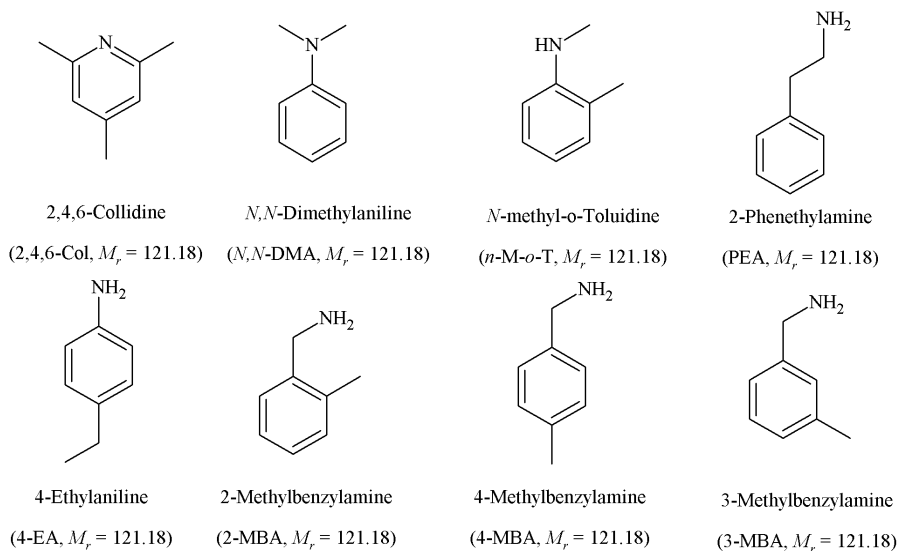


Figure 6. Isomeric amines studied with IMS in Paper III.

2.2 Oil fractioning (Papers IV-V)

The procedure for fractioning 20 crude oil samples in Paper IV was adopted from ref. [128]. Briefly, the LC fractionation was conducted by using a vertical glass column in atmospheric pressure to separate saturated, aromatic and polar fractions from crude oil. Approximately 100 mg of each oil sample was weighed with a calibrated analytical balance (± 0.1 mg) and dissolved in 500 μL of a dichloromethane solution with internal standard *n*-tetracosane- d_{50} at a concentration of 100 $\mu\text{g L}^{-1}$. This sample solution was placed on the top of a glass column (dimensions 13 \times 1 cm) packed with 3 g of Silica Gel 60 (particle size from 0.063 to 0.200 nm, Merck, Darmstadt, Germany), which was previously purified with hexane and activated in an oven at 120 $^{\circ}\text{C}$ for 12 hours. The samples were eluted into different fractions in the following order; saturated hydrocarbons with *n*-hexane (10 mL), aromatic hydrocarbons with *n*-hexane:dichloromethane (80:20%, 10 mL) and polar compounds with 10 mL of dichloromethane:methanol (90:10%, 10 mL). The fractions were collected in 50 mL flasks, and the solvent was evaporated by a rotary evaporator under reduced pressure. Each fraction was then transferred to a 2 mL vial (pre-weighed) using dichloromethane, which was subsequently evaporated under a nitrogen gas flow (from bottle), after which the vial was weighed again. In the Paper V the 11 crude oil samples crude oils, from the north to the south regions of Brazil, were pre-fractionated to saturated hydrocarbon and aromatic fractions by CENPES (Centro de Pesquisas e Desenvolvimento Leopoldo Américo Miguez de Mello, Rio de Janeiro, Brazil). They were also classified by CENPES using proprietary classifying methods (Table 1).

2.3 Separation of *n*-alkanes from branched and cyclic saturated hydrocarbons by urea adduct formation (Papers IV-V)

In order to separate *n*-alkanes from branched (B) and cyclic (C) saturated hydrocarbon in the saturated hydrocarbon fraction, urea adducts of *n*-alkanes were formed, as has previously been presented in references [128, 129]. The saturated hydrocarbon fraction was dissolved in 1000 μL of *n*-hexane and a 500 μL aliquot was transferred to a test tube of 18 \times 180 mm. 1 mL of acetone and 1 mL of *n*-hexane were added to the test tube, and the mixture was vortexed. To prepare a saturated solution of

urea, 30 g of urea was dissolved in 100 mL of methanol. The solution was stored in a refrigerator at 8 ° C. 1 mL of the saturated urea solution was added slowly to the test tube containing the saturated hydrocarbon fraction, and the immediate precipitation of urea crystals was observed. The test tube was heated in a water bath at 50 ° C to dissolve all the crystals and then cooled to room temperature for recrystallization of the urea. The crystallization was terminated in a freezer at -20 °C for 12 hours. After this, the solvent was evaporated under a nitrogen flow to obtain dried crystals, which were rinsed five times with 2 mL of *n*-hexane. The supernatant containing the B/C fraction, was transferred into a 30 mL balloon. The solvent was evaporated under reduced pressure and the urea crystals were dissolved in distilled water. To obtain the branched and cyclic hydrocarbon (B/C) fractions, liquid-liquid extraction of urea crystals was carried out with 2 mL of *n*-hexane. The organic layer was transferred to a 30 mL flask with a Pasteur pipette. This extraction step was repeated five times. The solvent was evaporated under reduced pressure and the B/C fraction was transferred to a previously weighed 2 mL vial and weighed again. The residue was dissolved in 500 μ L of dichloromethane.

2.4 Ion mobility spectrometry instrumentation (Papers I-III)

Measurements with IMS were conducted with a custom-made cylinder drift tube ion mobility spectrometry attached to a Sciex API300 triple quadrupole MS (Applied Biosystems-SCIEX, Concord, Ontario, Canada), which is referred to as IMS-MS (Figure 8), and with a similar drift tube attached to a faraday plate detector, which is referred to as IMS-FP. A more detailed description of these instruments can be found elsewhere; IMS-MS [44] and IMS-FP [29]. Briefly, both drift tubes have a similar design and the ion sources used in this study could be applied in both of the IMS instruments. The measurement parameters are summarized in Table 6.

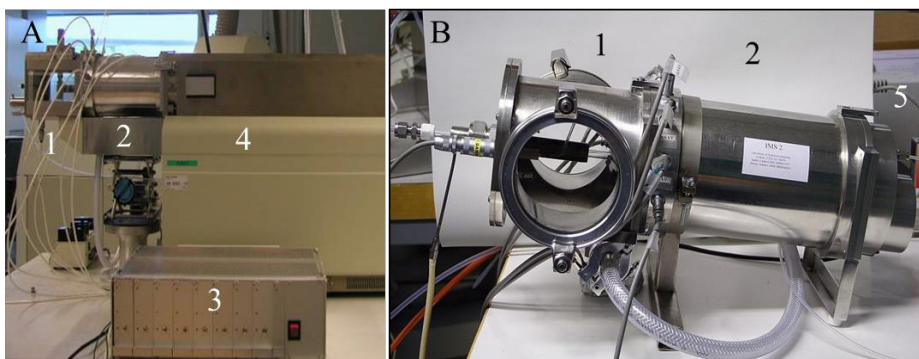


Figure 8. IMS connected to API300 MS (A) and to faraday plate detector (B): (1) ion source, (2) IMS drift tube, (3) control unit for IMS, (4) Sciex API300 triple quadrupole MS and (5) faraday plate (modified from ref [127]).

Table 6. Summary of IMS and MS parameters used in the study. The drift gas was nitrogen in all experiments, except in Paper III some of the experiments were carried out by using gas mixtures with varying proportions of nitrogen:argon and nitrogen:helium.

Parameter	(Paper I)	(Paper II)	(Paper III)
MS			
Declustering potential (V)	15-25	20-30	5
Focusing potential (V)	180-200	130-220	130
Entrance potential (V)	5		
IMS-MS			
Drift length (cm)	13.3		
Desolvation length (cm)	7.65		
Drift flow (L/min)	~2.4		
Gate opening time (μ s)	300		
Drift field (V/cm)	270-378	316-363	316
Desolvation field (V/cm)	230-260	272-303	304
Reflector plate in APPI experiments (kV)		0.8-1.6	1
Needle voltage ¹ (V)	1.3-1.5		
Needle voltage ² (V)	1.7-2.2		
IMS-FP			
Drift length (cm)	-	13.85	
Desolvation length (cm)	-	7.65	
Dirft flow (L/min)	-	2.1	1.9-2.5
Gate opening time (μ s)	-	100	200
Drift field (V/cm)	-	378	316
Desolvation field (V/cm)	-	378	316
Reflector plate in APPI experiments (kV)	-	2	
Needle volt. APCI (V)	-		2.0-2.2

¹ nebulizer gas was nitrogen, ² nebulizer gas was air (80:20 nitrogen:oxygen).

The IMS-MS instrument was operated either at full scan mode, typically a mass range of m/z 30-300 or 50-500, or with selected ion monitoring (SIM) mode. In the MS full scan mode, both B-N gates in the IMS were open, and in SIM mode the gates were pulsed to obtain a mobility window, which is described in more details [44]. The drift times of two ions were typically monitored simultaneously. The gates and voltage of IMS were controlled by a LabVIEW (National Instruments, Austin, US) based on a custom-made program, and the data was collected with Analyst 1.4.1 (Applied Biosystems/MDS SCIEX, Concord, ON, Canada). The data was further processed with Microsoft Excel 2002 (Microsoft Corporation, Redmond, WA, USA) applying Equation

(4) to calculate reduced mobilities. The IMS-FP instrument was operated with one B-N gate. A similar custom-made program as used in IMS-MS was also used to control the IMS-FP instrument and data processing to combine 2000 mobility spectra together. The data was further processed in ChemStation rev. 10.02 (Agilent Technologies, Inc., Palo Alto, CA, USA) with custom-written macros to calculate reduced mobility values.

A custom-made heated nebulizer was used to transfer the liquid sample to gas phase [29, 43, 130]. A syringe pump was used to deliver the liquid sample flow at a steady speed of typically 120-180 $\mu\text{L}/\text{h}$ to the nebulizer (nitrogen or air) gas flow.

The nitrogen gas for the nebulizer and drift gas was produced from compressed air and is described in Papers I and II. Additional measurements in Paper I were conducted using bottled air (80:20 % nitrogen:oxygen) as the nebulizer gas. Mainly, all the experiments were carried out nitrogen being the drift gas. Only some of the experiments in Paper III were carried out by using gas mixtures of nitrogen:argon and nitrogen:helium. All the measurements were conducted at ambient pressure, which was monitored with a pressure meter (Series 902; MKS Instrument, Andover, MA, USA).

2.5 Temperature of ion mobility drift tube (Paper I)

Most of the experiments were performed at room temperature, and when the drift tube was heated the temperature was calculated using 2,6-di-*tert*-butylpyridine as a thermometer compound. Briefly, since 2,6-DtBPyr is a sterically hindered and inert molecule, it has linear temperature dependence [12]. Taking into account that the mobility of a compound is proportional to temperature (Equation 4) when other parameters except T and t_d are constant, the Equation 4 can be reduced to Equation 5:

$$K \propto \left(\frac{273}{T} \right) \quad (5)$$

Where K is the mobility of 2,6-DtBPyr.

The mobility value of 2,6-di-*tert*-butylpyridine without temperature and pressure correction measured in our laboratory, $K_{2,6\text{-DtBPyr}} = 1.63 \text{ cm}^2/\text{Vs}$, at the room temperature (296 K). This was used as the calibration point for the calculations for the temperature range (296-335K) of the IMS drift tube.

2.6 Two-dimensional gas chromatography – time-of-flight mass spectrometry instrumentation (Papers IV-V)

The GC×GC-TOF-MS analyses were performed using the same instrumental setup as in the references [112, 131] using a Pegasus 4D (Leco, St. Joseph, MI, USA) GC×GC-TOF-MS, composed of an Agilent 6890 GC (Palo Alto, CA, USA) equipped with a secondary oven, a cryogenic modulator which uses liquid nitrogen for the cold jet and a Pegasus III (Leco, St. Joseph, MI, USA) TOF-MS (Figure 7). A DB-5 column (Agilent Technologies, Palo Alto, CA, USA), containing 5% phenyl–95% methylsiloxane (30 m, 0.25 mm i.d., 0.25 μm d_f) was used as the first dimension column (¹D). A BPX-50 column (SGE, Ringwood, VIC, Australia), containing 50% phenyl–50% methylsiloxane (1.5 m, 0.1 mm i.d., 0.1 μm d_f) was used as the second dimension column (²D). The ²D column was connected to the TOF-MS inlet by a 0.5 m x 0.25 mm i.d. uncoated deactivated fused silica capillary, SGE mini-unions and Siltite™ metal ferrules of 0.1–0.25 mm i.d. (Ringwood, VIC, Australia).

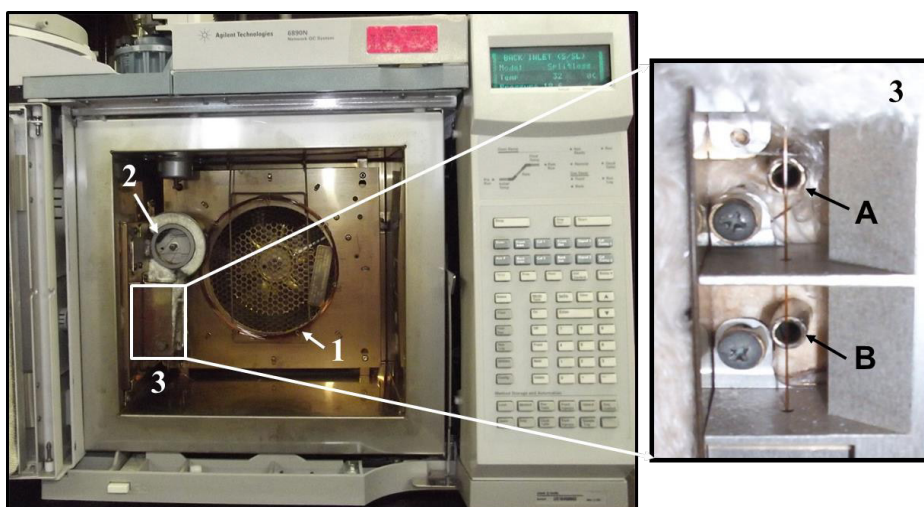


Figure 7. Modified GC oven: (1) ^1D GC column, (2) added ^2D oven and the ^2D GC column and (3) cryogenic modulator between the two columns (A and B are tubes for cold and hot jets); in the small figure (3) the cryogenic modulator is rotated 90° towards the door of the GC oven.

The GC conditions for the ^1D include: splitless injection of $1\ \mu\text{L}$ at $290\ ^\circ\text{C}$, purge time of 60 s, and purge flow of $5\ \text{mL}/\text{min}$. Helium was used as the carrier gas at a constant flow rate of $1.5\ \text{mL}/\text{min}$. The primary oven temperature program began at $70\ ^\circ\text{C}$ for 1 min, and was then increased to $170\ ^\circ\text{C}$ at $20\ ^\circ\text{C}/\text{min}$, and further to $325\ ^\circ\text{C}$ at $2\ ^\circ\text{C}/\text{min}$. The secondary oven temperature program was $10\ ^\circ\text{C}$ higher than the primary one. The modulation period was 8 s with a 2 s cold and hot pulses, and the cryogenic modulator temperature was set $30\ ^\circ\text{C}$ higher than the primary GC oven temperature program. The transfer line to the MS was set at $280\ ^\circ\text{C}$, the electron energy in electron ionization (EI) was 70 eV, the mass range was m/z 50–600 and the ion source temperature $230\ ^\circ\text{C}$. The detector was always set +50 V above the daily measured auto-tune value, and the acquisition rate was 100 spectra/s. Compound identification was performed by a comparison of mass spectra, retention time and elution order with data published in the literature.

2.8 Principle component analysis (Papers IV-V)

The software package Statistica 8 (Statsoft Inc.) was used in all statistical calculations in this work. Principal Component Analysis (PCA) was based on the covariance matrix. All variables were mean centered and scaled by the sample standard deviation. 42 geochemical parameters from 20 samples reported in Tables 10 and 11 (Paper IV) were used to create a matrix of the petroleum system in Recôncavo Basin. 42 parameters of maturity and source from 11 samples reported in Tables 12 and 13 (Paper V) were used to study correlations. Also these same 11 samples were evaluated by analysis of 101 normalized peak areas: area of compounds / area of internal standard (A_c/A_{is}).

3. RESULTS AND DISCUSSION

3.1 Behavior of sterically hindered phenols in IMS-MS (Paper I)

In Paper I, gas phase mobility properties of phenolic compounds with varying numbers of *tert*-butyl groups were studied with negative APCI-IMS-MS to determine their suitabilities as mobility standards (Figure 5). 2,4,6-trinitrotoluene was also included in this study as it has been used previously as a reference compound [18], and its behavior has been studied in more detail after our study [31]. The same set of phenolic compounds as used in this study has not been reported earlier in IMS literature.

The measured mass spectrometric data show that all the compounds produced deprotonated $[M-H]^-$ molecules. In the negative ion APCI mass spectra measured for 2-*t*BPh an oxygen insertion ion $[M-H+O]^-$ at m/z 165 was observed, in addition to the $[M-H]^-$ ion at m/z 149. When air was used as the nebulizer gas, instead of nitrogen, this oxygen insertion ion was observed more clearly. A similar observation was made for 2,4,6-TNT, since the oxygen adduct $[M+O]^-$ ion at m/z 243 was seen more clearly when the nebulizer gas was air. Table 7 illustrates other typical ions produced by 2,4,6-TNT: $[M-NO]^-$ at m/z 197, $[M-H]^-$ at m/z 226, M^- at m/z 227, and with a lower intensity $[M-OH]^-$ at m/z 210. All these 2,4,6-TNT ions observed are in line with ions reported in the literature [17, 31, 132]. In addition, ions at m/z 183 and 213 were observed sometimes in full scan MS spectra in the presence of the oxygen adduct ion. The formation of these ions could therefore be due to loss of one or two NO groups from the oxygen adduct

ion. However, in a recent article it was reported that the ion at m/z 213 is 1,3,5-trinitrobenzenanion, which is produced in the degradation of 2,4,6-TNT by ozone in an APCI ion source [133]. With the current data, it is not possible to conclude which explanation is correct.

The absolute reduced mobilities of selected identified analyte ions, at room temperature, are summarized in Table 7. Analytes produced more than one mobility peak due to dimerization or adduct formation. The variations in mobility values were typically <2%. The reduced mobility value of 2,4,6-TNT ion $[M-H]^-$ is within 2% agreement with values presented at the literature [31].

Table 7. Summary of reduced mobilities K_0 (cm^2/Vs) measured with negative APCI-IMS-MS with nitrogen as the nebulizer gas. The standard compounds were dissolved in hexane, unless otherwise stated. The numbers represent the peak numbers in the order they appear in the mass-selected mobility spectra. The structures of the standard compounds are presented in Figure 5 (adapted from Paper I).

Compound	Mass (u)	Ion formula	Measured ion, m/z	1st (K_0)	2nd (K_0)	3rd (K_0)	4th (K_0)
2- <i>t</i> BPh	150	$[M-H+O]^-$	165 ^a	1.63	1.13 ^b		
		$[M-H]^-$	149	1.63	1.53	1.14 ^b	
2,4- <i>Dt</i> BPh	206	$[M-H]^-$	205	1.34	1.29		
2,6- <i>Dt</i> BPh	206	$[M-H]^-$	205	1.43	1.37		
2,6- <i>Dt</i> B-4-MPh	220	$[M-H]^-$	219	1.36	1.29		
2,4,6- <i>Tt</i> BPh	262	$[M-H]^-$	261	1.23	1.18		
2,4,6-TNT	227	$[M+O]^-$	243 ^{a,c}	1.53			
		M^-	227 ^c	1.58 ^d	1.53	1.35	
		$[M-H]^-$	226 ^c	1.58	1.48	1.36	
		$[M-OH]^-$	210 ^c	1.53			
		$[M-NO]^-$	197 ^c	1.64	1.53	1.42	1.36

^a nebulizer gas was air; ^b dimer; ^c solvent ACN; ^d most likely the ¹³C isotope peak of the ion at m/z 226

The compounds 2,6-*Dt*BPh (Figure 9A), 2,6-*Dt*BP-4-MPh and 2,4,6-*Tt*BPh showed similar mobility peak patterns with two relatively large mobility peaks (Table 7). One requirement for the IMS instrumental standard is that the mobility value is independent of the IMS drift field. Therefore in our study, the variation in drift field (270-344 V/cm) was also tested for these three phenolic compounds. It was observed that all the reduced mobility values remained the same within the experimental error. However, the temperature variation (296-335 K) study done for 2,6-*Dt*BP-4-MPh and 2,4,6-*Tt*BPh showed that the intensity of the peak with a higher mobility value (1st peak in Table 7)

increased when the temperature increased. This is an indication that at least the lower mobility peak (2nd peak in Table 7) is an adduct ion, for example an adduct with O₂ or NO_x. However, no adducts were observed in the measured mass spectra. This is likely as they dissociate in the MS interface.

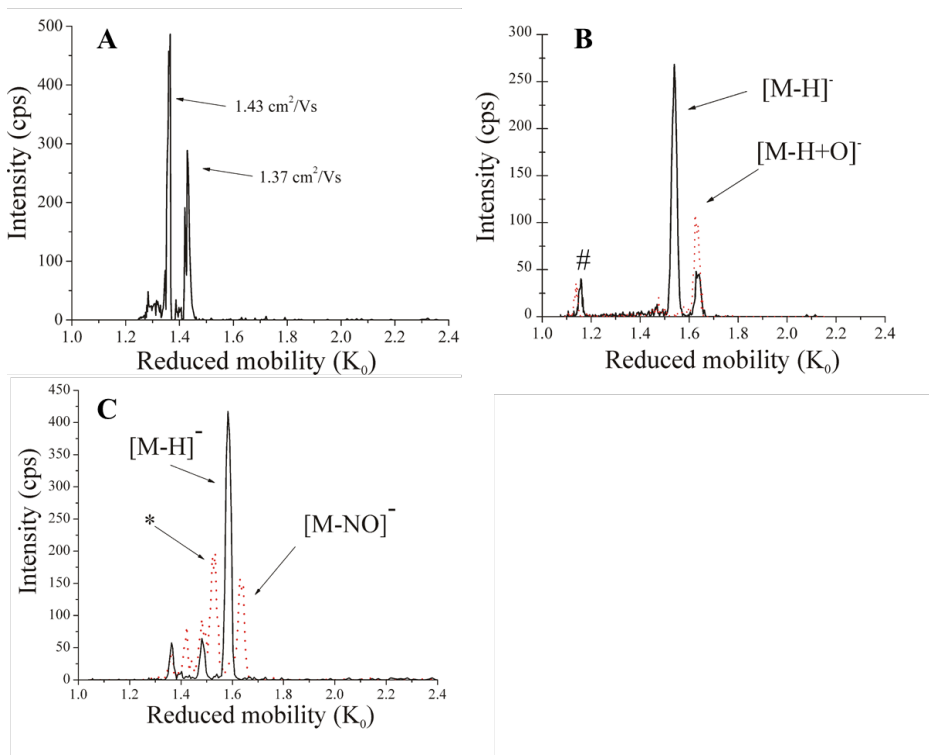


Figure 9. Negative APCI-IMS-MS mass-selected ion mobility spectrum of (A) [M-H]⁻ ion of 2,6-DtBPh at m/z 205, (B) [M-H]⁻ and [M-H+O]⁻ ions of 2-*t*BPh at m/z 149 (solid line) and m/z 165 (dotted line), respectively, (C) [M-H]⁻ and [M-NO]⁻ ions of 2,4,6-TNT at m/z 197 (2nd peak is marked with asterisk, dotted line) and m/z 226 (solid line), respectively. The measurements were carried out in room temperature (296 K) using nitrogen as the drift and nebulizer gases (A, C) and using nitrogen as the drift gas and air as the nebulizer gas (B). # most likely the analyte dimer.

The mass selected mobility spectra of the [M-H]⁻ ion of 2-*t*BPh typically showed three peaks; one (2nd, Table 7, Figure 9B) peak due to the deprotonated molecule at m/z 149, another peak (1st, Table 7, Figure 9B) due to the oxygen insertion ion [M-H+O]⁻ at m/z 165 and the third one (3rd, Figure 9B, marked with #) most likely due to the analyte dimer. In tandem mass spectrometric measurements the oxygen insertion ion at m/z 165 produced an ion at m/z 149 as a product ion (results not shown). Interestingly, the

oxygen insertion ion had a higher mobility than the lighter $[M-H]^-$ ion. This could be due to the fact that the $[M-H]^-$ ion exists initially as an adduct (e.g. O_2 or NO_x), which subsequently breaks down into the $[M-H]^-$ ion in the MS interface. An alternative explanation is that by the oxygen insertion a $-OH$ group is formed in the *ortho*-position of the oxygen atom allowing for the formation of an internal hydrogen bond. Due to this, the internal hydrogen bond is shielding the charge, resulting in a decreased interaction of the $[M-H+O]^-$ ion with the drift gas compared to the $[M-H]^-$ ion.

The two isomeric compounds, 2,4- and 2,6-DtBPh, both had two mobility peaks in the mass-selected ion mobility spectrum of the $[M-H]^-$ ion at m/z 205. As can be seen from Table 7, there is a clear difference, of about 0.1 units, in the reduced mobility values of both peaks when the mobility values of these two isomers are compared. This could be because, in the case of the ionized 2,4-DtBPh, the charge is exposed more to interactions with the drift gas than in the case of 2,6-DtBPh, which has two *tert*-butyl groups shadowing the ionization site (Figure 5). It was later observed that 2,4-DtBPh also formed a small quantity of dioxygen adduct $[M+O_2]^-$ ions at m/z 238, which had the same reduced mobility ($K_0 = 1.29 \text{ cm}^2/\text{Vs}$) as the second mobility peak of $[M-H]^-$ ion [134]. This indicates that the dioxygen adduct $[M+O_2]^-$ is initially present in the ionization chamber and is broken down after the IMS analysis to form an $[M-H]^-$ ion.

2,4,6-TNT produced several mass-selected mobility peaks (Table 7). The $[M-H]^-$ ion at m/z 226 showed three mobility peaks, of which the 1st peak ($K_0 = 1.58 \text{ cm}^2/\text{Vs}$) had the highest intensity (Figure 9C). The $[M-NO]^-$ ion at m/z 197 produced four mobility peaks, of which the 1st and the 2nd ($K_0 = 1.64 \text{ cm}^2/\text{Vs}$ and $K_0 = 1.53 \text{ cm}^2/\text{Vs}$, respectively) were the most intense. Interestingly, the 2nd mobility peak of $[M-NO]^-$ ion (marked with an asterisk in Figure 9C) shared the same mobility with $[M-OH]^-$ at m/z 210, M^- at m/z 227 and $[M+O]^-$ at m/z 243. This could be because in the drift tube the precursor ion $[M+O]^-$ moves across the drift region, forming the rest of the ions (m/z 197, m/z 210 and m/z 227) at the MS interface after the IMS separation. Note, that even though the mass difference of the $[M-H]^-$ and the M^- ions at m/z 226 and m/z 227, respectively, is only one mass unit, the mobility difference ($K_0 = 1.58 \text{ cm}^2/\text{Vs}$ and $K_0 = 1.53 \text{ cm}^2/\text{Vs}$, respectively) is relatively large. This supports the interpretation that the M^- ion originates from the oxygen adduct ion $[M+O]^-$. Also the mass difference between $[M-H]^-$ and $[M+O]^-$ ions is large enough to explain the mobility difference.

In summary, two isomeric phenols, 2,4-DtBPh and 2,6-DtBPh, could be separated with IMS-MS. Three of the phenols, namely 2,6-DtBPh, 2,6-DtB-4-MPh and 2,4,6-TtBPh, produced typically two mobility peaks in the mass-selected mobility spectra measured for the $[M-H]^-$ ion. These three phenolic compounds behaved similarly under different measuring conditions and they could be used as instrumental standards alongside with 2,4,6-TNT. Further characterization is still required for example at higher drift tube temperatures.

3.2 Separation of different ion structures with IMS (Paper II)

The aim of the study in Paper II was to investigate the capacity of IMS to separate different ion structures of pyridine and naphthol compounds (Figure 5) in the gas phase. The ionization conditions in APPI were selected so that different ion structures, radical cation M^+ and protonated molecule $[M+H]^+$ ions, could be created for the same molecule. The MS literature has examples of how APPI can be used to produce different ion forms by altering the solvent and / or the dopant [36, 135, 136].

When the analytes (Figure 5) were dissolved in hexane, APPI produced mainly protonated molecules $[M+H]^+$ at m/z 145, 145, 192 and 206 for 1- and 2-naphthol, 2,6-DtBPyr and 2,6-Dt-4-BPyr, respectively. However, when the analytes were dissolved into hexane:toluene (90:10%) they also produced radical cations M^+ (m/z 144, 144, 191 and 205). In the case of 2,6-DtBPyr and 2,6-Dt-4-BPyr, the M^+ ions were observed together with unexpected dioxygen adducts $[M+O_2]^+$ at m/z 223 and m/z 237, respectively. Product ion mass spectra for the M^+ and $[M+O_2]^+$ ions of 2,6-DtBPyr and 2,6-DtB-4-MPyr produced similar fragment ions, expect that for the $[M+O_2]^+$ ion the first fragmentation step was the loss of O_2 . For pyridine and 2-tBPyr, both solvents efficiently produced only protonated molecules at m/z 80 and 136, respectively. In addition to the $[M+H]^+$ ion, pyridine produced also a $[M+91]^+$ ion at m/z 170, when hexane:toluene (90:10%) was used as the solvent. Further tandem MS inspections of the $[M+91]^+$ ions structure indicated that it could be a benzyl cation adduct of pyridine.

In the next step, the absolute reduced mobilities of most of the identified analyte ions were recorded (Table 8). The mobility values for the analyte ions, obtained with hexane and hexane:toluene (90:10%) solvents, were the same. The repeatability of the mobility measurements was evaluated by measuring the mass-selected reduced mobility values

for the $[M+H]^+$ ion of 2,6-DtBPyr in hexane, because it has been previously used as a mobility standard [12]. The relative standard deviation for 2,6-DtBPyr was 0.7% ($n = 13$, $K_0 = 1.49 \text{ cm}^2/\text{Vs}$).

Pyridine produced two main (1st and 2nd, Table 8) mobility peaks for the $[M+H]^+$ ion with $K_0 = 2.04$ (monomer) and $1.69 \text{ cm}^2/\text{Vs}$ (dimer), when hexane was used as the solvent. Interestingly, the use of hexane:toluene (90:10%) as the solvent produced an additional 3rd peak at $K_0 = 1.63 \text{ cm}^2/\text{Vs}$ at m/z 80 with nearly the same mobility ($1.64 \text{ cm}^2/\text{Vs}$) as for the $[M+91]^+$ ion at m/z 170. This is in line with the earlier tandem MS findings, suggesting that the m/z 170 ion is a benzyl cation adduct which is formed in the desolvation or ionization region of the IMS. 2-tBPyr produced a single mobility peak ($K_0 = 1.73 \text{ cm}^2/\text{Vs}$) for the $[M+H]^+$ with both hexane and hexane:toluene (90:10%) solvents.

Table 8. Summary of the reduced mobilities K_0 (cm^2/Vs) measured with positive APPI-IMS-MS. The standard compounds were dissolved in hexane or hexane:toluene (90:10%) and the values shown are based on measurements with both solvents. The numbers represent the peak numbers in decreasing mobility order. The structures of the standard compounds are presented in Figure 5 (adapted from Paper II).

Compound	Mass (u)	Ion formula	Measured ion, m/z	1st (K_0)	2nd (K_0)	3rd (K_0)
Pyridine	79	$[M+H]^+$	80	2.04	1.69 ^a	1.63 ^b
		$[M+91]^+$	170 ^b	1.64		
2-tBPyr	135	$[M+H]^+$	136	1.73		
2,6-DtBPyr	191	M^{++}	191 ^b	1.45		
		$[M+H]^+$	192	1.50	1.45 ^{b,c}	
		$[M+O_2]^{++}$	223 ^b	1.45		
2,6-DtB-4-MPyr	205	M^{++}	205 ^b	1.38		
		$[M+H]^+$	206	1.42	1.38 ^{b,c}	
		$[M+O_2]^{++}$	237 ^b	1.39		
1-Naphthol	144	M^{++}	144	1.72		
		$[M+H]^+$	145	1.68	1.50 ^d	1.32 ^d
		$[M+H+10]^+$	155	1.68		
2-Naphthol	144	M^{++}	144	1.73		
		$[M+H]^+$	145	1.67	1.50 ^d	1.32 ^d
		$[M+H+10]^+$	155	1.67		

^a dimer, ^b peaks observed clearly only in hexane:toluene (90:10%), ^c most likely ¹³C isotope peak of the m/z 191 or 205 ions, and ^d minor peaks which are observed sporadically.

2,6-DtBPyr and 2,6-DtB-4-MPyr behaved similarly in the IMS analysis, and the 1st mobility peaks of their protonated molecules had higher mobilities ($K_0 = 1.50$ and 1.42 cm^2/Vs , respectively) than the peaks of their radical cations ($K_0 = 1.45$ and 1.38 cm^2/Vs , respectively, Figure 10A). Their dioxygen adducts $[\text{M}+\text{O}_2]^+$ had the same mobilities as the radical cations ($K_0 = 1.45$ and 1.39 cm^2/Vs , within experimental error, Figure 10B). The mass difference for the protonated molecules and the dioxygen adducts could explain the mobility difference.

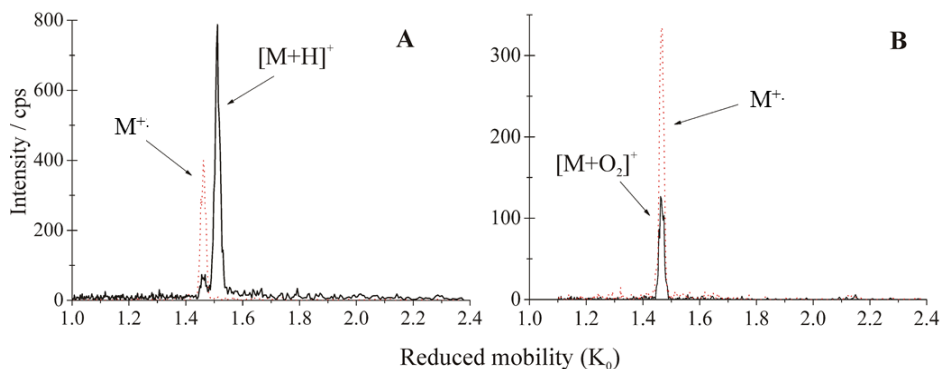


Figure 10. Positive ion APPI mass-selected mobility spectra of 2,6-DtBPyr dissolved in hexane:toluene (90:10%). (A) M^+ at m/z 191 (dotted line) and $[\text{M}+\text{H}]^+$ at m/z 192 (solid line). (B) M^+ (dotted line) and $[\text{M}+\text{O}_2]^+$ (solid line) at m/z 191 and m/z 223, respectively, shared the same mobility [127].

Interestingly, the radical cations of 1- and 2-naphthol at m/z 144 had higher mobilities ($K_0 = 1.72$ and 1.73 cm^2/Vs) than their protonated molecules at m/z 145 ($K_0 = 1.68$ and 1.68 cm^2/Vs , Table 8). However, in the case of 2,6-DtBPyr and 2,6-DtB-4-MPyr the M^+ had lower mobilities due to the formation of dioxygen adducts. This is because the $[\text{M}+\text{H}]^+$ ions of 1- and 2-naphthol interact more with the residual water in the drift gas than the M^+ , as similarly reported for anilines [74]. Additional support for our results is given by Fernández-maestre *et al.* who showed that the reduced mobility of $[\text{M}+\text{H}]^+$ ion of 2,6-DtBPyr is independent of the water concentration in the drift gas [15].

Additional mobility measurements were done for 2,6-DtBPyr with an APPI-IMS-FP instrument. These measurements showed the same mobility peaks for 2,6-DtBPyr as in the IMS-MS measurement, as well as an reaction ion peak (RIP). Typically, a FP detector measures all the ions, and therefore also a RIP is seen. With IMS-MS, the mobilities are measured only for selected analyte ions, and therefore a RIP is not seen.

A RIP is not necessarily observed with IMS-FP instruments either, for example Borsdorf *et al.* [70, 74] does not report a RIP in his APPI-IMS studies. This could be due to different sample introduction methods and ionization conditions. Borsdorf *et al.* introduced the analytes directly into the gas phase by heating the pure analytes without dissolving them in solvents. However, in our studies the analytes were introduced to the ionization chamber along with the solvent and / or dopant.

To summarise, depending on the ionization conditions, 2,6-D*t*BPyr and 2,6-D*t*B-4-MPyr efficiently produced both radical cations M^+ and protonated $[M+H]^+$ molecules. The radical cations M^+ had longer drift times. Further analysis revealed the presence of dioxygen adduct ions $[M+O_2]^+$, which also had the same mobility as the radical cations M^+ . Since 2-*t*BPyr does not produce the dioxygen adduct, its formation is likely to be dependent on the presence of two *tert*-butyl groups on both sides of the nitrogen “locking” the dioxygen in the middle. In cases of 1- and 2-naphthols, the radical cations M^+ had higher mobilities than the protonated molecules $[M+H]^+$, which is opposite to 2,6-D*t*BPyr and 2,6-D*t*B-4-MPyr. The $[M+O_2]^+$ formation of the M^+ ions of 2,6-D*t*BPyr and 2,6-D*t*B-4-MPyr increases the mass, and therefore both M^+ and $[M+O_2]^+$ ions have lower mobilities than the $[M+H]^+$ ions.

3.3 Separation of isomeric amines with IMS-FP (Paper III)

The aim of this study was to investigate how structural differences in isomeric compounds can affect their separation in IMS. Eight model isomeric amine standard compounds ($M_r=121$, $C_8H_{11}N$, Figure 6 and Table 9) were studied using positive APCI- and APPI-IMS-FP instrument. Literature reports mobility values for some of the amines used in our study, namely 4-ethylaniline [75], *N,N*-dimethylaniline [137, 138] and 2,4,6-collidine [138-140], but the same set of isomeric amines measured in our study was not included to the previous studies.

Mass spectrometric measurements showed that with APCI and APPI ionization techniques protonated molecules $[M+H]^+$ at m/z 122 were formed for all the amines. 2,6-D*t*BPyr was used as an instrumental standard and its $[M+H]^+$ ion was observed at m/z 192. Reduced mobilities of the analytes measured with IMS-FP and some literature values are presented in Table 9. The reproducibility of mobility experiments was

evaluated using a mobility value for the 2,6-DtBPyr measured with APCI ($n = 8$, on two different days, $K_0 = 1.47 \text{ cm}^2/\text{Vs}$), which had a standard deviation of 0.3%.

Reduced mobility measured with APCI and APPI for 2,4,6-Col is well in line with values reported in the literature (1.82 [138, 139] and 1.84 cm^2/Vs [140]). The mobility differences of *N,N*-DMA between our experiments and the values reported in the literature (Table 9) could be explained by a different drift tube design, different ionization conditions, or a higher drift tube temperature (323-473 K) than that used in our experiments (296 K). Karpas et al. [137, 138] used a ^{63}Ni β ion source to produce $[\text{M}+\text{H}]^+$ ions, and they reported two different mobility peaks for *N,N*-DMA. They were suspected to be due to different protonation sites in the molecule, i.e., the proton could be attached to the N atom or to the ring [137]. In our experiments, we observed only one mobility peak for all the amines. In the case of 4-EA one obvious explanation for the difference in the reported mobility values is the ion measured, i.e. radical cation by Borsdorf et al. [75] and protonated molecule in our study.

Some amines had distinctly different mobility values, while others shared nearly the same mobilities (Table 9). The compound class had an important role in mobility values. For instance, compounds with a *N*-heterocyclic aromatic ring (2,4,6-Col, 1.81 cm^2/Vs), tertiary (*N,N*-DMA, 1.75 cm^2/Vs) or secondary amines (*N*-M-*o*-T, 1.70 cm^2/Vs) had the highest mobility values and were separated clearly. The rest of the compounds were primary amines, which had lower mobilities (Table 9, Figure 11). It is suggested that the protonated $-\text{NH}_2$ group ($-\text{NH}_3^+$) interacts more with the drift gas, and therefore the primary amines had lower mobilities, whereas in tertiary and secondary amines the protonated group is more protected from interactions with the drift gas. This is a similar “shielding” effect, where two *tert*-butyl groups of 2,6-DtBPyr are protecting the charge in both sides of the protonated nitrogen [12, 15]. Interestingly, PEA and 4-EA were separated ($K_0 = 1.62$ and 1.58 cm^2/Vs , respectively), which could be because the protonated PEA forms a “loop” via $-\text{NH}_3^+$ interaction with the benzene ring. Therefore, it has a “closed” shape and is likely to interact less with the drift gas than the protonated 4-EA. The side chain of 4-EA is too short to form a “loop” leaving it with the “open” shape. In the IMS literature, protonated diamines and polyamines have been reported to form also a “loop” [141].

Table 9. Summary of the reduced mobility K_0 (cm^2/Vs) values for the isomeric amines ($M_r = 121$) and 2,6-di-*tert*-butylpyridine ($M_r = 191$) measured with an IMS-FP instrument using nitrogen as the drift gas. The mobility values have not been normalized with the mobility of 2,6-DtBPyr. The structures of the standard compounds are presented in Figure 6 (adapted from Paper III).

Compound	Abbreviation	APCI [M+H] ⁺ K_0 (cm^2/Vs)	APPI [M+H] ⁺ K_0 (cm^2/Vs)	Literature values K_0 (cm^2/Vs)
2,4,6-Collidine ^a	2,4,6-Col	1.81	1.80	1.82 [138, 139], 1.84 [140], [M+H] ⁺
<i>N,N</i> -Dimethylaniline ^a	<i>N,N</i> -DMA	1.75	1.75	1.87 [137], 1.81 [137, 138], [M+H] ⁺
<i>N</i> -methyl- <i>o</i> -Toluidine ^a	<i>n</i> -M- <i>o</i> -T	1.70	1.69	
2-Phenethylamine ^b	PEA	1.62	1.62	
4-Ethylaniline ^b	4-EA	1.58	1.58	1.77 [75], M ⁺
2-Methylbenzylamine ^c	2-MBA	1.61	1.61	
4-Methylbenzylamine ^c	4-MBA	1.60	1.57	
3-Methylbenzylamine ^c	3-MBA	1.60	1.58	
2,6-di- <i>tert</i> -butylpyridine ^d	2,6-DtBPyr	1.47		

^a Measured from Mix A; ^b Measured from Mix B; ^c Measured individually; ^d Measured from Mix B and Mix C.

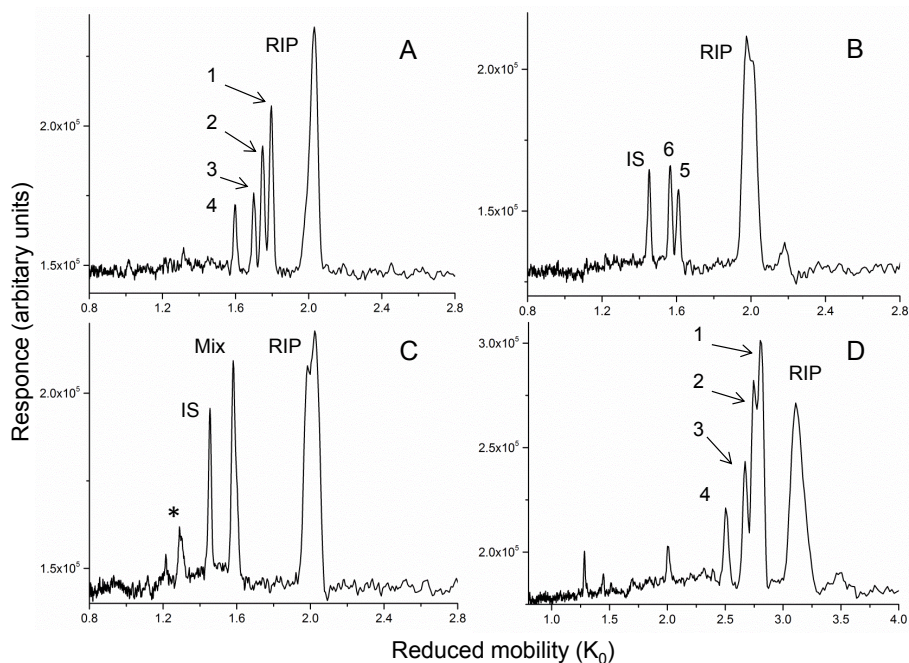


Figure 11. Positive APCI ion mobility spectra of mixtures of isomeric amines measured with IMS-Faraday plate detector (A, D) 1 = 2,4,6-Col, 2 = *N,N*-DMA, 3 = *n*-M-*o*-T and 4 = 2-MBA, (B) 5 = PEA and 6 = 4-EA, and (C) Mix = 2-, 3-, and 4-MBA. In (A, C) the drift gas was nitrogen and in (D) 33% helium and 67% nitrogen. RIP = reaction ion peak, IS = 2,6-DfBPy and the asterisk (*) indicates possible amine cluster ions.

The most common drift gases are air and nitrogen. The change of the drift gas physical properties could result in better separation of the analytes that share the same mobility with nitrogen as the drift gas [142]. For example, chloroaniline and iodoaniline are not separated when nitrogen is used as drift gas, but when helium is used as drift gas they are clearly separated [142]. Therefore, in our experiments the drift gas was modified by mixing argon or helium to the nitrogen nitrogen in order to study if enhanced separation is obtained. The presence of heavier argon molecules shifted the mobilities of all the amines towards lower values, while in the presence of lighter helium molecules the mobility shifted towards higher values (Figure 12). Similar trends have been reported in the literature, where the mobility of compounds increased when helium was used as the drift gas instead of nitrogen, and decreased when argon was

used [138, 142]. However, the change of drift gas did not result in better separation of the unresolved compounds.

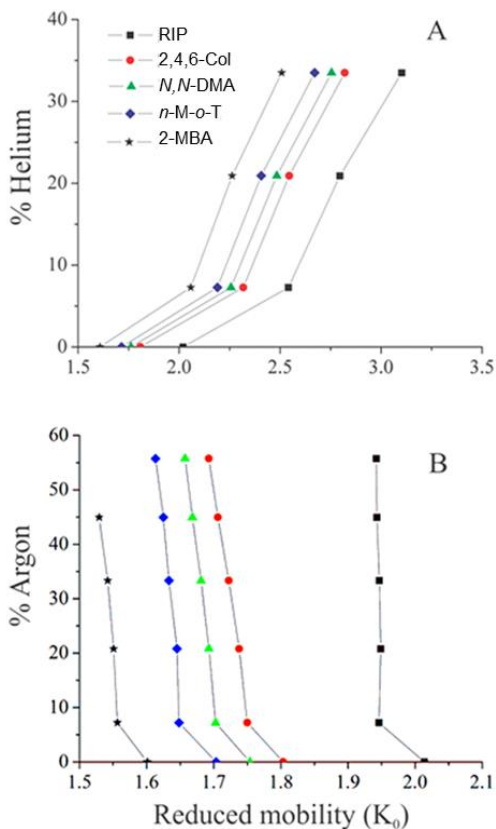


Figure 12. Reduced mobility values of isomeric amines measured with positive APCI-IMS-FP. The drift gas was nitrogen mixed with helium (A) or argon (B) (adapted from Paper III).

As a summary, the isomeric amines formed protonated molecules $[M+H]^+$ with both ionization techniques: APCI and APPI. 2,4,6-Col, *N,N*-DMA and *n*-*M-o*-T were separated clearly from each other with IMS, while the rest of the amines had mobility values very close to each other. However, PEA and 4-EA were separated. The major explanation for the different reduced mobilities is different shielding of the protonated nitrogen by the adjacent functional groups. In other words, the more protected the charge is e.g. *N*-heterocyclic aromatic ring (2,4,6-Col) vs. primary amines, the less the

ionized analyte can interact with the drift gas, and therefore it can move faster through the drift tube.

3.4 Geochemistry of Recôncavo Basin, Brazil, oils (Paper IV)

Most of the crude oil samples from the Recôncavo Basin, Brazil, share similar biological source material and thermal maturation levels, therefore it is not easy to differentiate between them by using conventional analyzing techniques such as GC-MS. In Paper IV the differentiation of 20 oil samples from the Recôncavo Basin was made with GC×GC-TOF-MS.

The Recôncavo Basin with an area of approx. 11500 km² is located in Bahia, northeastern Brazil and it has started to form in the late Jurassic-early Cretaceous period [143]. Petroleum exploration of this basin, which is now in a mature stage, dates back to the 1930's. Lacustrine shales are considered to be the predominant source rock units of the basin and the main reservoirs are pre-rift sandstones [144, 145].

All the samples were measured using the GC×GC-TOF-MS instrument and the peak areas of geochemically interesting compounds were calculated from the measurement data. In addition to traditionally used geochemically interesting compounds (Paper IV), some non-conventional biomarkers were included in this study. The most significant variations in concentration between the oil samples were observed in geochemical compounds namely, β -carotane; 20S + 20R C₂₇ 5 α ,14 α ,17 α -cholestanes; C₃₀ 17 α -diahopane; gammacerane; C₃₁ 17 α (H),21 β (H)-homohopane; C₃₀ 17 α (H),21 β (H)-hopane; C₃₁ 3 β -methylhopane; 8 α (H), 14 α (H)-onocerane; 8 α (H), 14 β (H)-onocerane; C₂₄ tetracyclic terpane; and C₂₆ tricyclic terpane. In total 52 geochemically interesting compounds were identified (excluding diamondoids). The peak areas of these compounds were used to calculate peak area ratios, which are typically called geochemical parameters. These parameters and their significance have been described by Peters et al. [123]. For example, in Paper IV the geochemical parameters provided information about different geochemical conditions, such as variations in biological source input material (Table 1 and 2, Paper IV) and the thermal stress conditions (Table 3 and 4, Paper IV). Biodegradation of crude oil by bacteria can also alter the geochemical parameters. This information can be used in oil exploration to distinguish between different oil samples.

Based on the plots presenting geochemical ratios of β -carotane or gammacerane / C_{30} $17\alpha(H),21\beta(H)$ -hopane (β -car / H_{30} , Figure 13; Gam/ H_{30} , Figure 14) as a function of C_{30} $17\alpha(H),21\beta(H)$ -hopane / $20S + 20R$ C_{27} $5\alpha,14\alpha,17\alpha$ -cholestanes (H_{30}/St) ratio, it was observed that the samples with high ratios of β -car/ H_{30} and Gam/ H_{30} were mainly located in the central area of the basin. The presence of an elevated concentration of β -carotane is associated with saline lacustrine paleoenvironments and the elevation in the concentration of gammacerane is commonly related to hypersalinity, highly specific for water-column stratification [123]. Our results (Figures 13 and 14) reveal that the salinity was not constant through time or throughout the whole ancient lake in the Recôncavo Basin.

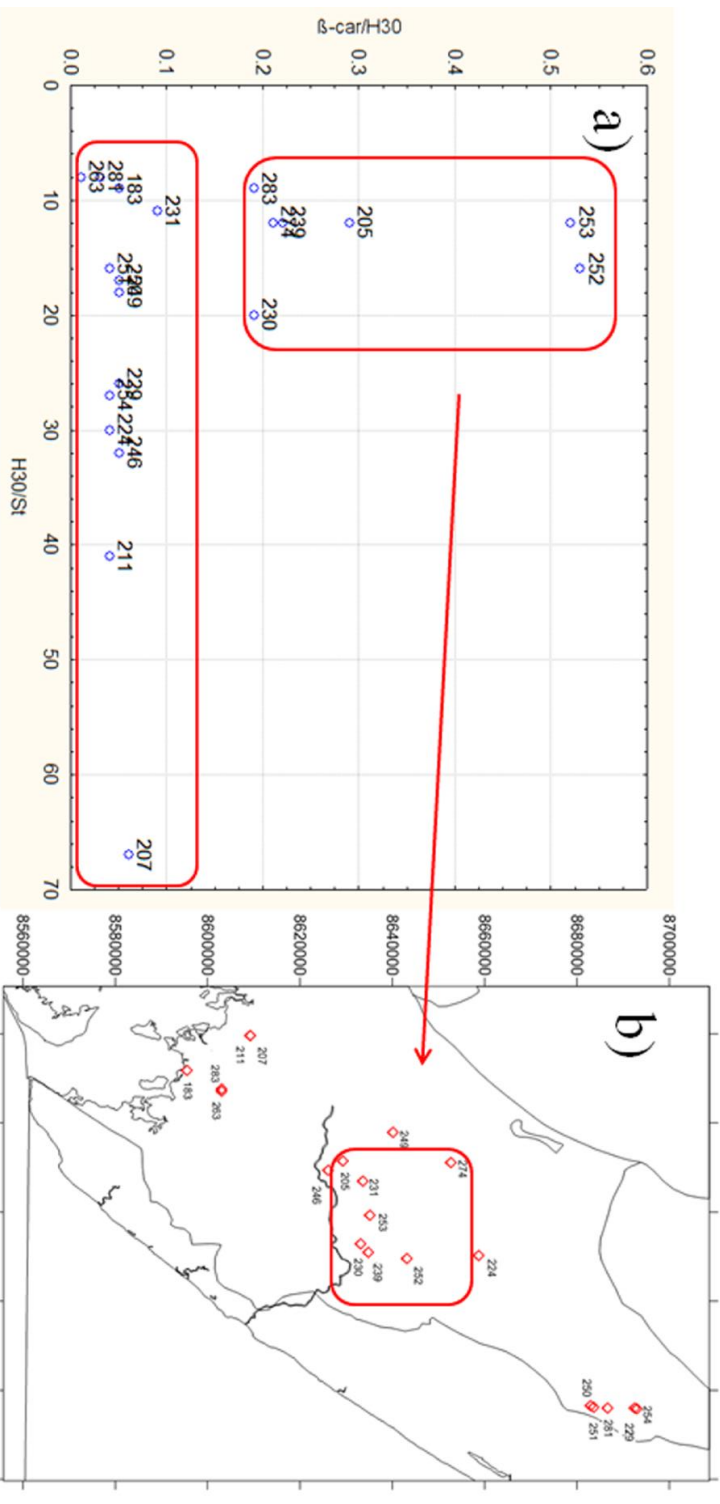


Figure 13. (A) β -carotene / $C_{30} 17\alpha(H), 21\beta(H)$ -hopane (β -car/ H_{30}) ratio vs. $C_{30} 17\alpha(H), 21\beta(H)$ -hopane / $20S + 20R C_{27} 5\alpha, 14\alpha, 17\alpha$ -cholestanes (H_{30}/St) graph, and (B) Recôncavo Basin map with samples from the central region highlighted. A larger map of the Recôncavo Basin is presented in Figure 1, Paper IV (adapted from Paper IV).

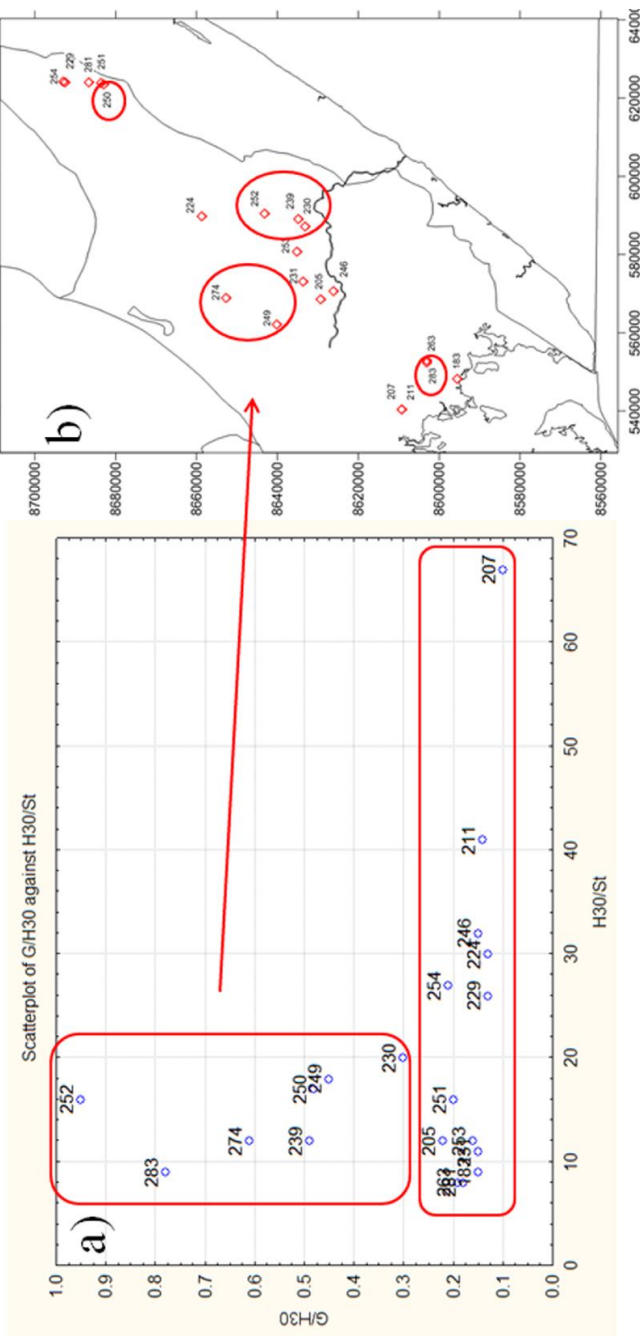


Figure 14. (A) Gammacerane / C₃₀ 17 α (H),21 β (H)-hopane (G/H₃₀) ratio vs. C₃₀ 17 α (H),21 β (H)-hopane / 20S + 20R C₂₇ 5 α ,14 α ,17 α -cholestanes (H₃₀/St) graph and (B) Recôncavo Basin map with samples from the central region highlighted. A large map of the Recôncavo Basin is presented in Figure 1, Paper IV (adapted from Paper IV).

To further simplify the large number of geochemical parameters, the statistical method, PCA was used to transform the complex results into a clear format. Figure 15 shows PCA results where principle components 1 and 2 are presented on the x and y-axis, respectively. Through this analysis only samples 253 and 274 were separated from the other samples. A further study of the results, showed that in the case of sample 253 (Figure 16A) the ratios mainly responsible for the separation, according to the score contributions, were $8\alpha(\text{H}), 14\alpha(\text{H})\text{-onocerane} / \text{C}_{30} 17\alpha(\text{H}),21\beta(\text{H})\text{-hopane}$ (ONII/ H_{30}); $8\alpha(\text{H}), 14\beta(\text{H})\text{-onocerane} / \text{C}_{30} 17\alpha(\text{H}),21\beta(\text{H})\text{-hopane}$ (ONIII/ H_{30}); and $\text{C}_{30} 17\alpha\text{-diahopane} / \text{C}_{30} 17\alpha(\text{H}),21\beta(\text{H})\text{-hopane}$ (Dia $\text{H}_{30}/\text{H}_{30}$). Onoceranes are associated with restricted basins in warm and humid tropical climates such as Brazil [112]. Their origin is unclear, but it is thought to be related to terrigenous dominated ferns and flowering plants [123]. Diahopanes are most likely formed by oxidation and rearrangement of hopenes [146]. For sample 274, the PCA score contributions showed that the ratios of $\text{C}_{31} 3\beta\text{-methylhopane} / \text{C}_{30} 17\alpha(\text{H}),21\beta(\text{H})\text{-hopane}$ ($3\beta\text{MH}_{31}/\text{H}_{30}$); C_{24} tetracyclic terpene / C_{26} tricyclic terpene (TeT $_{24}/\text{Tr}_{26}$); and $\text{C}_{31} 17\alpha(\text{H}),21\beta(\text{H})\text{-homohopane} / \text{C}_{30} 17\alpha(\text{H}),21\beta(\text{H})\text{-hopane}$ ($\text{H}_{31}\text{R}/\text{H}_{30}$) mainly contributed to its separation (Figure 16B). The precursor of $3\beta\text{-methylhopane}$ is the $3\beta\text{-methyl-hopanoid}$ synthesized by several types of methanotrophic bacteria [147, 148] and the oils with $3\beta\text{MH}_{31}/\text{H}_{30}$ ratio 1% are typically from lacustrine source rocks [111]. The geochemical significance of tri- and tetracyclic terpenes are discussed in the next chapter (Geochemistry and identification of compounds in Brazilian crude oils). The high $\text{H}_{31}\text{R}/\text{H}_{30}$ ratio is associated with marine and marine carbonate oils [123]. The oils 253 and 274 were distinguished from the rest of the oils mainly by non-conventional biomarker ratios.

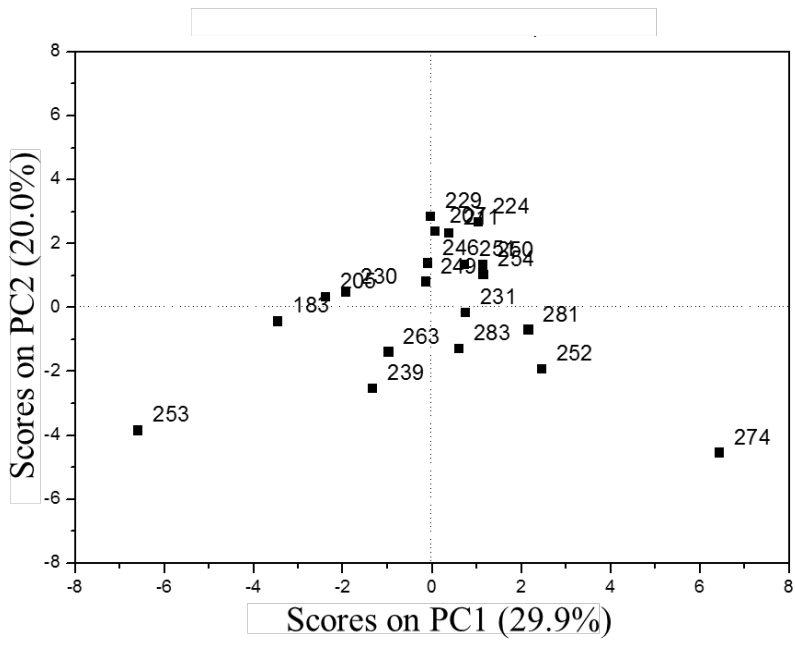


Figure 15. PCA score plots of geochemical source parameters (adapted from paper IV).

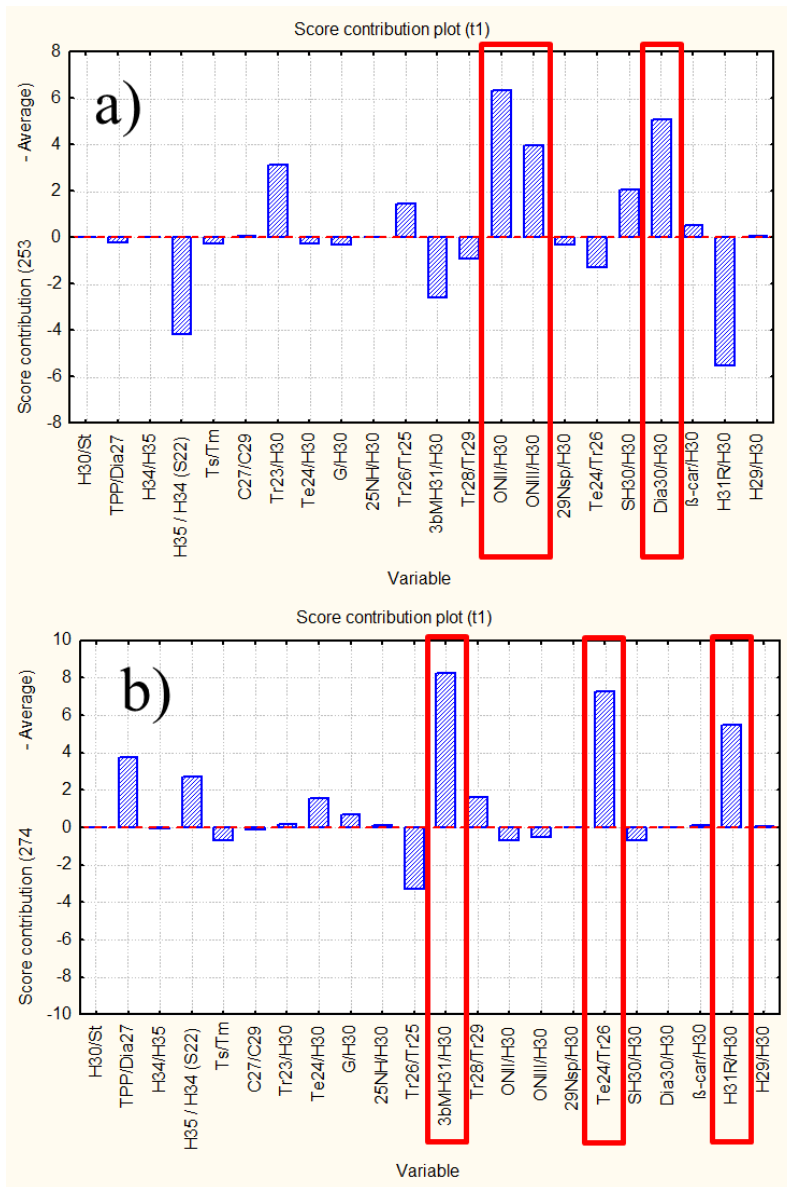


Figure 16. Parameter contributions to sample 253 (a) and 274 (b) in the PCA score plot illustrated in Figure 15. The red box illustrates biomarker ratios, which separated the sample (adapted from Paper IV).

3.5 Geochemistry and identification of compounds in Brazilian crude oils (Paper V)

In Paper V, eleven crude oil samples from different regions of Brazil, classified based on proprietary methods by the Research Center of Petrobras (CENPES) as having different source, biodegradation and maturity levels, were further analyzed with GC×GC-TOF-MS. The peak area data obtained was used for the calculation of the saturated and aromatic geochemical parameters. The saturated geochemical parameters assigned five (S01, S02, S08, S09 and S10), of the oils as originating from lacustrine source rocks, five from marine (S04, S05, S6, S07 and S11) and one (S03) as a mixture of marine and lacustrine source rocks. The 25-*nor*-hopane / C₃₀ 17 α (H),21 β (H)-hopane (25-NH/H₃₀) ratio assigned the oils S02 and S07 as biodegraded.

The saturated and aromatic geochemical parameters obtained from GC×GC-TOF-MS were analyzed by PCA (data not shown). However, the loading plot was difficult to read due to the large quantity of parameters, therefore another PCA was done with selected geochemical source parameters. This new calculation gave a similar result as the one with the large number of geochemical parameters, but produced Figures (Figure 17) which are easier to interpret. The PCA separated most mature oils (S05, S06 and S07, Figure 17A) and the loading plots in Figure 17B illustrate that the oils were mainly separated by parameters based on aromatic compounds and saturated maturity biomarker ratios.

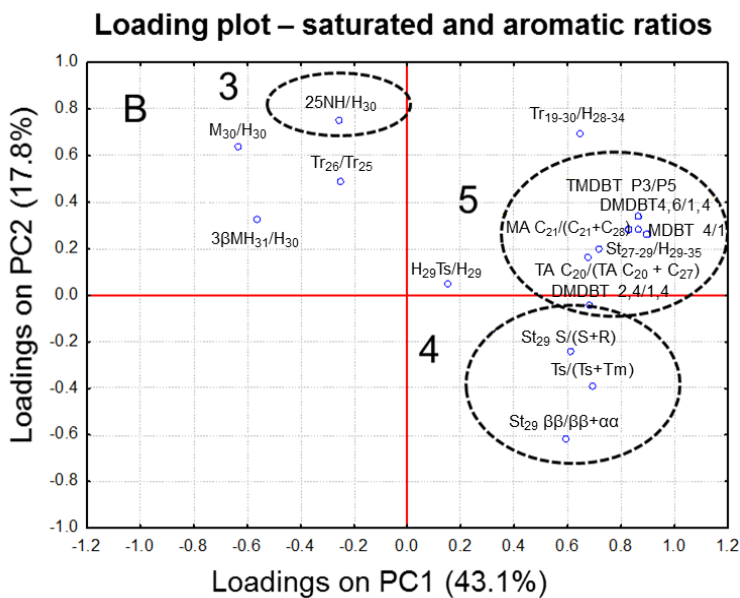
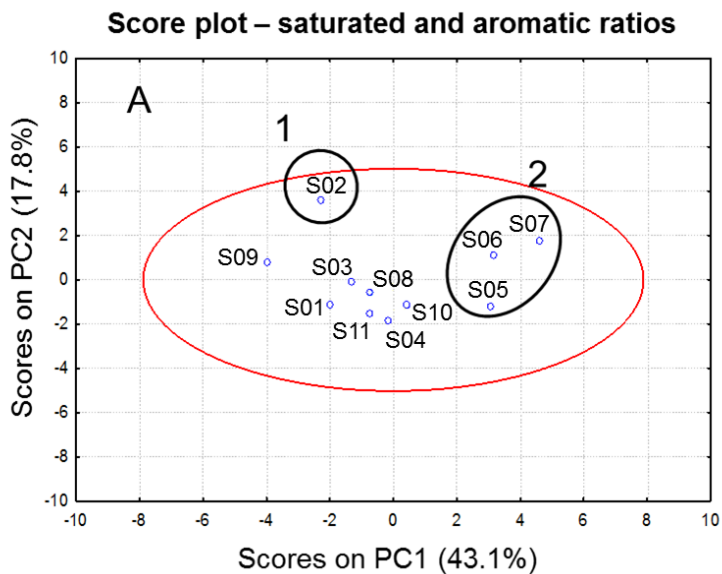


Figure 17. PCA score (A) and loading (B) plots for the first two principal components, based on saturated and aromatic biomarker parameters. [1] Oil S02; [2] Oils S05, S06 and S07; [3] 25NH/H₃₀ ratio; [4] some of the saturated maturity parameters; [5] aromatic geochemical parameters.

During the data analysis, eight unknown compounds (Figure 18), not reported earlier in the literature, were observed. These compounds had the molecular ion (M^+) at m/z 274, 288 or 316. Two of these compounds had a common characteristic fragment at m/z 191 in their EI mass spectrum, and the remaining six compounds had a common fragment at m/z 203. All the new (or unusual) compounds were found in the B/C oil fraction meaning that they are saturated hydrocarbons, *i.e.*, these compounds contain only carbon and hydrogen atoms. Therefore, it was straightforward to calculate the double bond equivalence (DBE), or degree of unsaturation, for all these compounds from the masses of the molecular ions. The DBE formula calculates how many hydrogens are “lost” from the saturated structure. The DBE for all the compounds was four.

The new compounds had different retention times in 1D and in 2D GC (Figure 18 and Table 10). In the chromatographic conditions used in this study (see section 2.6) the group type separation in the 2D dimension follows the order of: (i) tricyclic terpanes; (ii) steranes with 3 rings containing 6 carbon atoms and 1 ring containing 5 carbon atoms; (iii) tetracyclic terpanes with 4 rings containing 6 carbon atoms; (iv) pentacyclic terpanes with 4 rings containing 6 carbon atoms and 1 ring containing 5 carbon atoms and (v) pentacyclic terpanes with 5 rings containing 6 carbon atoms. In this group type separation, the observation that the eight new compounds are in the two dimensional separation plane somewhere between tricyclic terpanes and pentacyclic terpanes (Figure 18), and the DBE number of four, give reason to expect that the new compounds could be tetracyclic compounds.

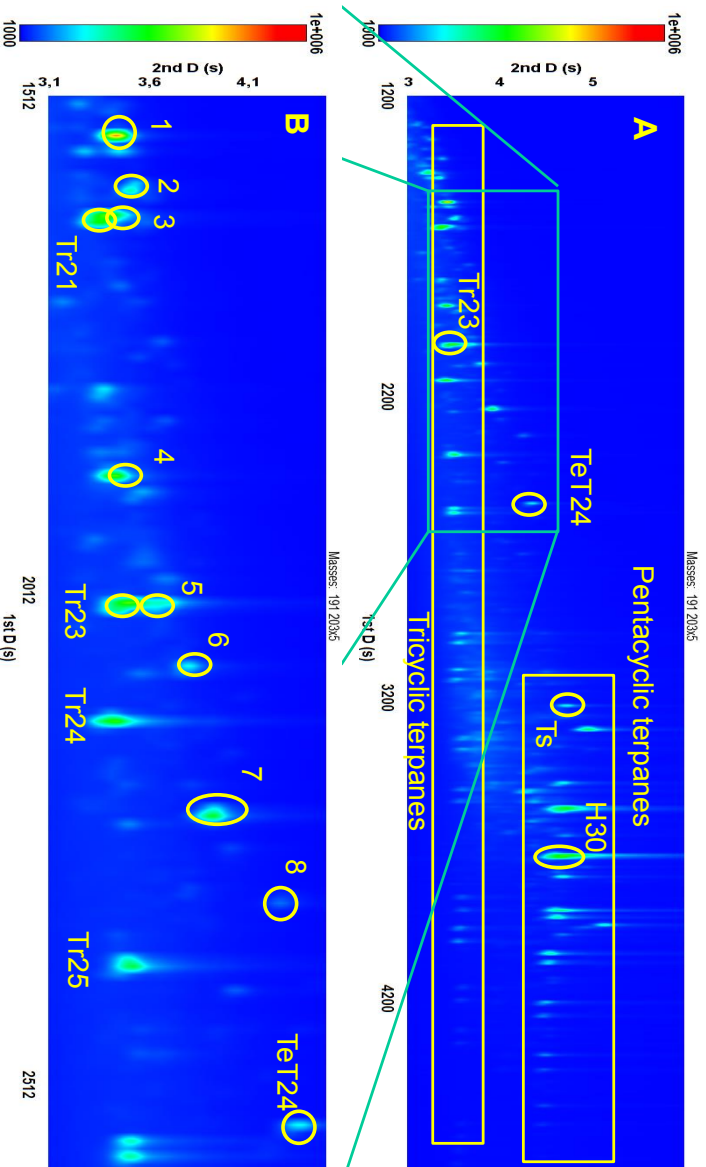


Figure 18. Crude oil sample S08: Partial extracted ion chromatogram with sums of ions at m/z 191 and 203 showing tri-, tetra-, and pentacyclic terpanes (A) and eight (1-8) new compounds (B). H30 = 17 α (H),21 β (H)-Hopane; TeT24 = C₂₄ tetracyclic terpane; Tr_n = C_n tricyclic terpane; Ts = C₂₇ 18 α -22,29,30-Trisnorneohopano (adapted from Paper V).

To achieve more information about the structures of the new compounds, the retention times of the compounds, for which the separation in a ^2D column was known, were plotted against the numerical values calculated based on the number of rings of 6 carbon atoms and number of rings of 5 carbon atoms in three reference compounds (Figure 19). The known reference compounds are C_{29} tricyclic terpane, which has three 6 carbon rings (with given ring number = 3); C_{29} $5\alpha(\text{H}),14\beta(\text{H}),17\beta(\text{H})$ -stigmastane 20R, which has three 6 carbon rings and one 5 carbon ring (with given ring number = 3.5) and C_{29} $17\alpha(\text{H}),21\beta(\text{H})$ hopane, which has four 6 carbon rings and one 5 carbon ring (with given ring number = 4.5) (see Figure 19 for structures). The ring numbers (Table 10) for the eight new compounds were assigned according to the best fit line obtained based on the known biomarker retention times. The ring numbers for the eight new compounds varied in the range from 2.86 to 3.91, representing approximately those of from tricyclic (3.00) to tetracyclic terpanes (4.00).

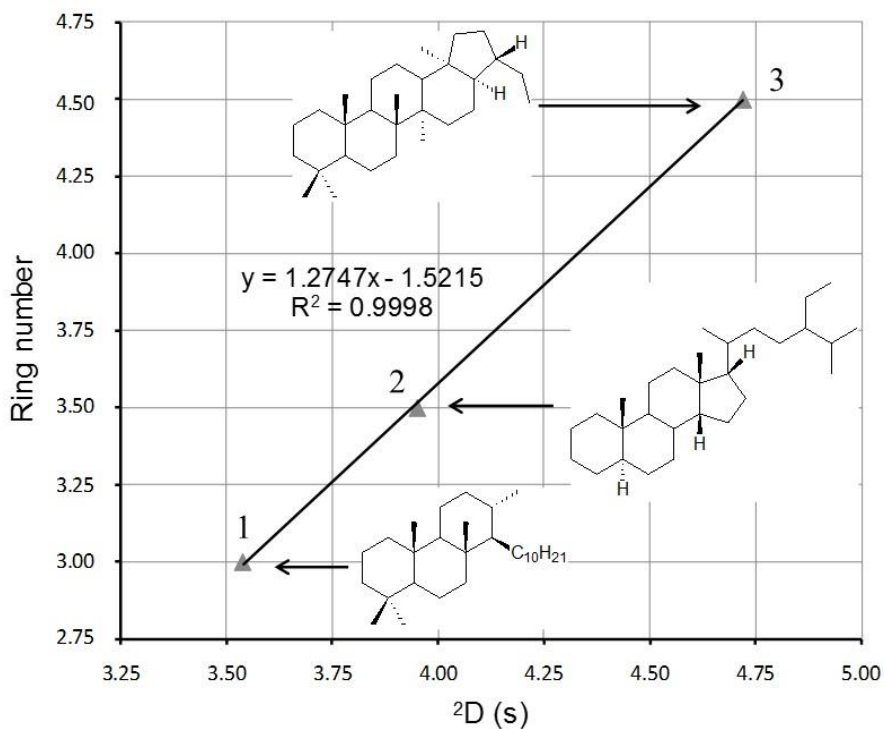


Figure 19. 2D retention time vs. ring number curve of (1) C_{29} tricyclic terpene, (2) C_{29} $5\alpha(H), 14\beta(H), 17\beta(H)$ -stigmastane 20R and (3) C_{29} $17\alpha(H), 21\beta(H)$ hopane, which were used to calculate the ring number values in Table 10 (adapted from Paper V).

Table 10. Retention times (t_R) in 1D (t_1) and 2D (t_2), and ring numbers for selected known biomarkers, as well as the calculated ring numbers for new tetracyclic compounds (Figure 19), which are marked with bold font. The numbers represent the new tetracyclic compounds observed in the chromatogram in Figure 18.

Name	MM	t_{R1} (s)	t_{R2} (s)	Carbons	Ring number
C ₂₀ tricyclic terpane	276	1448	3.24	20	3.00 ^b
C ₂₁ tricyclic terpane	290	1632	3.40	21	3.00 ^b
C ₂₄ tricyclic terpane	332	2144	3.43	24	3.00 ^b
C ₂₄ tetracyclic terpane	330	2552	4.36	24	4.00 ^b
C ₂₇ 13 β (H),17 α (H)-diacholestane 20R	372	2848	3.65	27	3.50 ^b
C ₂₇ 5 α (H),14 β (H),17 β (H)-stigmastane 20R	372	3112	3.89	27	3.50 ^b
C ₂₇ 22,29,30-trisnorneohopane (Ts)	370	3224	4.73	27	4.50 ^b
C ₂₇ 22,29,30-trisnorhopane (Tm)	370	3304	4.93	27	4.50 ^b
C ₂₉ tricyclic terpane	402	3136	3.54	29	3.00 ^b
C ₂₉ 5 α (H),14 β (H),17 β (H)-stigmastane 20R	400	3480	3.95	29	3.50 ^b
C ₂₉ Hopane	398	3568	4.72	29	4.50 ^b
Gammacerane	412	3952	5.14	30	5.00 ^b
8 α ,14 α Onocerane II	414	3576	3.83	30	2+2 ^b
#1, C₂₀H₃₄	274	1552	3.44	20	2.86 ^a
#2, C₂₀H₃₄	288	1608	3.63	21	3.11 ^a
#3, C₂₁H₃₆	288	1640	3.61	21	3.08 ^a
#4, C₂₃H₄₀	316	1896	3.44	23	2.86 ^a
#5, C₂₃H₄₀	316	2024	3.72	23	3.22 ^a
#6, C₂₃H₄₀	316	2088	3.81	23	3.34 ^a
#7, C₂₃H₄₀	316	2240	3.93	23	3.49 ^a
#8, C₂₃H₄₀	316	2328	4.26	23	3.91 ^a

^a The calculated ring number based on a linear trend line equation presented in Figure 19.

^b Given number according to the number of carbon rings in the molecule; a five-carbon ring reduces the number by 0.5.

Exact matches for the MS spectra of compounds 1-8 (Figure 20) were not found in the literature (Table 4, Paper V), therefore the structural identification, including ring configurations is relying on the compounds' retention times and MS fragmentation.

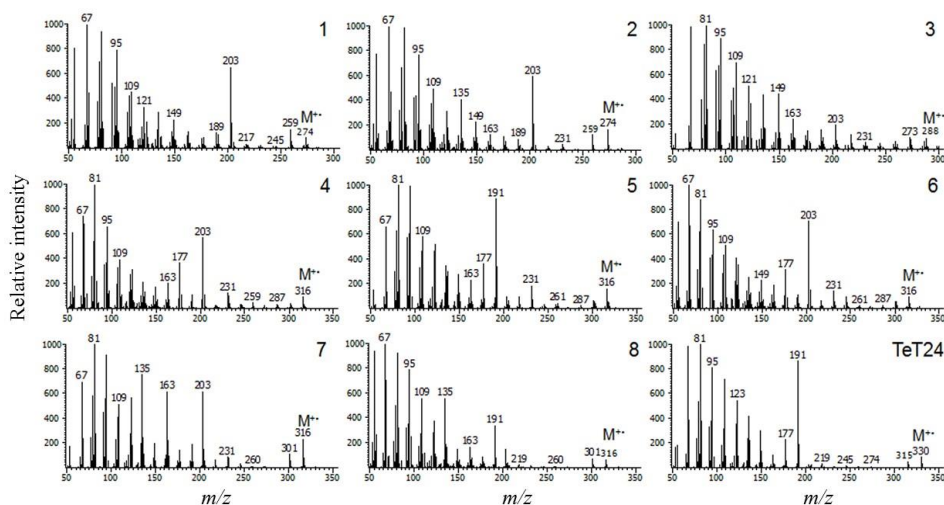


Figure 20. EI mass spectra of new compounds (1-8) and C_{24} tetracyclic terpene (TeT24) (adapted from Paper V).

Even when the measurements are conducted with a two dimensional gas chromatography obtaining “clean” EI mass spectra is not easy. This is demonstrated in Figure 21. The compound 4 co-eluted with another compound also in 2D , resulting in a single peak in TIC (marked with an asterisk in Figure 21). Careful spectral examination and software assisted deconvolution resulted in clear MS spectra for C_{23} tricyclic terpene (A, Figure 21) and compound 4 (B, Figure 20 and 21). The detection of this compound with conventional GC-MS would be very difficult, as in the detection of minor differences of oils in section 3.4. For example, $3\beta MH_{31}$ can not always be detected with GC-MS, because it elutes close to H_{31R} and Gam [111].

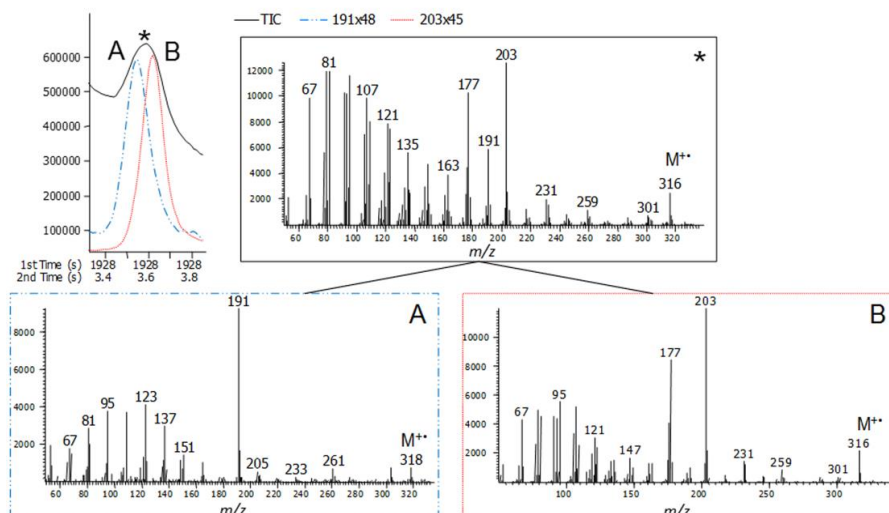


Figure 21. Top left: Total ion chromatogram (TIC) (*, black solid line); extracted ion chromatogram at m/z 191 (A, blue dashed line, peak intensity $\times 48$), and extracted ion chromatogram at m/z 203 (B, red solid line, peak intensity $\times 45$). Top right: mass spectrum at the top of the TIC peak. Bottom left: Mass spectrum of co-eluting possible C_{23} tricyclic terpene with diagnostic ion m/z 191 (A) taken at the top of the blue dashed line. Bottom right: New C_{23} tetracyclic compound (Compound 4, Figure 18B and 21) with diagnostic ion m/z 203 (B) taken at the top of the red solid line (adapted from Paper V).

The chromatographic and MS information for the new compounds were combined and the most likely tentative structures for compounds 1, 3, 4 and 8 are proposed (Figure 22). For instance, compound 4 has retention time close to tricyclic terpanes and it has a 4 ring structure. Therefore it could be possible to have a of the ring C, which could cause a reduction in retention time in 2D . Compounds 6 and 7 have similar MS spectra to compound 4, but a higher retention times in 2D , which indicate a different ring structure. Compound 8 has a retention time in 2D close to the C_{24} tetracyclic terpene and a fragment ion at m/z 191. This ion is typical to C_{24} tetracyclic terpene [150], and therefore compound 8 could be a C_{23} tetracyclic terpene. Compound 2 could have a similar structure as compound 1, because their retention times in 2D are similar and in MS spectrum they have similar fragment ions. The MS spectrum of compound 5 is close to compound 8, and therefore compound 5 could have a partially similar structure. To summarise, all the new compounds are assumed to have a tetracyclic saturated structure.

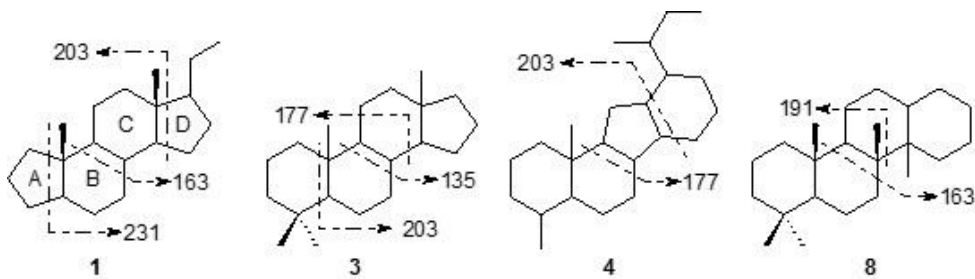


Figure 22. Tentative structures and possible fragmentations for new biomarkers (1, 3, 4 and 8) in Figure 18 (adapted from Paper V).

The new tetracyclic compounds were encountered with varying concentrations in all 11 crude oil samples collected from different regions of Brazil.

The peak areas of the new tetracyclic compounds were divided with the peak area of C₂₄ tetracyclic terpane (A_c/TeT₂₄, Supplementary material, Table 2S, Paper V). The new ratios were analyzed with PCA together with already known saturated and aromatic geochemical parameters as presented in Figure 17. The loading plot results showed that A_c/TeT₂₄ ratios acted in the same direction as dibenzothiophene ratios, which indicates that some of the new compounds could respond to changes in maturation in a similar way as dibenzothiophenes. Similar results were observed in score plots when the ratios of compound 7/TeT₂₄ and compound 8/TeT₂₄ were plotted with the ratio of dimethyldibenzothiophene (DMDBT) 4,6/1,4. The samples S06 and S07, which both showed high ratios of compound 7/TeT₂₄ and 8/TeT₂₄ when the ratio of DMDBT 4,6/1,4 was high.

A more detailed score plot (data not shown) examination of the samples revealed a correlation between the peak areas of compound 7 and TeT₂₄, which could mean that compound 7 is formed from TeT₂₄ during the maturation process, or the compounds could have a common precursor. Therefore, it is proposed that the ratios of compound 7 / TeT₂₄ could be used as potential new maturity parameter, for more mature oils, similar to benzothiophenes, which have been used for oils in the maturity window for vitrinite reflectance $R_0 \sim 1.3-1.5$ (Chakhmakhchev et al., 1997). Nevertheless, the maturation working range of these tetracyclic compounds should be determined in more detail.

4. CONCLUSIONS

Two different pre-separation techniques, IMS (Papers I-III) and GC×GC (IV-V) combined with MS, were studied in this thesis. Their capacity in difficult analytical tasks was demonstrated by separating model isomeric compounds with IMS and by oil analysis with GC×GC-TOF-MS.

Paper I studied the behavior of selected phenolic compounds and 2,4,6-TNT using negative APCI-IMS-MS. 2-*t*BPh formed two ion species $[M-H]^-$ and $[M-H+O]^-$, interestingly; the heavier $[M-H+O]^-$ ion had a shorter drift time than the lighter $[M-H]^-$ ion. This could be due to the fact that the $[M-H]^-$ ion forms an adduct, for example with NO_x or O_x , which is separated from analyte after IMS separation and is not detected with MS. The increased mass of an adduct ion $[M-H+?]$ could result in a longer drift time than $[M-H+O]^-$ ion, or the interaction with the drift gas is different for these two ion species. Where $[M-H]^-$ ion is more prone to interactions than $[M-H+O]^-$, which could form an internal hydrogen bond resulting in the charge being more protected. Three compounds, 2,6-*Dt*BPh, 2,6-*Dt*B-4-MPh and 2,4,6-*Tt*BPh, behaved similarly in the different IMS measuring conditions used in this study, producing two mobility peaks for the $[M-H]^-$ ion, which are not dependent on the measuring conditions used. Therefore, it can be suggested that these three phenolic compounds could be used as mobility standards in addition to 2,4,6-TNT, but further characterization is required. In addition, two isomeric compounds 2,4-*Dt*BPh and 2,6-*Dt*BPh were clearly separated with IMS.

Paper II demonstrated that in correct APPI ionization conditions, 2,6-*Dt*BPyr and 2,6-*Dt*B-4-MPyr efficiently produce both radical cations M^+ and protonated $[M+H]^+$ molecules. Also, dioxygen adduct ions $[M+O_2]^+$, which had the same mobility as M^+ , were observed. Therefore, it can be proposed that the M^+ ions are formed together with $[M+O_2]^+$ ions. The lower mobility of $[M+O_2]^+$ ions than of $[M+H]^+$, can be explained by the mass difference, i.e., heavier ions have longer drift times than lighter ions. The dioxygen adduct formation is likely to depend on the presence of two *tert*-butyl groups on both sides of the nitrogen “locking” the dioxygen in the middle. The naphthols produced both M^+ and $[M+H]^+$ ions. Interestingly, the M^+ ions had higher mobilities than the $[M+H]^+$ ions, which is opposite to 2,6-*Dt*BPyr and 2,6-*Dt*B-4-MPyr, for which also oxygen adducts were formed. The mobility order of different naphthol ions could

be due to different locations of the charge, for example the $[M+H]^+$ ion could be protonated in the -OH group, whereas in the M^+ ion the charge could be delocalized in the benzene rings. This could result in different conformation of molecules with different collision cross-sections of ion species.

In Paper III, both APCI and APPI produced protonated molecules $[M+H]^+$ for isomeric amines. Clear separation was recorded for 2,4,6-collidine, *N,N*-dimethylaniline, *N*-methyl-*o*-toluidine, phenethylamine and 4-ethylaniline with IMS, while the rest of the amines had mobility values very close to each other. This can be explained by the structures of isomers. For instance, the shielded molecules, i.e., with a protected charge (e.g. 2,4,6-collidine), interact less with the drift gas than the molecules with more open structures, such as primary amines.

In Paper IV, crude oil analysis from Recôncavo Basin was carried out with GC×GC-TOF-MS. Important geochemical parameters were calculated based on the GC×GC-TOF-MS results and evaluated. The PCA of the geochemical parameters was able to separate two oils from a total of twenty oils. The geochemical parameters also indicated that β -carotane can be used to reconstruct salinity variations in the late Jurassic to early Cretaceous time in an ancient lake during the fragmentation of the Pangaea supercontinent.

In Paper V, the source and maturity-related geochemical parameters were measured for eleven Brazilian crude oils using GC×GC-TOF-MS. A relationship between the retention time in 2D and the carbon ring structure was observed for several biomarkers already known from the literature. Since all the analyte compounds were saturated hydrocarbons (their polarity did not vary significantly), it is assumed that the shape of the molecule has an important role in the interactions with the column surface. The data about a relationship between the retention time in 2D and the carbon ring was used to achieve more structural information about eight new compounds found during the analysis. Using mass spectral data to calculate the DBE and the information from retention time in 2D , it could be suggested that these new compounds had tetracyclic structures, some of them similar to nor-steranes. It was also observed that compound 7/TeT24 ratio increases together with the DMDBT 4,6/1,4 ratio. This could be due to the fact that the compound 7 is more stable than the C_{24} tetracyclic terpane or it is produced during the maturation process. The compound 7/TeT24 ratio could be used in the future, in parallel with other maturation indicators such as benzothiophenes (R_0

~1.3-1.5) to evaluate oils from mature to overmature levels. Still, the maturity range for these new tetracyclic compounds should be characterized in more detail.

IMS is a faster measuring technique (typical analysis time is ~1 sec) with smaller peak capacity $\sim 10^2$ (total number of theoretical plates) [151] than GC×GC, which has peak capacity $>2 \times 10^4$ [90] with slower analysis time (typical analysis time is ~1 h). In IMS and GC×GC the separation of coeluting compounds can be improved in some cases by optimizing the measuring conditions, such as the polarity of the drift gas in IMS or the polarity of the columns in GC×GC. Furthermore, in IMS, ionized compounds are separated in a drift region and in GC×GC, the neutral molecules are separated. The shape of the molecule can change during the ionization process therefore these two techniques complement each other. IMS can be miniaturized for field analysis, while GC×GC instruments are typically benchtop size for laboratory use.

Both IMS and GC×GC, are capable of separating isomers. In IMS the most important property for separation of isomeric compounds is their shape (collision cross section). In addition to this, it was shown that different isomers have differing tendencies to form adducts. For example, in the negative APCI mode the formation of dioxygen adduct was seen for 2,4-DtBPh but not for 2,6-DtBPh. The dioxygen adduct of 2,4-DtBPh increased the mass of the ion resulting in a slower drift time than for the lighter [M-H]⁺ ion of 2,6-DtBPh. This basic finding could be adapted in different fields of chemistry to increase the understanding of the fundamental behavior of regio isomers. For example, isomers have a significant role in complex biological processes. Adducts (e.g. dioxygen) are well known in IMS and MS literature, but commonly they are dissociated in MS interface with declustering voltage or with curtain gas. Reactive oxygen species, such as hydrogen peroxide or peroxyxynitrite, are part of the production of dioxygen radical ions in living cells. It could be possible that dioxygen adducts are formed with molecules, which have similar structure than model compounds in this work, in real biological process. In the future, it would be interesting to study these adducts.

REFERENCES

1. Watson, J.T., Sparkman, O.D.: Introduction to Mass Spectrometry. John Wiley & Sons, Ltd. p. 862 (2008)
2. Hamilton, R.J.: Introduction to high performance liquid chromatography. In: Hamilton R.J., Sewell P.A. (eds.). Springer Netherlands, p. 248 (1982)
3. James, A.T., Martin, A.J.P.: Gas-liquid partition chromatography: the separation and micro-estimation of volatile fatty acids from formic acid to dodecanoic acid. *Biochemical Journal*. **50**, 679-690 (1952)
4. Eiceman, G.A., Karpas, Z., Hill, H.H.: Ion Mobility Spectrometry, 3rd ed., CRC Press Taylor & Francis, Boca Raton. p. 444 (2013)
5. Adahchour, M., Beens, J., Vreuls, R.J.J., Brinkman, U.A.T.: Recent developments in comprehensive two-dimensional gas chromatography (GCxGC): I. Introduction and instrumental set-up. *Trends in Analytical Chemistry*. **25**, 438-454 (2006)
6. Adahchour, M., Beens, J., Vreuls, R.J.J., Brinkman, U.A.T.: Recent developments in comprehensive two-dimensional gas chromatography (GCxGC): II. Modulation and detection. *Trends in Analytical Chemistry*. **25**, 540-553 (2006)
7. Adahchour, M., Beens, J., Vreuls, R.J.J., Brinkman, U.A.T.: Recent developments in comprehensive two-dimensional gas chromatography (GCxGC): III. Applications for petrochemicals and organohalogenes. *Trends in Analytical Chemistry*, **25**, 726-741 (2006)
8. Bertsch, W.: Two-Dimensional Gas Chromatography. Concepts, Instrumentation, and Applications – Part 1: Fundamentals, Conventional Two-Dimensional Gas Chromatography, Selected Applications. *Journal of High Resolution Chromatography*. **22**, 647-665 (1999)
9. Marriott, P.J., Chin, S.-T., Maikunthod, B., Schmarr, H.-G., Bieri, S.: Multidimensional gas chromatography. *Trends in Analytical Chemistry*. **34**, 1-21 (2012)
10. Mason, E.A.: Plasma Chromatography, Plenum, New York. p. 259 (1984)
11. Viidanoja, J., Sysoev, A., Adamov, A., Kotiaho, T.: Tetraalkylammonium halides as chemical standards for positive electrospray ionization with ion mobility spectrometry/mass spectrometry. *Rapid Communications in Mass Spectrometry*. **19**, 3051-3055 (2005)
12. Eiceman, G.A., Nazarov, E.G., Stone, J.A.: Chemical standards in ion mobility spectrometry. *Analytica Chimica Acta*. **493**, 185-194 (2003)
13. Kaur-Atwal, G., O'Connor, G., Aksenov, A., Bocos-Bintintan, V., Paul Thomas, C.L., Creaser, C.: Chemical standards for ion mobility spectrometry: a review. *International Journal for Ion Mobility Spectrometry*. **12**, 1-14 (2009)
14. Viitanen, A.K., Mauriala, T., Mattila, T., Adamov, A., Pedersen, C.S., Mäkelä, J.M., Marjamäki, M., Sysoev, A., Keskinen, J., Kotiaho, T.: Adjusting mobility scales of ion mobility spectrometers using 2,6-DiBP as a reference compound. *Talanta*. **76**, 1218-1223 (2008)
15. Fernandez-Maestre, R., Harden, C.S., Ewing, R.G., Crawford, C.L., Hill, H.H.: Chemical standards in ion mobility spectrometry. *Analyst*. **135**, 1433-1442 (2010)
16. Thomas, C.L.P., Rezgui, N.D., Kanu, A.B., Munro, W.A.: Measuring the temperature of the drift gas in an ion mobility spectrometer: a technical note. *International Journal for Ion Mobility Spectrometry*. **5**, 31-36 (2002)

17. Crawford, C.L., Hauck, B.C., Tufariello, J.A., Harden, C.S., McHugh, V., Siems, W.F., Hill, H.H.: Accurate and reproducible ion mobility measurements for chemical standard evaluation. *Talanta*. **101**, 161-170 (2012)
18. Kanu, A.B., Hill Jr, H.H.: Identity confirmation of drugs and explosives in ion mobility spectrometry using a secondary drift gas. *Talanta*. **73**, 692-699 (2007)
19. Spangler, G.E., Collins, C.I.: Reactant ions in negative ion plasma chromatography. *Analytical Chemistry*. **47**, 393-402 (1975)
20. Kanu, A.B., Dwivedi, P., Tam, M., Matz, L., Hill, H.H.: Ion mobility–mass spectrometry. *Journal of Mass Spectrometry*. **43**, 1-22 (2008)
21. Clemmer, D.E., Jarrold, M.F.: Ion Mobility Measurements and their Applications to Clusters and Biomolecules. *Journal of Mass Spectrometry*. **32**, 577-592 (1997)
22. Wittmer, D., Chen, Y.H., Luckenbill, B.K., Hill, H.H.: Electrospray Ionization Ion Mobility Spectrometry. *Analytical Chemistry*. **66**, 2348-2355 (1994)
23. Bothner, B., Siuzdak, G.: Electrospray Ionization of a Whole Virus: Analyzing Mass, Structure, and Viability. *ChemBioChem*. **5**, 258-260 (2004)
24. Borsdorf, H., Schelhorn, H., Flachowsky, J., Döring, H.-R., Stach, J.: Corona discharge ion mobility spectrometry of aliphatic and aromatic hydrocarbons. *Analytica Chimica Acta*. **403**, 235-242 (2000)
25. Pedersen, C.S., Lauritsen, F.R., Sysoev, A., Viitanen, A.-K., Mäkelä, J.M., Adamov, A., Laakia, J., Mauriala, T., Kotiaho, T.: Characterization of Proton-Bound Acetate Dimers in Ion Mobility Spectrometry. *Journal of the American Society for Mass Spectrometry*. **19**, 1361-1366 (2008)
26. Borsdorf, H., Nazarov, E.G., Miller, R.A.: Time-of-flight ion mobility spectrometry and differential mobility spectrometry: A comparative study of their efficiency in the analysis of halogenated compounds. *Talanta*. **71**, 1804-1812 (2007)
27. Sielemann, S., Baumbach, J.I., Schmidt, H., Pilzecker, P.: Detection of alcohols using UV-ion mobility spectrometers. *Analytica Chimica Acta*. **431**, 293-301 (2001)
28. Menéndez, M., Garrido-Delgado, R., Arce, L., Valcárcel, M.: Direct determination of volatile analytes from solid samples by UV-ion mobility spectrometry. *Journal of Chromatography A*. **1215**, 8-14 (2008)
29. Adamov, A., Mauriala, T., Teplov, V., Laakia, J., Pedersen, C.S., Kotiaho, T., Sysoev, A.A.: Characterization of a high resolution drift tube ion mobility spectrometer with a multi-ion source platform. *International Journal of Mass Spectrometry*. **298**, 24-29 (2010)
30. Rahel, J., Pavlik, M., Holubcik, L., Sobek, V., Skalny, J.D.: Relaxing Phenomena in Negative Corona Discharge: New Aspects. *Contributions to Plasma Physics*. **39**, 501-513 (1999)
31. Crawford, C.L., Hill, H.H.: Comparison of reactant and analyte ions for ⁶³Nickel, corona discharge, and secondary electrospray ionization sources with ion mobility-mass spectrometry. *Talanta*. **107**, 225-232 (2013)
32. Skalny, J.D., Orszagh, J., Mason, N.J., Rees, J.A., Aranda-Gonzalvo, Y., Whitmore, T.D.: Mass spectrometric study of negative ions extracted from point to plane negative corona discharge in ambient air at atmospheric pressure. *International Journal of Mass Spectrometry*. **272**, 12-21 (2008)

33. Waltman, M.J., Dwivedi, P., Hill Jr, H.H., Blanchard, W.C., Ewing, R.G.: Characterization of a distributed plasma ionization source (DPIS) for ion mobility spectrometry and mass spectrometry. *Talanta*. **77**, 249-255 (2008)
34. Ross, S.K., Bell, A.J.: Reverse flow continuous corona discharge ionisation applied to ion mobility spectrometry. *International Journal of Mass Spectrometry*. **218**, L1-L6 (2002)
35. Kauppila, T.J., Kostiaainen, R., Bruins, A.P.: Anisole, a new dopant for atmospheric pressure photoionization mass spectrometry of low proton affinity, low ionization energy compounds. *Rapid Communications in Mass Spectrometry*. **18**, 808-815 (2004)
36. Kauppila, T.J., Kuuranne, T., Meurer, E.C., Eberlin, M.N., Kotiaho, T., Kostiaainen, R.: Atmospheric Pressure Photoionization Mass Spectrometry. Ionization Mechanism and the Effect of Solvent on the Ionization of Naphthalenes. *Analytical Chemistry*. **74**, 5470-5479 (2002)
37. Kauppila, T.J., Kotiaho, T., Kostiaainen, R., Bruins, A.P.: Negative ion-atmospheric pressure photoionization-mass spectrometry. *Journal of the American Society for Mass Spectrometry*. **15**, 203-211 (2004)
38. Kolakowski, B.M., Mester, Z.: Review of applications of high-field asymmetric waveform ion mobility spectrometry (FAIMS) and differential mobility spectrometry (DMS). *Analyst*. **132**, 842-864 (2007)
39. Tang, F., Wang, X., Xu, C.: FAIMS Biochemical Sensor Based on MEMS Technology, *New Perspectives in Biosensors Technology and Applications*, Prof. Pier Andrea Serra (Ed.), ISBN: 978-953-307-448-1, InTech, Available from: <http://www.intechopen.com/books/new-perspectives-in-biosensorstechnology-and-applications/faims-biochemical-sensor-based-on-mems-technology>. (2011)
40. Shvartsburg, A.A.: *Differential Ion Mobility Spectrometry*. CRC Press, p. 322 (2008)
41. Giles, K., Pringle, S.D., Worthington, K.R., Little, D., Wildgoose, J.L., Bateman, R.H.: Applications of a travelling wave-based radio-frequency-only stacked ring ion guide. *Rapid Communications in Mass Spectrometry*. **18**, 2401-2414 (2004)
42. Pringle, S.D., Giles, K., Wildgoose, J.L., Williams, J.P., Slade, S.E., Thalassinou, K., Bateman, R.H., Bowers, M.T., Scrivens, J.H.: An investigation of the mobility separation of some peptide and protein ions using a new hybrid quadrupole/travelling wave IMS/oa-ToF instrument. *International Journal of Mass Spectrometry*. **261**, 1-12 (2007)
43. Castellanos, A., Benigni, P., Hernandez, D.R., DeBord, J.D., Ridgeway, M.E., Park, M.A., Fernandez-Lima, F.: Fast screening of polycyclic aromatic hydrocarbons using trapped ion mobility spectrometry-mass spectrometry. *Analytical Methods*. **6**, 9328-9332 (2014)
44. Sysoev, A., Adamov, A., Viidanoja, J., Ketola, R.A., Kostiaainen, R., Kotiaho, T.: Development of an ion mobility spectrometer for use in an atmospheric pressure ionization ion mobility spectrometer/mass spectrometer instrument for fast screening analysis. *Rapid Communications in Mass Spectrometry*. **18**, 3131-3139 (2004)
45. Xia, Y.-Q., Wu, S.T., Jemal, M.: LC-FAIMS-MS/MS for Quantification of a Peptide in Plasma and Evaluation of FAIMS Global Selectivity from Plasma Components. *Analytical Chemistry*. **80**, 7137-7143 (2008)

46. Myung, S., Lee, Y.J., Moon, M.H., Taraszka, J., Sowell, R., Koeniger, S., Hilderbrand, A.E., Valentine, S.J., Cherbas, L., Cherbas, P., Kaufmann, T.C., Miller, D.F., Mechref, Y., Novotny, M.V., Ewing, M.A., Sporleder, R.C., Clemmer, D.E.: Development of High-Sensitivity Ion Trap Ion Mobility Spectrometry Time-of-Flight Techniques: A High-Throughput Nano-LC-IMS-TOF Separation of Peptides Arising from a *Drosophila* Protein Extract. *Analytical Chemistry*. **75**, 5137-5145 (2003)
47. Henderson, S.C., Valentine, S.J., Counterman, A.E., Clemmer, D.E.: ESI/Ion Trap/Ion Mobility/Time-of-Flight Mass Spectrometry for Rapid and Sensitive Analysis of Biomolecular Mixtures. *Analytical Chemistry*. **71**, 291-301 (1999)
48. Ruotolo, B.T., Gillig, K.J., Stone, E.G., Russell, D.H., Fuhrer, K., Gonin, M., Schultz, J.A.: Analysis of protein mixtures by matrix-assisted laser desorption ionization-ion mobility-orthogonal-time-of-flight mass spectrometry. *International Journal of Mass Spectrometry*. **219**, 253-267 (2002)
49. Valentine, S.J., Plasencia, M.D., Liu, X., Krishnan, M., Naylor, S., Udseth, H.R., Smith, R.D., Clemmer D.E.: Toward Plasma Proteome Profiling with Ion Mobility-Mass Spectrometry. *Journal of Proteome Research*. **5**, 2977-2984 (2006)
50. Ewing, R.G., Atkinson, D.A., Eiceman, G.A., Ewing, G.J.: A critical review of ion mobility spectrometry for the detection of explosives and explosive related compounds. *Talanta*. **54**, 515-529 (2001)
51. Lee, J., Park, S., Cho, S.G., Goh, E.M., Lee, S., Koh, S.-S., Kim, J.: Analysis of explosives using corona discharge ionization combined with ion mobility spectrometry–mass spectrometry. *Talanta*. **120**, 64-70 (2014)
52. Sabo, M., Malásková, M., Matejčík, Š.: Ion mobility spectrometry–mass spectrometry studies of ion processes in air at atmospheric pressure and their application to thermal desorption of 2,4,6-trinitrotoluene. *Plasma Sources Science and Technology*. **23**, 015025 (2014)
53. Armenta, S., Alcalá, M., Blanco, M.: A review of recent, unconventional applications of ion mobility spectrometry (IMS). *Analytica Chimica Acta*. **703**, 114-123 (2011)
54. Ewing, M.A., Glover, M.S., Clemmer, D.E.: Hybrid ion mobility and mass spectrometry as a separation tool. *Journal of Chromatography A*. **1439**, 3-25 (2016)
55. Wu, C., Hill, H.H., Rasulev, U.K., Nazarov, E.G.: Surface Ionization Ion Mobility Spectrometry. *Analytical Chemistry*. **71**, 273-278 (1999)
56. Tuovinen, K., Kolehmainen, M., Paakkanen, H.: Determination and identification of pesticides from liquid matrices using ion mobility spectrometry. *Analytica Chimica Acta*. **429**, 257-268 (2001)
57. Kotiaho, T., Lauritsen, F.R., Degn, H., Paakkanen, H.: Membrane inlet ion mobility spectrometry for on-line measurement of ethanol in beer and in yeast fermentation. *Analytica Chimica Acta*. **309**, 317-325 (1995)
58. Vautz, W., Zimmermann, D., Hartmann, M., Baumbach, J.I., Nolte, J., Jung, J.: Ion mobility spectrometry for food quality and safety. *Food Additives & Contaminants*. **23**, 1064-1073 (2006)
59. Strachan, N.J.C., Nicholson, F.J., Ogden, I.D.: An automated sampling system using ion mobility spectrometry for the rapid detection of bacteria. *Analytica Chimica Acta*. **313**, 63-67 (1995)

60. Fenn, L., Kliman, M., Mahsut, A., Zhao, S., McLean, J.: Characterizing ion mobility-mass spectrometry conformation space for the analysis of complex biological samples. *Anal Bioanal Chem.* **394**, 235-244 (2009)
61. Snyder, A.P., Harden, C.S., Brittain, A.H., Kim, M.G., Arnold, N.S., Meuzelaar, H.L.C.: Portable hand-held gas chromatography/ion mobility spectrometry device. *Analytical Chemistry.* **65**, 299-306 (1993)
62. Dwivedi, P., Wu, P., Klopsch, S., Puzon, G., Xun, L., Hill, H., Jr.: Metabolic profiling by ion mobility mass spectrometry (IMMS). *Metabolomics.* **4**, 63-80 (2008)
63. Dwivedi, P., Schultz, A.J., Jr, H.H.H.: Metabolic profiling of human blood by high-resolution ion mobility mass spectrometry (IM-MS). *International Journal of Mass Spectrometry.* **298**, 78-90 (2010)
64. Taraszka, J.A., Counterman, A.E., Clemmer, D.E.: Gas-phase separations of complex tryptic peptide mixtures. *Fresenius Journal of Analytical Chemistry.* **369**, 234-245 (2001)
65. Jin, L., Barran, P.E., Deakin, J.A., Lyon, M., Uhrin, D.: Conformation of glycosaminoglycans by ion mobility mass spectrometry and molecular modelling. *Physical Chemistry Chemical Physics.* **7**, 3464-3471 (2005)
66. McLean, J.A., Ruotolo, B.T., Gillig, K.J., Russell, D.H.: Ion mobility-mass spectrometry: a new paradigm for proteomics. *International Journal of Mass Spectrometry.* **240**, 301-315 (2005)
67. Fasciotti, M., Lalli, P.M., Klitzke, C.F., Corilo, Y.E., Pudenzi, M.A., Pereira, R.C.L., Bastos, W., Daroda, R.J., Eberlin; M.N.: Petroleomics by Traveling Wave Ion Mobility-Mass Spectrometry Using CO₂ as a Drift Gas. *Energy & Fuels.* **27**, 7277-7286 (2013)
68. Santos, J.M., Galaverna, R.d.S., Pudenzi, M.A., Schmidt, E.M., Sanders, N.L., Kurulugama, R.T., et al.: Petroleomics by ion mobility mass spectrometry: resolution and characterization of contaminants and additives in crude oils and petrofuels. *Analytical Methods.* **7**, 4450-4463 (2015)
69. Ahmed, A., Cho, Y., Giles, K., Riches, E., Lee, J.W., Kim, H.I., Choi, C.H., Kim, S.: Elucidating Molecular Structures of Nonalkylated and Short-Chain Alkyl (n < 5, (CH₂)_n) Aromatic Compounds in Crude Oils by a Combination of Ion Mobility and Ultrahigh-Resolution Mass Spectrometries and Theoretical Collisional Cross-Section Calculations. *Analytical Chemistry.* **86**, 3300-3307 (2014)
70. Ponthus, J., Riches, E.: Evaluating the multiple benefits offered by ion mobility-mass spectrometry in oil and petroleum analysis. *International Journal for Ion Mobility Spectrometry.* **16**, 95-103 (2013)
71. Borsdorf, H., Rudolph, M.: Gas-phase ion mobility studies of constitutional isomeric hydrocarbons using different ionization techniques. *International Journal of Mass Spectrometry.* **208**, 67-72 (2001)
72. Borsdorf, H.: Influence of structural features of isomeric hydrocarbons on ion formation at atmospheric pressure. *International Journal for Ion Mobility Spectrometry.* **11**, 27-33 (2008)
73. Borsdorf, H., Nazarov, E.G., Eiceman, G.A.: Atmospheric pressure ionization and gas phase ion mobility studies of isomeric dihalogenated benzenes using different ionization techniques. *International Journal of Mass Spectrometry.* **232**, 117-126 (2004)

74. Borsdorf, H., Stone, J.A., Eiceman, G.A.: Gas phase studies on terpenes by ion mobility spectrometry using different atmospheric pressure chemical ionization techniques. *International Journal of Mass Spectrometry*. **246**, 19-28 (2005)
75. Borsdorf, H., Neitsch, K., Eiceman, G.A., Stone, J.A.: A comparison of the ion chemistry for mono-substituted toluenes and anilines by three methods of atmospheric pressure ionization with ion mobility spectrometry. *Talanta*. **78**, 1464-1475 (2009)
76. Dwivedi, P., Bendiak, B., Clowers, B.H., Hill Jr, H.H.: Rapid Resolution of Carbohydrate Isomers by Electrospray Ionization Ambient Pressure Ion Mobility Spectrometry-Time-of-Flight Mass Spectrometry (ESI-APIMS-TOFMS). *Journal of the American Society for Mass Spectrometry*. **18**, 1163-1175 (2007)
77. Counterman, A.E., Clemmer, D.E.: Cis-Trans Signatures of Proline-Containing Tryptic Peptides in the Gas Phase. *Analytical Chemistry*. **74**, 1946-1951 (2002)
78. Wu, C., Siems, W.F., Klasmeier, J., Hill, H.H.: Separation of Isomeric Peptides Using Electrospray Ionization/High-Resolution Ion Mobility Spectrometry. *Analytical Chemistry*. **72**, 391-395 (2000)
79. Clowers, B.H., Dwivedi, P., Steiner, W.E., Hill Jr, H.H., Bendiak, B.: Separation of Sodiated Isobaric Disaccharides and Trisaccharides Using Electrospray Ionization-Atmospheric Pressure Ion Mobility-Time of Flight Mass Spectrometry. *Journal of the American Society for Mass Spectrometry*. **16**, 660-669 (2005)
80. Clowers, B.H., Hill, H.H.: Influence of cation adduction on the separation characteristics of flavonoid diglycoside isomers using dual gate-ion mobility-quadrupole ion trap mass spectrometry. *Journal of Mass Spectrometry*. **41**, 339-351 (2006)
81. Karas, M.: Separation of Components of an Analysis Sample in an Ion Mobility Spectrometer using a Supply of Selectively Interactive Gaseous Particles. US Patent. 0178340 A1 and US7015462 B2 (2004)
82. Dwivedi, P., Wu, C., Matz, L.M., Clowers, B.H., Siems, W.F., Hill, H.H.: Gas-Phase Chiral Separations by Ion Mobility Spectrometry. *Analytical Chemistry*. **78**, 8200-8206 (2006)
83. Benassi, M., Corilo, Y.E., Uria, D., Augusti, R., Eberlin, M.N.: Recognition and Resolution of Isomeric Alkyl Anilines by Mass Spectrometry. *Journal of the American Society for Mass Spectrometry*. **20**, 269-277 (2009)
84. Schenauer, M.R., Leary, J.A.: An ion mobility-mass spectrometry investigation of monocyte chemoattractant protein-1. *International Journal of Mass Spectrometry*. **287**, 70-76 (2009)
85. Ahonen, L., Fasciotti, M., Gennäs, G.B.a., Kotiaho, T., Daroda, R.J., Eberlin, M., Kostianen, R.: Separation of steroid isomers by ion mobility mass spectrometry. *Journal of Chromatography A*. **1310**, 133-137 (2013)
86. Borsdorf, H., Nazarov, E.G., Miller, R.A.: Atmospheric-pressure ionization studies and field dependence of ion mobilities of isomeric hydrocarbons using a miniature differential mobility spectrometer. *Analytica Chimica Acta*. **575**, 76-88 (2006)
87. Gabryelski, W., Froese, K.L.: Rapid and sensitive differentiation of anomers, linkage, and position isomers of disaccharides using High-Field Asymmetric Waveform Ion Mobility Spectrometry (FAIMS). *Journal of the American Society for Mass Spectrometry*. **14**, 265-277 (2003)

88. Barnett, D.A., Purves, R.W., Ells, B., Guevremont, R.: Separation of *o*-, *m*- and *p*-phthalic acids by high-field asymmetric waveform ion mobility spectrometry (FAIMS) using mixed carrier gases. *Journal of Mass Spectrometry*. **35**, 976-980 (2000)
89. Lalli, P.M., Iglesias, B.A., Toma, H.E., de Sa, G.F., Daroda, R.J., Silva Filho, J.C., Szulejko, J.E., Araki, K., Eberlin, M.N.,: Protomers: formation, separation and characterization via travelling wave ion mobility mass spectrometry. *Journal of Mass Spectrometry*. **47**, 712-719 (2012)
90. Dimandja, J.-M.D.: Peer Reviewed: GC X GC. *Analytical Chemistry*. **76**, 167 A-174 A (2004)
91. Meinert, C., Meierhenrich, U.J.: A New Dimension in Separation Science: Comprehensive Two-Dimensional Gas Chromatography. *Angewandte Chemie International Edition*. **51**, 10460-10470 (2012)
92. NIST: The National Institute of Standards and Technology (<http://chemdata.nist.gov/>).
93. Pani, O., Górecki, T.: Comprehensive two-dimensional gas chromatography (GC×GC) in environmental analysis and monitoring. *Anal Bioanal Chem*. **386**, 1013-1023 (2006)
94. Herrero, M., Ibáñez, E., Cifuentes, A., Bernal, J.: Multidimensional chromatography in food analysis. *Journal of Chromatography A*. **1216**, 7110-7129 (2009)
95. Koek, M., van der Kloet, F., Kleemann, R., Kooistra, T., Verheij, E., Hankemeier, T.: Semi-automated non-target processing in GC × GC–MS metabolomics analysis: applicability for biomedical studies. *Metabolomics*. **7**, 1-14 (2011)
96. Hagan, S., Dunn, W.B., Knowles, J.D., Broadhurst, D., Williams, R., Ashworth, J.J., Cameron, M., Kelly, D.B.: Closed-Loop, Multiobjective Optimization of Two-Dimensional Gas Chromatography/Mass Spectrometry for Serum Metabolomics. *Analytical Chemistry*. **79**, 464-476 (2007)
97. Ventura, G.T., Kenig, F., Reddy, C.M., Schieber, J., Frysinger, G.S., Nelson, R.K., Dinel, E., Gaines, R.B., Schaeffer, P.: Molecular evidence of Late Archean archaea and the presence of a subsurface hydrothermal biosphere. *Proceedings of the National Academy of Sciences*. **104**, 14260-14265 (2007)
98. Frysinger, G.S., Gaines, R.B., Xu, L., Reddy, C.M.: Resolving the Unresolved Complex Mixture in Petroleum-Contaminated Sediments. *Environmental Science & Technology*. **37**, 1653-1662 (2003)
99. Song, S.M., Marriott, P., Wynne, P.: Comprehensive two-dimensional gas chromatography—quadrupole mass spectrometric analysis of drugs. *Journal of Chromatography A*. **1058**, 223-232 (2004)
100. Mitrevski, B., S., Wilairat, P., Marriott, P., J.: Evaluation of World Anti-Doping Agency criteria for anabolic agent analysis by using comprehensive two-dimensional gas chromatography–mass spectrometry. *Analytical and Bioanalytical Chemistry*. **396**, 2503-2511 (2010)
101. Eiserbeck, C., Nelson, R.K., Grice, K., Curiale, J., Reddy, C.M.: Comparison of GC-MS, GC-MRM-MS, and GCxGC to characterise higher plant biomarkers in Tertiary oils and rock extracts. *Geochimica et Cosmochimica Acta*. **87**, 299-322 (2012)
102. Silva, R.S.F., Tamanqueira, J.B., Dias, J.C.M., Passarelli, F.M., Bidart, A.M.F., Aquino Neto, F.R., Azevedo, D.A.: Comprehensive two-dimensional gas

- chromatography with time of flight mass spectrometry applied to analysis of Fischer-Tropsch synthesis products obtained with and without carbon dioxide addition to feed gas. *Journal of the Brazilian Chemical Society*. **22**, 2121-2126 (2011)
103. Ávila, B.M.F., Aguiar, A., Gomes, A.O., Azevedo, D.A.: Characterization of extra heavy gas oil biomarkers using comprehensive two-dimensional gas chromatography coupled to time-of-flight mass spectrometry. *Advances in Organic Geochemistry 2009 Proceedings of the 24th International Meeting on Organic Geochemistry*. **41**, 863-866 (2010)
 104. Ávila, B.M.F., Pereira, R., Gomes, A.O., Azevedo, D.A.: Chemical characterization of aromatic compounds in extra heavy gas oil by comprehensive two-dimensional gas chromatography coupled to time-of-flight mass spectrometry. *Selected Papers from the 34th ISCC and the 7th GCxGC Symposium 34th International Symposium on Capillary Chromatography and 7th GCxGC Symposium*. **1218**, 3208-3216 (2011)
 105. Dutriez, T., Courtiade, M., Thiébaud, D., Dulot, H., Borrás, J., Bertocini, F., Hennion, M.-C.: Advances in Quantitative Analysis of Heavy Petroleum Fractions by Liquid Chromatography-High-Temperature Comprehensive Two-Dimensional Gas Chromatography: Breakthrough for Conversion Processes. *Energy & Fuels*. **24**, 4430-4438 (2010)
 106. Mahé, L., Courtiade, M., Dartiguelongue, C., Ponthus, J., Souchon, V., Thiébaud, D.: Overcoming the high-temperature two-dimensional gas chromatography limits to elute heavy compounds. *Journal of Chromatography A*. **1229**, 298-301 (2012)
 107. Aguiar, A., Aguiar, H.G.M., Azevedo, D.A., Aquino Neto, F.R.: Identification of Methylhopane and Methylmoretane Series in Ceará Basin Oils, Brazil, Using Comprehensive Two-Dimensional Gas Chromatography Coupled to Time-of-Flight Mass Spectrometry. *Energy & Fuels*. **25**, 1060-1065 (2011)
 108. Aguiar, A., Silva Júnior, A.I., Azevedo, D.A., Aquino Neto, F.R.: Application of comprehensive two-dimensional gas chromatography coupled to time-of-flight mass spectrometry to biomarker characterization in Brazilian oils. *Fuel*. **89**, 2760-2768 (2010)
 109. Soares, R.F., Pereira, R., Silva, R.S.F., Mogollon, L., Azevedo, D.A.: Comprehensive two-dimensional gas chromatography coupled to time of flight mass spectrometry: new biomarker parameter proposition for the characterization of biodegraded oil. *Journal of the Brazilian Chemical Society*. **24**, 1570-1581 (2013)
 110. Li, S., Cao, J., Hu, S., Zhang, D., Fan, R.: Analysis of terpanes in biodegraded oils from China using comprehensive two-dimensional gas chromatography with time-of-flight mass spectrometry. *Fuel*. **133**, 153-162 (2014)
 111. Kiepper, A.P., Casilli, A., Azevedo, D.A.: Depositional paleoenvironment of Brazilian crude oils from unusual biomarkers revealed using comprehensive two dimensional gas chromatography coupled to time of flight mass spectrometry. *Organic Geochemistry*. **70**, 62-75 (2014)
 112. Oliveira, C.R., Ferreira, A.A., Oliveira, C.J.F., Azevedo, D.A., Santos Neto, E.V., Aquino Neto, F.R.: Biomarkers in crude oil revealed by comprehensive two-dimensional gas chromatography time-of-flight mass spectrometry: Depositional paleoenvironment proxies. *Organic Geochemistry*. **46**, 154-164 (2012)

113. Oliveira, C.R., Oliveira, C.J.F., Ferreira, A.A., Azevedo, D.A., Aquino Neto, F.R.: Characterization of aromatic steroids and hopanoids in marine and lacustrine crude oils using comprehensive two dimensional gas chromatography coupled to time-of-flight mass spectrometry (GCxGC-TOFMS). *Organic Geochemistry*. **53**, 131-136 (2012)
114. Silva, R.C., Silva, R.S.F., de Castro, E.V.R., Peters, K.E., Azevedo, D.A.: Extended diamondoid assessment in crude oil using comprehensive two-dimensional gas chromatography coupled to time-of-flight mass spectrometry. *Fuel*. **112**, 125-133 (2013)
115. Bertocini, F., Vendevre, C., Thiébaud, D.: Interest and Applications of Multidimensional Gas Chromatography for Trace Analysis in the Petroleum Industry *Oil & Gas Science and Technology - Rev. IFP*. **60**, 937-950 (2005)
116. Bruckner, C.A., Prazen, B.J., Synovec, R.E.: Comprehensive Two-Dimensional High-Speed Gas Chromatography with Chemometric Analysis. *Analytical Chemistry*. **70**, 2796-2804 (1998)
117. Frysinger, G.S., Gaines, R.B.: Comprehensive Two-Dimensional Gas Chromatography with Mass Spectrometric Detection (GC × GC/MS) Applied to the Analysis of Petroleum. *Journal of High Resolution Chromatography*. **22**, 251-255 (1999)
118. Hua, R., Li, Y., Liu, W., Zheng, J., Wei, H., Wang, J., Lua, X., Konga, H., Xu, G.: Determination of sulfur-containing compounds in diesel oils by comprehensive two-dimensional gas chromatography with a sulfur chemiluminescence detector. *First International Symposium on Comprehensive Multidimensional Gas Chromatography*. **1019**, 101-109 (2003)
119. Marshall, A.G., Hendrickson, C.L., Jackson, G.S.: Fourier transform ion cyclotron resonance mass spectrometry: A primer. *Mass Spectrometry Reviews*. **17**, 1-35 (1998)
120. Marshall, A.G., Rodgers, R.P.: Petroleomics: The Next Grand Challenge for Chemical Analysis. *Accounts of Chemical Research*. **37**, 53-59 (2004)
121. Vaz, B.G., Silva, R.C., Klitzke, C.F., Simas, R.C., Lopes Nascimento, H.D., Pereira, R.C.L., Garcia, D.F., Eberlin, M.N., Azevedo, D.A.: Assessing Biodegradation in the Llanos Orientales Crude Oils by Electrospray Ionization Ultrahigh Resolution and Accuracy Fourier Transform Mass Spectrometry and Chemometric Analysis. *Energy & Fuels*. **27**, 1277-1284 (2013)
122. Hughey, C.A., Rodgers, R.P., Marshall, A.G., Walters, C.C., Qian, K., Mankiewicz, P.: Acidic and neutral polar NSO compounds in Smackover oils of different thermal maturity revealed by electrospray high field Fourier transform ion cyclotron resonance mass spectrometry. *Organic Geochemistry*. **35**, 863-880 (2004)
123. Peters, K.E., Walters, C.C., Moldowan, J.M.: The Biomarker Guide: Biomarkers in the environment and human history, Vol 1. **2nd**, p. 471 (2005)
124. Peters, K.E., Walters, C.C., Moldowan, J.M.: The Biomarker Guide, Biomarkers and Isotopes in Petroleum Exploration and Earth History, Vol 2. **2nd**, p. 684 (2005)
125. Eiserbeck, C., Nelson, R.K., Grice, K., Curiale, J., Reddy, C.M., Raiteri, P.: Separation of 18 α (H)-, 18 β (H)-oleanane and lupane by comprehensive two-dimensional gas chromatography. *Journal of Chromatography A*. **1218**, 5549-5553 (2011)

126. Ventura, G.T., Kenig, F., Reddy, C.M., Frysinger, G.S., Nelson, R.K., Mooy, B.V., et al.: Analysis of unresolved complex mixtures of hydrocarbons extracted from Late Archean sediments by comprehensive two-dimensional gas chromatography (GC×GC). *Organic Geochemistry*. **39**, 846-867 (2008)
127. Laakia, J.: Applications of ion mobility spectrometry - mass spectrometry using negative atmospheric pressure chemical ionization on selected phenols, and positive atmospheric pressure photoionization for the separation of different ion structures, Ph.Lic. Thesis. University of Helsinki. (2010)
128. Marotta, E., Aquino Neto, F.R., Azevedo, D.A.: Separation and quantitative determination of linear and cyclic/branched alkanes in Brazilian petroleum using urea adduction and gas chromatography: a case study revisited. *Química Nova*. **37**, 1692-1698 (2014)
129. Nwadinigwe, C.A., Nwobodo, I.O.: Analysis of *n*-paraffins in light crudes: Molecular sieve and urea adduction techniques revisited. *Fuel*. **73**, 779-782 (1994)
130. Laakia, J., Pedersen, C.S., Adamov, A., Viidanoja, J., Sysoev, A., Kotiaho, T.: Sterically hindered phenols in negative ion mobility spectrometry-mass spectrometry. *Rapid Communications in Mass Spectrometry*. **23**, 3069-3076 (2009)
131. Silva, R.S.F., Aguiar, H.G.M., Rangel, M.D., Azevedo, D.A., Aquino Neto, F.R.: Comprehensive two-dimensional gas chromatography with time of flight mass spectrometry applied to biomarker analysis of oils from Colombia. *Fuel*. **90**, 2694-2699 (2011)
132. Cody, R.B., Laramee, J.A.: Atmospheric pressure ion source cross reference to related application. US Patent, WO 10/732205, 2004. (2005)
133. Sabo, M., Michalczyk, B., Lichvanová, Z., Kavický, V., Radjenovic, B., Matejčík, Š.: Interactions of multiple reactant ions with 2,4,6-trinitrotoluene studied by corona discharge ion mobility-mass spectrometry. *International Journal of Mass Spectrometry*. **380**, 12-20 (2015)
134. Laakia, J., Pedersen, C.S., Adamov, A., Viidanoja, J., Syseov, A., Kotiaho, T.: Ion mobility spectrometry/ mass spectrometry (IMS/MS) for measurement of selected phenols, (Poster). IMSC 2009 (18th International Mass Spectrometry Conference, Bremen, Germany). (2009)
135. Robb, D.B., Blades, M.W.: Atmospheric Pressure Photoionization for Ionization of Both Polar and Nonpolar Compounds in Reversed-Phase LC/MS. *Analytical Chemistry*. **78**, 8162-8164 (2006)
136. Syage, J.A.: Mechanism of $[M + H]^+$ formation in photoionization mass spectrometry. *Journal of the American Society for Mass Spectrometry*. **15**, 1521-1533 (2004)
137. Karpas, Z., Berant, Z., Stimac, R.: An ion mobility spectrometry/mass spectrometry (IMS/MS) study of the site of protonation in anilines. *Structural Chemistry*. **1**, 201-204 (1990)
138. Karpas, Z.: Ion Mobility Spectrometry of Aliphatic and Aromatic Amines. *Analytical Chemistry*. **61**, 684-689 (1989)
139. Karpas, Z., Berant, Z.: Effect of drift gas on mobility of ions. *The Journal of Physical Chemistry*. **93**, 3021-3025 (1989)
140. Karasek, F.W., Kim, S.H., Rokushika, S.: Plasma chromatography of alkyl amines. *Analytical Chemistry*. **50**, 2013-2016 (1978)

141. Karpas, Z., Bell, S.E., Wang, Y.F., Walsh, M., Eiceman, G.A.: The structure of protonated diamines and polyamines. *Structural Chemistry*. **5**, 135-140 (1994)
142. Asbury, G.R., Hill, H.H.: Using Different Drift Gases To Change Separation Factors (α) in Ion Mobility Spectrometry. *Analytical Chemistry*. **72**, 580-584 (1999)
143. Matz, L.M., Hill Jr, H.H., Beegle, L.W., Kanik, I.: Investigation of drift gas selectivity in high resolution ion mobility spectrometry with mass spectrometry detection. *Journal of the American Society for Mass Spectrometry*. **13**, 300-307 (2002)
144. Figueiredo, A.M.F., Braga, J.A.E., Zabalaga, J.C., Oliveira, J.J., Aguiar, G.A., Silva, O.B., Mato, L.F., Daniel, L.M.F., Magnavita, L.P., Bruhn, C.H.L., .: Recôncavo Basin, Brazil: a prolific intracontinental rift basin. In: Landon, S.M. (Ed.), *Interior rift basins*. Memoir, 59. American Association of Petroleum Geologists, Tulsa. (1994)
145. Santos, C.F., Braga, J.A.E.: O estado da arte da Bacia do Recôncavo. *Boletim de Geociências da Petrobras*. **4**, (1990)
146. Coutinho, L.F.C.: *Análise do Balanço Material do Petróleo em uma Região em Fase de Exploração Matura – Bacia Do Recôncavo, Brasil*. PEC-COPPE/UFRJ. Thesis. (2008)
147. Nytoft, H.P., Lutnæs, B.F., Johansen, J.E.: 28-Nor-spergulanes, a novel series of rearranged hopanes. *Organic Geochemistry*. **37**, 772-786 (2006)
148. Eigenbrode, J.L., Freeman, K.H., Summons, R.E.: Methylhopane biomarker hydrocarbons in Hamersley Province sediments provide evidence for Neoproterozoic aerobicity. *Earth and Planetary Science Letters*. **273**, 323-331 (2008)
149. Welander, P.V., Summons, R.E.: Discovery, taxonomic distribution, and phenotypic characterization of a gene required for 3-methylhopanoid production. *Proceedings of the National Academy of Sciences*. **109**, 12905-12910 (2012)
150. Chen, B., Liang, C., Yang, J., Contreras, D.S., Clancy, Y.L., Lobkovsky, E.B., Yaghi, O.M., Dai, S.: A Microporous Metal–Organic Framework for Gas-Chromatographic Separation of Alkanes. *Angewandte Chemie*. **118**, 1418-1421 (2006)
151. Trendel, J.-M., Restle, A., Connan, J., Albrecht, P.: Identification of a novel series of tetracyclic terpene hydrocarbons (C₂₄-C₂₇) in sediments and petroleum. *Journal of the Chemical Society, Chemical Communications*. 304-306 (1982)
152. May, J.C., McLean, J.A.: Advanced Multidimensional Separations in Mass Spectrometry: Navigating the Big Data Deluge. *Annual Review of Analytical Chemistry*. **9**, 387-409 (2016)

Sterically hindered phenols in negative ion mobility spectrometry–mass spectrometry

Jaakko Laakia^{1*}, Christian Schack Pedersen², Alexey Adamov³, Jyrki Viidanoja^{1†}, Alexey Sysoev⁴ and Tapio Kotiaho^{1,3}

¹Laboratory of Analytical Chemistry, Department of Chemistry, P.O. Box 55, FI-00014 University of Helsinki, Finland

²University of Copenhagen, Department of Chemistry, Universitetsparken 5, DK-2100 Copenhagen Ø, Denmark

³Division of Pharmaceutical Chemistry, Faculty of Pharmacy, P. O. Box 56, FI-00014 University of Helsinki, Finland

⁴Moscow Engineering Physics Institute (State University), Kashirskoe shosse 31, 115409, Moscow, Russia

Received 10 June 2009; Revised 22 July 2009; Accepted 22 July 2009

Negative corona discharge atmospheric pressure chemical ionization (APCI) was used to investigate phenols with varying numbers of *tert*-butyl groups using ion mobility spectrometry–mass spectrometry (IMS-MS). The main characteristic ion observed for all the phenolic compounds was the deprotonated molecule $[M-H]^-$. 2-*tert*-Butylphenol showed one main mobility peak in the mass-selected mobility spectrum of the $[M-H]^-$ ion measured under nitrogen atmosphere. When air was used as a nebulizer gas an oxygen addition ion was seen in the mass spectrum and, interestingly, this new species $[M-H+O]^-$ had a shorter drift time than the lighter $[M-H]^-$ ion. Other phenolic compounds primarily produced two IMS peaks in the mass-selected mobility spectra measured using the $[M-H]^-$ ion. It was also observed that two isomeric compounds, 2,4-di-*tert*-butylphenol and 2,6-di-*tert*-butylphenol, could be separated with IMS. In addition, mobilities of various characteristic ions of 2,4,6-trinitrotoluene were measured, since this compound was previously used as a mobility standard. The possibility of using phenolic compounds as mobility standards is also discussed. Copyright © 2009 John Wiley & Sons, Ltd.

Ion mobility spectrometry (IMS) is based on the separation of ions in a drift tube by an electric field.¹ Molecules with different collision cross-sections have different drift velocities and are therefore separated from each other. The theory of drift tube IMS has been described in detail previously.^{1–3} IMS is a powerful tool in different areas, such as the monitoring of environmental pollutants,^{4–6} warfare agents,⁷ explosives,^{8–10} herbicides,¹¹ pesticides,^{12,13} petroleum products,¹⁴ and illicit/legal drugs.¹⁵ In addition, it is also used in peptide analysis^{16,17} and space exploration.¹⁸ Most of these studies have used various positive ion ionization methods, whereas fewer studies have been carried out in negative ion mode.

Negative reactant ions formed in radioactive ionization in IMS were first studied during the 1970s^{19,20} and then later using a plasma ionization or corona discharge ion source.^{21–23} The negative ion mode with radioactive ionization has been used, for example, to measure inorganic pollutant gases, such as SO₂, H₂S, HCl, and NO₂,⁶ anesthetics²⁴ and organic nitrogen compounds such as 2,4,6-trinitrotoluene (2,4,6-TNT)^{8,9,25} and chlorinated compounds such as 2,4-dichlorophenoxyacetic acid and 2,4-dichlorophenol.²⁶ Explosives and chemical warfare agents (e.g. blistering agents) have also been measured using negative ion electrospray ionization

(ESI)-IMS,²⁷ and negative ion APCI-IMS has been used to study fluorinated phenols²⁸ and non-polar isomeric hydrocarbons.²⁹ Negative ion APCI-IMS has also been used to measure the reaction rate constants for electron attachment with CCl₄, CHCl₃, and CH₂Cl₂.³⁰ A review on the detection of explosives has been published¹⁰ and 2,4,6-TNT has been used as a negative ion mobility standard.³¹

In this study the behavior of selected phenolic compounds (Fig. 1) in negative APCI ion mobility spectrometry–mass spectrometry (IMS-MS) was measured. The compounds studied include phenolic compounds with varying numbers of *tert*-butyl groups. These compounds are widely used in industry; e.g., 2,6-di-*tert*-butylphenol is used as an antioxidant for food additives, fuels, oils and gasolines.^{32,33} 2,4,6-TNT was also included in the study since it has been used previously as a reference compound.³¹ The possibility of using phenolic compounds as mobility standards in negative IMS is also discussed.

EXPERIMENTAL

Instrumentation and measuring conditions

A custom-made IMS drift tube was attached to a commercial Sciex API-300 triple quadrupole mass spectrometer (Applied Biosystems-SCIEX, Concord, Ontario, Canada). This combination is referred to here as IMS-MS and is described in more detail by Sysoev *et al.*³⁴ Briefly, a 13.3 cm long drift tube is constructed from a set of metal rings individually separated

*Correspondence to: J. Laakia, Department of Chemistry, P.O. Box 55, FI-00014 University of Helsinki, Finland.
E-mail: jaakko.laakia@helsinki.fi

† Present address: PerkinElmer Life and Analytical Sciences/Wallac Oy, Mustionkatu 6 (P.O. Box 10), FI-20101 Turku, Finland

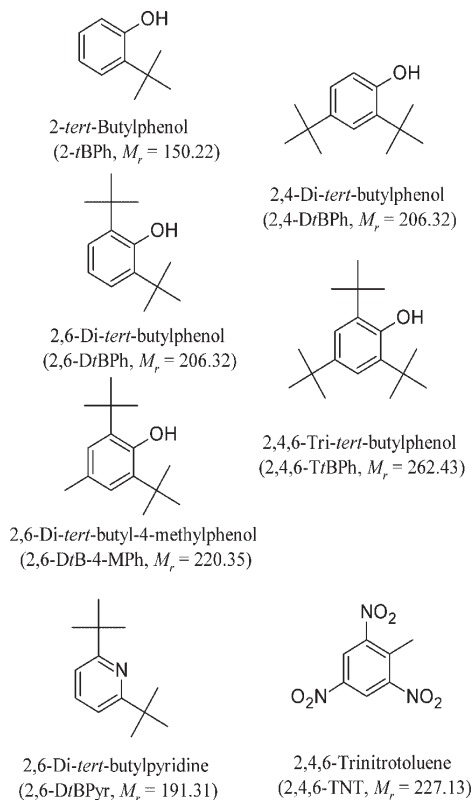


Figure 1. Structures of chemicals investigated in this study.

by Teflon rings. The desolvation area, which has a length of 7.65 cm, is separated by a Bradbury-Nielsen (B-N) gate from the drift region.³⁵ A second B-N gate is located in front of the MS interface. These two gates allow one to select a specific mobility window.^{34,36} The gate opening time for both B-N gates was 300 μ s for all the experiments. The B-N gates and the high voltages in the drift tube are controlled by a program written in-house and data is collected using the mass spectrometer operating software, the Analyst 1.4.1 program (Applied Biosystems/MDS SCIEX). The operating electric field varied between 270 and 378 V/cm in the drift region and between 230 and 260 V/cm in the desolvation area. This study uses absolute reduced mobilities, which are calculated according to Eqn. (1).

The instrument was operated using negative corona discharge APCI with a typical needle voltage of 1.3–1.5 kV in nitrogen and 1.7–2.2 kV in air. Most of the measurements were conducted in a nitrogen atmosphere, at atmospheric pressure. Pre-dried compressed air was passed through a NGLCMS20 nitrogen generator (Labgas Instrument Co., Espoo, Finland) to obtain 99.5% nitrogen. This was followed by a hydrocarbon and moisture trap. This nitrogen was used as both the nebulizer and the drift gas. The level of humidity was measured using a humidity gauge (Vaisala DMT242; Helsinki, Finland) downstream from the drift tube. In addition, compressed, bottled air (80% N₂, 20% O₂ with a purity of 4.0, AGA Ltd., Espoo, Finland) was used in certain experiments. A thermometer (Thermatag, Digitron Instrumentation Ltd., Torquay, UK) was attached to the nitrogen

storage tank and correlated well with the temperature being measured inside the drift tube, except in the case where the drift tube was heated above room temperature (see next section). The pressure meter (Series 902; MKS Instruments, Andover, MA, USA) was located within the laboratory and it correlated well with the prevailing ambient pressure in SMEAR III (60°20'N, 24°97'E), Helsinki, Finland.

Sample injections were conducted with a PHD 2000 advanced syringe pump (Harvard Apparatus GmbH, Hugstetten, Germany) with a typical injection speed of 180 μ L/h into the custom-made heated nebulizer, which was heated to 573 K. The nebulizer gas (nitrogen or air) flow rate in the nebulizer was typically 1.6–1.8 L/min. Sample concentrations were around 1–3 ppb unless otherwise stated. The drift flow was estimated to be \sim 2.4 L/min. The mass spectrometric parameters were as follows: declustering potential from -15 to -25 V, focusing potential from -180 to -200 V and an entrance potential of -5 V. Mass-selected mobility data was collected using the dual gate mode, which is presented in more detail in our previous publication.³⁴

Temperature and ion mobility

In our IMS-MS instrument the temperature of the device is measured with a thermometer which is mounted between the stainless steel metal drift rings and the outer core of the drift tube; therefore, it is expected that the temperature inside the drift tube will be somewhat different from the thermometer reading. To correlate the measured temperature with the real temperature inside the drift tube, the reduced mobility of 2,6-di-*tert*-butylpyridine (2,6-D-*t*BPyr) was measured at different temperatures in the positive APCI mode. Using this data, and recognizing that in the temperature range 310–523 K the reduced mobility of 2,6-D-*t*BPyr is constant,³⁷ the real temperature can be calculated as presented below. Correspondingly, the use of the reduced mobility of 2,4-lutidine has been used to calculate the real temperature inside a drift tube.³⁸ The reduced mobility of 2,6-D-*t*BPyr measured using the [M+H]⁺ ion at m/z 192 in positive ion APCI mode was 1.50 cm²/Vs within experimental error. The general formula for reduced mobility K_0 (cm²/Vs)³⁹ is:

$$K_0 = \left(\frac{l_d}{t_d V} \right) \left(\frac{273}{T} \right) \left(\frac{P}{760} \right) \quad (1)$$

where l_d = length of the drift region, t_d = drift time of the ion, V = the voltage drop over the drift region, P = pressure, and T = temperature. As the reduced mobility of 2,6-D-*t*BPyr is stable in the temperature range used (296–335 K) and all other variables, except T and t_d , are constant, the formula for reduced mobility of 2,6-D-*t*BPyr ($K_{2,6-D-*t*BPyr}$) without a temperature correction term can be rewritten as:

$$K_{2,6-D-*t*BPyr} \propto \left(\frac{273}{T} \right) \quad (2)$$

Based on this, when a room temperature (296 K) mobility value ($K_{2,6-D-*t*BPyr}$) of 2,6-D-*t*BPyr, 1.63 cm²/Vs, is used as a calibration point, its mobility values ($K_{2,6-D-*t*BPyr}$) of 1.72 and 1.85 cm²/Vs measured at thermometer readings 323 and 343 K represent the real temperatures in the drift tube of 313 and 335 K, respectively.

Chemicals

Phenolic compounds 2-*tert*-butylphenol (2-*t*BPh), 2,6-di-*tert*-butylphenol (2,6-D*t*BPh), 2,4-di-*tert*-butylphenol (2,4-D*t*BPh) and 2,6-di-*tert*-butyl-4-methylphenol (2,6-D*t*B-4-MPh), which all had a purity of >99%, 2,4,6-tri-*tert*-butylphenol (2,4,6-T*t*BPh), which had a purity of >98%, and 2,6-di-*tert*-butylpyridine (2,6-D*t*BPyr), which had a purity of >97%, were obtained from Sigma-Aldrich (Steinheim, Germany). The stock solutions (5 mM) were prepared first in hexane (Poch SA, Gliwice, Poland) and these were diluted further to give 50 or 500 μ M solutions. 2,4,6-Trinitrotoluene (2,4,6-TNT), 1000 μ g/mL in acetonitrile (ACN), with a purity of 99%, was purchased from Supelco (Bellefonte, PA, USA). This solution was diluted further in ACN (Lab-Scan, Dublin, Ireland).

RESULTS AND DISCUSSION

Reactant ions in negative corona discharge ionization

The identity of reactant ions in atmospheric pressure negative IMS has been studied previously^{19–21,23} and a general review of the corona discharge process has been published.⁴⁰ Briefly, based on these studies, one can state that the negative ionization process is more challenging and complex than the positive ion mode. In atmospheric pressure corona discharge chemical ionization, the charge is transferred first to oxygen and subsequently reactant ions are formed by various reactions. These depend, for example, on the concentration levels of different gases or chemicals present in the ion source atmosphere, and even trace amounts of chemicals (e.g. water, NO_x) can affect the ionization process. This generally complicates the measurements and reduces the consistency of the experiments. Due to this, the ionization conditions were kept as constant as possible.

Mass spectrometric measurements showed that the main reactant ions typically observed were [CO₃][−] at *m/z* 60 and [NO₂][−] at *m/z* 46, but [NO₃][−] at *m/z* 62 and [CNO][−] at *m/z* 42 were normally also seen at low intensities. However, depending on the ionization conditions (e.g. sample gas, corona needle voltage, and solvent) changes in relative abundances of these ions were observed. In addition, daily variations in ambient trace gas concentrations occur⁴¹ and could also have an effect on the ionization processes. Similar ions have also been reported in other corona discharge ionization IMS studies.^{21–23,42} Since the analytes were dissolved in different solvents, the solvent effect on the reactant ions was tested. Injection of solvents (e.g. hexane or acetonitrile) together with nebulizer gas clearly decreased the [CO₃][−] signal. When air was used instead of nitrogen as a nebulizer gas, the intensity of [CO₃][−] remained at about the same level. This was also the case in the presence of a solvent.

Ionization of model compounds

All the phenolic compounds formed [M–H][−] ions under negative ion APCI in nitrogen atmosphere. For some compounds, measurements were also carried out in air; e.g., for 2-*t*BPh, in addition to the [M–H][−] ion at *m/z* 149, an intense [M–H+O][−] ion at *m/z* 165 was observed. Formation of the [M–H+O][−] ion could occur by the formal insertion of

oxygen into a C–H bond during the ionization processes. A similar phenomenon was previously reported for benzene with positive corona discharge ionization.⁴³ In our study the origin of the oxygen is probably from the O₂. The product ion mass spectra of both the oxygen insertion ion of 2-*t*BPh (*m/z* 165) and the [M–H][−] ion of 2-*t*BPh (*m/z* 149) indicated the loss of 16 mass units (corresponding to the mass of a single oxygen atom) forming product ions *m/z* 149 and 133, respectively.

2,4,6-TNT typically produced three main characteristic ions, namely [M–NO][−] at *m/z* 197, [M–H][−] at *m/z* 226 and [M][−] at *m/z* 227, in nitrogen using corona discharge ionization (Fig. 2). When a mass spectrum was measured in air, an oxygen adduct ion [M+O][−] was more clearly seen at *m/z* 243. When the oxygen adduct ion was seen, ions *m/z* 213 and 183 were also typically observed in the mass spectrum, probably formed by loss of one or two NO groups from the oxygen adduct ion. A fragment ion [M–OH][−] at *m/z* 210, with a lower intensity, was also often seen in the mass spectra. Most of these characteristic ions of 2,4,6-TNT have been reported previously with different atmospheric pressure ionization techniques.^{9,42,44,45}

Mobilities of model compounds

In the next step, mobilities for the identified analyte ions were measured. The data is discussed below, compound by compound, and is summarized in Table 1. Typically, variations in reduced mobility values in different experiments were below 2%. 2,4,6-Trinitrotoluene (2,4,6-TNT) was also included in the compounds studied, since it has been used as a reference compound.³¹ The reduced mobility for its [M–H][−] ion equals 1.58 cm²/Vs, which is in agreement with the reported value of 1.53–1.55 cm²/Vs.¹⁰ The small difference is considered to be due to different drift tube designs and variations in measuring conditions.

2-*tert*-Butylphenol (2-*t*BPh)

The mass-selected mobility spectrum of the [M–H][−] ion of 2-*t*BPh shows one major mobility peak with a reduced mobility

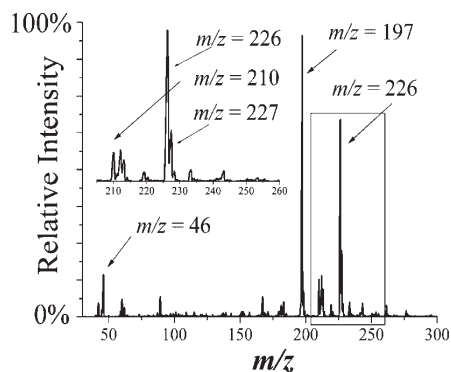


Figure 2. Negative ion APCI mass spectrum of 2,4,6-TNT. The gas-phase concentration of 2,4,6-TNT was around 1 ppb; 2,4,6-TNT was dissolved in acetonitrile and the nebulizer gas was nitrogen. The main peaks are the [M–NO][−] ion at *m/z* 197, [M–H][−] at *m/z* 226 and [M][−] at *m/z* 227. The [NO₂][−] ion at *m/z* 46 is a reactant ion.

Table 1. Summary of the reduced mobilities K_0 (cm^2/Vs) measured at room temperature. Nitrogen was used as a nebulizer gas and samples were dissolved in hexane unless otherwise stated. The numbers represent the peak numbers in the order they appear in the mass-selected mobility spectra

Molecule	Mass (u)	1st (K_0)	2nd (K_0)	3rd (K_0)	4th (K_0)
2- <i>t</i> BPh ($[\text{M}-\text{H}+\text{O}]^-$ m/z 165) ^b	150	1.63	1.13 ^c		
2- <i>t</i> BPh ($[\text{M}-\text{H}]^-$ m/z 149)	150	1.63	1.53	1.14 ^c	
2,4-D <i>t</i> BPh ($[\text{M}-\text{H}]^-$ m/z 205)	206	1.34	1.29		
2,6-D <i>t</i> BPh ($[\text{M}-\text{H}]^-$ m/z 205)	206	1.43	1.37		
2,6-D <i>t</i> B-4-MPh ($[\text{M}-\text{H}]^-$ m/z 219)	220	1.36	1.29		
2,4,6-T <i>t</i> BPh ($[\text{M}-\text{H}]^-$ m/z 261)	262	1.23	1.18		
2,4,6-TNT ($[\text{M}+\text{O}]^-$ m/z 243) ^{a,b}	227	1.53			
2,4,6-TNT ($[\text{M}]^-$ m/z 227) ^a	227	1.58 ^d	1.53	1.35	
2,4,6-TNT ($[\text{M}-\text{H}]^-$ m/z 226) ^a	227	1.58	1.48	1.36	
2,4,6-TNT ($[\text{M}-\text{OH}]^-$ m/z 210) ^a	227	1.53			
2,4,6-TNT ($[\text{M}-\text{NO}]^-$ m/z 197) ^a	227	1.64	1.53	1.42	1.36

^aSolvent is ACN.^bNebulizer gas is air.^cDimer.^dProbably ¹³C isotope peak of the m/z 226 ion.

of $1.53 \text{ cm}^2/\text{Vs}$ at room temperature and in a nitrogen atmosphere (Fig. 3(A)). Typically, two minor peaks with mobilities of 1.14 and $1.63 \text{ cm}^2/\text{Vs}$ were also seen. The mobility peak of $1.63 \text{ cm}^2/\text{Vs}$ is probably due to an oxygen insertion ion $[\text{M}-\text{H}+\text{O}]^-$ at m/z 165, since the intensity of this peak increased in the mass spectrum and the abundance of this mobility peak in the mobility spectrum also increased when air instead of nitrogen was used as the nebulizer gas (Fig. 3(B)). The fact that the oxygen insertion ion drifts faster than the main peak of 2-*t*BPh indicates that the main peak has an adduct, e.g. O_2 or NO_x , attached to the analyte or that the oxygen insertion ion interacts less with the drift gas due to its structure, i.e. a possible internal hydrogen bond between the OH group and the negatively charged oxygen atom in the ortho position, than the $[\text{M}-\text{H}]^-$ ion. Oxygen and chloride adduct formation has been reported previously for fluorinated phenols.²⁸ The peak with a mobility of $1.14 \text{ cm}^2/\text{Vs}$ is

probably due to dimer formation. A dimer peak, $[\text{2M}-\text{H}]^-$ at m/z 299, was observed in a mass spectrum measured with a sample concentration about 100 times greater, and a relatively wide mobility peak was observed in about the same position in the mass-selected mobility spectrum measured using the ion m/z 149 at this higher concentration. It was also observed that the reduced mobility of the major peak of 2-*t*BPh, the $[\text{M}-\text{H}]^-$ ion at m/z 149, remained stable within experimental error when the temperature was increased from 296 to 335 K.

2,6-Di-*tert*-butylphenol (2,6-D*t*BPh), 2,6-di-*tert*-butyl-4-methylphenol (2,6-D*t*B-4-MPh) and 2,4,6-tri-*tert*-butylphenol (2,4,6-T*t*BPh)

The mass-selected $[\text{M}-\text{H}]^-$ ion mobility spectra of all these compounds, measured at room temperature and in a nitrogen atmosphere, look remarkably similar; typically

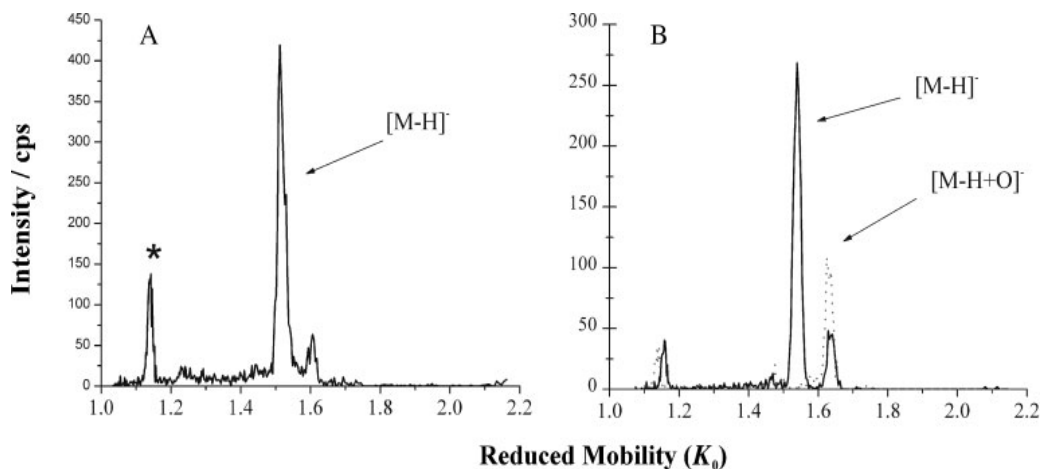


Figure 3. Negative ion APCI mass-selected ion mobility spectra of 2-*tert*-butylphenol. The gas-phase concentration of 2-*t*BPh was about 2 ppb; the sample was dissolved in hexane and measurements were made at room temperature. Mass-selected mobility spectra of (A) the $[\text{M}-\text{H}]^-$ ion at m/z 149 in nitrogen atmosphere and (B) ions $[\text{M}-\text{H}]^-$ at m/z 149 (solid line) and $[\text{M}-\text{H}+\text{O}]^-$ at m/z 165 (dotted line) in air (80% N_2 , 20% O_2). A dimer peak (marked with an asterisk) with lower mobility is also observed.

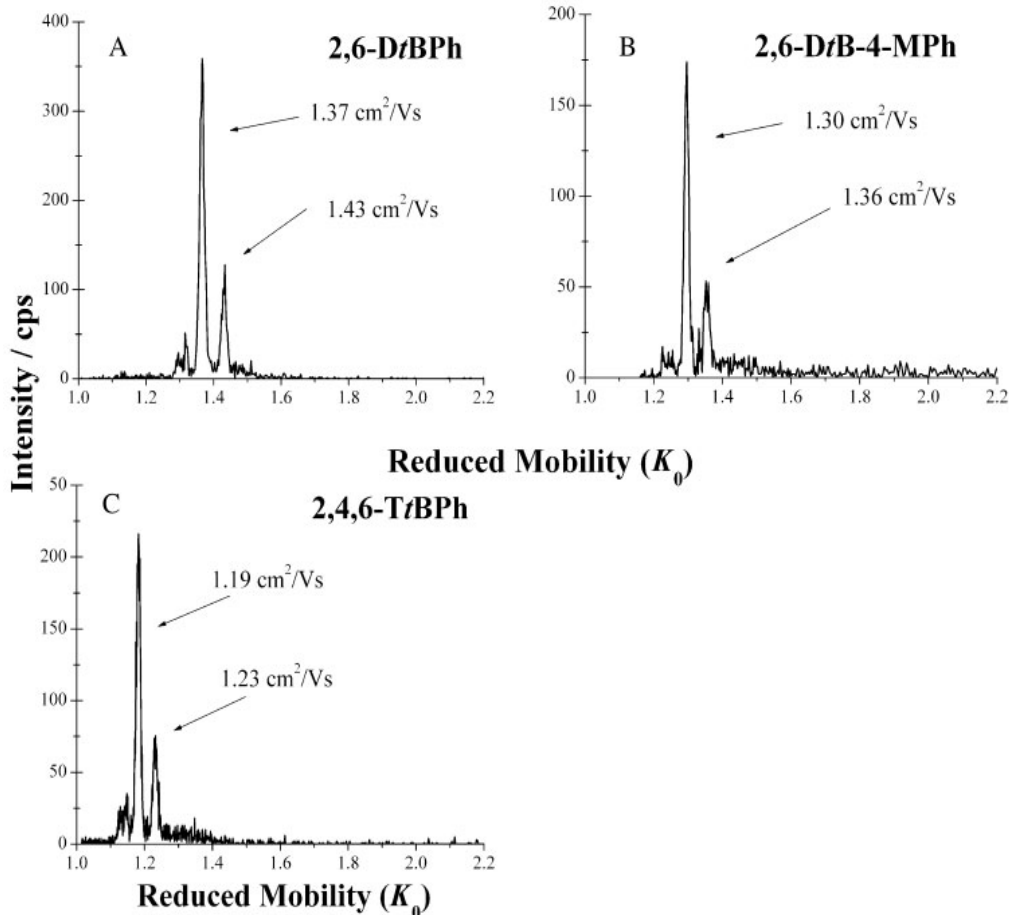


Figure 4. Negative ion APCI mass-selected ion mobility spectra for (A) the 2,6-DtBPh $[\text{M}-\text{H}]^-$ ion at m/z 205, (B) the 2,6-DtB-4-MPh $[\text{M}-\text{H}]^-$ ion at m/z 219, and (C) the 2,4,6-TtBPh $[\text{M}-\text{H}]^-$ ion at m/z 261. Gas-phase concentrations were between 1 and 2 ppb; samples were dissolved in hexane and measurements were made at room temperature in nitrogen atmosphere. The drift field was $308 \text{ cm}^2/\text{Vs}$.

two major peaks and sometimes one or two minor peaks (Fig. 4 and Table 1). The peak intensities changed somewhat between the different measurements, probably due to slight changes in the measuring conditions, but the absolute reduced mobilities were stable within experimental error. The multiple peaks are most likely due to different adduct ions formed, for example, with O_2 and NO_x . Due to the similarity of the ion mobility spectra the effect of temperature was studied in more detail for 2,6-DtB-4-MPh and 2,4,6-TtBPh. When the temperature was increased for 2,6-DtB-4-MPh (Fig. 5) the relative abundance of the first peak increased. This is an indication that at least the lower mobility peaks are due to adducts. Eiceman *et al.* have also reported that, at higher temperatures, adduct peaks decrease in height or disappear.²⁸ Similar behavior was also observed in our study for 2,4,6-TtBPh.

As expected, the mobilities of these compounds remained stable in the different drift fields of 270 and 344 V/cm. This is in agreement with earlier studies where varying the drift

field had a negligible effect on the mobilities of sterically hindered molecules.^{37,46} In addition, changing the nebulizer gas to air (80% N_2 , 20% O_2) was tested with 2,6-DtB-4-MPh and it did not affect the mobility of the $[\text{M}-\text{H}]^-$ ion.

2,6-Di-tert-butylphenol (2,6-DtBPh) and 2,4-di-tert-butylphenol (2,4-DtBPh)

The $[\text{M}-\text{H}]^-$ ion of these isomeric compounds had clearly different reduced mobilities (Table 1). The mass-selected ion mobility spectrum of the $[\text{M}-\text{H}]^-$ ion at m/z 205 of 2,4-DtBPh typically showed one large peak with a reduced mobility of $1.29 \text{ cm}^2/\text{Vs}$ and a smaller peak with a higher mobility of $1.34 \text{ cm}^2/\text{Vs}$, whereas the main peaks of the $[\text{M}-\text{H}]^-$ ion of 2,6-DtBPh had K_0 values of 1.43 and $1.37 \text{ cm}^2/\text{Vs}$. One explanation for the clearly different mobilities could be that the charge is more exposed to interactions in the 2,4-DtBPh than in 2,6-DtBPh. A similar explanation has been suggested to explain why the mobilities of acetate monomers are lower than those of acetate dimers with the same mass.⁴⁷

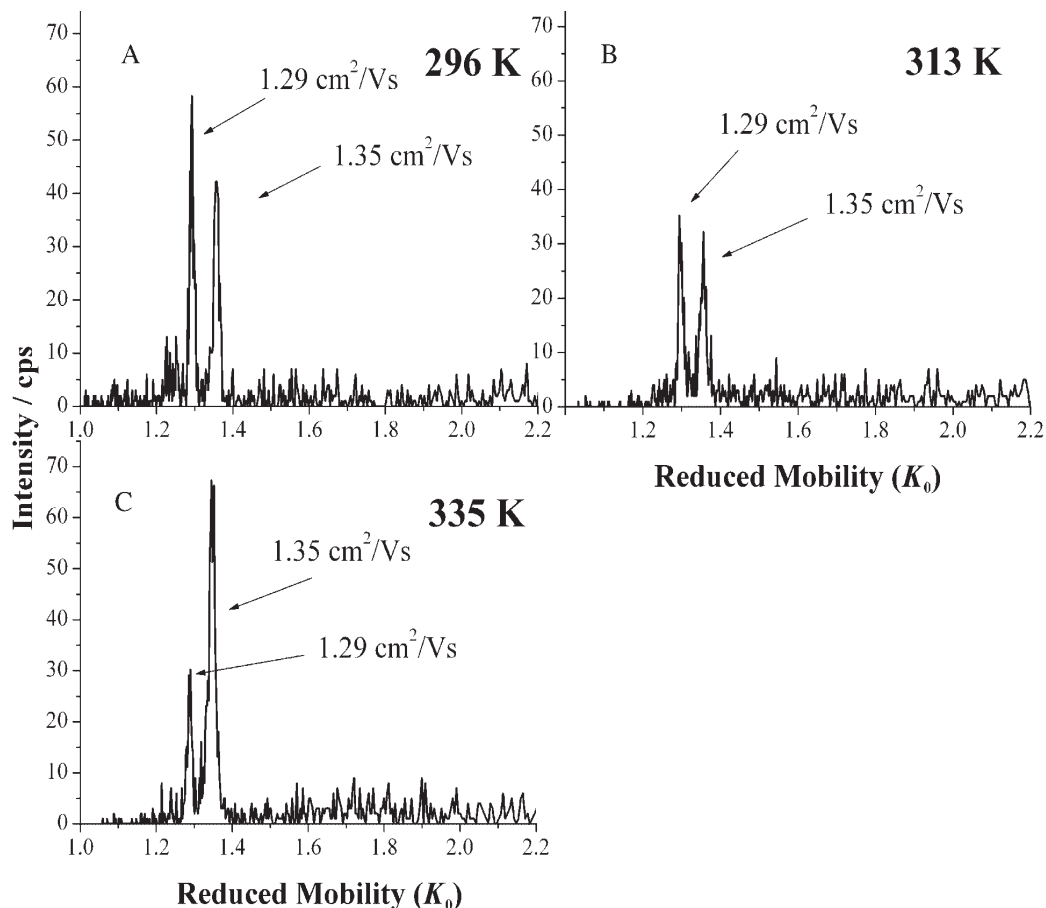


Figure 5. Negative ion APCI mass-selected ion mobility spectra of 2,6-di-*tert*-butyl-4-methylphenol $[M-H]^-$ ion at m/z 219. Gas-phase concentrations were 2 ppb; samples were dissolved in hexane and measurements were made at (A) 296, (B) 313, and (C) 335 K in nitrogen atmosphere. The drift field was $270 \text{ cm}^2/\text{Vs}$.

2,4,6-Trinitrotoluene (2,4,6-TNT)

For 2,4,6-TNT mass-selected mobility spectra were measured for the main ions m/z 226 and 197, and some other interesting ions m/z 227, 210 and 243 seen in the mass spectra (Table 1). The mobility spectra of the ions m/z 227, 226 and 197 showed multiple peaks with varying intensities, but typically there were one or two more intense peaks. The first peak of the $[M-NO]^-$ ion at m/z 197, $K_0 = 1.64 \text{ cm}^2/\text{Vs}$, has higher mobility than the first peak of the $[M-H]^-$ ion at m/z 226 with a mobility of $1.58 \text{ cm}^2/\text{Vs}$. Other ions did not produce peaks at these mobility values, except for a mobility peak for the ion m/z 227 which also had a K_0 of $1.58 \text{ cm}^2/\text{Vs}$, but based on its intensity it is probably the isotope peak of the m/z 226 ion. The mobility difference between these peaks could be due to the mass difference of these ions. The second peak of the ions m/z 197 and 227 has a mobility value of $K_0 = 1.53 \text{ cm}^2/\text{Vs}$ and a peak in the mass-selected mobility spectra of the ions m/z 210 and 243 with the same mobility can also be seen (Table 1). This could indicate that all the species with $K_0 = 1.53 \text{ cm}^2/\text{Vs}$ are formed at least partly from the one precursor ion, i.e. the oxygen adduct ion $[M+O]^-$ ion at m/z 243, which fragments after IMS separation. However, formation of this mobility peak due to the presence of an intact molecular anion or its

fragmentation to m/z 197 and 210 could also be possible. Similarly to what was reported previously,⁹ it was observed that the radical ion $[M]^-$ at m/z 227 of 2,4,6-TNT drifts more slowly than the $[M-H]^-$ ion at m/z 226 (Table 1). In our study the peaks with a K_0 of less than $1.50 \text{ cm}^2/\text{Vs}$ are probably due to various adducts, as their intensities decrease when the temperature is elevated to 335 K (Fig. 6).

Mobility standard

One of the goals of this study was to find out if phenolic compounds with protective *tert*-butyl groups could be used as mobility standards in negative ion mode IMS, in the same way as 2,6-di-*tert*-butylpyridine (2,6-DtBPyr), which has been used as a mobility standard for positive mode IMS.³⁷ A mobility standard is needed since differences in drift tube designs and measuring conditions lead to varying absolute reduced mobilities. An ideal standard for IMS has a constant reduced mobility over a wide range of temperatures and, in different drift fields, has a low tendency to form clusters or dimers, can be ionized with various atmospheric pressure ionizations methods and is safe to use.⁴⁸ 2,6-DtBPyr tetraalkylammonium halides (TAAH) have been identified as mobility standards for positive mode ESI-IMS⁴⁶ and also

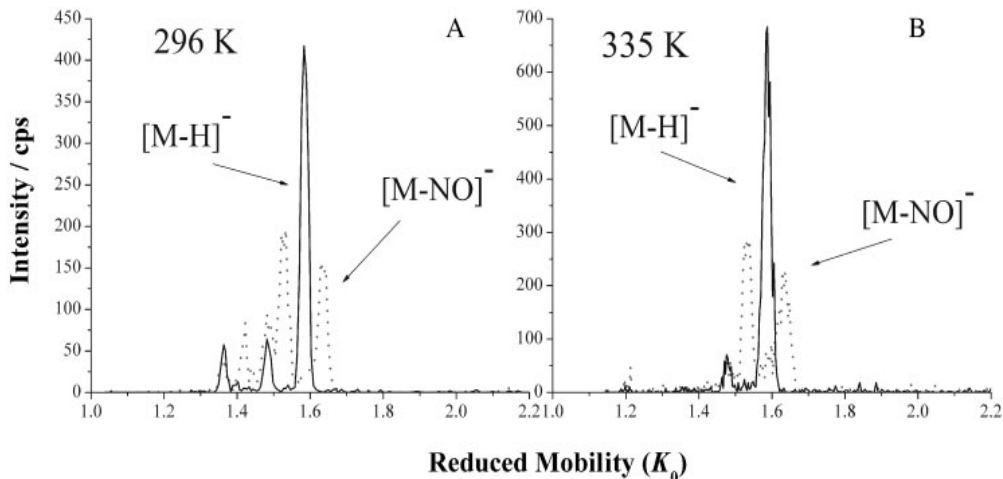


Figure 6. Negative ion APCI mass-selected ion mobility spectra of 2,4,6-trinitrotoluene. Gas-phase concentration was 1 ppb; samples were dissolved in acetonitrile and measurements were made in nitrogen atmosphere: (A) the $[M-NO]^-$ ion at m/z 197 (dotted line) and the $[M-H]^-$ ion at m/z 226 (solid line) at room temperature (296 K); (B) the same ions monitored at 335 K. The drift field was $308 \text{ cm}^2/\text{Vs}$.

suggested for use as standards for aerosol instruments.⁴⁹ In addition, 2,6-DtBPyr has been used to measure effective length of different drift tubes.⁵⁰ In negative ion mode IMS, 2,4,6-TNT has been used as a mobility standard.³¹

Our study indicates good reproducibility of the measured reduced mobilities in the conditions reported for 2,6-DtBPyr, 2,6-DtB-4-MPh and 2,4,6-TtBPyr. These compounds could be used as standards because they are easily available, inexpensive and safe to use. They should, however, be further tested using various instruments/measurement conditions and also other ionization methods before a final conclusion about their suitability as general mobility standards can be reached. 2,4,6-TNT also shows suitable behavior for use as a mobility standard. Compared with 2,4,6-TNT the main advantage of the phenols is that they produce less fragmentation under negative APCI and thereby simpler gas-phase chemistry and ion mobility spectra. Furthermore, the phenols have the advantage of being part of a homologous series which means that it is possible to tune the reduced mobility to avoid coeluting peaks and to tune the mass to avoid isobaric overlap.

CONCLUSIONS

The behavior of selected phenols and 2,4,6-TNT in negative corona discharge APCI-IMS was investigated. In our study, reduced mobilities of the main peaks of the $[M-H]^-$ ions of all the phenolic compounds are smaller than for the $[M-H]^-$ m/z 226 ion of 2,4,6-TNT, although the masses of some of the phenols are less than that of 2,4,6-TNT. These compounds are from different chemical families, and therefore they can interact differently with the drift gas, so that different reduced mobilities are observed.³ The mass-selected mobility spectrum of the $[M-H]^-$ ion of 2-tBPyr produced one major peak. When air was used as a nebulizer gas, a mobility peak due to an oxygen insertion ion $[M-H+O]^-$ was also

clearly seen. This species had a shorter drift time than the main peak of the $[M-H]^-$ ion of 2-tBPyr, indicating that the main peak may have an adduct present or that the interactions with drift gas differ. Interestingly, the two isomeric compounds 2,4-DtBPyr and 2,6-DtBPyr were clearly separated by IMS. Three of the phenols, namely 2,6-DtBPyr, 2,6-DtB-4-MPh and 2,4,6-TtBPyr, behaved very similarly, typically producing two major mobility peaks in the mass-selected mobility spectra measured for the $[M-H]^-$ ion under different conditions. This study suggests that these three phenols could be used as standards in addition to 2,4,6-TNT, but further characterization studies are required.

Acknowledgements

The Academy of Finland is thanked for their financial support. Victor Teplov is gratefully acknowledged for building the home-made nebulizer. Dr. Reno DeBono from Smith Detection is thanked for discussions regarding chemical standards. Thanks are given to Dr. Timo Mauriala for stimulating conversations. Dr. Raimo Timonen is acknowledged for discussions regarding reaction ion kinetics. The authors also acknowledge the Division of Atmospheric Sciences and Geophysics of University of Helsinki for the pressure data.

REFERENCES

1. Eiceman GA, Karpas Z. *Ion Mobility Spectrometry*. CRC Press Taylor & Francis: Boca Raton, 2005; 350.
2. Spangler GE. *Int. J. Mass Spectrom.* 2002; **220**: 399.
3. Mason EA. *Plasma Chromatography*. Plenum: New York, 1984; 259.
4. Eiceman GA, Sowa S, Lin S, Bell SE. *J. Hazard. Mater.* 1995; **43**: 13.
5. Kanu AB, Hill HH Jr, Gribb MM, Walters RN. *J. Environ. Monit.* 2007; **9**: 51.
6. Eiceman GA, Leasure CS, Vandiver VJ. *Anal. Chem.* 1986; **58**: 76.
7. Steiner WE, English WA, Hill HH Jr. *Jr. Anal. Chim. Acta* 2005; **532**: 37.
8. Matz LM, Tornatore PS, Hill HH. *Talanta* 2001; **54**: 171.

9. Spangler GE, Lawless PA. *Anal. Chem.* 1978; **50**: 884.
10. Ewing RG, Atkinson DA, Eiceman GA, Ewing GJ. *Talanta* 2001; **54**: 515.
11. Wu C, Hill HH, Rasulev UK, Nazarov EG. *Anal. Chem.* 1999; **71**: 273.
12. Tuovinen K, Kolehmainen M, Paakkanen H. *Anal. Chim. Acta* 2001; **429**: 257.
13. Jafari MT. *Talanta* 2006; **69**: 1054.
14. Spall WD, Mehlin K. IMS detection of chemical markers in petroleum products. *US Patent* 2004; 10/354,243: 3.
15. Matz LM, Hill HH Jr. *Anal. Chem.* 2001; **73**: 1664.
16. Valentine SJ, Counterman AE, Clemmer DE. *J. Am. Soc. Mass Spectrom.* 1999; **10**: 1188.
17. Tao L, McLean JR, McLean JA, Russell DH. *J. Am. Soc. Mass Spectrom.* 2007; **18**: 1232.
18. Johnson PV, Beegle LW, Kim HI, Eiceman GA, Kanik I. *Int. J. Mass Spectrom.* 2007; **262**: 1.
19. Carr TW. *Anal. Chem.* 1979; **51**: 705.
20. Spangler GE, Collins CI. *Anal. Chem.* 1975; **47**: 393.
21. Hill CA, Thomas CLP. *Analyst* 2003; **128**: 55.
22. Ross SK, Bell AJ. *Int. J. Mass Spectrom.* 2002; **218**: L1.
23. Waltman MJ, Dwivedi P, Hill HH Jr, Blanchard WC, Ewing RG. *Talanta* 2008; **77**: 249.
24. Eiceman GA, Shoff DB, Harden CS, Snyder AP, Martinez PM, Fleischer ME, Watkins ML. *Anal. Chem.* 1989; **61**: 1093.
25. Khayamian T, Tabrizchi M, Jafari MT. *Talanta* 2003; **59**: 327.
26. Daum KA, Atkinson DA, Ewing RG, Knighton WB, Grimsrud EP. *Talanta* 2001; **54**: 299.
27. Asbury RG, Klammeier J, Hill HH Jr. *Talanta* 2000; **50**: 1291.
28. Eiceman GA, Bergloff JF, Rodriguez JE, Munro W, Karpas Z. *J. Am. Soc. Mass Spectrom.* 1999; **10**: 1157.
29. Borsdorf H, Nazarov EG, Eiceman GA. *J. Am. Soc. Mass Spectrom.* 2002; **13**: 1078.
30. Tabrizchi M, Abedi A. *J. Phys. Chem. A* 2004; **108**: 6319.
31. Kanu AB, Hill HH Jr. *Talanta* 2007; **73**: 692.
32. Burton GW, Ingold KU. *J. Am. Chem. Soc.* 1981; **103**: 6472.
33. Hess MA, Haas MJ, Foglia TA, Marmer WN. *Energy Fuels* 2005; **19**: 1749.
34. Sysoev A, Adamov A, Viidanoja J, Ketola RA, Kostiaainen R, Kotiaho T. *Rapid Commun. Mass Spectrom.* 2004; **18**: 3131.
35. Bradbury NE, Nielsen RA. *Phys. Rev.* 1936; **49**: 388.
36. Tang X, Bruce JE, Hill HH Jr. *Rapid Commun. Mass Spectrom.* 2007; **21**: 1115.
37. Eiceman GA, Nazarov EG, Stone JA. *Anal. Chim. Acta* 2003; **493**: 185.
38. Thomas PCL, Rezgui ND, Kanu AB, Munro W. *Int. J. Ion Mobility Spectrom.* 2002; **5**: 31.
39. Steiner WE, English WA, Hill HH Jr. *J. Phys. Chem. A* 2006; **110**: 1836.
40. Chang J, Lawless PA, Yamamoto T. *IEEE Trans. Plasma Sci.* 1991; **19**: 1152.
41. Kukkonen J, Valkonen E, Walden J, Koskentalo T, Aarnio P, Karppinen A, Berkowicz R, Kartastenpää R. *Atmos. Environ.* 2001; **35**: 231.
42. Cody RB, Laramée JA. Atmospheric pressure ion source cross reference to related application. *US Patent*, WO 10/732205, 2004.
43. Ascenzi D, Franceschi P, Guella G, Tosi P. *J. Phys. Chem. A* 2006; **110**: 7841.
44. Evans CS, Sleeman R, Luke J, Keely BJ. *Rapid Commun. Mass Spectrom.* 2002; **16**: 1883.
45. Yinon J, McClellan JE, Yost RA. *Rapid Commun. Mass Spectrom.* 1997; **11**: 1961.
46. Viidanoja J, Sysoev A, Adamov A, Kotiaho T. *Rapid Commun. Mass Spectrom.* 2005; **19**: 3051.
47. Pedersen CS, Lauritsen FR, Sysoev A, Viitanen AK, Mäkelä JM, Adamov A, Laakia J, Mauriala T, Kotiaho T. *J. Am. Soc. Mass Spectrom.* 2008; **19**: 1361.
48. Kaur-Atwal G, O'Connor G, Aksenov A, Bocos-Bintintan V, Thomas CLP, Creaser C. *Int. J. Ion Mobility Spectrom.* 2009; **12**: 1.
49. Ude S, de la Mora JF. *J. Aerosol Sci.* 2005; **36**: 1224.
50. Viitanen AK, Mauriala T, Mattila T, Adamov A, Pedersen CS, Mäkelä JM, Marjamäki M, Sysoev A, Keskinen J, Kotiaho T. *Talanta* 2008; **76**: 1218.

Separation of Different Ion Structures in Atmospheric Pressure Photoionization-Ion Mobility Spectrometry-Mass Spectrometry (APPI-IMS-MS)

Jaakko Laakia,^a Alexey Adamov,^{a,b} Matti Jussila,^a Christian S. Pedersen,^c Alexey A. Sysoev,^{d,e} and Tapio Kotiaho^{a,b}

^a Laboratory of Analytical Chemistry, Department of Chemistry, University of Helsinki, Helsinki, Finland

^b Division of Pharmaceutical Chemistry, Faculty of Pharmacy, University of Helsinki, Helsinki, Finland

^c Department of Chemistry, University of Copenhagen, Copenhagen, Denmark

^d National Research Nuclear University MEPhI, Moscow, Russia

^e Linantec Ltd., Moscow, Russia

This study demonstrates how positive ion atmospheric pressure photoionization-ion mobility spectrometry-mass spectrometry (APPI-IMS-MS) can be used to produce different ionic forms of an analyte and how these can be separated. When hexane:toluene (9:1) is used as a solvent, 2,6-di-*tert*-butylpyridine (2,6-DtBPyr) and 2,6-di-*tert*-4-methylpyridine (2,6-DtB-4-MPyr) efficiently produce radical cations $[M]^{+\cdot}$ and protonated $[M + H]^+$ molecules, whereas, when the sample solvent is hexane, protonated molecules are mainly formed. Interestingly, radical cations drift slower in the drift tube than the protonated molecules. It was observed that an oxygen adduct ion, $[M + O_2]^{+\cdot}$, which was clearly seen in the mass spectra for hexane:toluene (9:1) solutions, shares the same mobility with radical cations, $[M]^{+\cdot}$. Therefore, the observed mobility order is most likely explained by oxygen adduct formation, i.e., the radical cation forming a heavier adduct. For pyridine and 2-*tert*-butylpyridine, only protonated molecules could be efficiently formed in the conditions used. For 1- and 2-naphthol it was observed that in hexane the protonated molecule typically had a higher intensity than the radical cation, whereas in hexane:toluene (9:1) the radical cation $[M]^{+\cdot}$ typically had a higher intensity than the protonated molecule $[M + H]^+$. Interestingly, the latter drifts slower than the radical cation $[M]^{+\cdot}$, which is the opposite of the drift pattern seen for 2,6-DtBPyr and 2,6-DtB-4-MPyr. (J Am Soc Mass Spectrom 2010, 21, 1565–1572) © 2010 American Society for Mass Spectrometry

In ion mobility spectrometry (IMS) ions move through an applied electric field in a drift gas flow [1]. Interactions between analyte ions and the drift gas result in a specific drift time for that ion, which is often converted to the reduced mobility (Formula 1) [1, 2]. Several general reviews of IMS exist [1, 3–8] and the theory behind drift tube ion mobility spectrometry has been presented in detail elsewhere [2, 9].

$$K_0 = \left(\frac{l_d^2}{t_d V} \right) \left(\frac{273}{T} \right) \left(\frac{P}{760} \right) \quad (1)$$

where l_d = length of the drift region, t_d = drift time of ion, V = voltage drop over the drift region, T = temperature, and P = pressure.

Address reprint requests to Mr. J. Laakia, Department of Chemistry, P.O. Box 55, FI-00014 University of Helsinki, Finland. E-mail: jaakko.laakia@helsinki.fi or Prof. Tapio Kotiaho, Faculty of Pharmacy, Division of Pharmaceutical Chemistry, P.O. Box 56 (Viikinkaari 5E), 00014 University of Helsinki, Finland and Laboratory of Analytical Chemistry, Department of Chemistry, A.I. Virtasen aukio 1 (P.O. Box 55), 00014 University of Helsinki, Finland. E-mail: tapio.kotiaho@helsinki.fi

The most common IMS devices are stand-alone instruments, which are commonly used to screen the environment for significant chemicals such as warfare agents, explosives, and illegal drugs [1, 10–12]. These devices are often tuned to detect certain chemicals; when more specific information is required, IMS is often combined with other instruments, for example with gas chromatography (GC-IMS) [4, 13]. Ion mobility spectrometry-mass spectrometry (IMS-MS) is also becoming more and more popular in various application fields, especially in bioanalysis [5]. Several different types of ion mobility spectrometers have been combined with mass spectrometers, e.g., drift tube IMS-MS [1, 5, 14], field asymmetric ion mobility spectrometry (FAIMS-MS) [5, 15–17], and also an aspiration IMS method has been combined with MS [18]. In bioanalysis, a common application of IMS-MS is structural studies of peptides and proteins [19–22]. Lately, it has also been shown that drift tube IMS-MS can be used, for example, to separate carbohydrate isomers [23] and enantiomers of model compounds [24, 25].

Ionization in ion mobility spectrometry is usually conducted with radioactive ionization (e.g., ⁶³Ni), how-

ever ionization techniques such as electrospray ionization (ESI) and atmospheric pressure chemical ionization (APCI) have also often been used [1, 5, 22, 26–29]. Atmospheric pressure photoionization (APPI) is an ionization technique that has shown its strength, especially in LC-MS during the past decade [30, 31]. However, APPI has already been used with IMS in 1980s [13]. An important advantage of APPI compared to ESI is that APPI is capable of ionizing less polar compounds [30, 32]. Together with drift tube ion mobility spectrometry, APPI has been used for example to detect alcohols [33] and toluene [34]. Borsdorf et al. have compared APPI with APCI and ^{63}Ni in the analysis of various aromatic compounds and terpenes and observed some variance in the mobility spectra depending on the ionization method [35–38]. Still, the number of publications with APPI-IMS is limited. In our group APPI-IMS has been used, for example, to measure mobility of 2,6-di-*tert*-butylpyridine (2,6-DtBPyr), which has been proposed for use as a mobility standard [39]. Interestingly, in some of these measurements, two different mobility peaks were observed using our high-resolution drift tubes. Preliminary mass-selected mobility measurements showed that one of the peaks was due to the $[\text{M}]^+$ ion of 2,6-DtBPyr and the other one due to the $[\text{M} + \text{H}]^+$ ion [40]. To further study this observation and possibility separate radical cations and protonated molecules of the same compound by IMS, a set of analytes was selected (Figure 1); the fact that depending on the ionization conditions radical cations or protonated molecules can be produced in APPI guided the selection [41–43]. The results of these studies and the reasons for the observed differences in mobilities of different ions of the model compounds are presented.

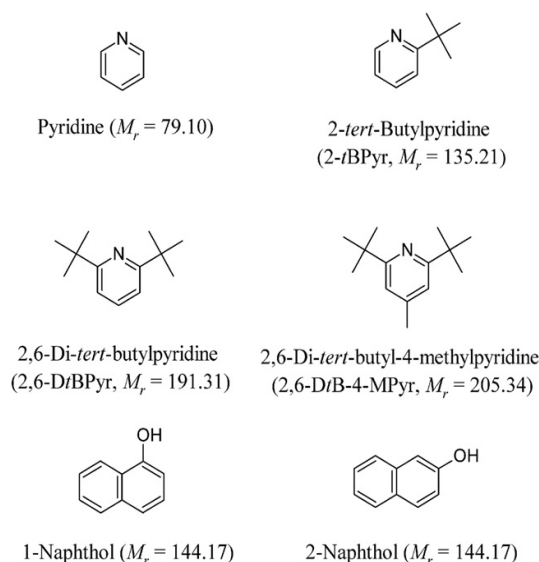


Figure 1. The structures of the compounds investigated in this study.

Experimental

Instrumentation

Two different drift tube IMS instruments were used in this study. Most of the measurements were done with the IMS-MS instrument described in more detailed previously [14]. In addition, some measurements were done with an ion mobility spectrometer-faraday plate detector (IMS-FP) instrument [44]. Briefly, in the IMS-MS instrument, the dual Bradbury-Nielsen (B-N) [45] gate cylinder drift tube is attached to a commercial triple-quadrupole mass spectrometer API-300 (SCIEX Applied Biosystems, Toronto, ON, Canada). These two B-N gates allow the selection of a mobility window [14, 46]. The gate opening time for both B-N gates was 300 μs . Nitrogen was used as the drift gas with a flow of ~ 2.4 L/min. The length of the drift region is 13.3 cm and voltage drop was set from 4.20 to 4.83 kV (from 316 to 363 V/cm), unless stated otherwise. Mass spectrometric parameters were typically a declustering potential from 20 to 30 V, unless otherwise stated, a focusing potential of 130 to 220 V, and an entrance potential of 5 to 10 V. Full scan mass spectra were usually collected in the range of m/z 30–300 in 1-s scan time, and sometimes with a range of m/z 50–500. Product ion mass spectra were measured in a mass range of m/z 30 to 200 or 300, and the collision energy varied from 15 to 40 V. Mass-selected ion mobility data were measured using the selected ion monitoring (SIM) mode of the instrument and the typical mobility spectrum measurement time was ~ 10 –15 min. The software used for data collection was Analyst 1.4.1 (Applied Biosystems/MDS SCIEX, Concord, ON, Canada). In the IMS-FP instrument, the total drift length is 13.85 cm and it was operated with one B-N gate with a gate opening time of 100 μs . The drift voltage was 5.24 kV, which equals 378 V/cm, and the nitrogen drift gas flow was set to 2.1 L/min. Data were collected by utilizing a custom-made program in a LabVIEW environment (National Instruments, Austin, TX, USA). Also, some data were transferred to a ChemStation rev. 10.02 (Agilent Technologies, Inc., Palo Alto, CA, USA) and further processed with custom-made macros. In this study, 2000 measurements were combined for the mobility spectra. A nitrogen delivery system, which produces 99.5% pure nitrogen gas from compressed air for drift and nebulizer gas, was described previously [14, 47, 48]. Experiments were conducted at room temperature and atmospheric pressure. Temperature was measured with a thermometer (Thermatag; Digitron Instrumentation Ltd., Torquay, England) which was attached to the nitrogen storage tank, and the pressure meter (Series 902; MKS Instrument, Andover, MA, USA) was located within the laboratory.

In both instruments, atmospheric pressure photoionization was carried out using a custom-made ion source in which a krypton discharge lamp is used (model PKS 100; Heraeus Noblelight, Cambridge, UK). It produces two energy packets, with 10 eV (main packet) and 10.6 eV,

which equal in wave lengths of 124 and 117 nm, respectively. Sample feeding to the ion source was carried out with a custom-made heated nebulizer, which was heated up to 573 K. Samples were injected into the nebulizer with a PHD 2000 Advanced Syringe Pump (Harvard Apparatus GmbH, Hugstetten, Germany). The nebulizer nitrogen gas flow was typically set at 1.6 to 1.8 L/min. In some measurements, a custom-made gas calibrator was used for sample introduction. In this system, analyte solutions are directly injected, without heating, into the nitrogen sample gas stream (1.9 L/min) using the syringe pump.

Chemicals

Chemicals used in the study were: *n*-hexane with a purity of >95% (POCH, SA, Gliwice, Poland), HPLC-grade toluene (Lab-Scan, Dublin, Ireland), *n*-pentane with a purity of >99% (Fluka, Steinheim, Germany), HPLC-gradient-grade methanol (J. T. Baker, Denver, Holland), pyridine with a purity of >99.5% (Merck, Darmstadt, Germany), 1-naphthol, 2-naphthol, 2-*tert*-butylpyridine (2-*t*BPyr), 2,6-di-*tert*-butylpyridine (2,6-D*t*BPyr) with a purity of >97% and 2,6-di-*tert*-butyl-4-methylpyridine (2,6-D*t*B-4-MPyr from Sigma-Aldrich, Steinheim, Germany) with a purity of >98%. All the chemicals were purchased and used as received. Solutions of 2,6-di-*tert*-butylpyridine, at two different concentrations, were made in the solvent to give 50 or 500 μM (IMS-FP measurements), which equals a gas-phase concentration of 2 or 20 ppb, respectively. Other compounds typically had solution concentrations of 50 or 100 μM , which equal gas-phase concentrations of about 1 to 10 ppb, depending on the compound concerned. Most of the solutions were prepared in hexane, or hexane:toluene (9:1). Only a few solutions were made in methanol:toluene (9:1), or pentane:toluene (9:1).

Results and Discussion

Atmospheric Pressure Photoionization (APPI)

One of the main points of the study was to select the APPI ionization conditions so that a radical cation and/or protonated molecule could be efficiently formed for the model compounds (Figure 1). All the pyridine compounds produced a protonated molecule $[\text{M} + \text{H}]^+$ in APPI when they were dissolved in hexane. Low level production of the $[\text{M}]^+$ ion was also observed for 2,6-D*t*BPyr and 2,6-D*t*B-4-MPyr in hexane (Figure 2a). However, when the sample solvent was hexane:toluene (9:1), radical cations were clearly observed for 2,6-D*t*BPyr and 2,6-D*t*B-4-MPyr (Figure 2b). In these conditions, pyridine and 2-*t*BPyr formed efficiently only the protonated molecule. A radical cation $[\text{M}]^{\cdot+}$ of toluene at m/z 92 was typically observed in the APPI mass spectra measured for samples in hexane:toluene (9:1). This is in good agreement with the results reported earlier [41]. The fact that the toluene radical

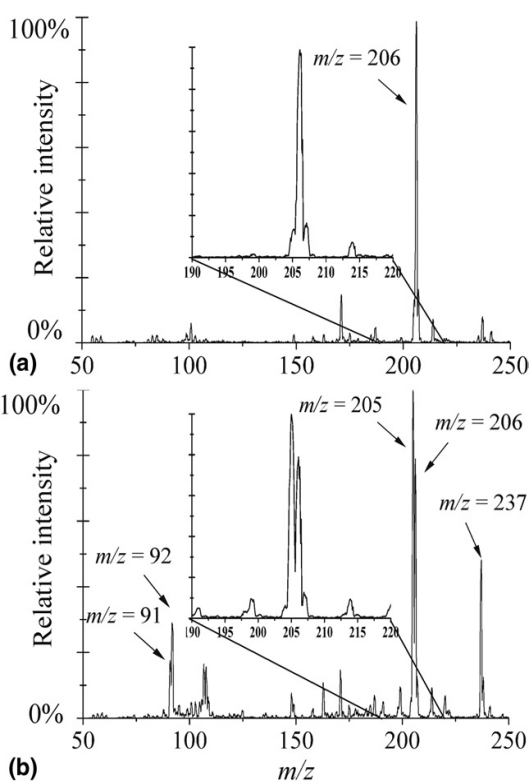


Figure 2. Positive ion APPI mass spectra of 2,6-D*t*B-4-MPyr, which have a gas-phase concentration of ~ 2 ppb. (a) The analyte is dissolved in hexane and (b) in hexane:toluene (9:1). The main peaks are the $[\text{M}]^+$ ion at m/z 205, $[\text{M} + \text{H}]^+$ at m/z 206, and $[\text{M} + \text{O}_2]^+$ at m/z 237. Toluene produces the ion $[\text{M} - \text{H}]^+$ at m/z 91 and radical cation $[\text{M}]^{\cdot+}$ at m/z 92. Declustering potential = 28 V.

cation is seen together with the analyte radical cation suggests that it is needed for effective formation of the $[\text{M}]^{\cdot+}$ ion.

For 2,6-D*t*BPyr and 2,6-D*t*B-4-MPyr, oxygen adduct $[\text{M} + \text{O}_2]^+$ ions at m/z 223 and 237, respectively, were observed in some of the APPI mass spectra, which turned out to be useful in explaining the mobility data (see the Mobilities of the Compounds section). For the samples dissolved in hexane:toluene (9:1) this ion was clearly observed (Figure 2b). Previously, O_2 adduct ions have been observed to be formed in positive APPI for benzene [49], for a β -distonic ion ($\text{C}_5\text{H}_5\text{N}^+-\text{CH}_2\text{C}_2\text{H}_2$) reacting with O_2 [50] and for distonic isomers of pyridine radical cation [51]. To confirm the structures of the oxygen adducts, their product ion mass spectra were measured and compared to product ion mass spectra of the radical cations and protonated molecules of 2,6-D*t*BPyr and 2,6-D*t*B-4-MPyr (Table 1). For both of the oxygen adducts oxygen (O_2) loss was observed and the other product ions seen in the mass spectrum were similar to the ones observed for the radical cation of the studied molecules. For both the radical cations and the protonated molecule of 2,6-D*t*BPyr and 2,6-D*t*B-4-MPyr, fragmentation of the side groups was observed. Product ion

Table 1. Product ion mass spectra of 2,6-di-*tert*-butylpyridine and 2,6-di-*tert*-butyl-4-methylpyridine with and without toluene in the sample solution

Compound	PI	Product ions, proposed cleaved species					CE	
2,6-DtBPyr in hexane	192	177 (70) (-CH ₃)	176 (100) (-CH ₄)	162 (70) (-C ₂ H ₆)	149 (10) (-C ₃ H ₇)	135 (10) (-C ₄ H ₉)	40	
	2,6-DtBPyr in hexane:toluene (9:1)	191	176 (40) (-CH ₃)	149 (100) (-C ₃ H ₆)			15	
2,6-DtB-4-MPyr in hexane	192	177 (70) (-CH ₃)	176 (100) (-CH ₄)	162 (70) (-C ₂ H ₆)	161 (20) (-C ₂ H ₇)	149 (20) (-C ₃ H ₇)	135 (20) (-C ₄ H ₉)	40
	223	191 (80) (-O ₂)	176 (30) (-O ₂ -CH ₃)	149 (100) (-O ₂ -C ₃ H ₆)				22
	206	191 (100) (-CH ₃)	190 (80) (-CH ₄)	176 (40) (-C ₂ H ₆)	163 (10) (-C ₃ H ₇)	149 (10) (-C ₄ H ₉)		38
2-DtB-4-MPyr in hexane:toluene (9:1)	205	204 (10) (-H)	190 (30) (-CH ₃)	163 (100) (-C ₃ H ₆)	149 (10) (-C ₄ H ₈)			15
	206	191 (100) (-CH ₃)	190 (80) (-CH ₄)	176 (50) (-C ₂ H ₆)	163 (20) (-C ₃ H ₇)	149 (10) (-C ₄ H ₉)		38
	237	205 (100) (-O ₂)	204 (20) (-O ₂ -H)	190 (30) (-O ₂ -CH ₃)	163 (100) (-O ₂ -C ₃ H ₆)			22

Relative abundances of product ions and the species lost are presented in brackets. Product ions with a relative abundance equal to or more than 10% are presented. All the analytes have a gas phase concentration of 2 to 4 ppb. PI = precursor ion (*m/z*); CE = collision energy (V).

spectra of the ions *m/z* 191 and 205 indicated that traces of oxygen adduct ion were sometimes observable in the product ion spectra. This further indicates that for the both radical cation species oxygen adduct formation is favorable.

1- and 2-naphthol behaved similarly in mass spectrometric analysis, and the APPI mass spectra measured for samples dissolved in hexane show both the radical cation [M]⁺ at *m/z* 144 and protonated molecule [M + H]⁺ at *m/z* 145 with varying relative intensities; typically, the [M + H]⁺ ion has a clearly higher intensity and the peak *m/z* 144 is relatively small. But when the samples are dissolved in hexane:toluene (9:1), the radical cation [M]⁺ at *m/z* 144 clearly has the higher intensity and a relatively small peak is seen at *m/z* 145. This is quite well in line with an earlier study where 2-naphthol in acetonitrile produced only the [M]⁺ ion at *m/z* 144 when the dopant was toluene or anisole [52], and when the solvent was hexane and toluene was dopant a small amount of the [M + H]⁺ ion at *m/z* 145 was produced along with the radical cation [41].

In addition to these two ions, which are most relevant for this study, an interesting ion-molecule reaction product ion with an additional 10 mass units compared with the [M + H]⁺ ion was observed at *m/z* 155 for both the naphthols. This ion was observed clearly when the [M + H]⁺ ion had a large intensity with a high declustering potential (80 V). At these conditions a small peak at *m/z* 127 was also seen in the APPI mass spectra, most likely formed via water loss from the protonated molecule. In the product ion mass spectrum of *m/z* 155, fragment ions *m/z* 127 and 145 are seen. Interestingly, the ion *m/z* 155 was also often observed in the product ion mass spectrum of *m/z* 145, where the ion *m/z* 127 is also observed. These findings suggest that the [M + H]⁺ ion, at *m/z* 145, loses water (M_r = 18) to form *m/z* 127, which reacts further, for example with CO (M_r = 28)

or other species capable of donating CO, to form ion [M + H - H₂O + CO]⁺ at *m/z* 155, a reaction which can also happen in reverse in the collision chamber. The origin of reacting neutral species could be trace impurities in the collision gas. The corresponding reaction product, i.e., removal of CO and addition of water, has recently been reported to occur for isoquinoline-3-carboxamides [53].

Mobilities of the Compounds

The mass-selected mobility data is summarized in Table 2, where the values are absolute reduced mobilities calculated using Formula 1. The behavior of the compounds is discussed below in more detail. Since 2,6-DtBPyr is proposed to be used as a mobility standard [39], the repeatability of the mobility measurements for it was looked into in more detail. The relative standard deviation of mass-selected reduced mobility for the [M + H]⁺ ion of 2,6-DtBPyr in hexane and with a gas-phase concentration of about 2 ppb was 0.7% (*n* = 13, K₀ = 1.49 cm²/Vs).

Pyridine

The mass-selected mobility spectrum of the pyridine [M + H]⁺ ion at *m/z* 80 shows two main peaks, K₀ = 2.04 and 1.69 cm²/Vs, when hexane is the solvent (Figure 3a). The latter mobility peak is expected to be due to a proton-bound dimer because its intensity increases when the gas-phase concentration of pyridine was doubled; even a dimer mass peak was not observed in a full scan mass spectrum. Symmetric proton-bound dimers are commonly formed under ambient conditions for a wide range of molecules: alcohols, ketones, ethers, acetates, aliphatic amines, and aromatic amines [54–56]. An additional reason for us to expect that the

Table 2. Summary of the reduced mobilities, K_0 (cm^2/Vs), measured with IMS-MS. Samples are dissolved in hexane or hexane:toluene (9:1) and typically the values are based on measurements made using both of the solvents. Typically the mobility values obtained with different solvents were the same within the experimental error. The numbers represent the peak numbers in decreasing mobility order as they appear in the mass-selected mobility spectra

Molecule	Mass (u)	1st (K_0)	2nd (K_0)	3rd (K_0)
Pyridine ($[\text{M} + \text{H}]^+$ m/z 80)	79	2.04	1.69 ^a	1.63 ^b
Pyridine ($[\text{M} + 91]^+$ m/z 170) ^b	79	1.64		
2-tBPyr ($[\text{M} + \text{H}]^+$ m/z 136)	135	1.73		
2,6-DtBPyr ($[\text{M}]^{+\cdot}$ m/z 191) ^b	191	1.45		
2,6-DtBPyr ($[\text{M} + \text{H}]^+$ m/z 192)	191	1.50	1.45 ^{b,c}	
2,6-DtBPyr ($[\text{M} + \text{O}_2]^{+\cdot}$ m/z 223) ^b	191	1.45		
2,6-DtB-4-MPyr ($[\text{M}]^{+\cdot}$ m/z 205) ^b	205	1.38		
2,6-DtB-4-MPyr ($[\text{M} + \text{H}]^+$ m/z 206)	205	1.42	1.38 ^{b,c}	
2,6-DtB-4-MPyr ($[\text{M} + \text{O}_2]^{+\cdot}$ m/z 237) ^b	205	1.39		
1-Naphthol ($[\text{M}]^{+\cdot}$ m/z 144)	144	1.72		
1-Naphthol ($[\text{M} + \text{H}]^+$ m/z 145)	144	1.68	1.50 ^d	1.32 ^d
1-Naphthol ($[\text{M} + \text{H} - \text{H}_2\text{O} + \text{CO}]^+$ m/z 155)	144	1.68		
2-Naphthol ($[\text{M}]^{+\cdot}$ m/z 144)	144	1.73		
2-Naphthol ($[\text{M} + \text{H}]^+$ m/z 145)	144	1.67	1.50 ^d	1.32 ^d
2-Naphthol ($[\text{M} + \text{H} - \text{H}_2\text{O} + \text{CO}]^+$ m/z 155)	144	1.67		

^aDimer.

^bPeaks observed only clearly in hexane:toluene (9:1).

^cMost likely ^{13}C isotope peak of the ion m/z 191 or 205.

^dMinor peaks that are observed sporadically.

second peak is a dimer peak is the observation that during one measurement day it was observed that the first peak changed relatively much, about 0.06 units, to lower mobility, but the second peak still had a mobility of $1.69 \text{ cm}^2/\text{Vs}$. We believe that the change could be due to sample solvent somehow “overloading” the drift tube on this one day, since the next day’s measurement of the mobility of the first peak was as expected. It has been reported that mobility of monomers can be more dependent on measuring conditions than dimers [57]. Interestingly, when hexane:toluene (9:1) is used, a new peak with a lower mobility, $K_0 = 1.63 \text{ cm}^2/\text{Vs}$, appears while measuring mass-selected mobility of the ion m/z 80 (Figure 3b). This mobility peak is most likely due to some kind of pyridine adduct ion. It was also observed that an adduct ion m/z 170 produced a mobility peak with this same mobility, i.e., $K_0 = 1.63 \text{ cm}^2/\text{Vs}$. An ion m/z 170 was typically seen with low intensity in APPI mass spectra of pyridine measured from hexane:toluene (9:1) solution. Its product ion mass spectrum indicated the presence of a fragment ion m/z 91, which could mean that the ion m/z 170 is a benzyl cation adduct of pyridine $[\text{M} + 91]^+$. The presence of some other product ions was also indicated (e.g., m/z 78 and 80) but unfortunately the quality of the product ion spectrum was not very good. Identification of the structure of the ion m/z 170 is not possible without further measurements.

2-tert-Butylpyridine, 2,6-di-tert-Butylpyridine and 2,6-di-tert-butyl-4-Methylpyridine

The mass-selected mobility spectra of 2-tBPyr measured for its $[\text{M} + \text{H}]^+$ ion produced one peak with a mobility of $K_0 = 1.73 \text{ cm}^2/\text{Vs}$ (Table 2) when the solvent was hexane or hexane:toluene (9:1). For 2,6-DtBPyr (Figure

4a and b) and 2,6-DtB-4-MPyr one clear mobility peak was observed in the mass-selected mobility spectra of the $[\text{M} + \text{H}]^+$ ion, with $K_0 = 1.50$ and $1.42 \text{ cm}^2/\text{Vs}$, respectively, whereas for the $[\text{M}]^{+\cdot}$ ions mobility peaks were observed at $K_0 = 1.45$ and $1.38 \text{ cm}^2/\text{Vs}$, respectively. Small mobility peaks were also observed at $K_0 = 1.45$ and $1.38 \text{ cm}^2/\text{Vs}$ for the $[\text{M} + \text{H}]^+$ ion of 2,6-DtBPyr and 2,6-DtB-4-MPyr, respectively, but it is expected that these are isotope peaks of ions m/z 191 and 205, respectively. Mass-selected mobility spectra of the $[\text{M} + \text{O}_2]^{+\cdot}$ ions of these two compounds produced mobility peaks with corresponding mobilities as measured for their $[\text{M}]^{+\cdot}$ ions (Table 2). Some mobility measurements were also done for 2,6-DtBPyr using the IMS-FP instrument and APPI. Two mobility peaks were observed when the sample solvent was either hexane:toluene (Figure 5) or pentane:toluene, with mobilities of $K_0 = 1.47$ and $1.42 \text{ cm}^2/\text{Vs}$ and $K_0 = 1.46$ and $1.42 \text{ cm}^2/\text{Vs}$, respectively. A reaction ion peak was also observed. However, when the sample solvent was methanol:toluene (9:1) only one mobility peak, at $K_0 = 1.46 \text{ cm}^2/\text{Vs}$, was seen. The small difference in reduced mobility between these two instruments was examined previously and it could be corrected by adjusting the mobility scale [58].

Interestingly, for both 2,6-DtBPyr and 2,6-DtB-4-MPyr the radical cation has a lower mobility than the protonated molecule. It is most likely that 2,6-DtBPyr and 2,6-DtB-4-MPyr form oxygen adducts $[\text{M} + \text{O}_2]^{+\cdot}$, causing slower drift time due to the increased mass. However, we could not entirely rule out the possibility that radical cations interact strongly with the residual oxygen in the drift gas and therefore drift slower. Borsdorf et al. have previously reported that protonated anilines have lower reduced mobilities than radical

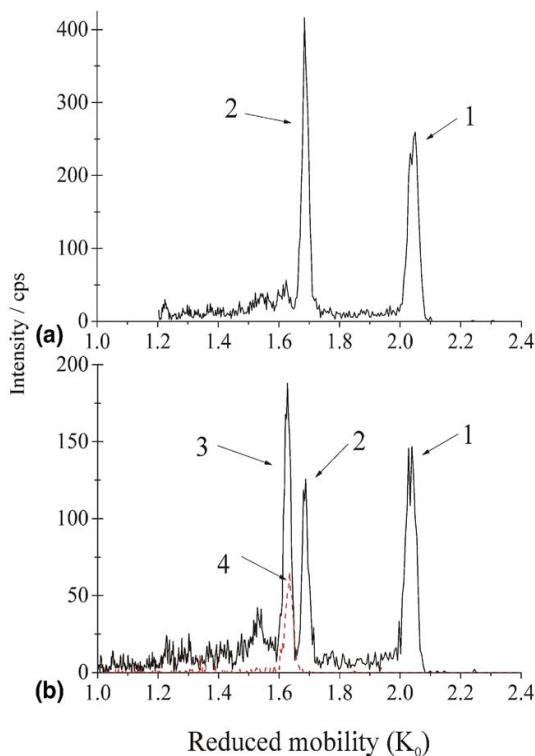


Figure 3. Positive ion APPI mass-selected ion mobility spectra of pyridine. (a) $[M + H]^+$ ion at m/z 80 (solid line); the gas-phase concentration is ~ 10 ppb and the sample is dissolved in hexane. (b) $[M + H]^+$ ion at m/z 80 (solid line) and $[M + 91]^+$ ion at m/z 170 (dotted line); the gas-phase concentration is ~ 5 ppb and the sample is dissolved in hexane:toluene (9:1). Peaks are: (1) monomer ion with $K_0 = 2.04$ cm^2/Vs , (2) dimer ion with $K_0 = 1.69$ cm^2/Vs , (3) and (4) adduct ion with mobilities of $K_0 = 1.63$ and 1.64 cm^2/Vs for ions at m/z 80 and 170, respectively.

cations [38], which is the opposite of our case. The explanation given was that in the experimental conditions used, protonated anilines interact significantly more with water in the drift tube than the radical cations. Due to this, protonated anilines are heavier and drift slower than radical cations. The solvation and clustering of protonated amines and pyridines has been studied by Meot-Ner et al. with NBS pulsed high-pressure mass spectrometer [59], the results of which suggest that steric effects cause unfavorable entropy effects for hydration of protonated 2,6-DtBPyr [59]. Based on this, we are expecting that protonated 2,6-DtBPyr and 2,6-DtB-4-MPyr do not interact strongly with water in the drift tube. Formation of an oxygen adduct $[M + O_2]^+$ was not observed for pyridine and 2-tBPyr. This could mean that both of the *tert*-butyl groups are needed to “lock” the oxygen atom together with ionized 2,6-DtBPyr and 2,6-DtB-4-MPyr to form a stable adduct. Also, it is clear based on the data that radical cations are needed for oxygen adduct formation, and the data show that formation of radical cations for pyridine and 2-tBPyr is not very favorable in the

conditions used. We could not find ionization energies (IE) for the *tert*-butyl substituted pyridines, but we are expecting that formation of a radical cation via charge-transfer from a toluene radical cation is favorable only for 2,6-DtBPyr and 2,6-DtB-4-MPyr, so that the IE of toluene (IE = 8.828 eV) is higher than that of these two pyridines. This estimation is based on literature values for pyridine, 2-methylpyridine, and 2,6-dimethylpyridine, which have ionization energies of IE = 9.26 eV, 9.2 eV (range given is 9.02–9.4) and 8.86 eV, respectively [60].

Note that 2,6-DtBPyr is used as a mobility standard [61] by some research groups [39, 58, 62]. It can be used for calibration if one makes sure, by selecting appropriate ionization conditions, that the mobility of the protonated molecule is measured.

1- and 2-Naphthol

These two isomeric compounds produced within experimental error the same mobility values for their radical cations and protonated molecules (Table 2). Mass-selected mobilities of the radical cation and protonated molecule of 1-naphthol measured for a sample in hex-

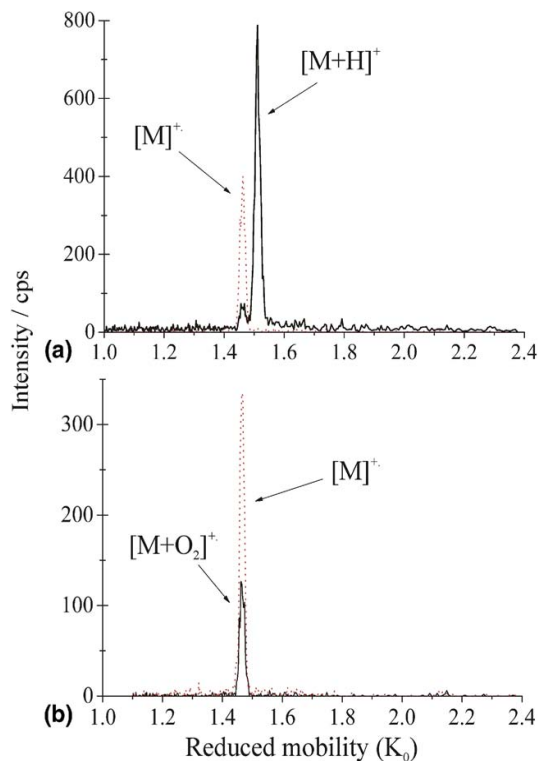


Figure 4. Positive ion APPI mass-selected mobility spectra of 2,6-DtBPyr. The gas-phase concentration is ~ 2 ppb and the sample is dissolved in hexane:toluene (9:1). (a) Ion $[M]^+$ at m/z 191 (dotted line) has a $K_0 = 1.45$ cm^2/Vs and ion $[M + H]^+$ at m/z 192 (solid line) has a $K_0 = 1.49$ cm^2/Vs . (b) Both ions $[M]^+$ at m/z 191 (dotted line) and $[M + O_2]^+$ at m/z 223 (solid line) have the same mobility, $K_0 = 1.45$ cm^2/Vs .

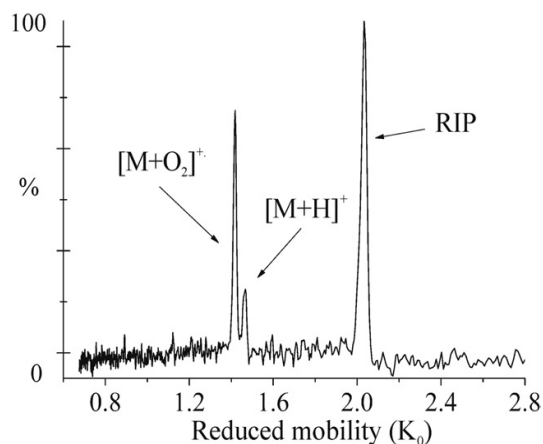


Figure 5. Positive ion APPI ion mobility spectrum of 2,6-DtBPyR measured with IMS-Faraday plate detector. The gas-phase concentration is ~20 ppb and the sample is dissolved in hexane:toluene (9:1). The reduced mobilities of peaks $[M + H]^+$ and $[M + O_2]^+$ are 1.47 and 1.42 cm^2/Vs , respectively. Analyte peak identification is based on IMS-MS data. RIP = reaction ion peak.

ane were $K_0 = 1.72 \text{ cm}^2/\text{Vs}$ and $K_0 = 1.68 \text{ cm}^2/\text{Vs}$, respectively, whereas the corresponding values for 2-naphthol were $K_0 = 1.73 \text{ cm}^2/\text{Vs}$ and $K_0 = 1.67 \text{ cm}^2/\text{Vs}$. The mobilities of the radical cations for both compounds measured in hexane:toluene (9:1) were the same as in hexane, within experimental error. In these conditions the mass selected mobility measurement of the ion m/z 145 produced a small peak with the same mobility as measured for the ion m/z 144, most likely due to isotope effects. Minor peaks with lower mobilities are also sometimes observed for both compounds. Mobility of the ion molecule reaction product $[M + H - H_2O + CO]^+$ ion at m/z 155 has the same mobility for both compounds than their protonated molecules. Interestingly, the radical cation $[M]^+$ has a higher mobility than the protonated ion $[M + H]^+$, which is the opposite of what is observed for 2,6-DtBPyR and 2,6-DtB-4-MPyR. For 2,6-DtBPyR and 2,6-DtB-4-MPyR, the slower mobility of the radical cation was explained by its ability to form an oxygen adduct ion. In the case of 1- and 2-naphthol, no other than $[M + H - H_2O + CO]^+$ adduct ions were identified from the measured mass spectra. The most likely explanation for the observed mobility order of the $[M]^+$ and $[M + H]^+$ ions of 1- and 2-naphthol is the explanation given by Borsdorf et al. for anilines [38], i.e., protonated molecules interact more with the residual water in the drift gas than radical cations.

Conclusions

This study demonstrates how radical cations and protonated molecules can be produced and separated with APPI-IMS-MS. Under appropriate measurement conditions, 2,6-DtBPyR and 2,6-DtB-4-MPyR efficiently produced both radical cations $[M]^+$ and protonated $[M +$

$H]^+$ molecules. The radical cation $[M]^+$ was observed to have a longer drift time. Further mass spectrometry analysis also revealed the formation of the oxygen adduct ion $[M + O_2]^+$, which has the same mobility as the radical cation $[M]^+$. The formation of the oxygen adduct is likely to be dependent on the presence of two *tert*-butyl groups. In case of 1- and 2-naphthol, the radical cation $[M]^+$ has a higher mobility than the protonated $[M + H]^+$, which is opposite compared with 2,6-DtBPyR and 2,6-DtB-4-MPyR. For pyridine and 2-tB-Pyr, protonated molecules were the main ions observed and their mobilities are reported. Overall, these findings illustrated how high-resolution IMS is used to separate different ion structures of model compounds, and how MS is used to obtain more information about the different peaks observed with IMS.

Acknowledgments

The authors acknowledge support for this project by the Academy of Finland (project numbers:114132 and 122018). Jyrki Viidanoja is acknowledged for stimulating conversations. The authors also acknowledge Markus Haapala and Jari Yli-Kauhala from the Division of Pharmaceutical Chemistry of the University of Helsinki. Jaroslaw Puton from the Military University of Technology, Warsaw, Poland, Elina Kalenius from the Department of Chemistry, University of Eastern Finland, and Glenn Spangler are thanked for help.

References

- Eiceman, G. A.; Karpas, Z. *Ion Mobility Spectrometry*, 2nd ed.; CRC Press Taylor and Francis: Boca Raton, 2005; p. 350.
- Mason, E. A. *Ion Mobility: Its Role in Plasma Chromatography*. In *Plasma Chromatography*, Carr T. W., Eds.; Plenum: New York, 1984; p. 259.
- Creaser, C. S.; Griffiths, J. R.; Bramwell, C. J.; Noreen, S.; Hill, C. A.; Thomas, C. L. P. *Ion Mobility Spectrometry: A Review. Part 1. Structural Analysis by Mobility Measurement*. *Analyst* **2004**, *129*, 984–994.
- Kanu, A. B.; Hill, H. H. Jr. *Ion Mobility Spectrometry Detection for Gas Chromatography*. *J. Chromatogr. A* **2008**, *1177*, 12–27.
- Kanu, A. B.; Dwivedi, P.; Tam, M.; Matz, L.; Hill, H. H. Jr. *Ion Mobility-Mass Spectrometry*. *J. Mass Spectrom.* **2008**, *43*, 1–22.
- Baumbach, J. *Ion Mobility Spectrometry in Scientific Literature and in the International Journal for Ion Mobility Spectrometry (1998–2007)*. *Int. J. Ion Mobility Spectrom.* **2008**, *11*, 3–11.
- Borsdorf, H.; Eiceman, G. A. *Ion Mobility Spectrometry: Principles and Applications*. *Appl. Spectrosc. Rev.* **2006**, *41*, 323–375.
- Baumbach, J. *Process Analysis Using Ion Mobility Spectrometry*. *Anal. Bioanal. Chem.* **2006**, *384*, 1059–1070.
- Spangler, G. E. *Expanded Theory for the Resolving Power of a Linear Ion Mobility Spectrometer*. *Int. J. Mass Spectrom.* **2002**, *220*, 399–418.
- Tarver, E. *External Second Gate, Fourier Transform Ion Mobility Spectrometry: Parametric Optimization for Detection of Weapons of Mass Destruction*. *Sensors* **2004**, *4*, 1–13.
- Asbury, R. G.; Klammeier, J.; Hill, H. H. Jr. *Analysis of Explosives Using Electrospray Ionization/Ion Mobility Spectrometry (ESI/IMS)*. *Talanta* **2000**, *50*, 1291–1298.
- Kanu, A. B.; Hill, H. H. Jr. *Identity Confirmation of Drugs and Explosives in Ion Mobility Spectrometry using a Secondary Drift Gas*. *Talanta* **2007**, *73*, 692–699.
- Baim, M. A.; Eatherton, R. L.; Hill, H. H. Jr. *Ion Mobility Detector for Gas Chromatography with a Direct Photoionization Source*. *Anal. Chem.* **1983**, *55*, 1761–1766.
- Sysoev, A.; Adamov, A.; Viidanoja, J.; Ketola, R. A.; Kostianen, R.; Kotiaho, T. *Development of an Ion Mobility Spectrometer for use in an Atmospheric Pressure Ionization Ion Mobility spectrometer/mass Spectrometer Instrument for Fast Screening Analysis*. *Rapid Commun. Mass Spectrom.* **2004**, *18*, 3131–3139.
- Guevremont, R.; Thekkadath, G.; Hilton, C. K. *Compensation Voltage (CV) Peak Shapes Using a Domed FAIMS with the Inner Electrode Translated to Various Longitudinal Positions*. *J. Am. Soc. Mass Spectrom.* **2005**, *16*, 948–956.
- Sultan, J.; Gabryelski, W. *Structural Identification of Highly Polar Nontarget Contaminants in Drinking Water by ESI-FAIMS-Q-TOF-MS*. *Anal. Chem.* **2006**, *78*, 2905–2917.

17. Xia, Y.; Wu, S. T.; Jemal, M. LC-FAIMS-MS/MS for Quantification of a Peptide in Plasma and Evaluation of FAIMS Global Selectivity from Plasma Components. *Anal. Chem.* **2008**, *80*, 7137–7143.
18. Adamov, A.; Viidanoja, J.; Kärpänoja, E.; Paakkanen, H.; Ketola, R. A.; Kostiaainen, R.; Sysyov, A.; Kotiaho, T. Interfacing an Aspiration Ion Mobility Spectrometer to a Triple Quadrupole Mass Spectrometer. *Rev. Sci. Instrum.* **2007**, *78*, 044101–044105.
19. Henderson, S. C.; Valentine, S. J.; Counterman, A. E.; Clemmer, D. E. ESI/Ion Trap/Ion Mobility/Time-of-Flight Mass Spectrometry for Rapid and Sensitive Analysis of Biomolecular Mixtures. *Anal. Chem.* **1999**, *71*, 291–301.
20. Valentine, S. J.; Counterman, A. E.; Clemmer, D. E. A Database of 660 Peptide Ion Cross Sections: Use of Intrinsic Size Parameters for Bona Fide Predictions of Cross Sections. *J. Am. Soc. Mass Spectrom.* **1999**, *10*, 1188–1211.
21. Kaur-Atwal, G.; Weston, D. J.; Green, P. S.; Crosland, S.; Bonner, P. L. R.; Creaser, C. S. Analysis of Tryptic Peptides using Desorption Electrospray Ionization Combined with Ion Mobility spectrometry/mass Spectrometry. *Rapid Commun. Mass Spectrom.* **2007**, *21*, 1131–1138.
22. Merenbloom, S. I.; Koening, S. L.; Valentine, S. J.; Plasencia, M. D.; Clemmer, D. E. IMS-IMS and IMS-IMS-IMS/MS for Separating Peptide and Protein Fragment Ions. *Anal. Chem.* **2006**, *78*, 2802–2809.
23. Dwivedi, P.; Bendiak, B.; Clowers, B. H.; Hill, H. H. Jr. Rapid Resolution of Carbohydrate Isomers by Electrospray Ionization Ambient Pressure Ion Mobility Spectrometry-Time-of-Flight Mass Spectrometry (ESI-APIMS-TOFMS). *J. Am. Soc. Mass Spectrom.* **2007**, *18*, 1163–1175.
24. Dwivedi, P.; Wu, C.; Matz, L. M.; Clowers, B. H.; Siems, W. F.; Hill, H. H. Jr. Gas-Phase Chiral Separations by Ion Mobility Spectrometry. *Anal. Chem.* **2006**, *78*, 8200–8206.
25. Karas, M. Separation of Components of an Analysis Sample in an Ion Mobility Spectrometer Using a Supply of Selectively Interactive Gaseous Particles. *U.S. Patent* 2004, 0178340 A1.
26. Shumate, C. B.; Hill, H. H. Coronaspray Nebulization and Ionization of Liquid Samples for Ion Mobility Spectrometry. *Anal. Chem.* **1989**, *61*, 601–606.
27. Clowers, B. H.; Hill, H. H. Jr. Influence of Cation Adduction on the Separation Characteristics of Flavonoid Diglycoside Isomers Using Dual Gate-Ion Mobility-Quadrupole Ion Trap Mass Spectrometry. *J. Mass Spectrom.* **2006**, *41*, 339–351.
28. Ruotolo, B. T.; Giles, K.; Campuzano, I.; Sandercock, A. M.; Bateman, R. H.; Robinson, C. V. Evidence for Macromolecular Protein Rings in the Absence of Bulk Water. *Science* **2005**, *310*, 1658–1661.
29. Borsdorf, H.; Schelhorn, H.; Flachowsky, J.; Döring, H.; Stach, J. Corona Discharge Ion Mobility Spectrometry of Aliphatic and Aromatic Hydrocarbons. *Anal. Chim. Acta* **2000**, *403*, 235–242.
30. Robb, D. B.; Blades, M. W. State-of-the-Art in Atmospheric Pressure Photoionization for LC/MS. *Anal. Chim. Acta* **2008**, *627*, 34–49.
31. Raffaelli, A.; Saba, A. Atmospheric Pressure Photoionization Mass Spectrometry. *Mass Spectrom. Rev.* **2003**, *22*, 318–331.
32. Cai, S.-S.; Syage, J. A. Comparison of Atmospheric Pressure Photoionization, Atmospheric Pressure Chemical Ionization, and Electrospray Ionization Mass Spectrometry for Analysis of Lipids. *Anal. Chem.* **2006**, *78*, 1191–1199.
33. Sielemann, S.; Baumbach, J. I.; Schmidt, H.; Pilzecker, P. Detection of Alcohols Using UV-Ion Mobility Spectrometers. *Anal. Chim. Acta* **2001**, *431*, 293–301.
34. Baumbach, J. I.; Sielemann, S.; Xie, Z.; Schmidt, H. Detection of the Gasoline Components Methyltert-Butyl Ether, Benzene, Toluene, and m-Xylene using Ion Mobility Spectrometers with a Radioactive and UV Ionization Source. *Anal. Chem.* **2003**, *75*, 1483–1490.
35. Borsdorf, H.; Rudolph, M. Gas-Phase Ion Mobility Studies of Constitutional Isomeric Hydrocarbons using Different Ionization Techniques. *Int. J. Mass Spectrom.* **2001**, *208*, 67–72.
36. Borsdorf, H.; Nazarov, E. G.; Eiceman, G. A. Atmospheric Pressure Ionization and Gas Phase Ion Mobility Studies of Isomeric Dihalogenated Benzenes using Different Ionization Techniques. *Int. J. Mass Spectrom.* **2004**, *232*, 117–126.
37. Borsdorf, H.; Stone, J. A.; Eiceman, G. A. Gas Phase Studies on Terpenes by Ion Mobility Spectrometry using Different Atmospheric Pressure Chemical Ionization Techniques. *Int. J. Mass Spectrom.* **2005**, *246*, 19–28.
38. Borsdorf, H.; Neitsch, K.; Eiceman, G. A.; Stone, J. A. A Comparison of the Ion Chemistry for Mono-Substituted Toluenes and Anilines by Three Methods of Atmospheric Pressure Ionization with Ion Mobility Spectrometry. *Talanta* **2009**, *78*, 1464–1475.
39. Eiceman, G. A.; Nazarov, E. G.; Stone, J. A. Chemical Standards in Ion Mobility Spectrometry. *Anal. Chim. Acta* **2003**, *493*, 185–194.
40. Laakia, J.; Adamov, A.; Jussila, M.; Pedersen, C. S.; Sysyov, A.; Kotiaho, T. Observation of Different Ion Structures in Ion Mobility Spectrometer with Photoionization (APPI). *Proceedings of the 17th Annual Conference on Ion Mobility Spectrometry*; (ISIMS 2008). Ottawa, Canada, July, 2008.
41. Kauppila, T. J.; Kuuranne, T.; Meurer, E. C.; Eberlin, M. N.; Kotiaho, T.; Kostiaainen, R. Atmospheric Pressure Photoionization Mass Spectrometry. Ionization Mechanism and the Effect of Solvent on the Ionization of Naphthalenes. *Anal. Chem.* **2002**, *74*, 5470–5479.
42. Syage, J. A. Mechanism of $[M + H]^+$ Formation in Photoionization Mass Spectrometry. *J. Am. Soc. Mass Spectrom.* **2004**, *15*, 1521–1533.
43. Robb, D. B.; Blades, M. W. Atmospheric Pressure Photoionization for Ionization of both Polar and Nonpolar Compounds in Reversed-Phase LC/MS. *Anal. Chem.* **2006**, *78*, 8162–8164.
44. Adamov, A.; Mauriala, T.; Teplov, V.; Laakia, J.; Pedersen, C. S.; Kotiaho, T.; Sysyov, A. Characterization of a High Resolution Drift Tube Ion Mobility Spectrometer with a Multi-Ion Source Platform. *Int. J. Mass Spectrom.* (Accepted). (doi:10.1016/j.jms.2010.02.008)
45. Bradbury, N. E.; Nielsen, R. A. Absolute Values of the Electron Mobility in Hydrogen. *Phys. Rev.* **1936**, *49*, 388–393.
46. Tang, X.; Bruce, J. E.; Hill, H. H. Jr. Design and Performance of an Atmospheric Pressure Ion Mobility Fourier Transform Ion Cyclotron Resonance Mass Spectrometer. *Rapid Commun. Mass Spectrom.* **2007**, *21*, 1115–1122.
47. Viidanoja, J.; Sysyov, A.; Adamov, A.; Kotiaho, T. Tetra-Alkylammonium Halides as Chemical Standards for Positive Electrospray Ionization with Ion Mobility spectrometry/mass Spectrometry. *Rapid Commun. Mass Spectrom.* **2005**, *19*, 3051–3055.
48. Laakia, J.; Pedersen, C. S.; Adamov, A.; Viidanoja, J.; Sysyov, A.; Kotiaho, T. Sterically Hindered Phenols in Negative Ion Mobility Spectrometry-Mass Spectrometry. *Rapid Commun. Mass Spectrom.* **2009**, *23*, 3069–3076.
49. Tubaro, M.; Marotta, M.; Seraglia, R.; Traldi, P. Atmospheric Pressure Photoionization Mechanisms. 2. The Case of Benzene and Toluene. *Rapid Commun. Mass Spectrom.* **2003**, *17*, 2423–2429.
50. Yu, S. J.; Holliman, C. L.; Rempel, D. L.; Gross, M. L. The β -Distonic Ion from the Reaction of Pyridine Radical Cation and Ethene: A Demonstration of High-Pressure Trapping in Fourier Transform Mass Spectrometry. *J. Am. Chem. Soc.* **1993**, *115*, 9676–9682.
51. Jobst, K. J.; De Winter, J.; Flammang, R.; Terlouw, J. K.; Gerbaux, P. Differentiation of the Pyridine Radical Cation from its Distonic Isomers by Ion-Molecule Reactions with Dioxide. *Int. J. Mass Spectrom.* **2009**, *286*, 83–88.
52. Kauppila, T.; Kostiaainen, R.; Bruins, A. P. Anisole, a New Dopant for Atmospheric Pressure Photoionization Mass Spectrometry of Low Proton Affinity, Low Ionization Energy Compounds. *Rapid Commun. Mass Spectrom.* **2004**, *18*, 808–815.
53. Beuck, S.; Schwabe, T.; Grimme, S.; Schlörer, N.; Kamber, M.; Schänzer, W.; Thevis, M. Unusual Mass Spectrometric Dissociation Pathway of Protonated Isoquinoline-3-Carboxamides due to Multiple Reversible Water Adduct Formation in the Gas Phase. *J. Am. Soc. Mass Spectrom.* **2009**, *20*, 2034–2048.
54. Ewing, R. G.; Eiceman, G. A.; Stone, J. A. Proton-Bound Cluster Ions in Ion Mobility Spectrometry. *Int. J. Mass Spectrom. Ion Process* **1999**, *193*, 57–68.
55. Pedersen, C. S.; Lauritsen, F. R.; Sysyov, A.; Viitanen, A. K.; Mäkelä, J. M.; Adamov, A.; Laakia, J.; Mauriala, T.; Kotiaho, T. Characterization of Proton-Bound Acetate Dimers in Ion Mobility Spectrometry. *J. Am. Soc. Mass Spectrom.* **2008**, *19*, 1361–1366.
56. Karpas, Z. Ion Mobility Spectrometry of Aliphatic and Aromatic Amines. *Anal. Chem.* **1989**, *61*, 684–689.
57. Putton, J. IMS in Quantitative Measurements, IMS Workshop 11.05.2009 in Mikkeli, Finland.
58. Viitanen, A. K.; Mauriala, T.; Mattila, T.; Adamov, A.; Pedersen, C. S.; Mäkelä, J. M.; Marjamäki, M.; Sysyov, A.; Keskinen, J.; Kotiaho, T. Adjusting Mobility Scales of Ion Mobility Spectrometers using 2,6-DtBP as a Reference Compound. *Talanta* **2008**, *76*, 1218–1223.
59. Meot-Ner, M.; Sieck, L. W. The Ionic Hydrogen Bond. 1. Sterically Hindered Bonds. Solvation and Clustering of Protonated Amines and Pyridines. *J. Am. Chem. Soc.* **1983**, *105*, 2956–2961.
60. NIST Chemistry WebBook. NIST Standard Reference Database Number 69 (<http://webbook.nist.gov/chemistry/>). **2008**.
61. Kaur-Atwal, G.; O'Connor, G.; Aksenov, A.; Bocos-Bintintan, V.; Paul Thomas, C.; Creaser, C. Chemical Standards for Ion Mobility Spectrometry: A Review. *Int. J. Ion Mobility Spectrom.* **2009**, *12*, 1–14.
62. Tadjimukhamedov, F.; Stone, J.; Papanastasiou, D.; Rodriguez, J.; Mueller, W.; Sukumar, H.; Eiceman, G. Liquid Chromatography/Electrospray Ionization/Ion Mobility Spectrometry of Chlorophenols with Full Flow from Large Bore LC Columns. *Int. J. Ion Mobility Spectrom.* **2008**, *11*, 51–60.



ELSEVIER

Contents lists available at ScienceDirect

Talanta

journal homepage: www.elsevier.com/locate/talanta

Short communication

Separation of isomeric amines with ion mobility spectrometry

Jaakko Laakia^{a,b,*}, Tiina J. Kauppila^c, Alexey Adamov^{b,c}, Alexey A. Sysoev^{d,e},
Tapio Kotiaho^{b,c}



^a Federal University of Rio de Janeiro, Department of Chemistry, LAGOA-LADETEC, Ilha do Fundão, Rio de Janeiro, RJ 21941-909, Brazil

^b Laboratory of Analytical Chemistry, Department of Chemistry, University of Helsinki, P.O. Box 55, FI-00014, Finland

^c Division of Pharmaceutical Chemistry and Technology, Faculty of Pharmacy, University of Helsinki, P.O. Box 56, FI-00014, Finland

^d National Research Nuclear University MEPhI, Kashirskoe shosse 31, 115409 Moscow, Russia

^e Linantec Ltd., Kashirskoe shosse 31, 115409 Moscow, Russia

ARTICLE INFO

Article history:

Received 14 August 2014

Received in revised form

21 October 2014

Accepted 24 October 2014

Available online 31 October 2014

Keywords:

Ion mobility spectrometry (IMS)

Atmospheric pressure chemical ionization

(APCI)

Atmospheric pressure photoionization

(APPI)

Isomeric amines

ABSTRACT

Eight selected isomeric amines were ionized using atmospheric pressure chemical ionization and atmospheric pressure photoionization producing a protonated molecule $[M+H]^+$ for each amine. The mobility of these ions was measured by ion mobility spectrometry. The amine compound class was shown to have an important role in mobility separation of the amines. 2,4,6-collidine, *N,N*-dimethylaniline and *N*-methyl-*o*-toluidine with highest observed mobilities have a *N*-heterocyclic aromatic ring, or are tertiary or secondary amines, respectively, whereas the rest of the compounds with lower mobilities were primary amines. It is suggested that the protonated $-NH_2$ group ($-NH_3^+$) interacts more with the drift gas, and therefore the primary amines have lower mobilities. The effect of the drift gas was tested by mixing argon or helium with the nitrogen drift gas. The presence of argon shifted the mobilities towards lower values, while with helium the mobility shifted towards higher values. However, in neither case did this result in better separation of the unresolved compounds.

© 2014 Elsevier B.V. All rights reserved.

1. Introduction

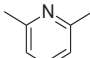
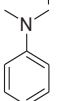
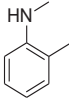
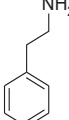
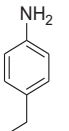
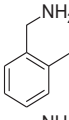
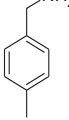
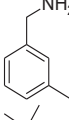
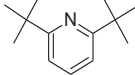
In ion mobility spectrometry (IMS) the analyte ions travel through a counter-flow drift gas in an electric field. The ions interact with the drift gas, which results in specific drift times for different ions. The analysis is commonly conducted at ambient pressure, which allows the construction of small portable IMS devices, which are widely used in field applications, for example, to detect explosives and warfare agents [1,2]. In the laboratory the IMS drift tube can be attached to a mass spectrometer (MS) [3,4]. This combination allows simultaneous access to mass and mobility data, for example to study different ionic structures of the same molecule [5,6], separating isomers of di-*tert*-butylphenol [7] or ovalbumin *N*-linked glycans [8] or distinguishing between different conformations of peptides [9].

Here, the main aim was to study the separation of isomeric amines ($M_r=121$, $C_8H_{11}N$, Table 1) with IMS in order to understand better how compound structure affects separation. In addition, it was investigated how the addition of helium and argon to the nitrogen drift gas affects the separation of these amines. This report completes the preliminary presentation of the results [10]. Some of the amines in our study, namely 4-ethylaniline [11], *N,N*-dimethylaniline [12,13] and 2,4,6-collidine [13–15], have been studied before with IMS, but the whole set of isomeric amines used in this study was not included to the compounds studied. The drift gas has a significant role in separating ions, and changes in drift gas polarizability and radius will result in different interaction with analyte ions, and can thus produce different drift times [14,16–18]. For the compounds studied here, the effect of the drift gas on the mobility has been studied earlier for 2,4,6-collidine by using nitrogen, air, helium, argon, carbon dioxide and sulfur hexafluoride as drift gases [14]. The drift gas studies include also for example the use of drift gases, such as nitrogen, helium, argon, and carbon dioxide for amines other than those studied here [14,17], as well as peptides [17], and cocaine and its metabolites, amphetamines and benzodiazepines [18]. Here, our aim was to investigate how the addition of different proportions of helium and argon to the nitrogen drift gas affects the separation of the model amines.

* Corresponding author at: Federal University of Rio de Janeiro, Department of Chemistry, LAGOA-LADETEC, Avenida Athos da Silveira Ramos, 149 - Centro de Tecnologia - Bloco A, Sala 603, Cidade Universitária, Ilha do Fundão, Rio de Janeiro, RJ 21941-909, Brazil. Tel.: +55 21 3938 7130/3938 7134; fax: +55 21 2260 3967/3938 7489.

E-mail addresses: laakia@iq.ufrj.br (J. Laakia), tapio.kotiaho@helsinki.fi (T. Kotiaho).

Table 1
Summary of the reduced mobility K_0 ($\text{cm}^2 \text{V}^{-1} \text{s}^{-1}$) values for the isomeric amines ($M_r=121$) and 2,6-di-*tert*-butylpyridine ($M_r=191$) measured with an IMS-FP instrument using nitrogen as the drift gas. Mobility values are not normalized with the mobility of 2,6-DtBPyr (average of eight measurements). The mobility values of amines are the average of four measurements; two within one day, which were then repeated on the second day.

Compound	Abbreviation	Structure	K_0 ($\text{cm}^2 \text{V}^{-1} \text{s}^{-1}$) APCI	K_0 ($\text{cm}^2 \text{V}^{-1} \text{s}^{-1}$) APPI
2,4,6-collidine ^a	2,4,6-Col		1.80	1.81
<i>N,N</i> -dimethylaniline ^a	<i>N,N</i> -DMA		1.75	1.75
<i>N</i> -methyl- <i>o</i> -toluidine ^a	<i>n</i> -M- <i>o</i> -T		1.70	1.69
2-phenethylamine ^b	PEA		1.62	1.62
4-ethylaniline ^b	4-EA		1.58	1.58
2-methylbenzylamine ^c	2-MBA		1.61	1.61
4-methylbenzylamine ^c	4-MBA		1.60	1.57
3-methylbenzylamine ^c	3-MBA		1.60	1.58
2,6-di- <i>tert</i> -butylpyridine ^d	2,6-DtBPyr		1.47	

^a Measured from Mix A.

^b Measured from Mix B.

^c Measured individually.

^d Measured from Mix B and Mix C.

2. Experimental section

2.1. Chemicals

The amines *N*-methyl-*o*-toluidine (> 95%), 2-methylbenzylamine (> 96%), 4-methylbenzylamine (> 97%), 3-methylbenzylamine and 4-ethylaniline (> 98%), 2-phenethylamine (> 99%), *N,N*-dimethylaniline (> 99.5%) and 2,6-di-*tert*-butylpyridine (> 97%) were purchased from Sigma-Aldrich (Steinheim, Germany) and 2,4,6-collidine (> 99%) from Merck (Darmstadt, Germany). Stock solutions (5 mM) were prepared in methanol (HPLC, Lab-scan, Dublin, Ireland) and diluted further with methanol:toluene (95:5%) (HPLC, Baker, Deventer, Holland) to give 50 and 100 μM solutions.

2.2. Instrumentation

The mobility distributions were recorded using a custom-made drift tube ion mobility spectrometer equipped by a Faraday plate detector (IMS-FP) [19] and the mass spectrometric data were recorded using an ion mobility spectrometer-mass spectrometer (IMS-MS) [3]. In the IMS-FP the length of the drift region was 13.85 cm. The instrument was operated using a Bradbury-Nielsen (B-N) type ion gate with a 200 μs gate opening time. The drift gas flow was set to 1.9–2.5 L min^{-1} and measurements were conducted at room temperature (294–297 K). Nitrogen, and mixtures of nitrogen and argon or helium were used as drift gases. The desolvation and drift fields were both set to 316 V cm^{-1} .

A custom-made program was used to operate the instrument. During the total measurement time of 25 s 500 drift time transients were summed up to achieve drift time distribution. The obtained data were processed by a ChemStation 10.02 program code (Agilent Technologies, Inc., PaloAlto, CA, USA), with custom-made macros to calculate reduced mobilities of the ions detected. The IMS-MS was operated in continuous ion flow mode (both B–N gates open) to record the mass spectra [3]. The desolvation and drift fields were set to 304 and 316 V cm⁻¹, respectively. The nitrogen drift gas flow was ~2.4 L min⁻¹. The mass spectrometer was a triple-quadrupole mass spectrometer API-300 (SCIEX Applied Biosystems, Toronto, ON, Canada) operated in positive ion mode with a declustering potential of 5 V, and a mass range of *m/z* 30–300. The data were collected by Analyst 1.4.1 program code (Applied Biosystems/MDS SCIEX, Concord, ON, Canada).

2.3. Gases

Nitrogen for the drift and nebulizer gases was produced from compressed air with a heatless dryer Dominic Hunter Pneudri MiDAS 4 (Parker Hannifin Ltd., Gateshead, England) and a NGLCMS20 (Labgas Instrument Co., Espoo, Finland) or N2-MISTRAL-0 (LNI Schmidlin AG, Neuheim, Switzerland) nitrogen generator. The N₂ gas was further purified using a hydrocarbon and moisture trap. The level of humidity was measured using a humidity gauge (Vaisala DMT242; Helsinki, Finland) downstream from the drift tube. The bottled gases were purchased from AGA (Espoo, Finland) with a 99.999% purity for argon and 99.996% for helium. The drift gas mixtures were produced using two EL-Flow mass flow controllers (Bronkhorst, Ruurlo, the Netherlands).

2.4. Ionization

The samples were delivered to the ionization region using a custom-made heated nebulizer [19], which was heated up to 423 K. The samples were delivered with a PHD 2000 Advanced Syringe Pump (Harvard Apparatus GmbH, Hugstetten, Germany) into a nebulizer (the injection speed was 180 μL h⁻¹), where the nitrogen gas flow at 1.6–1.8 L min⁻¹ carried the sample vapor to the ionization region. Two different ionization methods were used in this study: (1) atmospheric pressure chemical ionization (APCI) was conducted using an acupuncture needle (the corona needle potential was 2.0–2.2 kV), and (2) atmospheric pressure photoionization (APPI), using a krypton discharge lamp (PKS-100, Cathodeon, Ltd., Cambridge, England) with 10 and 10.6 eV photons.

3. Results and discussion

3.1. Ionization

Most of the experiments were conducted with an IMS-FP instrument operated in positive ion APCI or APPI mode. Mass spectra measured with the IMS-MS instrument confirmed that all the amines produced protonated molecules [M+H]⁺ with positive APCI and APPI. Furthermore, both ionization methods resulted in a reaction ion peak (RIP).

3.2. Mobilities

All the reduced mobilities for isomeric amines were recorded with IMS-FP using APCI or APPI, and are summarized in Table 1. The mobility measurements were mainly done using three different mixtures of the analytes: Mix A (2,4,6-Col, *N,N*-DMA, *n*-*M-o*-T and 2-MBA), Mix B (PEA, 4-EA and 2,6-DtBPyr) and Mix C (2-, 3- and 4-MBA, and 2,6-DtBPyr). The mobility order was confirmed by

measuring the amines individually. As an example of the reproducibility of the measurements the reduced mobility of 2,6-DtBPyr $K_0 = 1.47 \text{ cm}^2 \text{ V}^{-1} \text{ s}^{-1}$ with the relative standard deviation of 0.3% ($n=8$, on two different days) measured using APCI is reported. 2,6-DtBPyr is nowadays a commonly used IMS standard [19–22]. However, in this study reduced mobility values were not normalized with the reduced mobility of 2,6-DtBPyr.

Due to the different experimental conditions it is difficult to compare the reduced mobility values obtained in this study to the ones previously published [11–15]. However, the reduced mobility values in Ref [13] for 2,4,6-Col ($1.83 \text{ cm}^2 \text{ V}^{-1} \text{ s}^{-1}$) and *N,N*-DMA ($1.81 \text{ cm}^2 \text{ V}^{-1} \text{ s}^{-1}$) measured at 150 °C and using air as the drift gas are close to the values reported in Table 1, showing the same mobility order, but smaller differences in mobilities. Interestingly, Karpas et al. have reported that anilines typically form two mobility peaks, one for nitrogen-protonated, and one for ring-protonated species [12,13]. Later, this has been proven by mobility separation of different forms of protonated aniline molecules formed by electrospray ionization, and interpreting the subsequently measured collision induced dissociation (CID) mass spectra of the mobility separated protonated molecules [6]. It was observed that the nitrogen-protonated ions had longer drift time than the ring-protonated ions due to stronger interaction with the drift gas. However, in our study photoionization and corona discharge ionization produced only one mobility peak for each amine meaning that only one protonation site (most likely nitrogen) was preferable.

Based on the reduced mobility values presented in Table 1 and Fig. 1, two different amine groups can be separated. The first group contains the amines 2,4,6-Col, *N,N*-DMA and *n*-*M-o*-T, which contain a *N*-heterocyclic aromatic ring, or a tertiary or secondary amino group, respectively. These amines have clearly faster mobilities than the second group containing primary NH₂-groups (PEA, 4-EA, and 2-, 3- and 4-MBA). From Fig. 1A and Table 1 it can be seen that the amines in the first group can be separated from each other, and they have clearly different mobility values. Fig. 1A shows also that the first group of amines can be easily separated from a second group amine 2-MBA. Reduced mobilities of the amines in the second group are very close to each other. PEA and 4-EA could be separated from each other (Fig. 1B), but the mixture of 2-, 3- and 4-MBA produced a single mobility peak (Fig. 1C).

The clear separation of isomeric amines 2,4,6-Col, *N,N*-DMA and *n*-*M-o*-T could be explained by the varying number of carbon containing groups attached to the nitrogen atom, or by the aromatic nitrogen being surrounded by two methyl groups in *ortho* position, i.e. the charge in the *N*-protonated molecule is shielded by the alkyl groups, resulting in decreased interaction of the protonated molecule with the drift gas, and therefore higher mobility. Because of a similar shielding effect of the charged site, some molecules, such as 2,6-DtBPyr [20,21] and tetraalkylammonium halides [23], have been found suitable as IMS instrumental standards, and their reduced mobilities have been observed to be minimally affected by e.g. impurities of the drift gas. Interestingly, PEA was separated from 4-EA, even though both compounds have –NH₂ groups (Fig. 1B). The reason for this might be that the protonated PEA forms a “loop” via –NH₃⁺ interaction with the benzene ring, resulting in a more closely-packed shape. Therefore protonated PEA is likely to interact less with the drift gas than the protonated 4-EA, which cannot form a similar “loop”. This is also supported by the slightly higher mobility of PEA (Table 1, Fig. 1B). Similar loop formation has been reported in an IMS study for protonated diamines and polyamines [24]. In addition, very recently it has been shown by infrared multiple-photon dissociation spectroscopy that for the protonated phenylalkylamines, C₆H₅(CH₂)_{*n*}NH₃⁺ ($n=2-4$), the most stable ion geometry has

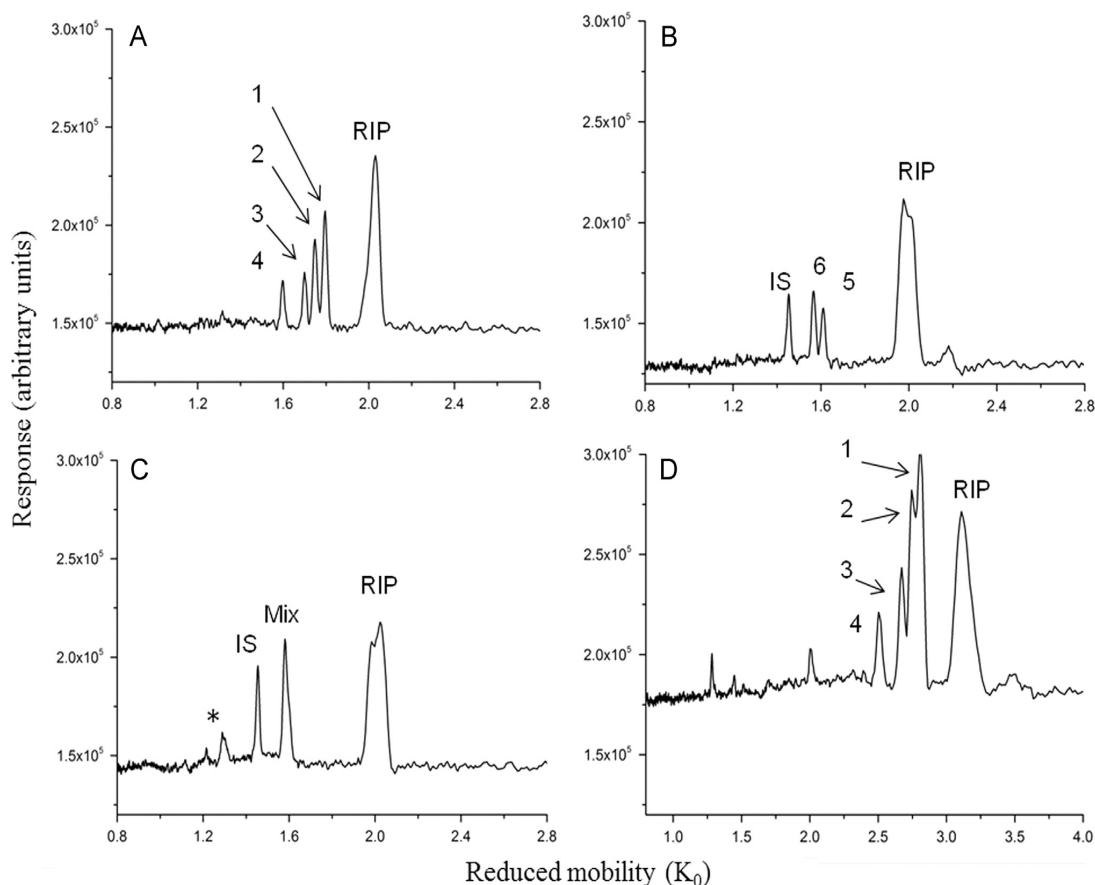


Fig. 1. Positive APCI ion mobility spectra of mixtures of isomeric amines measured with IMS-FP instrument (A and D) 1=2,4,6-Col, 2=*N,N*-DMA, 3=*n*-*M*-*o*-T and 4=2-MBA, (B) 5=PEA and 6=4-EA, and (C) Mix=2-, 3-, and 4-MBA. In Fig. (A)–(C) the drift gas was nitrogen and in Fig. (D) the drift gas mixture was 33% helium and 67% nitrogen. RIP=reaction ion peak, IS=2,6-DtBPyr and the asterisk indicates possible amine cluster ions.

interactions between the aromatic ring and the $-\text{NH}_3^+$ group causing folding of the side chain [25].

The effect of drift gas composition was studied using positive APCI-IMS-FP, sample mixture A, and a varying amount of helium or argon in the nitrogen drift gas. The addition of helium shifted all the peaks towards higher mobility (Fig. 2A), and separation of the amines was deteriorated at higher helium concentrations (Fig. 1D vs. 1A). On the contrary, the addition of argon to the nitrogen drift gas shifted all the peaks towards lower mobility (Fig. 2B), but the reduced mobility of the reaction ion peak (RIP) stayed more or less constant after the first argon addition. In addition, it was observed that peak heights of the analytes increased as the amount of helium in the drift gas increased, but with increasing amount of argon in the drift gas the peak heights were observed to decrease. These results are in good agreement with literature, where it has been reported for many compounds that reduced mobilities increase, when helium is used as the drift gas instead of nitrogen, and decrease, when argon is used as the drift gas [14,18]. Of the compounds used here, for 2,4,6-collidine clearly higher mobility in helium than in argon has been reported [14]. The observed changes in the peak height, and the effect of helium on resolution are also in good agreement with literature. It has been reported that helium provides clearly better sensitivity and argon lower, when compared to the use of nitrogen as drift gas [17]. In the same study it was hypothesized that the sensitivity changes are due to increased amount of reactions in the drift tube, since longer drift times allow more reactions, and the presence of different

gases may cause differences in ionization efficiency in the electrospray process. In the same study it was also reported that shorter drift times in helium drift gas provide lower resolving power. Comparison of Fig. 1A and D confirms this observation.

4. Conclusions

The selected isomeric amines produced $[\text{M}+\text{H}]^+$ ions with APCI and APPI. Both ionization methods produced a single mobility peak for each amine. Two subgroups from the model compounds could be identified based on reduced mobility. Compounds with *N*-heterocyclic aromatic ring, tertiary or secondary amino groups (2,4,6-collidine, *N,N*-dimethylaniline and *N*-methyl-*o*-toluidine, respectively) had clearly higher reduced mobilities than the rest of the amines, which had a primary $-\text{NH}_2$ group (2-phenethylamine, 4-ethylaniline, and 2-,3- and 4-methylbenzylamine). 2,4,6-Col, *N,N*-DMA and *n*-*M*-*o*-T could also be separated from each other, while the primary amines had mobility values very close to each other. However, PEA could be separated from 4-EA. The extent of how much the adjacent groups are shielding the protonated nitrogen is expected to be the major explanation for the different reduced mobilities. In other words: the more protected the charge, the less the ionized analyte can interact with the drift gas, and therefore it can move faster through the drift tube.

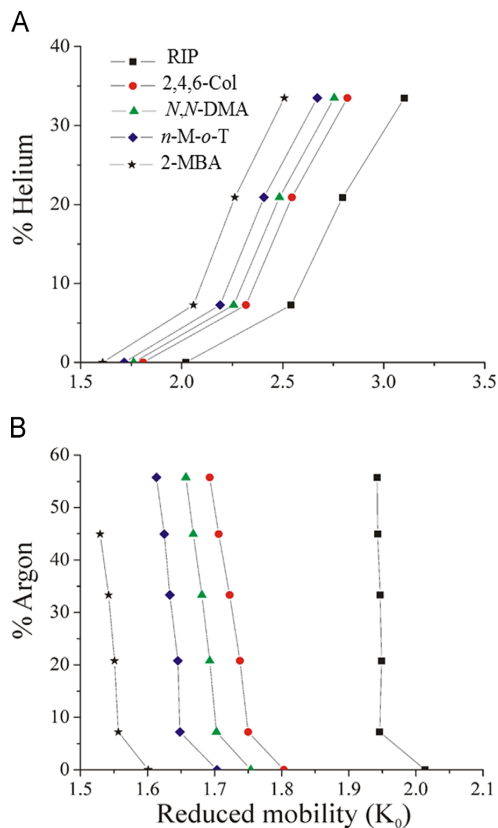


Fig. 2. Reduced mobility values of isomeric amines measured with a positive APCI-IMS-FP instrument. Helium (A) or argon (B) mixed in the nitrogen drift gas.

When argon was mixed with nitrogen drift gas all the peaks shifted towards lower reduced mobility, and a reduction in the peak height was observed, whereas the opposite behavior was observed with helium, which shifted all the peaks towards higher reduced mobility and increased peak height.

Acknowledgments

The project was supported by the Academy of Finland (Project nos.: 114132, 122018, 125758 and 255559). Docent Elina Kalenius and Jyrki Viidanoja are thanked for stimulating conversations. Prof. Herbert H. Hill, Jr. is acknowledged for a conversation regarding the structures of protonated amines.

References

- [1] G.A. Eiceman, Z. Karpas, *Ion Mobility Spectrometry*, second ed., CRC Press Taylor & Francis, Boca Raton, 2005.
- [2] G.A. Eiceman, J.A. Stone, *Anal. Chem.* 76 (2004) 390 A–397 A.
- [3] A. Sysoev, A. Adamov, J. Viidanoja, R.A. Ketola, R. Kostianen, T. Kotiaho, *Rapid Commun. Mass Spectrom.* 18 (2004) 3131–3139.
- [4] A.B. Kanu, P. Dwivedi, M. Tam, L. Matz, H.H. Hill, *J. Mass Spectrom.* 43 (2008) 1–22.
- [5] J. Laakia, A. Adamov, M. Jussila, C.S. Pedersen, A.A. Sysoev, T. Kotiaho, *J. Am. Soc. Mass Spectrom.* 21 (2010) 1565–1572.
- [6] P.M. Lalli, B.A. Iglesias, H.E. Toma, G.F. de Sa, R.J. Daroda, J.C. Silva Filho, J.E. Szulejko, K. Araki, M.N. Eberlin, *J. Mass Spectrom.* 47 (2012) 712–719.
- [7] J. Laakia, C.S. Pedersen, A. Adamov, J. Viidanoja, A. Sysoev, T. Kotiaho, *Rapid Commun. Mass Spectrom.* 23 (2009) 3069–3076.
- [8] M.D. Plasencia, D. Isailovic, S.I. Merenbloom, Y. Mechref, D.E. Clemmer, *J. Am. Soc. Mass Spectrom.* 19 (2008) 1706–1715.
- [9] A.E. Counterman, D.E. Clemmer, *Anal. Chem.* 74 (2002) 1946–1951.
- [10] J. Laakia, A. Adamov, A. Sysoev, T. Kotiaho, Separation of isomeric amines with ion mobility spectrometry, in: *Proceedings of the 19th Annual Conference on Ion Mobility Spectrometry (ISIMS 2010)*, Albuquerque, USA, 2010.
- [11] H. Borsdorf, K. Neitsch, G.A. Eiceman, J.A. Stone, *Talanta* 78 (2009) 1464–1475.
- [12] Z. Karpas, Z. Berant, R. Stimac, *Struct. Chem.* 1 (1990) 201–204.
- [13] Z. Karpas, *Anal. Chem.* 61 (1989) 684–689.
- [14] Z. Karpas, Z. Berant, *J. Phys. Chem.* 93 (1989) 3021–3025.
- [15] F.W. Karasek, S.H. Kim, S. Rokushika, *Anal. Chem.* 50 (1978) 2013–2016.
- [16] A.B. Kanu, H.H. Hill Jr., *Talanta* 73 (2007) 692–699.
- [17] G.R. Asbury, H.H. Hill, *Anal. Chem.* 72 (2000) 580–584.
- [18] L.M. Matz, H.H. Hill Jr, L.W. Beegle, I. Kaniak, *J. Am. Soc. Mass Spectrom.* 13 (2002) 300–307.
- [19] A. Adamov, T. Mauriala, V. Toplev, J. Laakia, C.S. Pedersen, T. Kotiaho, A.A. Sysoev, *Int. J. Mass Spectrom.* 298 (2010) 24–29.
- [20] G.A. Eiceman, E.G. Nazarov, J.A. Stone, *Anal. Chim. Acta* 493 (2003) 185–194.
- [21] R. Fernandez-Maestre, C.S. Harden, R.G. Ewing, C.L. Crawford, H.H. Hill, *Analyst* 135 (2010) 1433–1442.
- [22] A.K. Viitanen, T. Mauriala, T. Mattila, A. Adamov, C.S. Pedersen, J.M. Mäkelä, M. Marjamäki, A. Sysoev, J. Keskinen, T. Kotiaho, *Talanta* 76 (2008) 1218–1223.
- [23] J. Viidanoja, A. Sysoev, A. Adamov, T. Kotiaho, *Rapid Commun. Mass Spectrom.* 19 (2005) 3051–3055.
- [24] Z. Karpas, S.E. Bell, Y.F. Wang, M. Walsh, G.A. Eiceman, *Struct. Chem.* 5 (1994) 135–140.
- [25] B. Chiavarino, M.E. Crestoni, M. Schütz, A. Bouchet, S. Piccirillo, V. Steinmetz, O. Dopfer, S. Fornarini, *J. Phys. Chem. A* 118 (2014) 7130–7138.



High resolution molecular organic geochemistry assessment of Brazilian lacustrine crude oils[☆]



Alessandro Casilli^{a,*}, Renzo C. Silva^a, Jaakko Laakia^a, Cleverson J.F. Oliveira^b, Alexandre A. Ferreira^b, Maria Regina B. Loureiro^a, Débora A. Azevedo^{a,*}, Francisco R. Aquino Neto^a

^a Universidade Federal do Rio de Janeiro, Instituto de Química, LAGOA-LADETEC, Ilha do Fundão, Rio de Janeiro, RJ 21941-909, Brazil

^b Division of Geochemistry, PETROBRAS Research and Development Center (CENPES), PETROBRAS, Rua Horácio Macedo, 950, Ilha do Fundão, Rio de Janeiro, RJ 21941-915, Brazil

ARTICLE INFO

Article history:

Received 14 October 2013

Received in revised form 13 January 2014

Accepted 16 January 2014

Available online 27 January 2014

ABSTRACT

As most of the oils in the Recôncavo Basin are genetically related and have experienced nearly equivalent thermal stress, it is difficult to differentiate them using standard techniques. However, differentiation can be accomplished using new analytical techniques, including comprehensive two-dimensional gas chromatography (GC×GC)-time of flight mass spectrometry (TOFMS). In this investigation, GC×GC-TOFMS was applied for the characterization of 20 selected Recôncavo Basin crude oils from a wide geographical distribution. Source and maturation parameters were determined based on the analysis of saturated hydrocarbons, aromatic compounds and diamondoids using GC×GC-TOFMS. Chemometric techniques were applied in order to expand the overall understanding of the sample characteristics. It was found that β-carotane and gammacerane were highly important for differentiating oils from the central portion of the basin, while two southern oils were differentiated by their sulfur-containing aromatic compounds. Diamondoid analysis was fundamental to evaluating maturity. The results of this study show how previously overlooked, minor oil components are important for differentiating genetic groups, compounds that were neglected prior to the application of GC×GC-TOFMS.

© 2014 Elsevier Ltd. All rights reserved.

1. Introduction

The Recôncavo Basin is located in northeastern Brazil (State of Bahia) and its evolution is related to the fragmentation of the Gondwana paleocontinent and the opening of the South Atlantic Ocean, in the late Jurassic-early Cretaceous time (Figueiredo et al., 1994). The basin encompasses approximately 11,500 km² and corresponds to the southern part of the Recôncavo-Tucano-Jatobá rift (Fig. 1) (Milani and Davison, 1988; Magnavita and Da Silva, 1995). Petroleum exploration in the prolific Recôncavo Basin, which now is in a mature stage, dates back to the 1930s (see, for instance, Figueiredo et al., 1994). In the South Tucano sub-basin there are some small gas fields. Northward, no liquid petroleum accumulations have been found. In the Recôncavo Basin, the lacustrine shales of the Candeias Formation (early Cretaceous) are considered to be the predominant source rock units. The main reservoirs are sandstones of the pre-rift Sergi Formation (Santos et al., 1990; Coutinho, 2008).

A deep understanding of crude oil potential demands a detailed characterization of its constituents. This challenging task involves different analytical techniques. Traditionally, the most commonly adopted is one-dimensional (1D) capillary gas chromatography (GC), which, despite the impressive results achieved in the past, has encountered limitations in many cases. GC coupled with mass spectrometry (MS), acquiring key ions in single ion monitoring (SIM) mode (Chakhmakhchev et al., 1997) or tandem MS (MS-MS) in metastable reaction monitoring (MRM) has overcome many of these limitations (Moldowan et al., 1986). More recently, GC coupled to triple quadrupole mass spectrometry (GC-QqQ) has been implemented and other mass spectrometry analyzers might come into play. Despite these technological advances, the complexity of the matrix is still generating restricted access to the bulk of information. Most of them also suffer from the lack of full mass spectra information, being limited target oriented methods. Another issue is the mixtures of stereoisomers, which have similar structures, generating coelutions and similar mass spectral fragmentations. Thus, chromatographic coelution as well as the lack of mass spectral data, significantly limit the information gathered by these analytical techniques. Therefore, it is important to use complementary techniques to overcome such limitations. GC×GC and GC×GC-TOFMS are certainly among these techniques for the reasons highlighted below (Eiserbeck et al., 2011).

[☆] This study was presented at the 26th IMOG Meeting, Tenerife, September 16–20th, 2013.

* Corresponding authors. Tel.: +55 21 25627488, +55 21 22603967; fax: +55 21 22603967 (A. Casilli).

E-mail addresses: casilli@iq.ufrj.br (A. Casilli), debora@iq.ufrj.br (D.A. Azevedo).

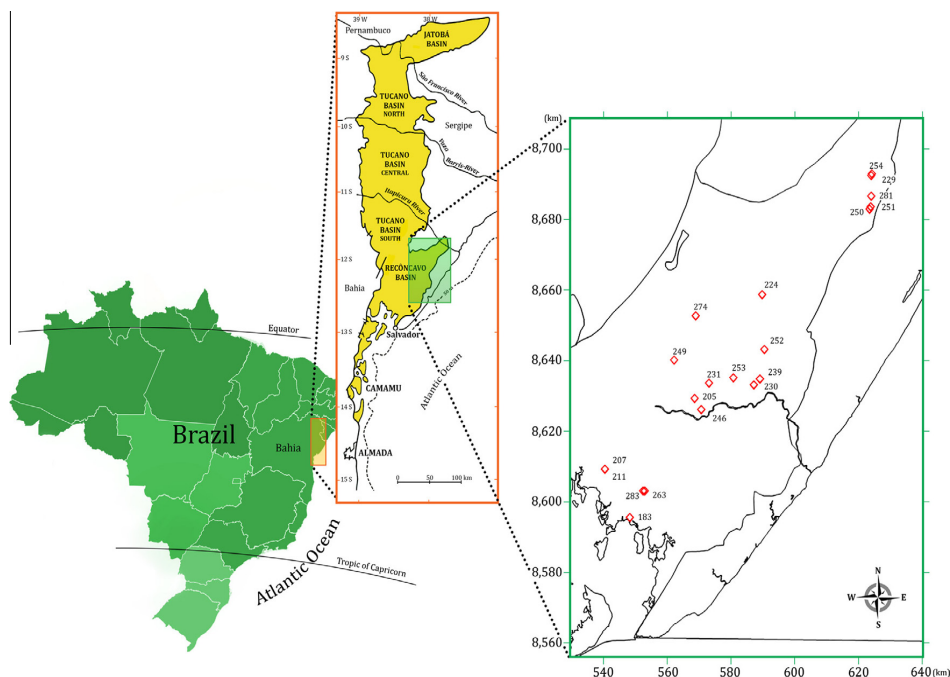


Fig. 1. Location map of Recôncavo Basin and position of the studied oils.

Since the commercial availability of comprehensive two-dimensional gas chromatography instruments (GC×GC), analyses that were previously performed by one-dimensional chromatography techniques have been improved. GC×GC allows for the reduction of coelutions, particularly common in complex mixtures such as crude oil. Time of flight mass spectrometers (TOFMS) provide the mass spectrum of each component, which maximizes the extraction of the biomarker structural information content embedded in the complexity of petroleum samples.

GC×GC-TOFMS has been used for advanced biomarker and diamondoid evaluation. Sound statements of the advantages provided by this technique in organic geochemistry have been recently reported (Ventura et al., 2010, 2012; Aguiar et al., 2011; Silva et al., 2011, 2013; Eiserbeck et al., 2012; Oliveira et al., 2012a, 2012b). Noteworthy is its application in the search for better data from traditional biomarkers as well as the search for non-conventional biomarkers carrying specific geochemical diagnostic features, the latter rarely monitored in routine analysis by conventional 1D-GC or monitored by GC-MS-MS.

Therefore, GC×GC-TOFMS is the first analytical technique with the potential to allow for a breakthrough in traditional biomarker based study of petroleum systems, paving the path for the development of a true high resolution molecular organic geochemistry (HRMOG). The present study illustrates this potential in the assessment of 20 crude oil samples from the Recôncavo Basin. Gaglianone and Trindade (1998) investigated the biomarkers distribution in a set of oils from this basin. The oils have been classified as belonging to the same family, with only minor compositional variations related to maturation; to the best of our knowledge, this is the only work reported in literature, concerning the biomarkers distribution in this basin.

Analyses were performed on saturated and aromatic hydrocarbons, organo-sulfur compounds and diamondoids. The primary goal was to differentiate oils considered to come from source rocks deposited in similar environments and with similar levels of thermal maturity.

2. Geological setting

The lacustrine freshwater shales of the Gomo and Tauá members of the Candeias Formation (syn-rift) are considered to be the main source rocks of the basin. Previous geochemical studies (e.g., Mello et al., 1994; Aragão et al., 1998) identified the depositional paleoenvironment as a freshwater lake or lakes. Sediments were deposited under anoxic conditions, which favored organic matter preservation. Total organic carbon (%TOC) content varies from 0.8–4%, but can reach 10% in some organic rich facies. Rock-Eval pyrolysis shows a petroleum potential (S_2 peak) of around 16 mg HC/g rock, although in some facies the values may rise to 70 mg HC/g rock. Hydrogen index ($HI = (S_2/TOC) \times 100$) values may reach 700 mg HC/g TOC, and chemical and petrographic analyses indicate a type I kerogen.

Based on the vitrinite reflectance results of Coutinho (2008), the source rocks are at oil window and wet gas window levels of thermal maturity in the south and central parts of the basin. In the northeastern part of the basin, the organic matter is still immature to marginally mature.

Three basic types of reservoirs and traps have been proposed for the Recôncavo Basin (Figueiredo et al., 1994; Magnavita and Da Silva, 1995). (1) Pre-rift system: The main reservoirs are in the Sergi and Água Grande Formations and account for around 57% of the proven oil volume of the basin. They are fluvial/eolian sands and the traps are mainly structural. (2) Syn-rift Candeias system: This petroleum system comprises approximately 16% of the proven oil reserves of the basin. The reservoirs are typically lacustrine turbidites with stratigraphic and combined traps. (3) Syn-rift Ilhas system: The oil volume of this system corresponds to around 27% of the total proven oil of the basin. The principal reservoirs are deltaic sands, and there are structural, combined and stratigraphic traps.

3. Samples and methods

Twenty crude oil samples from the Recôncavo Basin were analyzed. The geographic location of the respective wells is shown in

Fig. 1. Samples 254, 229, 281, 251 and 250 belong to the northeast part of the basin. Another group comprises samples 224, 274, 249, 246, 205, 231, 253, 230, 239, 252 and 224, located in the central part of the basin, while samples 183, 263, 283, 211 and 207 are located in the southern part of the basin.

3.1. Sample preparation

The oil samples were subjected to liquid chromatography with pre-activated silica as the stationary phase. The crude oil samples were dissolved in hexane and applied to the top of a column containing activated silica gel (120 °C overnight). The samples (ca. 100 mg each) were separated into saturated hydrocarbons, aromatic hydrocarbons and polar compounds, through *n*-hexane (10 ml), *n*-hexane:dichloromethane (8:2, v:v, 10 ml) and dichloromethane:methanol (9:1, v:v, 10 ml), respectively. The solvent from each fraction was evaporated and 500 µl of dichloromethane was added. One microlitre of the saturated hydrocarbon and aromatic fraction was analyzed by GC×GC-TOFMS.

Urea adduction of the saturated hydrocarbon fraction was performed to remove the *n*-alkanes (Nwadinigwe and Nwobodo, 1994; Marotta, 2010). Briefly, the saturated hydrocarbon fraction was dissolved in 1 mL of *n*-hexane in a test tube, and 1 ml of acetone was added. A saturated solution of urea in methanol was added and the precipitation of urea was immediately observed. The solution was heated to 50 °C until the urea was completely dissolved; afterwards, the solution was cooled and the formation of urea crystals observed. The solvents were carefully evaporated under nitrogen flow, and the dried crystals were washed with hexane (5 × 2 ml). After centrifugation, the washing solvent containing the cyclic and branched saturated hydrocarbons was obtained. This fraction, after evaporation by nitrogen flow, was dissolved in dichloromethane and analyzed by GC×GC-TOFMS.

In order to analyze diamondoids, another procedure was performed. Approximately 100 mg of each crude oil was deposited in the top of a dry silica gel column and was then eluted with 5 ml of *n*-hexane, similarly to procedures published elsewhere (Azevedo et al., 2008; Springer et al., 2010). Eluted solutions were rapidly sealed and analyzed by GC×GC-TOFMS. Deuterated *n*-dodecane-*d*₂₆ and *n*-tetracosane-*d*₅₀ standard solutions were used to spike the samples before the fractionation procedure. A set of diamondoid standards purchased from Chiron AS (Stiklestadveien, Norway) was used as reference for the identification of adamantane and diamantane. Internal deuterated standards (*n*-dodecane-*d*₂₆ and *n*-tetracosane-*d*₅₀) were used for relative quantification of diamondoids and saturated hydrocarbons, respectively (Silva et al., 2013).

3.2. GC×GC-TOFMS and data processing

Analyses were performed on a Pegasus 4D (Leco, St. Joseph, MI, USA) GC×GC-TOFMS, composed of an Agilent 6890 GC (Palo Alto, CA, USA) equipped with a secondary oven, a non-moving quadrupole dual-stage modulator and a Pegasus III (Leco, St. Joseph, MI, USA) time of flight mass spectrometer. A DB-5 column (Agilent Technologies, Palo Alto, CA, USA), 5% phenyl-95% methylsiloxane (30 m, 0.25 mm i.d., 0.25 µm *d*_f) was used as the first dimension column (¹D). A BPX-50 column (SGE, Ringwood, VIC, Australia), 50% phenyl-50% methylsiloxane (1.5 m, 0.1 mm i.d., 0.1 µm *d*_f) was used as the second dimension column (²D). The 2D column was connected to the TOFMS by means of a 0.5 m × 0.25 mm i.d. uncoated deactivated fused silica capillary, via SGE mini-unions and Silitite™ metal ferrules 0.1–0.25 mm i.d. (Ringwood, VIC, Australia) (Silva et al., 2011; Oliveira et al., 2012a).

The GC conditions for the first dimension include: splitless mode injection of 1 µl at 290 °C, a purge time of 60 s, and a purge

flow of 5 ml/min. Helium was used as the carrier gas at a constant flow rate of 1.5 ml/min. The primary oven temperature program began at 70 °C for 1 min, and was then increased to 170 °C at 20 °C/min, and further to 325 °C at 2 °C/min. The secondary oven temperature program was 10 °C higher than the primary one. The modulation period was 8 s with a 2 s hot pulse duration, and the modulator temperature was 30 °C higher than the primary oven temperature. The transfer line to the MS was set at 280 °C, the electron ionization mode was set at 70 eV, the mass range was 50–600 Da, the ion source temperature was 230 °C, the detector was 1550 V, and the acquisition rate was 100 spectra/s. Compound identification was performed by comparison with literature mass spectra, mass spectral examination, retention time and elution order.

Diamondoid analyses were carried out using the same instrument and column. GC conditions differ by a 5 °C offset used between the dimensions during the GC program, which was initially stabilized at 50 °C and the first dimension temperature was raised to 350 °C at 4 °C/min. The modulation period was chosen to be 6 s, with a 2 s hot pulse. Transfer line and ion source temperatures were held at 290 °C and 200 °C, respectively. GC×GC-TOFMS data acquisition and processing were performed with ChromaTOF software version 4.42 (Leco, St. Joseph, MI, USA). Individual peaks were automatically detected on the basis of a 10:1 signal/noise ratio.

3.3. Chemometric analyses

The software package Statistica 8 (Statsoft Inc.) was used in all statistical calculations in this work. Principal Component Analysis (PCA) was based on the covariance matrix. All variables were mean centred and scaled by the sample standard deviation. Data reported in Tables 1–4 have been partially or totally processed. In the latter case, a matrix $X_{(20 \times 42)}$ containing maturity parameters from saturated biomarker, aromatics and diamondoid data was used.

4. Results and discussion

4.1. Saturated hydrocarbons

Tri- and tetracyclic terpanes (*m/z* 191), regular and rearranged hopanes (*m/z* 191), methyl-hopanes (*m/z* 205), secohopanes (*m/z* 123), onoceranes (*m/z* 123), steranes (*m/z* 217, 218), β-carotane (*m/z* 125) and other compounds (e.g., gammacerane, tetracyclic polyprenoid (TPP) (*m/z* 191, 259) were detected in the saturate fractions of the Recôncavo oils by monitoring extracted ion chromatograms (EIC). The detailed procedure adopted for structural characterization is extensively reported in previous works (e.g., Aguiar et al., 2010, 2011; Oliveira et al., 2012a, 2012b).

The tricyclic terpene series (Tr_n) was identified in all samples, with the corresponding carbon numbers varying from C₁₉ to C₄₁. The regular hopane series was detected in the range from C₂₇ to C₃₇. Moretanes were detected from C₂₉ to C₃₄. Diahopanes were also often detected in oils; the complete series from C₃₀ to C₃₅ was assigned in the current investigation. The 28-*nor*-spergulane series, another type of rearranged hopane, was detected in the range from C₂₉ to C₃₂. Using the GC×GC-TOFMS method, each class of compounds was successfully separated in the chromatographic plane, as can be seen in the representative example of the tri-, tetra- and pentacyclic terpanes reported in Fig. 1S. Fig. 2 shows examples of pentacyclic terpene fingerprints of the two most chromatographically distinct samples, 263 and 252.

Besides the above mentioned traditional biomarkers, less common ones were also investigated, for example, the 3β-methyl-hopane

Table 1
Traditional source parameters from saturated biomarkers as analyzed by GC×GC-TOFMS.^a

Sample	Region	H ₃₀ /St	TPP/Dia ₂₇	H ₃₄ /H ₃₅	H ₃₅ S ₂₂ /H ₃₄ S ₂₂	Ts/Tm	C ₂₇ /C ₂₉	Tr ₂₃ /H ₃₀	Te ₂₄ /H ₃₀	Gam/H ₃₀	25NH/H ₃₀	Tr ₂₆ /Tr ₂₅
183	South	9	1.62	1.90	tr	4.45	1.94	0.93	0.21	0.15	0.01	1.74
205	Central	12	2.04	2.00	tr	3.60	1.88	0.87	0.13	0.22	0.02	1.89
207	South	67	1.94	2.38	0.35	2.04	1.34	0.18	0.08	0.10	0.01	1.18
211	South	41	2.92	2.50	0.34	1.97	1.25	0.06	0.04	0.14	0.01	1.82
224	Central	30	1.25	2.19	0.47	1.31	2.72	0.29	0.08	0.13	0.01	1.11
229	Northeast	26	1.40	3.40	0.45	1.91	3.12	0.31	0.11	0.13	0.01	1.74
230	Central	20	2.13	1.47	tr	1.95	2.03	0.4	0.10	0.30	0.02	1.94
231	Central	11	2.12	1.61	0.43	1.10	1.10	0.27	0.09	0.15	0.03	1.50
239	Central	12	3.21	1.82	0.34	1.42	1.21	0.46	0.08	0.49	0.12	1.48
246	Central	32	1.68	2.41	0.41	2.12	2.25	0.36	0.11	0.15	0.01	1.02
249	Central	18	2.39	2.94	0.46	2.62	1.80	0.35	0.07	0.45	0.04	1.44
250	Northeast	17	4.61	3.34	0.39	1.26	2.32	0.2	0.05	0.48	0.04	1.71
251	Northeast	16	4.21	2.40	0.47	1.69	1.74	0.19	0.06	0.20	0.02	1.78
252	Central	16	1.87	1.75	0.53	1.42	1.42	0.49	0.30	0.95	0.02	1.58
253	Central	12	2.53	1.87	tr	1.56	1.90	1.47	0.09	0.16	0.03	1.92
254	Northeast	27	2.65	2.32	0.43	1.89	1.49	0.25	0.11	0.21	0.03	1.39
263	South	8	1.36	2.42	0.39	1.25	1.98	1.18	0.34	0.19	0.08	1.06
274	Central	12	8.55	1.08	0.57	1.11	1.20	0.55	0.42	0.61	0.07	0.55
281	Northeast	8	4.00	1.84	0.54	1.04	2.18	0.40	0.19	0.18	0.05	1.27
283	South	9	5.07	1.77	0.54	1.58	1.22	0.65	0.12	0.78	0.03	1.79

^a H₃₀, C₃₀ 17 α (H),21 β (H)-hopane; St, Σ C₂₇ $\alpha\alpha\alpha$ + $\alpha\beta\beta$ cholestanes (S + R); TPP, C₃₀ tetracyclic poliprenoid; Dia₂₇, C₂₇ 13 β (H),17 α (H)-diacholestanes (S + R); H₃₄, C₃₄ 17 α (H),21 β (H)-tetrakisohomohopane (22S + 22R); H₃₅, C₃₅ 17 α (H),21 β (H)-pentakisohomohopane (22S + 22R); T_s, C₂₇ 22,29,30-trisnorneohopane; T_m, C₂₇ 22,29,30-trisnorhopane; C₂₇, Σ C₂₇ $\alpha\alpha\alpha$ + $\alpha\beta\beta$ cholestanes(S + R); C₂₉, C₂₉ $\alpha\alpha\alpha$ + $\alpha\beta\beta$ 24-ethyl-cholestanes (S + R); Tr_n, C_n 13 β (H),14 α (H)-tricyclic terpane (sum of A + B isomers); Te₂₄, C₂₄ tetracyclic terpane; G, gammacerane; SH₃₀, C₃₀ 8 α (H),14 α (H),17 α (H),21 β (H)-secohopane; 25NH, 25-nor-hopane. tr = trace level.

Table 2
Non-conventional source parameters from saturated biomarkers as analyzed by GC×GC-TOFMS.^a

Sample	Region	3 β MH ₃₁ /H ₃₀	Tr ₂₈ /Tr ₂₉	ONII/H ₃₀	ONIII/H ₃₀	29Nsp/H ₃₀	Te ₂₄ /Tr ₂₆	SH ₃₀ /H ₃₀	DH ₃₀ /H ₃₀	β -car/H ₃₀	H ₃₁ R/H ₃₀	H ₂₉ /H ₃₀
183	South	0.02	1.44	2.06	tr	0.15	0.30	2.14	0.88	0.05	0.13	0.31
205	Central	0.02	1.50	tr	tr	0.03	0.16	1.41	0.24	0.29	0.1	0.57
207	South	0.03	1.67	0.15	0.21	0.04	0.93	0.21	0.20	0.06	0.12	0.52
211	South	0.04	2.19	0.13	tr	0.04	0.71	0.23	0.21	0.04	0.15	0.55
224	Central	0.03	4.9	0.13	tr	0.03	0.97	0.67	0.14	0.04	0.12	0.45
229	Northeast	0.03	2.63	0.11	0.12	0.03	0.85	0.55	0.15	0.05	0.16	0.73
230	Central	0.02	1.07	0.82	tr	0.04	0.27	0.84	0.21	0.19	0.08	0.58
231	Central	0.05	2.59	0.31	0.27	0.05	0.61	0.29	0.23	0.09	0.16	0.84
239	Central	0.02	1.18	0.55	0.30	0.04	0.23	5.27	0.22	0.22	0.1	0.69
246	Central	0.03	1.45	0.23	0.17	0.05	0.83	0.92	0.20	0.05	0.11	0.83
249	Central	0.05	2.13	0.70	0.30	0.06	0.93	1.14	0.30	0.05	0.15	0.66
250	Northeast	0.05	2.11	0.1	0.05	0.06	0.48	0.51	0.07	0.05	0.17	0.75
251	Northeast	0.04	2.05	0.16	0.05	0.08	0.36	0.41	0.16	0.04	0.17	0.54
252	Central	0.08	1.90	0.05	0.10	0.16	0.74	0.32	0.06	0.53	0.24	0.43
253	Central	tr	1.14	3.33	0.92	n.d.	0.07	3.37	1.14	0.52	tr	0.77
254	Northeast	0.04	2.41	0.25	tr	0.06	0.81	0.82	0.18	0.04	0.20	0.71
263	South	0.01	1.13	0.31	0.24	0.03	0.25	2.05	0.11	0.01	0.07	0.93
274	Central	0.13	3.46	0.20	0.04	0.06	4.48	0.38	0.25	0.21	0.28	0.80
281	Northeast	0.05	1.76	0.25	0.09	0.15	0.92	0.63	0.21	0.03	0.24	0.83
283	South	0.04	1.29	0.40	0.20	0.04	0.16	0.71	0.05	0.19	0.15	0.63

^a H₃₀, C₃₀ 17 α (H),21 β (H)-hopane;H₂₉, C₂₉ 17 α (H)-30-norhopane; β -car, β -carotane; 29Nsp, C₂₉ 28-nospergulane; Tr_n, C_n 13 β (H),14 α (H)-tricyclic terpane (sum of A + B isomers); SH₃₀, C₃₀ 8 α (H),14 α (H),17 α (H),21 β (H)-secohopane; Tr_n, C_n tricyclic terpane; ONII, 8 α (H),14 β (H)-onoceranone; ONIII, 8 α (H),14 β (H)-onoceranone; 3 β MH₃₁, C₃₁ 3 β -methylhopane; Te₂₄, C₂₄ tetracyclic terpane; H₃₁R, C₃₁17 α (H),21 β (H)-homohopane (R). tr = trace level.

series, whose precursors are the 3 β -methyl-hopanoids synthesized by several types of methanotrophic bacteria (Eigenbrode et al., 2008; Welander et al., 2012). These biomarkers, usually present in small amounts in crude oils, are a key example of the detection potential of GC×GC, due to its characteristics of high peak capacity and sensitivity, as previously shown by Oliveira et al. (2012a). The coelution between gammacerane and C₃₁ 3 β -methyl-hopane normally observed in monodimensional GC, was solved by utilizing GC×GC.

Gammacerane and TPP were also identified in all of the Recôncavo oils. High relative concentration of gammacerane is commonly related to hypersalinity, highly specific for water-column stratification during source rock deposition. TPP has an origin linked to precursors from freshwater algae. A relatively high concentration

of TPP is considered indicative of source rocks deposited in a lacustrine environment (Holba et al., 2003).

β -Carotane, thought to be derived from halo-tolerant unicellular algae which thrive in anoxic, saline lacustrine or highly restricted marine settings (Peters et al., 2005; Sousa Júnior et al., 2013), was also detected in the 20 oil samples.

Onoceranones are associated with restricted basins in warm and humid tropical climates such as Brazil (Oliveira et al., 2012a). Their origin is unclear, but is thought to be related to terrigenous dominated ferns and flowering plants (Peters et al., 2005).

The GC×GC-TOFMS identification and quantification of the compounds just described were used to establish origin, paleoenvironmental conditions and maturity of the oils (calculated and reported in Tables 1–3).

Table 3
Maturity parameters from saturated and aromatic compounds as analyzed by GC×GC-TOFMS.^a

Sample	Saturated biomarker				Aromatics				
	T _s /(T _s +T _m)	H ₃₂ S/(S+R)	C ₂₉ ααα S/(S+R)	C ₂₉ ββ/(ββ+αα)	TA/(TA+MA)	TA I/(I+II)	MDBT 4/1	DMDBT 4.6/1.4	DMDBT 2.4/1.4
183	0.87	0.58	0.45	0.67	0.28	0.94	9.16	3.29	3.34
205	0.78	0.61	0.46	0.54	0.60	0.65	2.94	1.57	1.82
207	0.67	0.59	0.44	0.53	0.64	0.48	2.88	2.66	1.67
211	0.66	0.58	0.41	0.56	0.54	0.53	1.75	2.64	1.61
224	0.57	0.58	0.46	0.67	0.47	0.47	2.28	1.59	1.00
229	0.66	0.59	0.47	0.53	0.54	0.52	1.80	1.63	1.75
230	0.66	0.61	0.43	0.48	0.35	0.81	2.26	2.03	3.54
231	0.52	0.59	0.44	0.62	0.31	0.45	2.03	2.00	1.68
239	0.59	0.69	0.50	0.58	0.52	0.34	2.34	2.45	1.17
246	0.68	0.58	0.56	0.41	0.37	0.48	1.46	1.43	1.69
249	0.58	0.51	0.52	0.57	0.24	0.87	4.12	3.28	1.19
250	0.53	0.51	0.47	0.46	0.49	0.37	3.29	1.18	1.03
251	0.61	0.50	0.41	0.56	0.58	0.39	2.35	1.28	1.24
252	0.59	0.57	0.42	0.55	0.41	0.13	1.76	1.70	1.31
253	0.68	0.60	0.42	0.56	0.52	0.43	3.12	2.03	1.60
254	0.65	0.63	0.40	0.54	0.54	0.44	5.09	1.49	1.11
263	0.56	0.60	0.41	0.54	0.16	0.96	12.56	6.78	3.87
274	0.47	0.46	0.46	0.57	0.39	0.50	3.71	1.32	1.99
281	0.51	0.54	0.49	0.50	0.39	0.71	1.81	1.23	0.99
283	0.61	0.59	0.49	0.64	0.45	0.09	1.12	2.19	1.09

^a T_s, C₂₇22,29,30-trisnorneohopane; T_m, C₂₇ 22,29,30-trisnorhopane; H₃₂, C₃₂ 17α(H),21β(H)-bishomohopane (22S+22R); C₂₉, Σααα+αββ St29 (S+R); C₂₉ ββ, 5α(H),14β(H),17β(H)-24-ethylcholestane; C₂₉ αα, 5α(H),14α(H),17α(H)-24-ethylcholestane; TA, triaromatic steroids; MA, monoaromatic steroids; TA I, triaromatic steroids with short-chain carbon; TA II, triaromatic steroids with long-chain carbon; MDBT, 4-methyl dibenzothiophene; MDBT, 1-methyl dibenzothiophene; DMDBT, 4,6-dimethyl dibenzothiophene; DMDBT, 1,4-dimethyl dibenzothiophene; DMDBT, 2,4-dimethyl dibenzothiophene.

Table 4
Diamondoid parameters obtained from GC×GC-TOFMS analyses.

Sample	Quantitative ^a			Diamondoid indexes ^b			
	3-MD + 4-MD (μg/g)	MAI	DMAI	EAI	TMA	MDI	DMDI
183	1.46	0.59	0.43	0.75	0.15	0.41	0.70
205	1.09	0.26	0.53	0.72	0.17	0.43	0.72
207	1.43	0.38	0.48	0.66	0.16	0.39	0.78
211	1.89	0.29	0.47	0.62	0.11	0.35	0.63
224	6.03	0.73	0.46	0.69	0.17	0.41	0.71
229	0.31	0.53	0.35	0.65	0.12	0.39	0.77
230	1.70	0.65	0.47	0.56	0.18	0.31	0.75
231	2.42	0.65	0.52	0.56	0.19	0.49	0.67
239	1.46	0.57	0.52	0.72	0.12	0.32	0.79
246	2.22	0.67	0.78	0.59	0.24	0.46	0.69
249	1.12	0.50	0.40	0.63	0.13	0.40	0.69
250	1.31	0.62	0.31	0.69	0.13	0.51	0.65
251	0.93	0.59	0.36	0.63	0.13	0.52	0.65
252	0.63	0.63	0.47	0.68	0.14	0.42	0.70
253	4.93	0.44	0.57	0.65	0.09	0.48	0.72
254	0.28	0.59	0.39	0.66	0.08	0.41	0.50
263	5.95	0.73	0.61	0.65	0.19	0.45	0.75
274	1.00	0.56	0.41	0.69	0.17	0.55	0.65
281	1.06	0.55	0.32	0.81	0.13	0.45	0.74
283	0.33	0.63	0.40	0.67	0.13	0.41	0.59

^a Relative quantification to *m/z* 66 fragment of *n*-hexadecane-*d*₃₄, MD = methyl-diamantane;

^b MAI = (1-methyl-adamantane)/(1-methyl-adamantane + 2-methyl-adamantane); MDI = (4-methyl-diamantane)/(4-methyl-diamantane + 1-methyl-diamantane + 3-methyl-diamantane); DMAI = (1,3-dimethyl-adamantane)/(1,2-dimethyl-adamantane + 1,3-dimethyl-adamantane); DMDI = (3,4-dimethyl-diamantane)/(4,9-dimethyl-diamantane + 3,4-dimethyl-diamantane); EAI = (2-ethyl-adamantane)/(1-ethyl-adamantane + 2-ethyl-adamantane); TMAI = (1,3,5-trimethyl-adamantane)/(1,3,5-trimethyl-adamantane + 1,3,4-trimethyl-adamantane).

4.2. Aromatic compounds

C ring monoaromatic (MA) steroid (*m/z* 253) and triaromatic (TA) steroid (*m/z* 231) distributions were investigated in the aromatic fractions of the Recôncavo oils. These biomarkers are common constituents in sediments and petroleum and have been successfully used as thermal maturity parameters (Hussler et al., 1981; Mackenzie et al., 1981; Riolo et al., 1986). The MAs were

assigned as C₂₁, C₂₂, C₂₇, C₂₈ and C₂₉ components, while the TAs were assigned as C₂₀, C₂₁, C₂₆, C₂₇ and C₂₈.

Benzothiophenes and dibenzothiophenes are not formally considered biomarkers because they cannot be related to specific biological precursors. Despite that, geochemical parameters based on benzothiophenes and dibenzothiophenes, which are abundant in mature oils, have been proposed and applied as thermal maturity indicators in source rocks and oils (Radke et al., 1982; Chakhmakhchev et al., 1997; Santamaría-Orozco et al., 1998; Heckmann et al., 2011). In all the Recôncavo oils investigated, 1- and 4-methyl-dibenzothiophene (MDBT; *m/z* 198), 1,4-dimethyl-dibenzothiophene (DMDBT; *m/z* 212), 2,4-DMDBT and 4,6-DMDBT and different isomers of trimethyl-dibenzothiophene (TMDBT; *m/z* 226) were identified. Fig. 2S shows a “roof tile effect” for the alkyl-dibenzothiophenes, where each family with the same carbon number is easily grouped.

Parameters for maturity assessment of the oils, based on aromatic compounds, have been calculated using the GC×GC-TOFMS peak areas and are reported in Table 3.

4.3. Diamondoids

Diamondoid analyses by GC×GC-TOFMS were published recently (Li et al., 2012; Silva et al., 2013), showing the advantages of GC×GC-TOFMS in analyzing extended diamondoids. Adamantanes (*m/z* 135, 136, 149, 163, 177 and 191), diamantanes (*m/z* 187, 188, 201 and 215), triamantanes (*m/z* 239, 240, 244, 253 and 267) and tetramantanes (*m/z* 291, 292 and 305) were investigated. However, the samples analyzed in this study did not show considerable amounts of tri- nor tetramantanes (signal-to-noise ratio lower than 10). Adamantanes and diamantanes were identified and their peak areas were used to calculate diamondoid ratios (Table 4).

5. High resolution molecular organic geochemistry

The use of GC×GC-TOFMS adds a new approach to geochemical analysis. Regarding the crude oils from the Recôncavo Basin, saturated compounds were investigated looking for minor

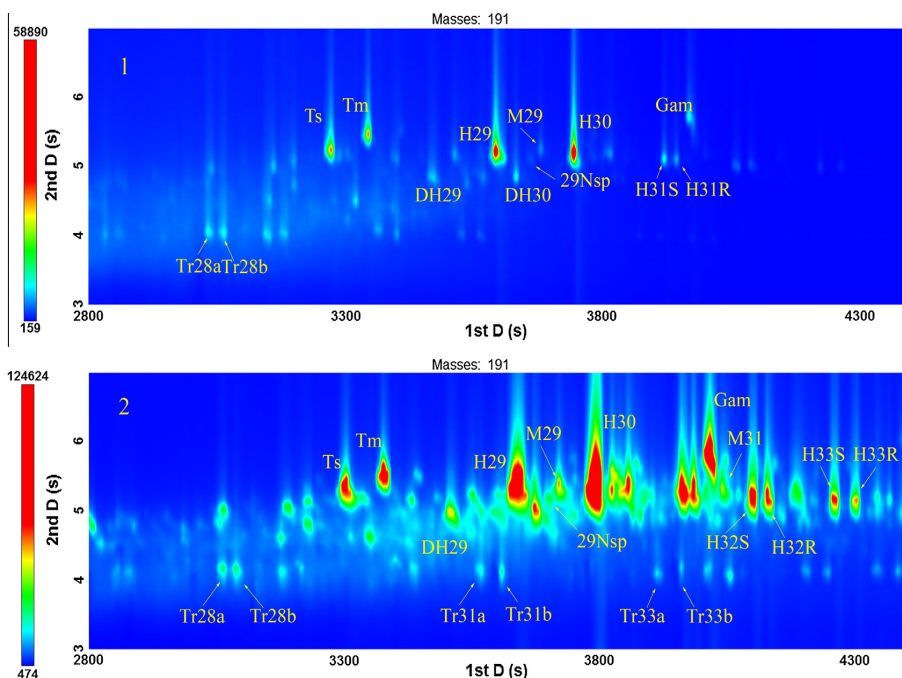


Fig. 2. Extracted ion chromatogram m/z 191 showing mainly pentacyclic terpanes (e.g. hopanes) eluate. Sample 263 [1] shows low abundance of m/z 191, whereas, sample 252 [2] presents high abundance. Tm = 17 α (H)-22,29,30 trisnorhopane; Ts = 18 α (H)-22,29,30 trisnorneohopane; Trn = C_n tricyclic terpane; H₂₉ = 17 α (H),21 β (H)-30-norhopane and C₂₉Ts = 18 α (H),21 β (H)-30-norneohopane; 29Nsp = C₂₉ 28-nor-spergulane, M₂₉ = 17 β (H),21 α (H)-30-norhopano; H₃₀ = 17 α (H),21 β (H)-hopane; M₃₀ = 17 β (H),21 α (H)-hopane; H₃₁₋₃₃ = C₃₁-C₃₃ homohopane; Gam = gammacerane; M₃₁ = 17 β (H),21 α (H)-30-homohopane; DH₃₀ = C₃₀ 17 α -diahopane.

differences related to depositional paleoenvironment. Maturity assessments were possible combining data from saturated biomarkers, aromatics and diamondoids using Principal Component Analysis (PCA).

5.1. Depositional environment

The lacustrine origin of the Recôncavo oils is clearly demonstrated by the high H₃₀/St ratios (C₃₀-17 α ,21 β -hopane 20S + 20R/C₂₇-5 α ,14 α ,17 α -cholestanes 20S + 20R) reported in Table 1 and is supported by the ratios of Tr₂₆/Tr₂₅ and TPP/Dia₂₇. The main purpose of this work was to identify minor compositional variations in the Recôncavo Basin oils using GC \times GC-TOFMS and thus provide more details about the original lacustrine environment. For instance, the detection of 3 β -methyl-hopanes in all the studied oils reinforces a lacustrine origin for the Recôncavo Basin. These biomarkers have been recently characterized in Brazilian lacustrine oils from the Potiguar and Cumuruxatiba basins as minor constituents (Oliveira et al., 2012a). Similarly, considering that all the samples contain β -carotane and gammacerane, a more detailed investigation of these compounds was undertaken. The β -carotane/17 α ,21 β -C₃₀-hopane ratio (β -car/H₃₀) for all samples was calculated and the values plotted against H₃₀/St (Fig. 3a). The separation of the 20 samples into at least two groups can be clearly established. It must be observed that in the group characterized by higher values of β -carotane, almost all the oils were from the center of the Recôncavo Basin (Fig. 3b). As β -carotane is associated with saline lacustrine paleoenvironments, data reveal that the salinity was not constant throughout ancient lake deposition in the Recôncavo Basin.

Gammacerane is usually found in oils at least at trace levels, but a high relative abundance indicates a stratified water column due to hypersalinity during source rock deposition (Sinninghe Damsté et al., 1995). In these samples, the G/H₃₀ ratio is not relatively high

compared to other studies (Petersen et al., 2012) even though it correlates with β -car/H₃₀ ratio (Fig. 4).

According to the literature (e.g., Coutinho, 2008), most of the hydrocarbons accumulated in the Recôncavo reservoirs are considered to be generated from the lacustrine freshwater shales in the Gomo and Tauá Members of the Candeias Formation. The elevated β -car/H₃₀ and G/H₃₀ ratios in some of the studied oils (Fig. 5) appear to suggest the existence of episodes of higher salinity during deposition of these source rocks.

It is well known that the conditions in lakes may change within relatively short periods of time (see, for instance, Killops and Killops, 2005), resulting in deposition of different organic facies. Based on the biomarker data described above, it is reasonable to suppose that there could have been halophilic protozoa and halotolerant microscopic algae, living in saline waters resulting the relatively higher concentrations of gammacerane and β -carotane in some samples.

In order to better understand the differences between the 20 samples, a statistical investigation based on PCA of the traditional (Table 1, Fig. 6a) and traditional plus non-conventional (Tables 1 + 2, Fig. 6b) source biomarker parameters has been carried out. The introduction of non-conventional parameters differentiated samples 253 and 274 from the main group. The score contribution analysis for these two samples, illustrated in Fig. 7 shows the importance of the unusual biomarkers for oil differentiation. The ratios of ONII/H₃₀, ONIII/H₃₀ and DH₃₀/H₃₀ were the main factors responsible for the separation of sample 253 (Fig. 7a), whereas for sample 274 the ratios of 3 β MH₃₁/H₃₀, Te₂₄/Tr₂₆ and H_{31R}/H₃₀ were the main factors (Fig. 7b).

5.2. Maturity

Internal deuterated standards were used to perform quantification of diamondoids, especially 3- and 4-methyl-diamantanes

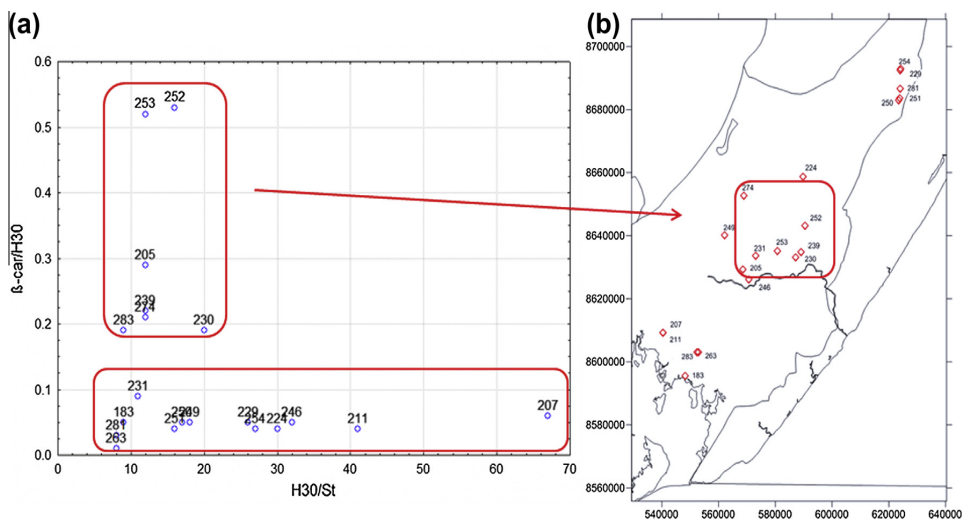


Fig. 3. (a) β -Carotane/ $17\alpha(\text{H}),21\beta(\text{H})$ -30-hopane ($\beta\text{-car}/\text{H}_{30}$) ratio vs. $17\alpha,21\beta\text{-C}_{30}$ -hopane/ $20\text{S} + 20\text{R}$ C_{27} $5\alpha,14\alpha,17\alpha$ -cholestanes (H_{30}/St) graph, and (b) Recôncavo Basin map with samples from the central region highlighted.

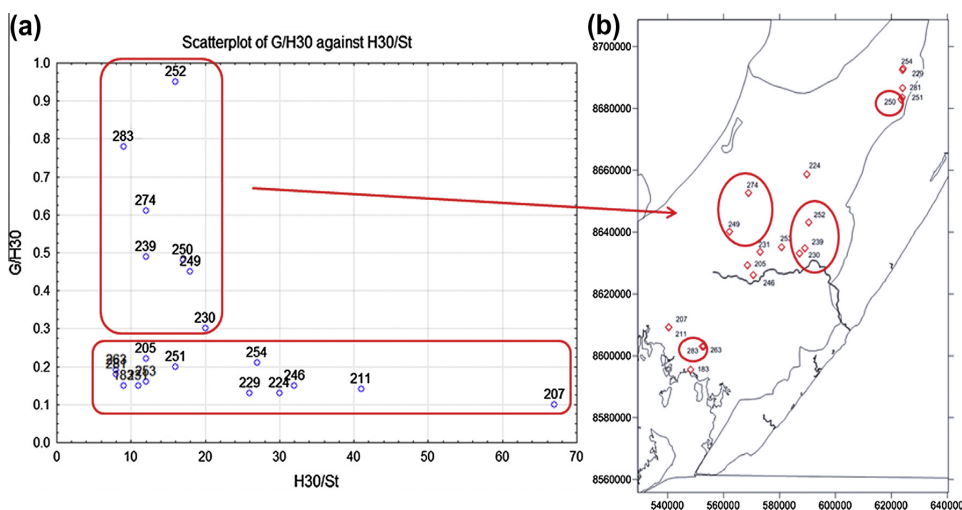


Fig. 4. (a) Gammacerane/ $17\alpha(\text{H}),21\beta(\text{H})$ -30-hopane (G/H_{30}) ratio vs. (H_{30}/St) graph, and (b) Recôncavo Basin map with samples from the central region highlighted.

which are used to plot the Dahl's diagram (Dahl et al., 1999; Silva et al., 2013) (Fig. 8).

Diamondoid ratios were also used to estimate thermal maturity as good relationships were recently found in simulation experiments by Fang et al. (2012). In their work, the authors assigned diamondoid ratios to the Easy%Ro scale, which is a vitrinite reflectance equivalence scale for thermal maturity simulation experiments as proposed by Sweeney and Burnham (1990). The results were plotted in Fig. 9 to fit the Recôncavo Basin samples in an Easy%Ro range calculated from EAI (ethyl-adamantane index) and DMAI (dimethyl-adamantane index) (Table 4).

Almost all samples are in the range of 1.0–1.5%, supporting Dahl's diagram suggestion that these oils have a thermal maturity near the boundary between biomarker cracking and cracking of the main components in the oils. Although the shape of Dahl's diagram for different petroleum systems is quite similar, the diamondoid baseline is characteristic of a particular petroleum system. For

these lacustrine oils, a baseline around 1–2 $\mu\text{g}/\text{g}$ was found. Noticeably three samples (253, 224, 263) presented diamondoid concentration compatible to an initial stage of cracking. In Fig. 10, samples 263 and 253 showed two of the three higher DMAI values, corroborating the quantitative diamondoid analysis. However, sample 246 shows a DMAI ratio which is not fully understood. Caution must be taken as (a) the low stigmasterane concentration are due to both thermal maturity and lacustrine deposition and (b) these parameters are known to be influenced by other variables such as lithofacies and organic matter type (Grice et al., 2000; Wei et al., 2006; Springer et al., 2010).

Apparently, the sample set exhibits thermal maturity in the narrow range in which traditional saturated biomarker ratios start to be inconclusive (i.e. ratios of $20\text{S}/(20\text{S} + 20\text{R})$ C_{29} $5\alpha(\text{H}),14\alpha(\text{H}),17\alpha(\text{H})$ -24-ethyl-cholestane (C_{29} $\alpha\alpha\alpha$) and C_{32} $22\text{S}/(22\text{S} + 22\text{R})$ $17\alpha(\text{H}),21\beta(\text{H})$ -bishomohopane (H_{32}) had values close to equilibrium) and diamondoids have been concentrated due to thermal

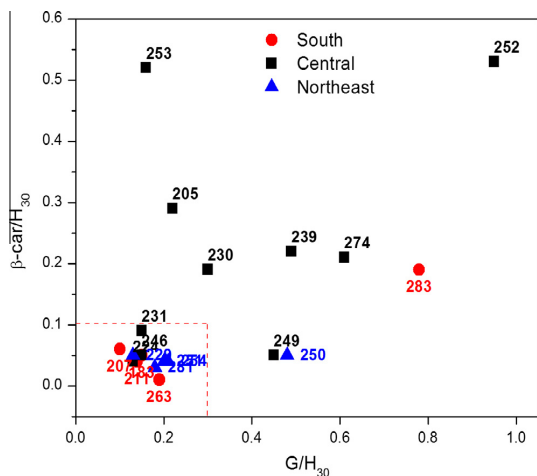


Fig. 5. Graph plotting ratios of (β -car/ H_{30}) vs. (G/H_{30}). The small dashed box illustrates low salinity.

stress, i.e. oil cracking. A more complete approach might consider all gathered data from GC \times GC-TOFMS experiments.

PCA was applied over the maturity variables calculated for the 20 oils resulting in the distinction of three groups (Fig. 10). The first

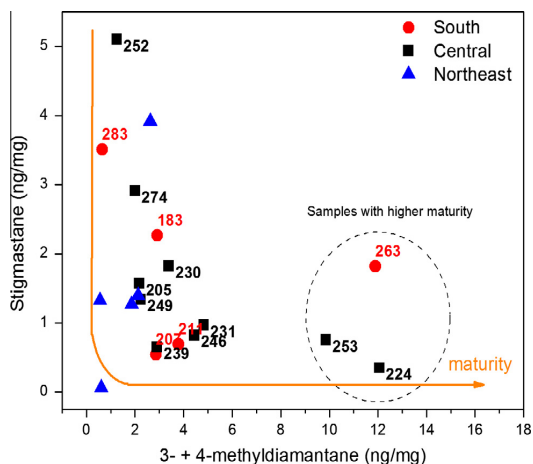


Fig. 8. Relation between biomarker (stigmastane) and diamondoid (methylidiamantanes) concentrations in oils with different thermal maturities, which shows that the biomarkers decrease in concentration with thermal maturity as the diamondoids increase.

group (A) comprises samples 224, 253 and 263, based on diamondoid concentrations ($> 10 \mu\text{g/g}$), (Fig. 8). Meanwhile, samples 250, 251, 252, 274, 281 and 283 are grouped (B) because of their higher

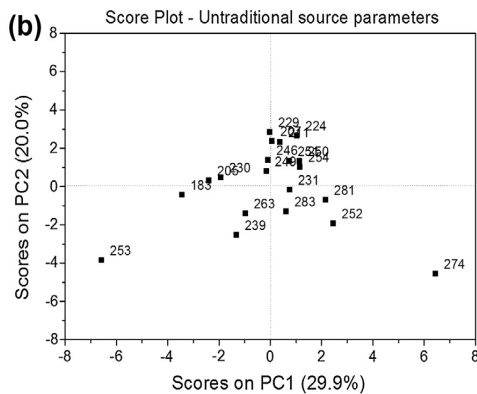
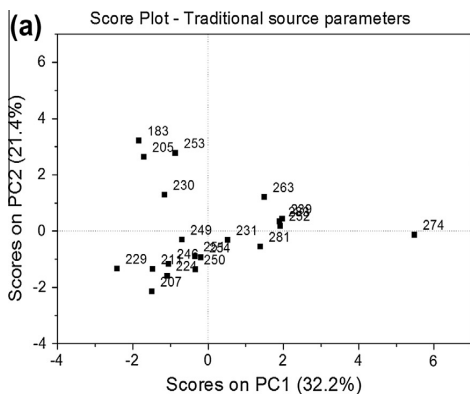


Fig. 6. PCA Score plots (a) traditional and (b) traditional plus non-conventional source parameters. See Table 1 and 2 for the parameters.

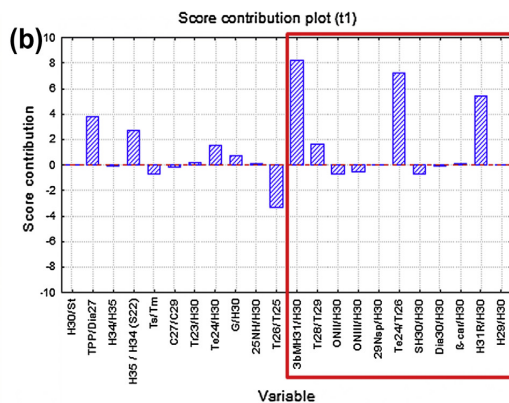
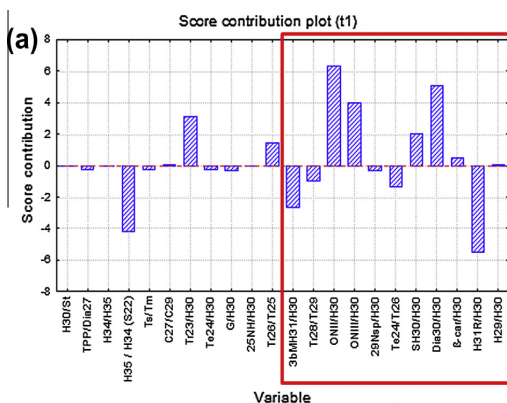


Fig. 7. Parameter contributions to sample 253 (a) and 274 (b) in PCA score plot (from Fig. 9).

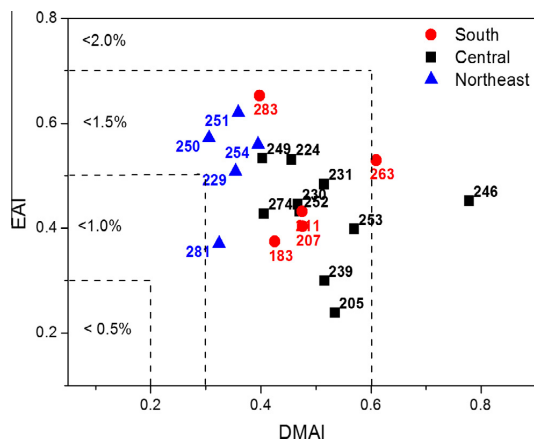


Fig. 9. Regions of estimated EasyRo(%) values from $EAI = (2\text{-ethyl-adamantane}) / (1\text{-ethyl-adamantane} + 2\text{-ethyl-adamantane})$ and $DMAI = (1,3\text{-dimethyl-adamantane}) / (1,2\text{-dimethyl-adamantane} + 1,3\text{-dimethyl-adamantane})$. Indexes boundaries were estimated from Fang et al. (2012).

saturated biomarker content being the most immature sample subset. The remaining samples form a group (C) with positive values on the second principal component. The loading plot suggests group C is differentiated by both diamondoid and aromatic components. In addition, Dahl's diagram displays group C near to the center of the plot. These two features suggest that this group corresponds to either mixed oils or oils altered by other reservoir processes. To better understand the influence of sulfur-containing aromatics, alkyldibenzothiophenes were evaluated. The plots shown in Fig. 3S display the higher abundance of DBTs in samples 183 and 263, both belonging to the southern area of the Recôncavo Basin (Fig. 4b).

Taking into account the highest diamondoid concentration of oils 224, 253 and 263, it is reasonable to speculate that these oils may have migrated short distances from mature source rocks of the Candeias Formation to adjacent reservoirs. In fact, this is one of the models proposed by Figueiredo et al. (1994) and Magnavita and Da Silva (1995) to explain the migration and accumulation of petroleum in the Recôncavo Basin. On the other hand, medium to long distance migration of hydrocarbons generated in the Candeias Formation was possibly involved in the accumulation of oils 250,

251, 252, 274, 281 and 283, the least mature among the 20 oil samples investigated in this study. The above assumptions are supported by Gussow's model of differential entrapment of oil and gas in interconnected reservoirs controlled by buoyancy forces (Gussow, 1953).

Regarding the biodegradation level of the oils analyzed, relatively small quantities of 25-norhopanes have been detected, suggesting that the samples have not undergone intensive biodegradation (Bennett et al., 2006).

6. Conclusions

The use of advanced analytical techniques and statistical routines have enhanced the understanding of petroleum systems of the Recôncavo Basin by allowing a more detailed assessment, using what has been called high resolution molecular organic geochemistry (HRMOG). Lacustrine Brazilian oils were investigated by GC×GC-TOFMS, resulting in a better detection of β -carotene and several other series of biomarkers that were useful to distinguish different source facies. In addition, maturity information from saturated biomarkers, aromatics and diamondoids was used to differentiate maturity throughout the basin, providing supporting information to the understanding of the petroleum system in Recôncavo Basin.

Acknowledgements

We thank CNPq, FAPERJ, FUJB and PETROBRAS (Contract 00500072201.11.9) for support. The Geologists Jarbas V.P. Guzzo and Luiz F.C. Coutinho (Petrobras R&D Center, PDGEO/Geochemistry) are gratefully acknowledged for the fruitful discussions, comments and suggestions. Special thanks go to the Associate Editor Ken Peters, Dr. Jeremy Dahl and an anonymous reviewer for the constructive comments and suggestions that have greatly improved the quality of this article.

Appendix A. Supplementary material

Supplementary data associated with this article can be found, in the online version, at <http://dx.doi.org/10.1016/j.orggeochem.2014.01.009>.

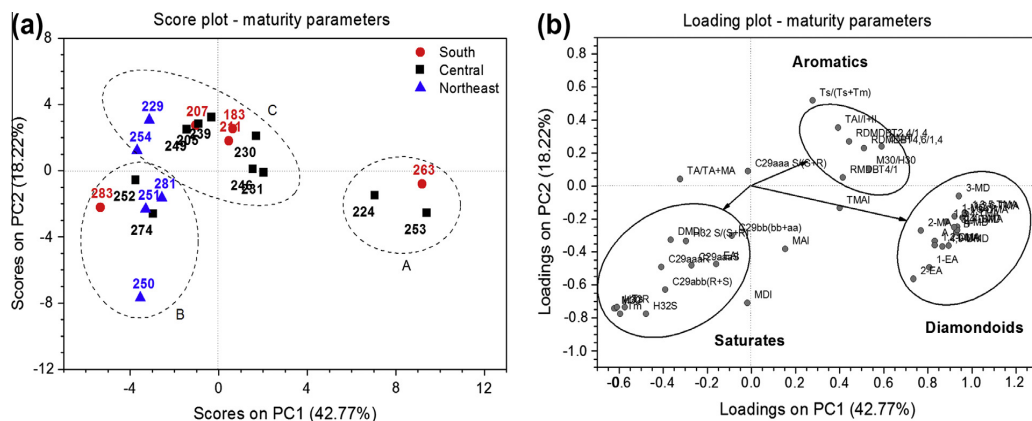


Fig. 10. PCA score [A] and loading [B] plots for the first two components, based on saturated hydrocarbons, aromatic compounds and diamondoid parameters.

References

- Aguiar, A., Silva Júnior, A.I., Azevedo, D.A., Aquino Neto, F.R., 2010. Application of comprehensive two-dimensional gas chromatography coupled to time-of-flight mass spectrometry to biomarker characterization in Brazilian oils. *Fuel* 89, 2760–2768.
- Aguiar, A., Aguiar, H.G.M., Azevedo, D.A., Aquino Neto, F.R., 2011. Identification of methylhopane and methylmoretane series in Ceará Basin oils, Brazil, using comprehensive two-dimensional gas chromatography coupled to time-of-flight mass spectrometry. *Energy & Fuels* 25, 1060–1065.
- Aragão, M.A.N.F., Trindade, L.A.F., Araujo, C.V., Silva, O.B., Scartezini, A.A., Oswald, F.H., Canário, J.A., Garcia, A.P., 1998. Distribution and controls of lacustrine source rocks in the Recôncavo Basin, Brazil. In: Mello, M.R., Yilmaz, P.O. (Eds.), *Extended Abstracts Volume, American Association of Petroleum Geologists International Conference and Exhibition, Rio de Janeiro*, p. 306.
- Azevedo, D.A., Tamaqueira, J.B., Dias, J.C.M., Carmo, A.P.B., Landau, L., Gonçalves, F.T.T., 2008. Multivariate statistical analysis of diamondoid and biomarker data from Brazilian basin oil samples. *Fuel* 87, 2122–2130.
- Bennett, B., Fustic, M., Farrimond, P., Huang, H., Larter, S.R., 2006. 25-Norhopanes: formation during biodegradation of petroleum in the subsurface. *Organic Geochemistry* 37, 787–797.
- Chakhmakhchev, A., Suzuki, M., Takayama, K., 1997. Distribution of alkylated dibenzothiophenes in petroleum as a tool for maturity assessments. *Organic Geochemistry* 26, 483–489.
- Coutinho, L.F.C., 2008. Analysis of the petroleum mass balance in a mature zone for exploration – Recôncavo Basin, Brasil. Ph.D. Thesis. Universidade Federal do Rio de Janeiro, Brazil.
- Dahl, J.E., Moldowan, J.M., Peters, K.E., Claypool, G.E., Rooney, M.A., Michael, G.E., Mello, M.R., Kohnen, M.L., 1999. Diamondoid hydrocarbons as indicators of natural oil cracking. *Nature* 399, 54–57.
- Eigenbrode, J.L., Freeman, K.H., Summons, R.E., 2008. Methylhopane biomarker hydrocarbons in Hamersley Province sediments provide evidence for Neoproterozoic Earth and Planetary. *Science Letters* 273, 323–331.
- Eiserbeck, C., Nelson, R.K., Grice, K., Curiale, J., Reddy, C.M., Raiteri, P., 2011. Separation of 18 α (H)-, 18 β (H)-oleanane and lupane by comprehensive two-dimensional gas chromatography. *Journal of Chromatography A* 1218, 5549–5553.
- Eiserbeck, C., Nelson, R.K., Grice, K., Curiale, J., Reddy, C.M., 2012. Comparison of GC-MS, GC-MRM-MS, and GC \times GC to characterise higher plant biomarkers in Tertiary oils and rock extracts. *Geochimica et Cosmochimica Acta* 87, 299–322.
- Fang, C., Xiong, Y., Liang, Q., Li, Y., 2012. Variation in abundance and distribution of diamondoids during oil cracking. *Organic Geochemistry* 47, 1–8.
- Figueiredo, A.M.F., Braga, J.A.E., Zabalaga, J.J., Oliveira, G.A., Aguiar, Silva, Mato, L.F., Daniel, L.M.F., Magnavita, L.P., Bruhn, C.H.L., 1994. Recôncavo Basin, Brazil: a prolific intracontinental rift basin. In: Landon, S.M. (Ed.), *Interior Rift Basins: American Association of Petroleum Geologists Memoir*, vol. 59, pp. 157–203.
- Gaglianone, P.C., Trindade, L.A.F., 1998. *Geochimica Brasiliensis. Caracterização geoquímica dos óleos da Bacia do Recôncavo* 2, 15–39.
- Grice, K., Alexander, R., Kagi, R.L., 2000. Diamondoid hydrocarbon ratios as indicators of biodegradation in Australian crude oils. *Organic Geochemistry* 31, 67–73.
- Gussow, W.C., 1953. Differential trapping of hydrocarbons. *American Society of Petroleum Geologists Journal* 1, 4–5.
- Heckmann, J.R., Pereira, R., Gonçalves, F.T.T., Landau, L., Azevedo, D.A., 2011. Geochemical evaluation of Brazilian oils with emphasis on aromatic hydrocarbons. *Química Nova* 34, 1328–1333.
- Holba, A.G., Dzou, L.L., Wood, G.D., Ellis, L., Adam, P., Schaeffer, P., Albrecht, P., Greene, T., Hughes, W.B., 2003. Application of tetracyclic polyprenoids as indicators of input from fresh-brackish water environments. *Organic Geochemistry* 34, 441–469.
- Hussler, G., Chappe, B., Wehrung, P., Albrecht, P., 1981. C27–C29 ring A monoaromatic steroids in Cretaceous black shales. *Nature* 294, 556–558.
- Killops, S., Killops, V., 2005. *Introduction to Organic Geochemistry*, second ed. Wiley-Blackwell, Oxford, UK.
- Li, M., Wang, T.G., Lillis, P.G., Wang, C., Shi, S., 2012. The significance of 24-norcholestanes, triaromatic steroids and dinosteroids in oils and Cambrian-Ordovician source rocks from the cratonic region of the Tarim Basin, NW China. *Applied Geochemistry* 27, 1643–1654.
- Mackenzie, A.S., Hoffmann, C.F., Maxwell, J.R., 1981. Molecular parameters of maturation in the Toarcian shales, Paris Basin, France—III. Changes in aromatic steroid hydrocarbons. *Geochimica et Cosmochimica Acta* 45, 1345–1355.
- Magnavita, L.P., Da Silva, H.T.F., 1995. Rift border system: the interplay between tectonics and sedimentation in the Recôncavo Basin, Northeastern Brazil. *American Association of Petroleum Geologists Bulletin* 79, 1590–1607.
- Marotta, E.C.G.B., 2010. Separation and Quantitative Determination of Linear and Cyclic/branched Alkanes from Brazilian Oils by Urea Adduction and Gas Chromatography. M.Sc. Dissertation. Universidade Federal do Rio de Janeiro, Brazil.
- Mello, M.R., Koutsoukos, E.A.M., Mohriak, W.U., Bacoccoli, G., 1994. Selected petroleum systems in Brazil. In: Magoon, L.B., Dow, W.G. (Eds.), *The Petroleum System – from Source to Trap*. American Association of Petroleum Geologists Memoir, vol. 60, pp. 499–512.
- Milani, E.J., Davison, I., 1988. Basement control and transfer tectonics in the Recôncavo-Tucano-Jatobá rift, Northeast Brazil. *Tectonophysics* 154, 41–70.
- Moldowan, J.M., Sundararaman, P., Schoell, M., 1986. Sensitivity of biomarker properties to depositional environment and/or source input in the Lower Toarcian of SW-Germany. *Organic Geochemistry* 10, 915–926.
- Nwadinigwe, C.A., Nwobodo, I.O., 1994. Analysis of *n*-paraffins in light crudes: molecular sieve and urea adduction techniques revisited. *Fuel* 73, 779–782.
- Oliveira, C.R., Ferreira, A.A., Oliveira, C.J.F., Azevedo, D.A., Santos Neto, E.V., Aquino Neto, F.R., 2012a. Biomarkers in crude oil revealed by comprehensive two-dimensional gas chromatography time-of-flight mass spectrometry: depositional paleoenvironment proxies. *Organic Geochemistry* 46, 154–164.
- Oliveira, C.R., Oliveira, C.J.F., Ferreira, A.A., Azevedo, D.A., Aquino Neto, F.R., 2012b. Characterization of aromatic steroids and hopanoids in marine and lacustrine crude oils using comprehensive two dimensional gas chromatography coupled to time-of-flight mass spectrometry (GC \times GC-TOFMS). *Organic Geochemistry* 53, 131–136.
- Peters, K.E., Walters, C.C., Moldowan, J.M., 2005. *The Biomarker Guide, Biomarkers and Isotopes in Petroleum Exploration and Earth History*, vol. 2. Cambridge University Press, Cambridge, UK.
- Petersen, H.L., Holland, B., Nytoft, H.P., Cho, A., Piasecki, S., de la Cruz, J., Cornec, J.H., 2012. Geochemistry of crude oils, seepage oils and source rocks from Belize and Guatemala: indications of carbonate-sourced petroleum systems. *Journal of Petroleum Geology* 35, 127–163.
- Radke, M., Welte, D.H., Willsch, H., 1982. Geochemical study on a well in the Western Canada Basin: relation of the aromatic distribution pattern to maturity of organic matter. *Geochimica et Cosmochimica Acta* 46, 1–10.
- Riolo, J., Hussler, G., Albrecht, P., Connan, J., 1986. Distribution of aromatic steroids in geological samples: their evaluation as geochemical parameters. *Organic Geochemistry* 10, 981–990.
- Santamaría-Orozco, D., Horsfield, B., Di Primio, R., Welte, D.H., 1998. Influence of maturity on distributions of benzo- and dibenzothiophenes in Tithonian source rocks and crude oils, Sonda de Campeche, Mexico. *Organic Geochemistry* 28, 423–439.
- Santos, C.F., Cupertino, J.A., Braga, J.A.E., 1990. Síntese sobre a geologia das bacias do Recôncavo, Tucano e Jatobá. In: Raja Gabaglia, G.P., Milani, E.J. (Eds.), *Origem e evolução das bacias sedimentares brasileiras*, Petrobras, Rio de Janeiro, pp. 235–266 (in Portuguese).
- Silva, R.S.F., Aguiar, H.G.M., Rangel, M.D., Azevedo, D.A., Aquino Neto, F.R., 2011. Comprehensive two-dimensional gas chromatography with time of flight mass spectrometry applied to biomarker analysis of oils from Colombia. *Fuel* 90, 2694–2699.
- Silva, R.C., Silva, R.S.F., Castro, E.V.R., Peters, K.E., Azevedo, D.A., 2013. Extended diamondoid assessment in crude oil using comprehensive two-dimensional gas chromatography coupled to time-of-flight mass spectrometry. *Fuel* 112, 125–133.
- Sinninghe Damsté, J.S., Kenig, F., Koopmans, M.P., Köster, J., Schouten, S., Hayes, J.M., de Leeuw, J.W., 1995. Evidence for gammacerane as an indicator of water column stratification. *Geochimica et Cosmochimica Acta* 59, 1895–1900.
- Sousa Júnior, G.R., Santos, A.L.S., de Lima, S.G., Lopes, J.A.D., Reis, F.A.M., Santos Neto, E.V., Chang, H.K., 2013. Evidence for euphotic zone anoxia during the deposition of Aptian source rocks based on aryl isoprenoids in petroleum, Sergipe-Alagoas Basin, northeastern Brazil. *Organic Geochemistry* 63, 94–104.
- Springer, M.V., Garcia, D.F., Gonçalves, F.T.T., Landau, L., Azevedo, D.A., 2010. Diamondoid and biomarker characterization of oils from the Llanos Orientales Basin, Colombia. *Organic Geochemistry* 41, 1013–1018.
- Sweeney, J.J., Burnham, A.K., 1990. Evaluation of a simple model of vitrinite reflectance based on chemical kinetics. *American Association of Petroleum Geologists Bulletin* 74, 1559–1570.
- Ventura, G.T., Raghuraman, B., Nelson, R.K., Mullins, O.C., Reddy, C.M., 2010. Compound class oil fingerprinting techniques using comprehensive two-dimensional gas chromatography (GC \times GC). *Organic Geochemistry* 41, 1026–1035.
- Ventura, G.T., Simoneit, B.R.T., Nelson, R.K., Reddy, C.M., 2012. The composition, origin and fate of complex mixtures in the maltene fractions of hydrothermal petroleum assessed by comprehensive two-dimensional gas chromatography. *Organic Geochemistry* 45, 48–65.
- Wei, Z., Moldowan, J.M., Dahl, J., Goldstein, T.P., Jarvie, D.M., 2006. The catalytic effects of minerals on the formation of diamondoids from kerogen macromolecules. *Organic Geochemistry* 37, 1421–1436.
- Welander, V.W., Summons, R.E., 2012. Discovery, taxonomic distribution, and phenotypic characterization of a gene required for 3-methylhopanoid production. *Proceedings of the National Academy of Sciences* 109 (32), 12905–12910.



Characterization of unusual tetracyclic compounds and possible novel maturity parameters for Brazilian crude oils using comprehensive two-dimensional gas chromatography-time of flight mass spectrometry



Jaakko Laakia^{a,*}, Alessandro Casilli^a, Bruno Q. Araújo^a, Félix T.T. Gonçalves^a, Elaine Marotta^a, Cleverson J.F. Oliveira^b, Carlos A. Carbonezi^b, Maria Regina B. Loureiro^a, Débora A. Azevedo^a, Francisco R. Aquino Neto^{a,*}

^a Universidade Federal do Rio de Janeiro, Instituto de Química, LAGOA/LADETEC, Ilha do Fundão, Rio de Janeiro, RJ 21941-598, Brazil

^b Division of Geochemistry, Petrobras Research and Development Center (CENPES), Petrobras, Ilha do Fundão, Rio de Janeiro, RJ 21941-915, Brazil

ARTICLE INFO

Article history:

Received 26 March 2016

Received in revised form 18 October 2016

Accepted 18 October 2016

Available online 24 October 2016

Keywords:

Biomarkers

Two-dimensional gas chromatography

Group-type separation

Mass spectrometry

Tetracyclic saturated biomarkers

Maturation

ABSTRACT

Eleven Brazilian oil samples from different sources, biodegradation and maturity levels were analyzed by comprehensive two-dimensional gas chromatography-time of flight mass spectrometry (GC×GC-TOFMS). Geochemical characterization associated with principal component analysis (PCA) allowed the identification of the three most mature oils. The GC×GC chromatographic conditions used in this study allowed us to perform group-type (or chemical class) separation in the following second dimension (²D) order: (i) tricyclic terpanes; followed by (ii) steranes with 3 rings containing 6 carbon atoms and 1 ring containing 5 carbon atoms; (iii) tetracyclic terpanes with 4 rings containing 6 carbon atoms; (iv) pentacyclic terpanes with 4 rings containing 6 carbon atoms and 1 ring containing 5 carbon atoms; and finally (v) pentacyclic terpanes with 5 rings containing 6 carbon atoms. This information was used to tentatively identify the ring structure of eight unusual compounds found in the saturated fraction of the oils. These compounds had the double bond equivalent (DBE) value four, which was calculated based on molecular ions M⁺ at *m/z* 274, 288 and 316, indicating possible tetracyclic structures. Two of them presented a diagnostic peak at *m/z* 191 and six at *m/z* 203. A trend between the ratios of two of these unusual compounds and the C₂₄ tetracyclic terpane versus 4,6/1,4 dimethyldibenzothiophene ratio shows promise as a maturation parameter. Thus, these unusual compounds are prone to respond to the maturation on a scale from mature to overmature, when compared with traditional maturation parameters.

© 2016 Elsevier Ltd. All rights reserved.

1. Introduction

Gas Chromatography (GC) coupled to Mass Spectrometry (MS) has been one of the most important techniques used to assess structural information of the large amounts of compounds observed in complex crude oil samples. Historically, one dimensional GC–qMS-instruments were used for single ion monitoring (SIM) because the full scan mode acquisition rate was not always fast enough to analyze a wide range of ions during GC runs (Sparkman et al., 2011). Nowadays, GC–MS–quadrupole combinations have achieved a sufficient acquisition rate for the monitoring of multiple fragment ions while superior sensitivity and selectivity

have been provided by GC–MS/MS–triple quadrupoles performing MS/MS tandem experiments. In spite of progress in GC–MS technology, a great number of chromatographic co-elution problems in complex sample analyses remain unsolved. Many of these co-elution issues can be addressed by multiple ion monitoring or by applying deconvolution algorithms, which separate overlapping peaks and reconstruct clean chromatograms and mass spectra for each component (Lu et al., 2008). However, this is ineffective when two co-eluting compounds have similar mass spectra and/or the same diagnostic ion.

One key instrumental setup that has the potential to address such issues is comprehensive two-dimensional gas chromatography-time of flight mass spectrometry (GC×GC-TOFMS) (Aguier et al., 2010). Unlike GC–MS analyses, GC×GC instrumentation produces full mass spectrum data with a high acquisition rate, which assures reliable qualitative and quantitative

* Corresponding authors.

E-mail addresses: jaakko.laakia@helsinki.fi (J. Laakia), radler@iq.ufrj.br (F.R. Aquino Neto).

results. In GC×GC, the increase in signal-to-noise ratio is achieved due to the focusing of the chromatographic peaks by a modulator, which generates narrow peaks. In addition, the chemical background of the column, which is typical for one dimensional ^1D GC, generates a characteristic bleeding that increases the baseline with the temperature program. In GC×GC, this bleeding is constantly modulated and separated as any analyte compound in each ^1D fraction. Therefore, some compounds with low abundances, which are commonly lost in the background noise in one dimensional ^1D GC, are more easily resolved in GC×GC-TOFMS. An example of how this technique is effective in displaying compounds hitherto unobservable due to problems of resolution and/or co-elution is found in Oliveira et al. (2012a) and Kiepper et al. (2014) where four isomers for C_{19} – C_{24} tricyclic terpanes and C_{31} β -methylhopane were identified respectively. Recently, Araújo and Azevedo (2016) also used GC×GC-TOFMS to identify unusual steranes in branched-cyclic hydrocarbon fractions of crude oils from the Sergipe-Alagoas Basin, Brazil.

Moreover, ^2D separation improves the quality of mass spectra, making peaks purer by separating mass fragments of co-eluting compounds. A clear example in crude oil research can be seen in the investigation of C_{27} $17\alpha(\text{H})$ -22,29,30-trisnorhopane (Tm) and C_{27} $18\alpha(\text{H})$ -22,29,30-trisnorhopane (Ts), which are commonly used for maturity evaluations (Seifert, 1978). Even though these two compounds are separated and analyzed in ^1D GC, a source dependence which can affect the maturity interpretation of the Ts/Tm ratio has previously been reported (Moldowan et al., 1986). This apparent source dependence can be explained by Ts co-eluting with the C_{30} tetracyclic terpane (TeT_{30}) (Rullkötter and Wendisch, 1982). Furthermore, the concentration of Tm could also be influenced by the C_{30} tricyclic terpane (Tr_{30}), which co-elutes with Tm on ^1D (Aguar et al., 2010). It is well established that the abundance of TeT_{30} and Tr_{30} can be influenced by this kind of organic matter input (Aquino Neto et al., 1983; Moldowan et al., 1983; Peters et al., 2005a). Since the majority of studies using Ts/Tm are conducted with ^1D GC, it is difficult to rule out that co-eluting compounds do not cause problems in interpretation. Therefore, the common solution in geochemical studies based only on one dimensional GC has been to use parallel biomarker parameters (Peters et al., 2005a).

GC×GC-TOFMS provides cleaner mass spectra and improves the accuracy of biomarker ratios by resolving co-eluting compounds in ^2D . Additionally, the deconvoluted ion current (DIC) in TOFMS analysis can be used for compounds which co-elute in ^2D . This is possible due to the fast spectral acquisition rate and absence of concentration skewing (Focant et al., 2004; Mitrevski et al., 2010). Hence, the GC×GC-TOFMS system improves the separation of minor compounds that co-elute in standard GC and GC-MS analyses. It is important to emphasize that the resolution of co-eluting components in GC×GC-TOFMS analyses is a result of an additional dimension for the separation system, which facilitates the identification of new or not often reported (unusual) compounds encountered in complex crude oil samples.

In this study, 11 Brazilian crude oils were examined from differing source rocks and depositional conditions (5 lacustrine, 5 marine and 1 mixture) and with varying biodegradation and maturity levels. The aim was to evaluate the degree of maturation of the oil samples by analyzing saturated and aromatic fractions with conventional and non-conventional biomarker ratios measured by GC×GC-TOFMS. This approach is made possible by the increased capacity of GC×GC-TOFMS in the separation of oil components which can overcome interference in the determination of these parameters caused by their diverse origin and geological history. The enhanced diagnosis capacity enabled by GC×GC-TOFMS leading to High Resolution Molecular Organic Geochemistry (HRMOG), has been previously used for maturation investigations

incorporating established parameters (Casilli et al., 2014). An outcome of this current study was the identification of eight unusual tetracyclic biomarkers in the saturated hydrocarbon fractions which may have potential as maturity indicators. The structure and geochemical significance of these tetracyclic compounds are discussed.

2. Material and methods

2.1. Sample preparation

Selected crude oils from the north to the south regions of Brazil were classified by the Research Center of Petrobras (Centro de Pesquisas Leopoldo Américo Miguez de Mello, CENPES, Rio de Janeiro, RJ, Brazil) using proprietary classifying methods (Table 1). These oils were also pre-fractionated by CENPES with medium pressure liquid chromatography (MPLC, model MKW, Margot Köhnen Willsch, Jülich, Germany) into saturated and aromatic fractions (Radke et al., 1980). The saturated fractions were further processed to remove the *n*-alkanes using urea adduction to separate branched and cyclic hydrocarbon fractions (B/C) (Lappas et al., 1997; Netzel and Rovani, 2007). The detailed experimental procedure for urea adduction and chromatographic analysis is described in Marotta et al. (2014) and Casilli et al. (2014), respectively. The B/C and aromatic fractions (total of 22 samples) were dissolved in dichloromethane (TediaBrasil, Rio de Janeiro, RJ, Brazil) with an internal standard of 20 $\mu\text{g}/\text{mL}$ of perdeuterated *n*-tetracosane- D_{50} and pyrene- D_{10} (Cambridge Isotope Laboratories, Andover, MA, USA) before chromatographic analyses.

2.2. GC×GC-TOFMS and data processing

Analyses were performed on a Pegasus 4D (Leco, St. Joseph, MI, USA) GC×GC-TOFMS, composed of an Agilent Technologies 6890 GC (Palo Alto, CA, USA) equipped with a secondary oven, a non-moving quad-jet dual-stage modulator and a Pegasus III (Leco, St. Joseph, MI, USA) time of flight mass spectrometer. A DB-5 column (Agilent Technologies, Palo Alto, CA, USA), 5% phenyl-95% methylsiloxane (30 m, 0.25 mm i.d., 0.25 μm d_f) was used as the first dimension column (^1D). A BPX-50 column (SGE, Ringwood, VIC, Australia) with 50% phenyl polysilphenylene-siloxane (1.5 m, 0.1 mm i.d., 0.1 μm d_f) was used as the second dimension column (^2D). The ^2D column was connected to the TOFMS by means of a 0.5 m × 0.25 mm i.d. uncoated deactivated fused silica capillary, using SGE mini-unions and Siltite™ metal ferrules 0.1–0.25 mm i.d. (Ringwood, VIC, Australia) (Silva et al., 2011; Oliveira et al., 2012a).

GC conditions were: splitless mode injection of 1 μL at 290 °C, a purge time of 60 s, and a purge flow of 5 mL/min. Helium was used as the carrier gas at a constant flow rate of 1.5 mL/min. The primary oven temperature program began at 70 °C for 1 min, and was then increased to 170 °C at 20 °C/min, and further to 325 °C at 2 °C/min. The secondary oven temperature program was 10 °C higher than the primary one. The modulation period was 8 s with a 2 s hot pulse duration, and the modulator temperature was 30 °C higher than the primary oven temperature. The transfer line to the MS was set at 280 °C, the electron ionization mode was set at 70 eV, the mass range was 50–600 Da, the ion source temperature was 230 °C, the detector was +50 V above the tune value, and the acquisition rate was 100 spectra/s. Compound identification was performed by mass spectral examination, comparison with literature mass spectra, retention time and elution order, which is extensively reported in previous works (Aguar et al., 2010, 2011; Oliveira et al., 2012a, 2012b).

Table 1
Geochemical parameters of selected Brazilian crude oils measured by GC×GC-TOFMS.

Geochemical parameters/classification ^a	S01 LS-NB Off	S02 LS-SB On	S03 MIX-BD Off	S04 MN-NB-MM Off	S05 MN-NB-HM Off	S06 MR-NB-HM On	S07 MR-BD-HM Off	S08 LS-NB-HM Off	S09 LF-SB On	S10 LF-NB On	S11 ME On
SAT% ^b	42	26	26	52	72	54	58	38	38	50	44
ARO% ^b	4	18	15	14	16	10	17	13	1	12	10
NSO% ^b	22	53	40	16	7	10	15	27	25	14	11
H ₃₀ /St ₂₇ ^c	9.30	3.80	2.40	3.60	1.70	0.91	3.80	9.70	22.0	85.0	4.40
Tr ₂₃ /H ₃₀	0.34	2.50	0.23	0.24	0.61	2.40	2.30	0.30	0.50	0.50	0.06
Tr ₂₆ /Tr ₂₅	0.91	1.14	1.21	0.71	0.99	1.23	0.96	1.09	1.46	0.29	0.96
2 α MH ₃₁ /H ₃₀ %	5.10	14.0	5.60	4.00	1.40	4.20	1.90	1.80	0.62	0.77	9.60
3 β MH ₃₁ /H ₃₀ % ^d	1.73	10.0	1.72	0.65	0.55	2.40	0.62	1.40	29.0	11.03	0.41
TeT ₂₄ /H ₃₀	0.10	0.79	0.04	0.04	0.08	0.10	0.20	0.08	0.11	0.07	0.02
TeT ₂₄ /Tr ₂₆	0.50	0.44	0.33	0.34	0.18	0.07	0.17	0.34	0.20	2.93	0.64
H ₂₉ /H ₃₀	0.60	1.48	0.48	0.48	0.39	0.70	0.38	0.58	0.55	0.57	0.52
H ₃₁ R/H ₃₀	0.34	0.08	0.20	0.22	0.13	0.26	0.14	0.20	0.18	0.12	0.10
Gam/H ₃₀	0.16	0.90	0.45	0.05	0.00	0.22	0.13	0.16	0.28	0.25	0.86
H ₃₅ (R + S)/H ₃₄ (R + S)	0.67	0.82	0.58	0.74	0.48	0.60	0.41	0.52	0.40	0.39	0.52
β -car/H ₃₀ ^e	0.05	0.15	0.22	0.19	0.15	1.56	0.35	0.05	0.06	0.03	0.12
TPP/Dia ₂₇ ^f	0.38	1.77	0.17	0.19	0.08	0.23	0.31	0.55	36.0	10.0	0.05
Tr ₂₁ /Tr ₂₃	0.83	0.71	0.85	0.59	0.60	0.80	0.77	0.84	0.75	0.74	0.66
Tr ₂₀ /Tr ₂₃	0.53	0.51	0.53	0.28	0.25	0.48	0.39	0.44	0.57	0.47	0.46
M ₃₀ /H ₃₀	0.11	0.28	0.13	0.10	0.06	0.14	0.08	0.13	0.22	0.16	0.13
Tr ₁₉₋₃₀ (S + R)/H ₂₈₋₃₄ (S + R) ^g	0.56	2.60	0.39	0.45	1.52	4.60	4.80	0.69	1.40	1.20	0.18
H ₃₂ 22S/(22S + 22R)	0.58	0.55	0.56	0.59	0.61	0.59	0.59	0.61	0.51	0.60	0.59
St ₂₉ 20S/(20S + 20R)	0.43	0.48	0.36	0.50	0.58	0.54	0.48	0.52	0.39	0.55	0.53
St ₂₉ $\beta\beta$ (S + R)/ $\beta\beta$ (S + R) + $\alpha\alpha$ (S + R)	0.48	0.32	0.42	0.59	0.63	0.61	0.51	0.52	0.48	0.56	0.51
Ts/(Ts + Tm)	0.32	0.27	0.42	0.55	0.83	0.47	0.62	0.29	0.32	0.46	0.64
25NH/H ₃₀ (m/z 177)	0.03	1.54	0.07	0.01	0.00	0.01	0.14	0.08	0.01	0.01	0.00

H₃₀, C₃₀ 17 α (H),21 β (H)-hopane; St₂₇, C₂₇ 5 α (H),14 α (H),17 α (H)-cholestanes (20S + 20R); Tr_n, C_n tricyclic terpane; 2 α MH₃₁, C₃₁ 2 α -methylhopane; 3 β MH₃₁, C₃₁ 3 β -methylhopane; TeT₂₄, C₂₄ tetracyclic terpane; H₂₉, C₂₉ 17 α (H), 21 β (H)-30-norhopane; H₃₁R, C₃₁ 17 α (H),21 β (H)-homohopane (R); Gam, gammacerane; H₃₄, C₃₄ 17 α (H),21 β (H)-tetrakisomohopane (22S + 22R); H₃₅, C₃₅ 17 α (H),21 β (H)-pentakisomohopane (22S + 22R); β -car, β -carotane; TPP, C₃₀ tetracyclic polyterpene; Dia₂₇, C₂₇ 13 β (H),17 α (H)-diacholestanes (20S + 20R); M₃₀, C₃₀ 17 β (H),21 α (H)-hopane; H₃₂, C₃₂ 17 α (H),21 β (H)-bishomohopane (22S + 22R); St₂₉, C₂₉ 5 α (H),14 α (H),17 α (H) + 5 α (H), 14 β (H), 17 β (H), 24-ethylcholestane (20S + 20R); Ts, C₂₇ 22,29,30-trisnorhopane; Tm, C₂₇ 22,29,30-trisnorhopane; LS, lacustrine saline; LF, lacustrine freshwater; MN, marine normal; MR, marine restricted; ME, marine evaporitic; MIX, Mixture (marine + lacustrine); NB, Non biodegraded; BD, biodegraded; SB, severe biodegraded; MM, medium maturation; HM, high maturation; Off, off shore; On, on shore.

^a The parameters are taken from Peters et al. (2005a) unless stated otherwise and the classification of crude oils was provided by CENPES.

^b Compound class distribution, in percentage (%), determined by liquid chromatography was provided by CENPES.

^c Mello et al. (1988).

^d Kiepper et al. (2014).

^e Casilli et al. (2014).

^f Silva et al. (2011).

^g Silva et al. (2008).

2.3. Chemometric analyses

The software package Statistica 8 (Statsoft Inc., Tulsa, OK, USA) was used in all statistical calculations in this work. Principal Component Analysis (PCA) was based on the covariance matrix. All variables were mean centered and scaled by the sample standard deviation. Data reported in Tables 1 and 2 were used to create matrix X_(11×42) containing maturity and source ratios from saturated biomarker and aromatic compounds. Also matrix X_(11×101) was constructed for the analysis of all the normalized peak areas: area of compounds/area of internal standard (A_c/A_{is}). In the calculations *n*-tetracosane-D₅₀

was used for compounds in B/C fraction and pyrene-D₁₀ for aromatic fraction.

3. Results and discussion

A range of geochemical parameters were determined by identifying and quantifying compounds of geochemical interest. Peak areas and relevant ratios were calculated and are listed in Tables 1 and 2, the majority of which have been described by Peters et al. (2005a). These parameters provide information about different geochemical conditions such as variations in biological source inputs, biodegradation and maturation.

Table 2
Geochemical compound ratios in aromatic fractions of selected crude oils measured by GC×GC-TOFMS.

Geochemical parameters/classification	S01	S02	S03	S04	S05	S06	S07	S08	S09	S10	S11
TA C ₂₀ /(TA C ₂₀ + C ₂₇) %	nd	18.0	5.7	5.1	53.0	18.0	25.0	12.0	nd	4.0	1.0
TA C ₁₉₋₂₁ /(TA C ₁₉₋₂₁ + TA C ₂₆₋₂₈) %	nd	16.0	3.5	3.8	45.0	14.0	37.0	10.0	nd	7.3	0.6
MA C ₂₁ /(MA C ₂₁ + C ₂₈) %	13.0	47.0	7.1	24.0	73.0	49.0	67.0	28.0	nd	43.0	13.0
MA C ₂₀₋₂₁ /(MA C ₂₀₋₂₁ + MA C ₂₇₋₂₉) %	7.4	40.0	5.5	17.0	63.0	42.0	54.0	27.0	nd	47.0	10.0
MDBT 4/1	1.7	1.7	2.8	3.6	5.4	11.0	17.0	2.7	nd	6.3	2.4
DMDBT 2,4/1,4	0.5	0.3	0.9	0.4	0.5	1.0	1.0	0.7	nd	1.0	0.5
DMDBT 4,6/1,4	1.2	0.7	1.5	1.2	1.9	4.6	7.3	1.2	nd	1.9	1.5
TMDBT peak 3/peak 5	nd	2.0	2.0	1.9	2.6	3.5	6.7	2.0	nd	2.4	1.6

TA, triaromatic steroids; MA, monoaromatic steroids; MDBT, methyl dibenzothiophene; DMDBT, dimethyl dibenzothiophene; TMDBT, trimethyl dibenzothiophene; nd, not determined.

3.1. Saturated hydrocarbons

Geochemically pertinent compounds such as tri-, tetra- and pentacyclic terpanes (m/z 191), methyl-hopanes (m/z 205), 25-norhopane (m/z 177), diasteranes and steranes (m/z 217 and 218), β -carotane (m/z 125), and tetracyclic polyprenoids (m/z 259) were detected in the B/C fractions of the Brazilian oils by monitoring extracted ion chromatograms (EIC). These were used for subsequent interpretations of source, alteration (Biodegradation) and maturity of the various oils.

3.1.1. Saturated hydrocarbon source parameters

The following biomarkers which are characteristic of source organic matter were detected in all B/C fractions of the oils: tricyclic terpane series (Tr_n) from C_{19} to C_{40} , C_{30} diahopane and regular hopanes from C_{28} to C_{36} , except C_{36} hopane was not detected in the oils S06 and S10. Common biomarker parameters used to elucidate source and environment of deposition are as follows. The hopane to steranes ratio, expressed as H_{30}/St_{27} , indicates relative inputs of heterotrophic bacterial biomass (H_{30}), versus eukaryotic organisms (St_{27}) such as algae and higher plants (Fu et al., 1990; Peters et al., 2005a). Low (< 4) H_{30}/St_{27} ratios are typically associated with marine source rocks (Mello et al., 1988) while a high 3β -MH $_{31}/H_{30}$ % ratio ($> 1\%$) indicates lacustrine sources (Kiepper et al., 2014).

The score plot of H_{30}/St_{27} and 3β -MH $_{31}/H_{30}$ % ratios illustrated that oils with low values in both parameters (oils S04–S07) were generated by marine source rocks (Supplementary material, Fig. 1S). It is noteworthy that oils S09 and S10 showed an abnormal elevation of C_{30} 17 α (H),21 β (H)-hopane.

The TPP/Dia $_{27}$ ratio is highly specific for lacustrine organic matter (Silva et al., 2011), with high TPP/Dia $_{27}$ values being characteristic of lacustrine conditions and biomass. Oils S02 and S11 show elevated Gam/ H_{30} ratios, sometimes indicative of hypersalinity in marine shales and is used as an indicator of water-column stratification during source rock deposition. Elevated concentrations of β -carotane were observed in oil S06, a compound which is associated with saline lacustrine paleoenvironments. High values for Tr_{26}/Tr_{25} ratios are typical for lacustrine oils, and low for marine oils. The Tr_{23}/H_{30} ratio responds in the opposite manner, i.e. is low in lacustrine settings (Peters et al., 2005a), although in our study this distinction was unclear. For instance, lacustrine oil (S10) had the lowest value of Tr_{26}/Tr_{25} ratio and a marine oil (S06) had the second highest value. Therefore we relied primarily on H_{30}/St_{27} , 3β -MH $_{31}/H_{30}$ % (Supplementary material, Fig. 1S) and TPP/Dia $_{27}$ to classify the oils as lacustrine, marine and mixed. Based on these geochemical parameters, S01, S02, S08, S09 and S10 are lacustrine oils, S04, S05, S06, S07 and S11 are marine oils; and S03 is a mixture of both sources.

3.1.2. Saturated hydrocarbon biodegradation parameters

During biodegradation hopanes and steranes are preferentially depleted relative to tricyclic terpanes, and consequently can affect the interpretation of geochemical parameters (Peters et al., 2005a). In our study the degree of biodegradation was evaluated using the 25-norhopane to C_{30} hopane (25NH/ H_{30}) ratio (Table 1) (Bennett et al., 2006). According to this parameter, samples S02 and S07 were significantly altered, putting into question the reliability of the Gam/ H_{30} and H_{30}/St_{27} ratios as indicators of biomass and depositional environment for these two samples. The tricyclic terpanes to pentacyclic terpanes (Tr_{19-30} (S + R)/ H_{28-34} (S + R)) ratio is used as an indicator for the level of biodegradation of crude oils (Wenger and Isaksen, 2002) and corroborates the fact that oils S02 and S07 in our study are biodegraded. Interestingly, oils S05, S06, S09 and S10 could also be considered biodegraded based on this ratio. However, these samples do not contain the series of

demethylated tricyclic terpanes (m/z 177) and had a very low 25NH/ H_{30} ratio and are assumed to be different from S02 and S07 in that they were (i) a mixture of a biodegraded oil and fresh oil and/or (ii) altered by different kinds of micro-organisms with different metabolic properties, which did not produce 25-norhopanes (Peters et al., 2005a). In summary oil S02 was clearly the most biodegraded.

3.1.3. Saturated hydrocarbon maturation parameters

Routine sterane and hopane maturity parameters (Table 1) indicate that most of the oils in our study have reached a moderate to high degree of maturity, i.e., are between the beginning of the oil window and the peak of oil generation (Gürgey, 1999; Peters et al., 2005a). Practically all the oils have reached the equilibrium value of 60% for the H_{32} 22S/(22S + 22R) ratio (vitrinite reflectance equivalent of approx. $R_o = 0.6\%$). There is greater variation among the samples for the St_{29} 20S/(20S + 20R) ratio, which reaches equilibrium at 55% (approx. $R_o = 0.9\%$; Gürgey, 1999) and for the St_{29} $\beta\beta$ (S + R)/ $\beta\beta$ (S + R) + $\alpha\alpha$ (S + R) ratio, which reaches equilibrium at 70% (approx. $R_o = 1.0\%$; Petersen et al., 2012). Oils S05 and S06 show the highest values for the sterane maturity parameters (Supplementary material, Fig. 2S) and are considered as the most mature, whereas oils S02, S03 and S09 showed lower values for these ratios, and therefore are considered less thermally evolved. Biodegradation may have altered the steranes in sample S02, since the St_{29} $\beta\beta$ (S + R)/ $\beta\beta$ (S + R) + $\alpha\alpha$ (S + R) ratio is relatively much lower than for the St_{29} 20S/(20S + 20R) ratio (Section 3.1.2).

Based on the moretane/hopane (M_{30}/H_{30}) ratio, which decreases with increasing maturation (Grantham, 1986), oils S05 and S07 are the most mature, while the oils S02 and S09 are the least mature. Finally, $Ts/(Ts + Tm)$ ratios indicate that S01, S02, S08 and S09 oil samples have the lowest degree of thermal maturity whereas S05, S07 and S11 are the most mature samples. It is important to consider that the $Ts/(Ts + Tm)$ ratio can also be influenced by the lithology and oxicity of the depositional setting (Rullkötter et al., 1985; Rullkötter and Marzi, 1988). The terpane and sterane ratios indicated that S06 has highest degree of maturity in contrast to its M_{30}/H_{30} and $Ts/(Ts + Tm)$ ratios, which indicated a lower maturity level. This may be explained by the fact that the S06 sample, which has a high Tr_{19-30} (S + R)/ H_{28-34} (S + R) ratio, was exposed to different maturation and/or biodegradation processes (e.g. removal of hopanes and no formation of 25NH) than oils S05 and S07 (Farrimond et al., 1998). In summary, oils S05 and S06 were the most mature samples based on sterane parameters (Supplementary material, Fig. 2S).

3.2. Aromatic fraction maturity parameters

Monoaromatic (MA, m/z 253) and triaromatic (TA, m/z 231) steroids, which are abundant in mature oils (Mackenzie et al., 1981, 1982; Peters et al., 2005a), were detected in most samples, except for oil S01 in which TA steroids were not detected, and S09, in which neither MA nor TA steroids were detected. Methyl- (MDBT, m/z 198), dimethyl- (DMDBT, m/z 212) and trimethyl-dibenzothiophenes (TMDBT, m/z 226) were found in all of the oil samples, except in sample S09. The following geochemical parameters were calculated for compounds in the aromatic fraction of our oils (Table 2). Methyl- (MDBT) and dimethyl-dibenzothiophenes (DMDBT) ratios, which are used as thermal maturity indicators in the range of mature to overmature oils (Chakhmakhchev et al., 1997; Heckmann et al., 2011), show the highest values for the S06 and S07 oil samples. The mono- and triaromatic steroid ratios, MA $C_{21}/(MA C_{21} + C_{28})$ % and TA $C_{20}/(TA C_{20} + C_{27})$ %, which increase with maturation, show the highest values in the S05 oil. Oil S09 had an extremely small

quantity of aromatic compounds (1% ARO, Table 1), therefore no aromatic geochemical parameters could be calculated.

In summary, ordinary saturated hydrocarbon maturation parameters (Section 3.1.3), indicate that oils S05 and S06 are the most mature samples. This is also supported by the aromatic compound parameters. In addition oil S07 was identified as a mature sample, as was illustrated in Section 3.1.3 with the ratios of M_{30}/H_{30} and $Ts/(Ts + Tm)$.

3.3. Identification of compounds

Eight unusual (or new) compounds were detected in most of the samples, although with varying relative intensities (Table 3). Their distribution is illustrated in the partial chromatogram of the B/C fraction of sample S08 shown in Fig. 1, as well as the respective mass spectra shown in Fig. 2. Compounds 1 and 2 have molecular ion M^+ at m/z 274, compound 3 at m/z 288 and compounds 4–8 at m/z 316. Fig. 3 illustrates the separation of compound 4 by software-assisted deconvolution in 2D from the co-eluting C_{23} tricyclic terpene, resulting in a cleaner mass spectrum where diagnostic and molecular ions are clearly distinguishable. Since the peaks were overlapping, deconvolution of the ion current (DIC) was only possible due to the high acquisition rate of the TOFMS (Focant et al., 2004).

The unusual compounds showed double bond equivalence (DBE) values equal to four, which indicate a tetracyclic saturated structure. Alkenes can be found in immature crude oils and rock extracts, but since double bonds are relatively susceptible to transformation in early diagenetic processes, structures with a double bond are generally absent or only found as trace quantities in oils. These compounds are more common in immature bitumen (Peters et al., 2005b). For example, de-A-diasterenes have been detected in immature marine shales (Peakman et al., 1986) and C_{23} tricyclic terp-12(13)-ene in asphaltenes (Yang et al., 2009). Taking into account that alkenes are rarely found in crude oils, especially in the saturated hydrocarbon fraction, and that their retention times in 2D being higher than those of tricyclic terpenes (Supplementary Material, Table 1S), we assign these eight unusual structures as saturated tetracyclic compounds.

Compounds 5 and 8 have m/z 191 as a diagnostic ion, which is typical for tetracyclic terpenes, whereas compounds 1–4, 6 and 7 have a diagnostic ion at m/z 203; in addition, compound 1 showed m/z 135 characteristic of A-nor-steranes (van Graas et al., 1982). In the literature (Table 4), the C_{20} tetracyclic diterpane, with a diagnostic ion at m/z 203 and molecular ion at m/z 274, has been reported in coal samples from Luquan, China (Sheng et al., 1992). Similarly the C_{23} C-10-demethylated tetracyclic terpene, with a diagnostic ion at m/z 177 and molecular ion at m/z 316 was detected in severely biodegraded oils in Zhungeer oil field in China (Zhusheng et al., 1990) and in Brazilian oils (Aguar et al., 2010). Recently, sterane derivatives with a diagnostic ion at m/z 203 related to a modified androstane carbon skeleton have been synthesized for biomarker confirmation (Bender et al., 2015).

Different pathways for the formation of tetracyclic compounds (Supplementary Material, Fig. 3S) have been proposed in the literature: (i) thermo-catalytic degradation of pentacyclic hopane precursors during geological maturation (Trendel et al., 1982); (ii) microbial opening of ring E of hopanoids, e.g. oxidation of hop-17(21)-enes, at an early stage of diagenesis, followed by a reduction in the corresponding alkanes (Trendel et al., 1982); (iii) cyclization of a squalene precursor stopping at ring D, leading to tetracyclic precursors which could be further reduced (Trendel et al., 1982); (iv) enzymatic cyclization of unsaturated aliphatic polyisoprenoids, i.e. isocomene formation from farnesol (Zalkow et al., 1977; Petrov et al., 1988); (v) precursors of tetracyclic diterpanes from pteridophyta, for example ferns (Sheng et al., 1992); (vi) biosynthesis of tetracyclic terpene series by bacteria or algae (Sheng et al., 1992); (vii) C_{19} A-nor-steranes which could originate from larger sterols observed in some sponges (Minale and Sodano, 1974; Grosjean et al., 2009). Interestingly, although sample S07 was classified as a marine oil and S08 as a lacustrine oil, both of them have high levels of these unusual tetracyclic compounds. This may indicate that both environments had organisms capable of producing precursors of these unusual compounds.

3.4. Number and size of rings of polycyclic alkanes

The unusual tetracyclic compounds 4–8 all have the same molecular ion m/z 316 but their retention times (t_R) differ in 1D and 2D . The GC×GC-TOFMS instrument is capable of performing compound class separations from complex hydrocarbons. Some examples of this capability are crude oils where ten different groups were separated (Ventura et al., 2010), diesel samples where compounds with different number of aromatic rings were separated (Marriott et al., 2004) and gasoline fuel where linear and branched alkanes were separated (Schoenmakers et al., 2000).

In this study, a similar GC×GC separation was observed in the hydrocarbon fraction with biomarkers based on retention time (t_R) in the second dimension in the following order: (i) tricyclic terpenes; (ii) steranes with 3 rings with 6 carbon atoms in ring and 1 ring with 5 carbon atoms in ring; (iii) tetracyclic terpenes with 4 rings with 6 carbon atoms; (iv) pentacyclic terpenes with 4 rings with 6 carbon atoms and 1 ring with 5 carbon atoms; (v) pentacyclic terpene with 5 rings with 6 carbon atoms (Fig. 4). A group-type separation was observed in the 2D order with the chromatographic conditions used in the GC×GC-TOFMS.

The main separation factor in the mid-polar 2D column is polarity of compounds, i.e., analytes with increasing polarity have increasing retention times. This rule is valid when analytes have ring structures (e.g. benzene) or functional groups with differing polarity (e.g. oxygen or nitrogen). In our study the polarity does not vary significantly between saturated compounds that contain only hydrogen and carbon atoms (hydrocarbons). Therefore, these distinct retention times may be explained by the three dimensional shape of molecules and small differences in polarizability of six member rings as compared to five member rings. These would

Table 3
Peak areas of unusual compounds and TeT_{24} divided by perdeuterated tetracosane (A_i/A_{is}).

Compounds/classification	S01	S02	S03	S04	S05	S06	S07	S08	S09	S10	S11
#1, $C_{20}H_{34}$	0.20	0.17	0.12	0.11	0.08	0.20	0.40	0.58	0.07	0.03	0.11
#2, $C_{20}H_{34}$	0.07	0.08	0.04	0.03	0.01	0.04	0.14	0.24	0.02	0.01	0.02
#3, $C_{21}H_{36}$	0.02	0.03	0.00	0.00	0.00	0.00	0.02	0.02	0.06	0.02	0.00
#4, $C_{23}H_{40}$	0.06	0.12	0.03	0.02	0.00	0.09	0.16	0.41	0.22	0.09	0.00
#5, $C_{23}H_{40}$	0.09	0.08	0.01	0.01	0.00	0.06	0.11	0.49	0.02	0.01	0.01
#6, $C_{23}H_{40}$	0.06	0.08	0.01	0.02	0.00	0.02	0.07	0.21	0.23	0.06	0.01
#7, $C_{23}H_{40}$	0.10	0.18	0.06	0.03	0.00	0.07	0.17	0.47	1.89	0.43	0.02
#8, $C_{23}H_{40}$	0.03	0.04	0.01	0.01	0.00	0.02	0.03	0.05	0.09	0.03	0.00
TeT_{24}	0.19	0.29	0.05	0.05	0.03	0.01	0.05	0.64	2.08	0.42	0.08

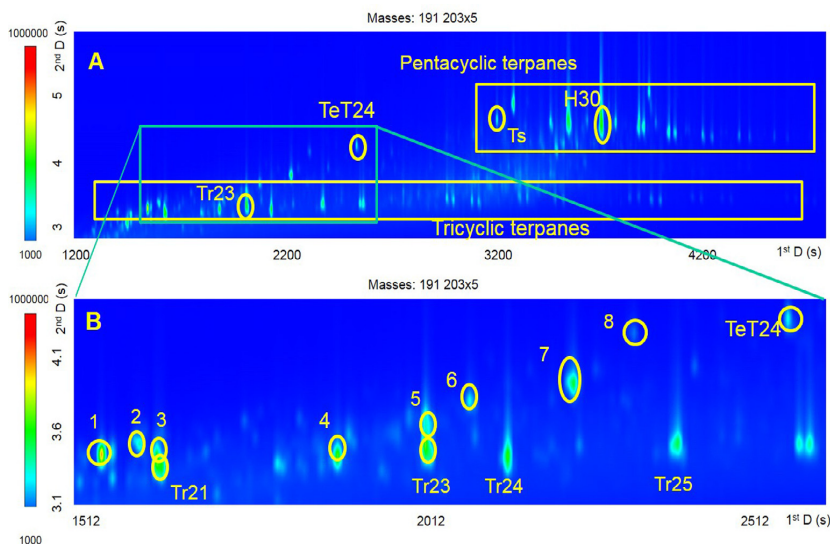


Fig. 1. Sample S08: Partial extracted ion chromatogram with sum of ions m/z 191 and 203 ($\times 5$) showing tri-, tetra-, and pentacyclic terpanes [A] and eight [1–8] unusual compounds [B]. $Tr_n = C_n$ tricyclic terpene; TeT24, C_{24} tetracyclic terpene.

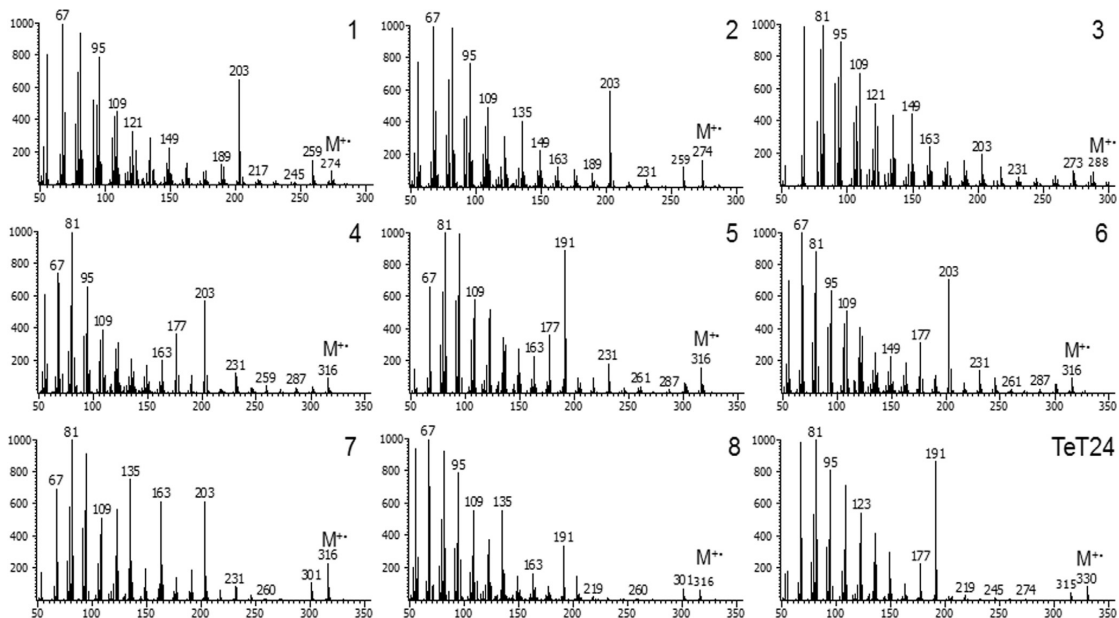


Fig. 2. Mass spectra of [1–8] unusual compounds. TeT24, C_{24} tetracyclic terpene.

be more twisted, thus allowing a larger surface area of six member rings for interaction with the stationary phase of the 2D column and resulting in longer retention times than five member rings. The analyte molecules could form a “van der Waals plane” which would increase the contact force with the column stationary phase similar to smaller hydrocarbon isomers such as 2-methyl butane and pentane which are separated in a GC with a MOF-508 column (Chen et al., 2006).

Generally, tri- and tetracyclic terpanes are assumed to have a more planar structure than steranes (with five-carbon ring) which disrupts the planarity of the structure and result in steranes having

lower retention times in 2D than tetracyclic compounds. Some variations inside the groups were also observed. For instance, in the tricyclic terpene group (i) C_{19} and C_{20} tricyclic terpanes had the lowest retention times in 2D , and show an increase in the 2t_R of the tricyclic terpene series and (ii) pentacyclic hopanes, with increasing carbon number, showed the opposite behavior of a reduction in 2D retention times (Supplementary Material, Table 1S). In the case of C_{19} and C_{20} tricyclic terpanes the variation can be explained by the fact that C_{20} and C_{21} tricyclic terpanes have four stereoisomers, and the $13\alpha(H),14\alpha(H)$ and $13\alpha(H),14\beta(H)$ isomers, respectively, are usually the most abundant ones in oils

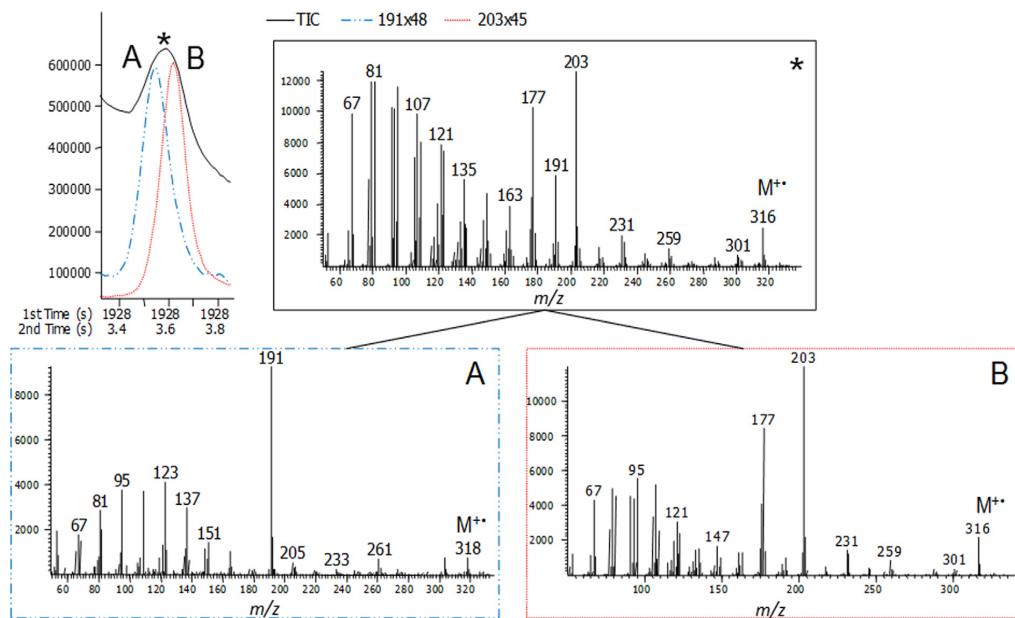


Fig. 3. Top left: Total ion chromatogram (*, black solid line); extracted ion chromatogram at m/z 191 (A, blue dashed line, peak intensity $\times 48$), and extracted ion chromatogram at m/z 203 (B, orange solid line, peak intensity $\times 45$). Top right: mass spectrum at peak top of TIC. Bottom left: Mass spectra of co-eluting possible C_{23} tricyclic terpene with diagnostic ion m/z 191 [A]. Bottom right: Unusual C_{23} tetracyclic compound [compound 4, Figs. 1 and 2] with diagnostic ion m/z 203 [B]. (For interpretation of the references to colour in this figure legend, the reader is referred to the web version of this article.)

Table 4

Summary of tetracyclic compounds (I to XIV, in Supplementary material Fig. 1S) found in oils or rock extracts.

Compounds	Empirical formula	$[M]^+$ (m/z)	Key ions (m/z)	Biological origin	Reference
C_{19} methyl-sterane (I)	$C_{19}H_{32}$	260	204, 203		Norden et al. (2011)
C_{19} methyl-18-nor-androstane (II)	$C_{19}H_{32}$	260	204, 203, 135		Bender et al. (2013)
C_{19} A-nor-sterane	$C_{19}H_{32}$	260	203		Grosjean et al. (2009)
C_{19} D-homo-13 β (H), 14 α (H)-androstane	$C_{19}H_{32}$	260	203, 204, 245		Norden et al. (2015)
C_{19} 5 α (H), 14 β (H)-androstane	$C_{19}H_{32}$	260	203, 204, 245		Bender et al. (2015)
C_{19} diterpane	$C_{19}H_{32}$	260	217, 177	Microbiological	Petrov et al. (1988)
C_{20} methyl-androstane (III)	$C_{20}H_{34}$	274	218, 217		Norden et al. (2011)
C_{20} tetracyclic diterpane	$C_{20}H_{34}$	274	259, 203, 177, 109	Fungal or lower plant	Sheng et al. (1992)
C_{20} phyllocladane (IV)	$C_{20}H_{34}$	274	274, 259, 231, 123	Higher plants, in the leaf resins of conifers	Noble et al. (1985), Schulze and Michaelis (1990), Zubrik et al. (2009)
C_{21} tetracyclic terpene	$C_{21}H_{36}$	288	273, 231, 203, 164, 123	Fungal or lower plant	Sheng et al. (1992)
C_{22} pregnane	$C_{22}H_{38}$	302	287, 218	Microbial	Lu et al. (2009)
C_{23} C-10 demethylated tetracyclic terpene (V)	$C_{23}H_{40}$	316	177	Biodegradation	Zhusheng et al. (1990), Aguiar et al. (2010)
nor-des-A-ursane/taraxastane	$C_{23}H_{40}$	316	177		Eiserbeck et al. (2012)
C_{23} unsaturated de-A-steroid (alkene) (VI)	$C_{23}H_{40}$	316	203	Immature shale	Peakman et al. (1986)
C_{24} tetracyclic terpene (VII)	$C_{24}H_{42}$	330	315, 191	Thermo degradation or microbial	Trendel et al. (1982)
C_{24} 4,4-dimethyl-homopregnane	$C_{24}H_{42}$	330	246, 177		Ten Haven et al. (1985)
C_{24} des-A-oleanane (VIII)	$C_{24}H_{42}$	330	315, 191, 177	Higher plant, Cretaceous or younger	Woodhouse et al. (1992), Samuel et al. (2010)
C_{24} des-A-lupane (IX)	$C_{24}H_{42}$	330	287, 192, 192, 123	Higher plant	Schmitter et al. (1981), Woodhouse et al. (1992)
C_{24} lanostane (X)	$C_{24}H_{42}$	330	315, 259	Sponge, dinoflagellate	Lu et al. (2011)
C_{26} A-nor-sterane (XI)	$C_{26}H_{46}$	358	343, 203, 135		van Graas et al. (1982)
C_{26} degraded bicadinane (XII)	$C_{26}H_{46}$	358	343, 315, 163, 149	Higher plant	Bao et al. (2013)
C_{27} nor-methyl-cholestane (XIII)	$C_{27}H_{48}$	372	357, 217, 149	Diatom, dinoflagellate	Schouten et al. (1994)
C_{30} onocerane I (XIV)	$C_{30}H_{54}$	414	399, 191, 123	Fern	Jacob et al. (2004)

(Oliveira et al., 2012a). The small difference in retention time in 2D could be due to different conformations of the two isomers.

In the case of the homologous series of hopanes, the systematic reduction in retention time in 2D can be explained by the degree of branching on the side chain, which increases with increasing car-

bon number. Sometimes chromatographic conditions can cause disruption in retention times. For example, the heat transfer inside the 2D oven can be more effective than in the 1D oven. Note, in Supplementary Material Fig. 4S, that the homologous series of tricyclic terpanes have a slightly increasing trend in retention time in 2D

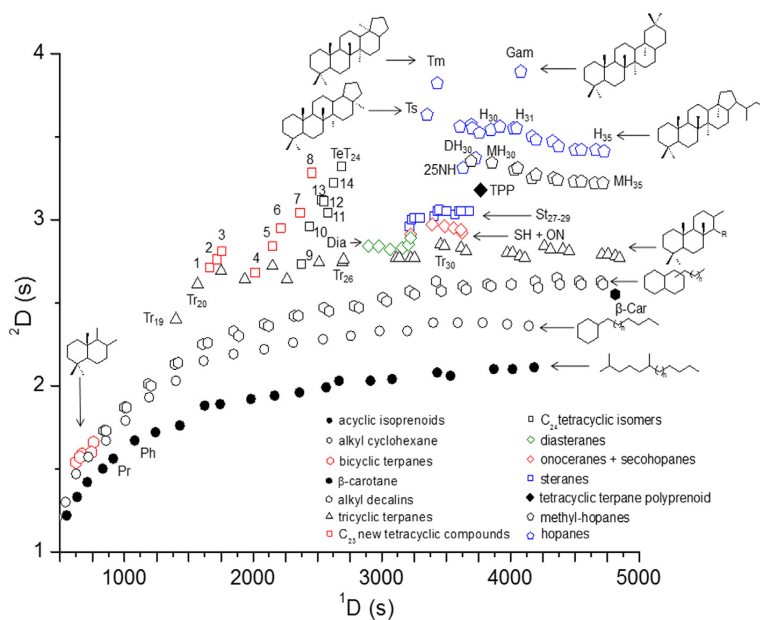


Fig. 4. GCxGC-TOFMS retention time plot (1D vs 2D) illustrating the behavior of hydrocarbons with differing ring structures.

which supports the hypothesis that the side chain of the hopanes could be more branched than the tricyclic terpanes. C_{27} 18 α (H)-2,2,9,30-trisnorhopane (Ts) has a retention time in 2D close to hopane, but C_{27} 17 α (H)-22,29,30-trisnorhopane (Tm) has a much higher retention time, closer to gammacerane, which has 6 rings with 6 carbon atoms (Hills et al., 1966). The difference in retention times could be due to fact that the structure of Tm is more planar than Ts (Dunlap et al., 1985). Onocerane II has a “broken” ring C, which could allow freedom of rotation of two different ring sets resulting in lower retention times in 2D than steranes, which have a fused ring structure. Also, additional methyl groups in fused ring structures are expected to hinder molecule-stationary phase interactions and result in a small reduction in retention times in 2D . Ring numbers were assigned to known biomarkers with C_{29} structure, namely C_{29} tricyclic terpene (Ring number = 3), C_{29} 5 α (H),14 β (H),17 β (H)-stigmastane 20R (Ring number = 3.5) and C_{29} 17 α (H),21 β (H)-30-norhopane (Ring number = 4.5), based on how many six-carbon rings they contain. If the structure had five carbons in one ring, then 0.5 was subtracted from the original number. This was plotted against their retention times (t_R) in 2D (see Supplementary Material, Fig. 5S). The resulting curve equation was used to calculate ring numbers for the eight unusual tetracyclic compounds (Supplementary Material, Table 1S). Since chromatographic conditions can affect retention time in 2D , C_{24} tricyclic terpene (Ring number = 3) and C_{24} tetracyclic terpene (Ring number = 4) were included for comparison (Supplementary Material, Table 1S) because they elute in the same region of the chromatogram as the unusual tetracyclic terpanes. Compound 5 and 6 were an exception, with ring numbers 3.22 and 3.34 that could represent a “closed” conformation of a sterane-like structure which has reduced interaction with the column phase. Differences in retention times (t_R) in 1D and 2D indicate structural differences. For example, in Fig. 5, tentative structures for unusual compounds 1, 3, 4 and 8 are presented which are based on compiled chromatographic and MS information. Compound 4 has a t_R close to tricyclic terpanes, but it has a 4 ring structure. Therefore, one could suggest a contraction of ring C, which could cause reduction in t_R in 2D . This change in 2D retention time is also observed for other compounds.

For example, t_R of C_{30} 17 α (H),21 β (H)-hopane with 5 carbon atoms in ring E is lower than that of gammacerane with 6 carbon atoms in ring E. Compound 4 has MS fragment ions m/z 177 and 203, which supports a hypothesis of the presence of having 5 carbon atoms in ring C. Whereas, compound 8 has t_R in 2D near the C_{24} tetracyclic terpene and a m/z 191 fragment ion, typical of C_{24} tetracyclic terpene (Trendel et al., 1982). This indicates that this compound could be a C_{23} tetracyclic terpene.

By evaluating the mass spectra data in combinations with retention times in the first and second dimensions, and by excluding chemical structures that present completely different mass spectra (Table 4) we suggest that the structures are tetracyclic saturated compounds with terpene and/or sterane hydrocarbon skeletons but with differing methyl group positions and/or on the ring sizes.

The mass spectra of des-A-ursane and des-A-oleanane (Zhusheng et al., 1990; Woodhouse et al., 1992; Samuel et al., 2010) do not match with the observed mass spectra. This also holds for kaurane (Sheng et al., 1992), phyllocladane (Sheng et al., 1992), beyerane (Noble et al., 1985), all of which are ruled out as they present ion m/z 123 as the base peak. Compounds related to methyl-estrane (Norden et al., 2011), methyl-androstane (Norden et al., 2011), methyl-nor-androstane (Bender et al., 2013) or *D-homo*-androstane (Bender et al., 2013) all have a base peak at m/z 203, and so we tentatively suggest that the unusual tetracyclic compounds could have the structure with a 5 carbon atom ring. Changing the position of only one methyl group, and/or changing the stereochemistry, can completely change the mass spectra. All the structures that showed m/z 203 are assigned as being steroid like structures presenting at least one 5 carbon atom ring.

3.5. High resolution molecular organic geochemistry

The CENPES provided a set of basic geochemical parameters for all the oils in our study as well as their interpreted classifications (Table 1). In addition to this information, biomarker parameters were calculated from GCxGC-TOFMS data (Tables 1 and 2). We

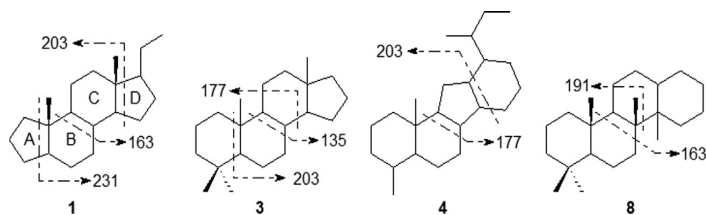


Fig. 5. Tentative structures and possible fragmentations for unusual biomarkers (1, 3, 4 and 8) in Fig. 1.

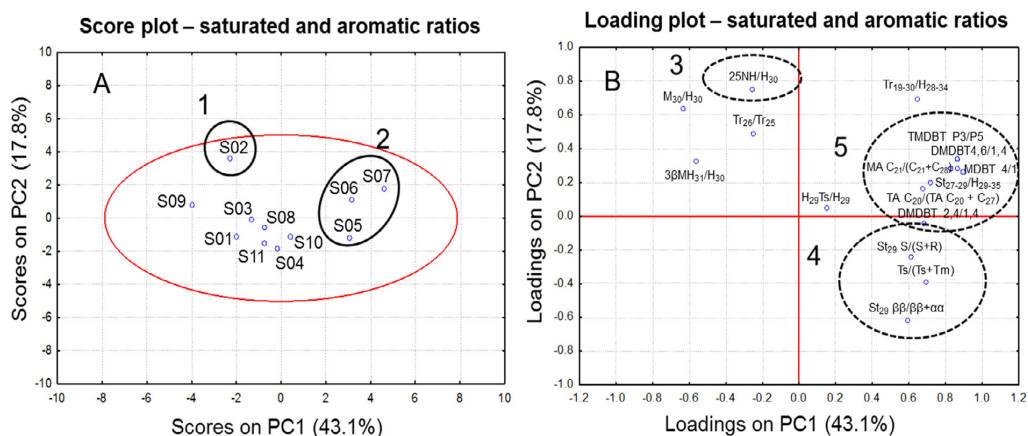


Fig. 6. PCA score [A] and loading [B] plots for the first two principal components, based on saturated and aromatic biomarker parameters. [1] Oil S02; [2] oils S05, S06 and S07; [3] 25NH/H₃₀ ratio; [4] some of saturated maturity parameters; [5] aromatic geochemical parameters.

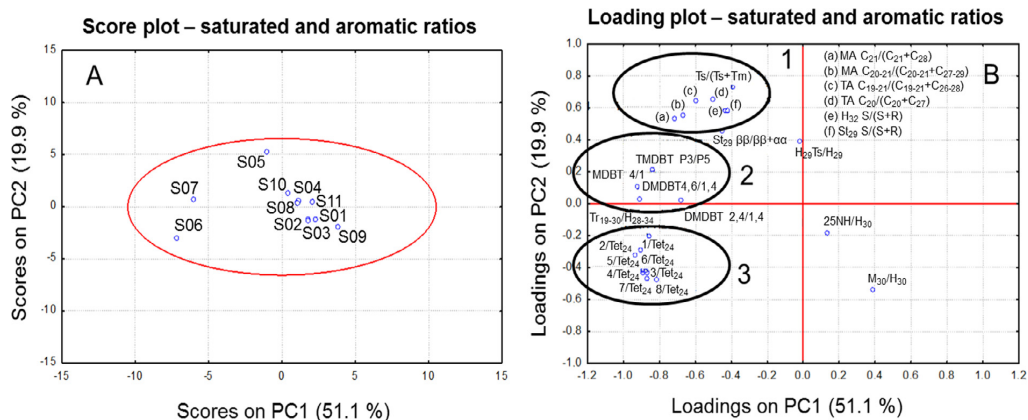


Fig. 7. PCA score [A] and loading [B] plots for the first two principal components, based on saturated and aromatic biomarker parameters. [1] Conventional saturated/aromatic maturation ratios; [2] dibenzothiophenes ratios; [3] unusual compounds 1–8/TeT24 ratios.

subjected these parameters to PCA with the following results. The S02 oil was separated based on the highest biodegradation level while the S05, S06 and S07 oils were separated as being the most mature (data not shown), supporting the earlier interpretation of saturated (Section 3.1.3) and aromatic (Section 3.2) maturation parameters. The result was similar when selected source parameters and all the saturated and aromatic maturation parameters were used for PCA analysis (Fig. 6A). The loading plot indicates that the most mature oils were mainly separated by parameters based on aromatic compounds and terpane ratios (Fig. 6B). The S09 oil could be considered immature, as this sample had extremely low

abundance of aromatic compounds, which is unusual. Therefore, a further investigation using PCA was conducted using only peak areas. The results showed that oil S09 was clearly separated from the other samples (Supplementary material, Fig. 6S). The contribution plot shows a high concentration of tri- and tetracyclic terpanes and an extremely low abundance of aromatic compounds, confirming the low maturity of this sample.

Finally, PCA was run with all the geochemical ratios in Tables 1 and 2 and also with the unusual biomarker compound ratios, obtained by dividing each of the peak areas by the peak area of the C₂₄ tetracyclic terpane (Fig. 7A; Supplementary Material,

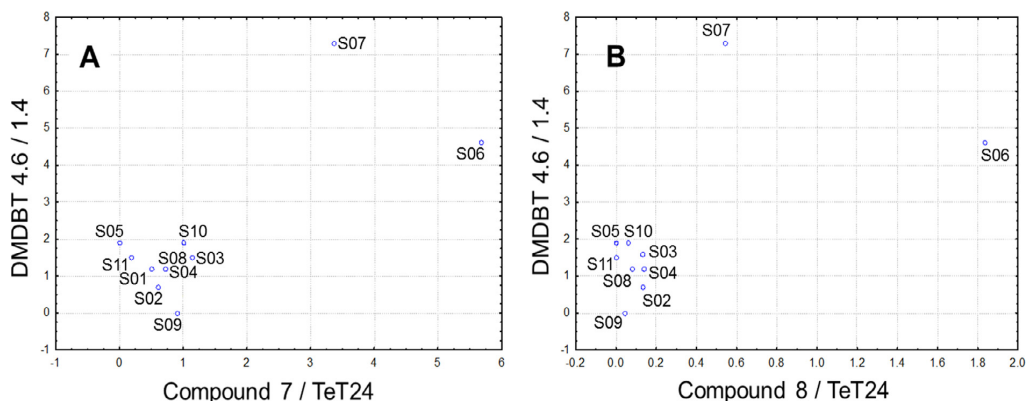


Fig. 8. The ratios of compound 7/TeT24 [A] and compound 8/TeT24 [B] follow about the same trend of ratio of DMBT 4,6/1,4.

Table 2S). The results show that source parameters have an insignificant role in the separation of the oils. Since PCA simplifies the results and can have overshadowed some parameters, the correlation of unusual compound ratios was tested by creating simple plots against source and environmental parameters. For example, elevated values of $\text{TeT}_{24}/\text{H}_{30}$ and $\text{TeT}_{24}/\text{Tr}_{26}$ may indicate carbonate or evaporite depositional environments whereas β -carotane/ H_{30} and Gam/H_{30} indicate elevated salinity and/or water column stratification levels in lacustrine environments (Sinninghe Damsté et al., 1995; Casilli et al., 2014). 2α -MH₃₁ is indicative of cyanobacteria and cyanobacterial mats and commonly elevated in oils from carbonate marine source rock (Summons et al., 1999). The outcome found no correlation between these known source and environment parameters and the unusual tetracyclic terpane ratios.

The key result of PCA analysis of the unusual biomarkers (group number 3, Fig. 7B) is a trend in the same loadings as the dibenzothiophenes (group number 2, Fig. 7B). A similar trend can be seen in score plots when ratios of compound 7/TeT24 (Fig. 8A) and compound 8/TeT24 (Fig. 8B) are plotted with DMBT 4,6/1,4. The oil S05 had no compound 7 or 8 and this could be because initial organic input material lacked precursors of these compounds. However, a correlation between normalized peak areas of compound 7 and TeT24 is seen (Table 3), which may mean that compound 7 is formed from TeT24 during maturation or they have a common precursor. Therefore, it is proposed that these ratios are potential maturity parameters for more mature oils, akin to benzothiophene parameters which have been used for oils in the maturity range of $R_o \sim 1.3$ – 1.5 (Chakhmakhchev et al., 1997). However, it is recommended that the working range of these tetracyclic compounds be determined in more detail.

4. Conclusions

Source and maturity-related geochemical parameters were measured for eleven Brazilian crude oils using GC×GC-TOFMS. $\text{H}_{30}/\text{St}_{27}$, 3β -MH₃₁/ H_{30} % and $\text{TPP}/\text{Dia}_{27}$ ratios suggested that oils S01, S02, S08, S09 and S10 were generated from lacustrine source rocks; S04, S05, S6, S07 and S11 from marine source rocks, and S03 is a mixture of both sources. PCA on the data indicate that the most mature oils are S05, S06 and S07 and the least mature is S09. The low maturity degree is also confirmed by the absence of aromatic compounds in this sample.

Eight unusual biomarkers were revealed by the GC×GC-TOFMS technique, some of which (compounds 3, 4 and 5) would not have been detected using one dimensional GC-MS. A relationship between retention time (t_R) in ²D and carbon ring number was

observed for known biomarkers and by using this correlation, we were able to obtain additional structural information about number of carbons in rings for the unusual tetracyclic compounds. Furthermore, mass spectral data point to tetracyclic structures, some of which appear similar to nor-steranes, and tentative structures for four of these compounds are proposed.

No correlation between these novel compounds and source parameters was observed. However, we did observe a trend between some of these tetracyclic compounds and maturity of the oils, e.g. the ratio of compound 7/TeT24 increasing with the ratio of DMBT 4,6/1,4. One explanation is that compound 7 is more stable than the C₂₄ tetracyclic terpane or is produced during the maturation process. Therefore, it is proposed that the compound 7/TeT24 ratio could be used in parallel with other maturation indicators such as benzothiophenes ($R_o \sim 1.3$ – 1.5) to evaluate oils from mature to overmature levels. The working range for these unusual tetracyclic compounds as maturity parameters needs to be characterized in more detail.

Acknowledgements

The authors thank CNPq, CAPES, and FAPERJ (Brazilian research councils) for scholarships and financial support, FUJB and PETROBRAS (Contract 00500072201.11.9) for their support. Alexandre A. Ferreira from Petrobras is thanked for his help. Special thanks go to the Editor-in-Chief, Erdem Idiz, Ph.D. and Associate Editor Dr. Marcus Elvert. Further thanks go to Dr. Will Meredith and to the anonymous reviewer for their comments.

Appendix A. Supplementary material

Supplementary data associated with this article can be found, in the online version, at <http://dx.doi.org/10.1016/j.orggeochem.2016.10.012>.

Associate Editor—Marcus Elvert

References

- Aguiar, A., Aguiar, H.G.M., Azevedo, D.A., Aquino Neto, F.R., 2011. Identification of methylhopane and methylmoretane series in Ceará Basin oils, Brazil, using comprehensive two-dimensional gas chromatography coupled to time-of-flight mass spectrometry. *Energy & Fuels* 25, 1060–1065.
- Aguiar, A., Silva Júnior, A.L., Azevedo, D.A., Aquino Neto, F.R., 2010. Application of comprehensive two-dimensional gas chromatography coupled to time-of-flight mass spectrometry to biomarker characterization in Brazilian oils. *Fuel* 89, 2760–2768.

- Aquino Neto, F.R., Trendel, J.M., Restle, A., Connan, J., Albrecht, P.A., 1983. Occurrence and formation of tricyclic and tetracyclic terpanes in sediments and petroleum. In: Bjørøy, M., Albrecht, P., Cornford, C. (Eds.), *Advances in Organic Geochemistry 1981*. John Wiley & Sons, New York, pp. 659–676.
- Araújo, B.Q., Azevedo, D.A., 2016. Uncommon steranes in Brazilian marginal crude oils: dinoflagellate molecular fossils in the Sergipe-Alagoas Basin, Brazil. *Organic Geochemistry* 99, 38–52.
- Bao, J., Zhu, C., Liu, Y., Wang, W., Liu, H., 2013. Novel C₂₆ tetracyclic degraded bicadinanes in oil sands from the Haitoubei-Maichen Sag of the Beibuwan Basin, South China Sea. *Organic Geochemistry* 58, 89–95.
- Bender, M., Schmidtman, M., Rullkötter, J., Summons, R.E., Christoffers, J., 2013. Identification of a fossil sterane biomarker in crude oil – an androstane with a modified carbon skeleton. *European Journal of Organic Chemistry* 2013, 5934–5945.
- Bender, M., Schmidtman, M., Summons, R.E., Rullkötter, J., Christoffers, J., 2015. A geomimetic approach to the formation and identification of fossil sterane biomarkers in crude oil: 18-nor-*p*-homo-androstane and 5 α ,14 β -androstane. *Chemistry – A European Journal* 21, 12501–12508.
- Bennett, B., Fustic, M., Farrimond, P., Huang, H., Larter, S.R., 2006. 25-Norhopanes: formation during biodegradation of petroleum in the subsurface. *Organic Geochemistry* 37, 787–797.
- Casilli, A., Silva, R.C., Laakia, J., Oliveira, C.J.F., Ferreira, A.A., Loureiro, M.R.B., Azevedo, D.A., Aquino Neto, F.R., 2014. High resolution molecular organic geochemistry assessment of Brazilian lacustrine crude oils. *Organic Geochemistry* 68, 61–70.
- Chakhmakhchev, A., Suzuki, M., Takayama, K., 1997. Distribution of alkylated dibenzothiophenes in petroleum as a tool for maturity assessments. *Organic Geochemistry* 26, 483–489.
- Chen, B., Liang, C., Yang, J., Contreras, D.S., Clancy, Y.L., Lobkovsky, E.B., Yaghi, O.M., Dai, S., 2006. A microporous metal-organic framework for gas-chromatographic separation of alkanes. *Angewandte Chemie* 118, 1418–1421.
- Dunlap, N.K., Sabol, M.R., Bauer, P.E., Watt, D.S., Reibenspies, J.H., Anderson, O.P., Seifert, W.K., Moldowan, J.M., 1985. Synthesis of biological markers in fossil fuels. 3. Degraded and rearranged C₂₇ hopanes. *The Journal of Organic Chemistry* 50, 1826–1829.
- Eiserbeek, C., Nelson, R.K., Grice, K., Curiale, J., Reddy, C.M., 2012. Comparison of GC-MS, GC-MRM-MS, and GC \times GC to characterise higher plant biomarkers in Tertiary oils and rock extracts. *Geochimica et Cosmochimica Acta* 87, 299–322.
- Farrimond, P., Taylor, A., Telnæs, N., 1998. Biomarker maturity parameters: the role of generation and thermal degradation. *Organic Geochemistry* 29, 1181–1197.
- Focant, J.-F., Sjödin, A., Patterson Jr., D.G., 2004. Improved separation of the 209 polychlorinated biphenyl congeners using comprehensive two-dimensional gas chromatography–time-of-flight mass spectrometry. *Journal of Chromatography A* 1040, 227–238.
- Fu, J., Sheng, G., Xu, J., Eglinton, G., Gowar, A.P., Jia, R., Fan, S., Peng, P., 1990. Application of biological markers in the assessment of paleoenvironments of Chinese non-marine sediments. *Organic Geochemistry* 16, 769–779.
- Grantham, P.J., 1986. Sterane isomerisation and moretane/hopane ratios in crude oils derived from Tertiary source rocks. *Organic Geochemistry* 9, 293–304.
- Grosjean, E., Love, G.D., Stalviès, C., Fike, D.A., Summons, R.E., 2009. Origin of petroleum in the Neoproterozoic-Cambrian South Oman Salt Basin. *Organic Geochemistry* 40, 87–110.
- Gürgey, K., 1999. Geochemical characteristics and thermal maturity of oils from the Thrace basin (western Turkey) and western Turkmenistan. *Journal of Petroleum Geology* 22, 167–189.
- Heckmann, J.R., Landau, L., Gonçalves, F.T.T., Pereira, R., Azevedo, D.A., 2011. Geochemical evaluation of Brazilian oils with emphasis on aromatic hydrocarbons. *Quimica Nova* 34, 1328–1333.
- Hills, I.R., Whitehead, E.V., Anders, D.E., Cummins, J.J., Robinson, W.E., 1966. An optically active triterpane, gammacerane in Green River, Colorado, oil shale bitumen. *Chemical Communications (London)*, 752b–754b.
- Jacob, J., Disnar, J.-R., Boussafir, M., Ledru, M.-P., Albuquerque, A.L.S., Sifeddine, A., Turcq, B., 2004. Onocerane attests to dry climatic events during the Quaternary in the tropics. *Organic Geochemistry* 35, 289–297.
- Kiepper, A.P., Casilli, A., Azevedo, D.A., 2014. Depositional paleoenvironment of Brazilian crude oils from unusual biomarkers revealed using comprehensive two dimensional gas chromatography coupled to time of flight mass spectrometry. *Organic Geochemistry* 70, 62–75.
- Lappas, A.A., Patiaka, D., Ikononou, D., Vasalos, I.A., 1997. Separation and characterization of paraffins and naphthenes from FCC feedstocks. *Industrial and Engineering Chemistry Research* 36, 3110–3115.
- Lu, H., Chen, T., Grice, K., Greenwood, P., Peng, P.A., Sheng, G., 2009. Distribution and significance of novel low molecular weight steranes in an immature evaporitic sediment from the Jinxian Sag, North China. *Organic Geochemistry* 40, 902–911.
- Lu, H., Liang, Y., Dunn, W.B., Shen, H., Kell, D.B., 2008. Comparative evaluation of software for deconvolution of metabolomics data based on GC-TOF-MS. *TrAC, Trends in Analytical Chemistry* 27, 215–227.
- Lu, H., Sheng, G., Peng, P.A., Ma, Q., Lu, Z., 2011. Identification of C₂₄ and C₂₅ lanostanes in Tertiary sulfur rich crude oils from the Jinxian Sag, Bohai Bay Basin, Northern China. *Organic Geochemistry* 42, 146–155.
- Mackenzie, A.S., Brassell, S.C., Eglinton, G., Maxwell, J.R., 1982. Chemical fossils: the geological fate of steroids. *Science* 217, 491–504.
- Mackenzie, A.S., Hoffmann, C.F., Maxwell, J.R., 1981. Molecular parameters of maturation in the Toarcian shales, Paris Basin, France—III. Changes in aromatic steroid hydrocarbons. *Geochimica et Cosmochimica Acta* 45, 1345–1355.
- Marotta, E., Aquino Neto, F.R., Azevedo, D.A., 2014. Separation and quantitative determination of linear and cyclic/branched alkanes in Brazilian petroleum using urea adduction and gas chromatography: a case study revisited. *Quimica Nova* 37, 1692–1698.
- Marriott, P.J., Massil, T., Hügel, H., 2004. Molecular structure retention relationships in comprehensive two-dimensional gas chromatography. *Journal of Separation Science* 27, 1273–1284.
- Mello, M.R., Telnaes, N., Gaglianone, P.C., Chicarelli, M.I., Brassell, S.C., Maxwell, J.R., 1988. Organic geochemical characterisation of depositional palaeoenvironments of source rocks and oils in Brazilian marginal basins. *Organic Geochemistry* 13, 31–45.
- Minale, L., Sodano, G., 1974. Marine sterols: unique β -hydroxymethyl-A-nor-5 α -steranes from the sponge *Axinella verrucosa*. *Journal of the Chemical Society, Perkin Transactions* 1, 2380–2384.
- Moldowan, J.M., Seifert, W.K., Gallegos, E.J., 1983. Identification of an extended series of tricyclic terpanes in petroleum. *Geochimica et Cosmochimica Acta* 47, 1531–1534.
- Moldowan, J.M., Sundaraman, P., Schoell, M., 1986. Sensitivity of biomarker properties to depositional environment and/or source input in the Lower Toarcian of SW-Germany. *Organic Geochemistry* 10, 915–926.
- Mitrevski, B.S., Wilairat, P., Marriott, P.J., 2010. Evaluation of World Anti-Doping Agency criteria for anabolic agent analysis by using comprehensive two-dimensional gas chromatography–mass spectrometry. *Analytical and Bioanalytical Chemistry* 396, 2503–2511.
- Netzel, D.A., Rovani, J.F., 2007. Direct separation and quantitative determination of (*n*-, iso-) alkanes in neat asphalt using urea adduction and high-temperature gas chromatography (HTGC). *Energy & Fuels* 21, 333–338.
- Noble, R.A., Alexander, R., Kagi, R.L., Knox, J., 1985. Tetracyclic diterpenoid hydrocarbons in some Australian oils, sediments and crude oils. *Geochimica et Cosmochimica Acta* 49, 2141–2147.
- Norden, S., Bender, M., Rullkötter, J., Christoffers, J., 2011. Androstanes with modified carbon skeletons. *European Journal of Organic Chemistry* 2011, 4543–4550.
- Oliveira, C.R., Ferreira, A.A., Oliveira, C.J.F., Azevedo, D.A., Santos Neto, E.V., Aquino Neto, F.R., 2012a. Biomarkers in crude oil revealed by comprehensive two-dimensional gas chromatography time-of-flight mass spectrometry: depositional paleoenvironment proxies. *Organic Geochemistry* 46, 154–164.
- Oliveira, C.R., Oliveira, C.J.F., Ferreira, A.A., Azevedo, D.A., Aquino Neto, F.R., 2012b. Characterization of aromatic steroids and hopanoids in marine and lacustrine crude oils using comprehensive two dimensional gas chromatography coupled to time-of-flight mass spectrometry (GC \times GC-TOFMS). *Organic Geochemistry* 53, 131–136.
- Peakman, T.M., Farrimond, P., Brassell, S.C., Maxwell, J.R., 1986. De-A-steroids in immature marine shales. *Organic Geochemistry* 10, 779–789.
- Peters, K.E., Walters, C.C., Moldowan, J.M., 2005a. *The Biomarker Guide: Biomarkers and Isotopes in Petroleum Exploration and Earth History*, vol. 2, second ed. pp. 684.
- Peters, K.E., Walters, C.C., Moldowan, J.M., 2005b. *The Biomarker Guide: Biomarkers in the Environment and Human History*, vol. 1, second ed. pp. 471.
- Petersen, H.I., Holland, B., Nytoft, H.P., Cho, A., Piasecki, S., de la Cruz, J., Cornec, J.H., 2012. Geochemistry of crude oils, seepage oils and source rocks from Belize and Guatemala: indications of carbonate-sourced petroleum systems. *Journal of Petroleum Geology* 35, 127–163.
- Petrov, A.A., Pehk, T.Y., Vorobieva, N.S., Zemskova, Z.K., 1988. Identification of some novel tetracyclic diterpene hydrocarbons in petroleum. *Organic Geochemistry* 12, 151–156.
- Radke, M., Willsch, H., Welte, D.H., 1980. Preparative hydrocarbon group type determination by automated medium pressure liquid chromatography. *Analytical Chemistry* 52, 406–411.
- Rullkötter, J., Wendisch, D., 1982. Microbial alteration of 17 α (H)-hopanes in Madagascar asphalts: removal of C-10 methyl group and ring opening. *Geochimica et Cosmochimica Acta* 46, 1545–1553.
- Rullkötter, J., Spiro, B., Nissenbaum, A., 1985. Biological marker characteristics of oils and asphalts from carbonate source rocks in a rapidly subsiding graben, Dead Sea, Israel. *Geochimica et Cosmochimica Acta* 49, 1357–1370.
- Rullkötter, J., Marzi, R., 1988. Natural and artificial maturation of biological markers in a Toarcian shale from northern Germany. *Organic Geochemistry* 13, 639–645.
- Samuel, O.J., Kildahl-Andersen, G., Nytoft, H.P., Johansen, J.E., Jones, M., 2010. Novel tricyclic and tetracyclic terpanes in Tertiary deltaic oils: structural identification, origin and application to petroleum correlation. *Organic Geochemistry* 41, 1326–1337.
- Schmitter, J.M., Arpino, P.J., Guiochon, G., 1981. Isolation of degraded pentacyclic triterpenoid acids in a Nigerian crude oil and their identification as tetracyclic carboxylic acids resulting from ring A cleavage. *Geochimica et Cosmochimica Acta* 45, 1951–1955.
- Schoenmakers, P.J., Oomen, J.L.M.M., Blomberg, J., Genuit, W., van Velzen, G., 2000. Comparison of comprehensive two-dimensional gas chromatography and gas chromatography–mass spectrometry for the characterization of complex hydrocarbon mixtures. *Journal of Chromatography A* 892, 29–46.
- Schouten, S., Sinnighe Damsté, J.S., Schoell, M., de Leeuw, J.W., 1994. A novel sterane, 27-nor-24-methyl-5 α -cholestane, in sediments. *Geochimica et Cosmochimica Acta* 58, 3741–3745.
- Schulze, T., Michaelis, W., 1990. Structure and origin of terpenoid hydrocarbons in some German coals. *Organic Geochemistry* 16, 1051–1058.

- Seifert, W.K., 1978. Steranes and terpanes in kerogen pyrolysis for correlation of oils and source rocks. *Geochimica et Cosmochimica Acta* 42, 473–484.
- Sheng, G., Simoneit, B.R.T., Leif, R.N., Chen, X., Fu, J., 1992. Tetracyclic terpanes enriched in Devonian cuticle humic coals. *Fuel* 71, 523–532.
- Silva, R.S.F., Aguiar, H.G.M., Rangel, M.D., Azevedo, D.A., Aquino Neto, F.R., 2011. Comprehensive two-dimensional gas chromatography with time of flight mass spectrometry applied to biomarker analysis of oils from Colombia. *Fuel* 90, 2694–2699.
- Silva, T.F., Azevedo, D.A., Rangel, M.D., Fontes, R.A., Aquino Neto, F.R., 2008. Effect of biodegradation on biomarkers released from asphaltenes. *Organic Geochemistry* 39, 1249–1257.
- Sinninghe Damsté, J.S., Kenig, F., Koopmans, M.P., Köster, J., Schouten, S., Hayes, J.M., de Leeuw, J.W., 1995. Evidence for gammacerane as an indicator of water column stratification. *Geochimica et Cosmochimica Acta* 59, 1895–1900.
- Sparkman, O.D., Penton, Z.E., Kitson, F.G., 2011. *Gas Chromatography and Mass Spectrometry*. Academic Press, Amsterdam, pp. 331–339.
- Summons, R.E., Jahnke, L.L., Hope, J.M., Logan, G.A., 1999. 2-Methylhopanoids as biomarkers for cyanobacterial oxygenic photosynthesis. *Nature* 400, 554–557.
- ten Haven, H.L., De Leeuw, J.W., Schenck, P.A., 1985. Organic geochemical studies of a Messinian evaporitic basin, northern Apennines (Italy) I: hydrocarbon biological markers for a hypersaline environment. *Geochimica et Cosmochimica Acta* 49, 2181–2191.
- Trendel, J.-M., Restle, A., Connan, J., Albrecht, P., 1982. Identification of a novel series of tetracyclic terpene hydrocarbons (C₂₄–C₂₇) in sediments and petroleum. *Journal of the Chemical Society, Chemical Communications*, 304–306.
- van Graas, G., de Lange, F., de Leeuw, J.W., Schenck, P.A., 1982. A-nor-steranes, a novel class of sedimentary hydrocarbons. *Nature* 296, 59–61.
- Wenger, L.M., Isaksen, G.H., 2002. Control of hydrocarbon seepage intensity on level of biodegradation in sea bottom sediments. *Organic Geochemistry* 33, 1277–1292.
- Ventura, G.T., Raghuraman, B., Nelson, R.K., Mullins, O.C., Reddy, C.M., 2010. Compound class oil fingerprinting techniques using comprehensive two-dimensional gas chromatography (GC×GC). *Organic Geochemistry* 41, 1026–1035.
- Woodhouse, A.D., Oung, J.N., Philp, R.P., Weston, R.J., 1992. Triterpanes and ring-A degraded triterpanes as biomarkers characteristic of Tertiary oils derived from predominantly higher plant sources. *Organic Geochemistry* 18, 23–31.
- Yang, C., Liao, Z., Zhang, L., Creux, P., 2009. Some biogenic-related compounds occluded inside asphaltene aggregates. *Energy & Fuels* 23, 820–827.
- Zalkow, L.H., Harris, R.N., Van Derveer, D., Bertrand, J.A., 1977. Isocomene: a novel sesquiterpene from *Isocoma Wrightii*. X-ray crystal structure of the corresponding diol. *Journal of the Chemical Society, Chemical Communications*, 456–457.
- Zhusheng, J., Fowler, M.G., Lewis, C.A., Philp, R.P., 1990. Polycyclic alkanes in a biodegraded oil from the Kelamayi oilfield, northwestern China. *Organic Geochemistry* 15, 35–46.
- Zubrik, A., Šaman, D., Vašíčková, S., Simoneit, B.R.T., Turčániová, L.U., Lovás, M., Cvačka, J., 2009. Phyllocladane in brown coal from Handlová, Slovakia: isolation and structural characterization. *Organic Geochemistry* 40, 126–134.

FINNISH METEOROLOGICAL INSTITUTE

Erik Palménin aukio 1

P.O. Box 503

FI-00101 HELSINKI

tel. +358 29 539 1000

WWW.FMI.FI

FINNISH METEOROLOGICAL INSTITUTE

CONTRIBUTIONS No. 131

ISBN 978-952-336-016-7 (paperback)

ISSN 0782-6117

Erweko

Helsinki 2017

ISBN 978-952-336-017-4 (pdf)

Helsinki 2017

